THE USE OF SURGE ARRESTERS IN PARALLEL FOR THE LIGHTNING PROTECTION OF POLE MOUNTED DISTRIBUTION TRANSFORMERS IN ESKOM

Baden George Chatterton

School of Electrical and Electronic Engineering

University of Natal

December 2002

Submitted in fulfilment of the academic requirements for the degree of Master of Science in the School of Electrical and Electronic Engineering at the University of Natal

" Our doubts are traitors
and make us loose the good we oft
might win by fearing to attempt "

William Shakespeare

" What lies behind us and what lies before us
are tiny matters compared to
what lies within us "

Oliver Holmes

DECLARATION OF OWN WORK

I declare that this dissertation is my own unaided work and the relevant sources that I have used or quoted, have been indicated accordingly in the text. The dissertation is being submitted for the Degree of Master of Science in Engineering at the University of Natal. The work has not been submitted before for any degree or examination at any other University in South Africa.

The research work was conducted at the University of Natal under the supervision of Dr. Derek Hoch, Department of Electrical Engineering and Mr. Rob Stephen, Eskom Distribution. The practical part of the Eskom experimental project was conducted by myself under the supervision of Dr. Hendri Geldenhuys, Eskom Distribution. The work forms part of an Eskom research project (R99-00852R) to reduce the pole mounted transformer failure rate in Distribution.

Baden George Chatterton

Date

12 th day of December 2002

ACKNOWLEDGEMENTS

I would like to thank the following people and organisations for their kind assistance, support and time during the period of my dissertation :

- My supervisors Dr. Derek Hoch and Mr. Rob Stephen for their time, enthusiastic assistance and technical guidance with the dissertation.
- The electrical workshop staff at the University of Natal, especially Mr. Tony Roos.
- Dr. Hendri Geldenhuys and Ian Ferguson from Eskom Distribution for supervising and assisting me with the project engineering of the experimental project at Glencoe. A special thank you must be given to Dr. Hendri Geldenhuys for always making time available to see me, answer my unending questions and for trying to impart some of his extensive technical knowledge onto myself.
- Tony Britten from TSI for his technical assistance and support of the dissertation and Kohlie Kohlmeyer from TSI for his administrative support with the Eskom research project.
- The Eskom Glencoe TSC staff for their enthusiasm and support with the project, especially Mr. Pieter Trichardt and Mr. Clem Waldeck.
- The Eskom Newcastle Plant staff for their help with the monthly data collection.
- Eskom Research (Envoor Moos and Minnesh Bipath) for funding the experimental project and for funding the overseas trip to the International Centre for Lightning Research and Testing (ICLRT), Florida, USA.
- Eskom Distribution Eastern Region management team for allowing the initial funding and continued support of the project.
- A special word of thanks to all my family and friends who constantly encouraged me.

ABSTRACT

Eskom (Electricity Supply Commission of South Africa) is the national electrical utility that provides the generation, transmission and distribution of electricity in South Africa. The majority of Eskom's electricity distribution is done with either 11kV or 22kV electrical overhead networks. An unacceptable number of Eskom's pole mounted power transformers on these networks have been failing over the past six years in the Kwa-Zulu Natal region. The average transformer failure rate for the Distribution Eastern Region was calculated to be 2.4% per annum. International norms seem to indicate a transformer failure rate of between 0.5% and 1.0% per annum as acceptable.

The estimated cost of these transformer failures was between R9 million and R13 million per annum for the Eastern Region. Eskom Distribution has seven regions and the total cost of these failures was considerable to the business. These transformer failures contributed an average of 5.3% per month of the Supply Loss Index (SLI) for the Eastern Region, with a maximum contribution of 14.5% per month of the SLI for the region. The SLI is an Eskom performance measure of the unavailability of supply of the networks.

The Eskom plant performance database (NAPI) was statistically analysed in detail and a number of field investigations conducted at transformer installations that had failed in the past. Transformer earth electrode resistance measurements were taken in an attempt to identify the cause of these transformer failures. Local transformer manufacturers were consulted and a national transformer refurbishment company's database was analysed during the investigation as part of a holistic approach to the industry related dissertation.

The main finding of the NAPI data analysis was that the majority of the transformers failed during lightning storm periods. Another similar Eskom investigation had a sample of failed transformers opened for internal inspection. Signs of lightning damage to either the primary side winding or the primary lead were found.

The proposed failure hypothesis was that the transformers required additional lightning protection of the primary side to protect the transformer against lightning. It seemed that the current specification of the Eskom distribution class surge arresters was inadequate to offer sufficient lightning protection of the pole mounted transformers.

Practical measures were implemented on existing Eskom 11kV networks in the Glencoe area as part of an Eskom research project to reduce the high failure rates of transformers. Two experimental networks were established and one control network was used as a reference line. The project implementation was completed at the end of October 1999.

The experimental project looked at applying additional primary side lightning protection of the transformers. The main emphasis of the lightning protection on the first network was the use of two distribution class arresters in parallel (double arrester configuration) for each transformer and an understrung conductor connected to the prior structure back from the transformer installation. The second network had the standard single arresters installed on the transformers. A 600mm wood path was placed in series with an earthed down conductor installed on each intermediate woodpole structure to ensure a basic insulation level of 300kV for the network. The control network also had single arresters installed and was a fully insulated network (no earthed down conductor on the woodpoles).

Each network was carefully monitored in terms of equipment failures and the performance levels of each network was measured with installed voltage dip recorders near the individual network circuit breakers. The Eskom Lightning Position and Tracking System (LPATS) data was collected and analysed to quantify the lightning activity before the project implementation to that of after project implementation.

For the period November 1999 to March 2002 not a single transformer or surge arrester had failed due to lightning on the double arrester and understrung conductor configuration experimental network. There were recorded transformer and surge arrester failures on the second experimental network and on the control network. It was found that the practical methods implemented on the networks did not have a negative impact on the performance levels of the networks.

Laboratory work was conducted in the high voltage laboratory at the University of Natal, on various metal oxide varistor (MOV) blocks of opened up new and failed surge arresters. This was to determine the effect of MOV blocks in parallel under power frequency and current impulse conditions. In particular, to determine what the effect of parallel MOV blocks with different voltage-current (V-I) characteristics would have on the current sharing and energy absorption capabilities of the individual blocks. The work was performed to simulate the behaviour of two surge arresters in parallel as in the experimental project.

The experimental project lines were modeled using the Alternative Transients Program (ATP) simulation package and various parametric studies performed in the single phase conductor simulations. Each network component (such as the line, transformer and surge arrester) and phenomena (such as the effect of corona, the transient earth electrode resistance and voltage flashover) were modeled. The effect of surge arresters in parallel and the use of an understrung conductor arrangement were quantified. A current sharing factor (k-factor) was introduced to quantify the sharing of currents through surge arresters in parallel with different V-I curves.

The main finding from the impulse laboratory work was that current sharing between parallel MOV blocks became better at higher currents. This finding was supported by other research work findings, particularly in the field of nuclear fusion research with parallel arresters. The results of the ATP simulations showed that the experimental network with the parallel arresters and understrung conductor arrangement considerably reduced the energy absorbed by the individual arresters. The effect of the double arrester configuration was to reduce the energy absorbed by the individual arresters even with arresters with different V-I characteristics and different manufacturers. The understrung conductor arrangement was found to be the major contributor towards the reduction of the energy absorbed by the arresters.

The equivalent circuit of a MOV block for transient studies was proposed and then simulated in ATP. The simulated results were compared to the measured waveforms obtained from the impulse laboratory work. A good agreement between the simulated and measured waveforms was obtained.

For existing Eskom networks with high arrester and transformer failure rates, the double arrester (distribution class) configuration would be the most time and cost effective solution. The alternative of using a single station class arrester is not proposed due to the costs involved and the availability of stock. The understrung conductor arrangement did significantly reduce the energy absorbed by the arresters but due to high labour costs and time requirements this would not be recommended for existing networks. It is suggested that Eskom investigate this practical method for new lines to be built in high lightning areas.

Even with arresters from different manufacturers, the use of the double arrester configuration would decrease the energy absorbed and hence reduce the risk of failure of the individual arresters protecting the transformer. This means that Eskom field staff can use different manufacturer arresters in parallel. This would be especially for times when replacing failed arresters or a faulty transformer under breakdown conditions and electrical supply has to be restored to the customer as soon as possible. It was proposed to perform arrester matching by ensuring that the both arresters were from the same manufacturer.

TABLE OF CONTENTS

LIST OF FIGURES

LIST OF TABLES

CHAPTER 1
INTRODUCTION

1.1 Background to the Dissertation

Eskom (Electricity Supply Commission of South Africa) is the national electrical utility that provides the generation, transmission and distribution of electricity in South Africa. The majority of Eskom's electricity distribution is done with either 11kV or 22kV electrical networks. In Eskom Distribution these voltage level electrical networks are referred to as *reticulation networks* and are classified as *medium voltage (MV)* networks. These networks consist of three separate, unshielded, bare wire overhead conductors with wood pole structures and small pole mounted power transformers. These reticulation networks feed rural farm houses, other rural supplies (such as pumps and boreholes) or domestic customers living in traditional rural villages (called electrification areas). Depending on the load requirements of the customer and the existing network configuration, the pole mounted power transformer can be three phase, dual phase or single phase. The secondary or low voltage (LV) side of the transformer supplies the customers.

The three phase step down transformers used are of voltage ratios 11kV/400V or 22kV/400V. The transformers are mounted on wood pole structures and are of power ratings ranging from of 25kVA to 500kVA. The LV side normally comprises aerial bundle conductor (ABC) or underground cable leading to the customer. Each phase of the primary or MV side of the transformer is fitted with a gapless metal oxide surge arrester to protect the transformer against lightning overvoltages that occur on the networks.

Due to the low *basic insulation level (BIL)* of the reticulation lines and the absence of a shield wire due to economic reasons, the reticulation lines are vulnerable to direct lightning strikes. Without the shield wire the lightning stroke may terminate directly on one of the phase conductors resulting in large voltage surges on the network.

Refer to chapter 1.2 for the proposed transformer failure hypothesis. In high lightning density countries such as South Africa, the failure rates of surge arresters and pole mounted transformers tends to be high.

In recent years (1990 to 2000), there was a large increase in the number of reticulation networks in Eskom Distribution. This was due to the increased number of rural and electrification customers requiring electricity in their homes and the natural expansion of the distribution system due to the interconnectivity of the networks. With this increase in the number of networks came an associated increase in the number of pole mounted transformers out in the field supplying the customers.

Eskom Distribution is divided into seven operating regions. One of these regions, Eastern Region covers the Kwa-Zulu Natal area (western part of South Africa with the city of Durban as the head office) of South Africa. Refer to Appendix A for a map of South Africa. This region comprises the Natal Midlands up to the Drakensberg mountain range and the north and south coast of Kwa-Zulu Natal. The Natal Midlands and Northern Natal areas are situated in known high lightning density areas.

The Eastern Region has been experiencing a high number of pole mounted transformer failures. In the period 1994 to 1998, there has been an average transformer failure rate of 2.4% per annum as shown in Table 1.1 below. A transformer failure rate of between 0.5% and 1% per annum is regarded as more acceptable. This percentage tends to vary depending on the local lightning levels and the country of the analysis.

Table 1.1 Reticulation transformer failures in Eskom Eastern Region

Year	Installed MV capacity (MVA)	Total number of transformers	Number of failures (p.a)	% failures (p.a)
1994	1713	24094	603	2.5%
1995	1859	26332	630	2.4%
1996	2130	30834	783	2.5%
1997	2492	37150	785	2.1%
1998	2850	42 300	990	2.4%

Typical Australian transformer failures rates were between 1% and 2% per annum (Darveniza et al, 1989). An average transformer failure rate of between 0.2% to 0.8% per annum was experienced by the utility Florida Power and Light (FPL) in Florida, USA (Parrish, 1991). Florida is also in a high lightning density region similar to South Africa.

In 1998 there were 990 recorded transformer failures out of an Eastern Region transformer population of 42 300. A total of 5504 MVA hours was lost due to these transformer failures. This resulted in a calculated financial loss of between R9 million and R13 million for 1998 (Chatterton, 1999a). There are seven regions (most in high lightning areas), thus the cost of these transformer failures to the Distribution business was considerable.

The transformer data for 1999 was unavailable due to the implementation of a new performance measurement database (NEPS) in Eskom and the difficulties with querying the records in the database. In this dissertation only the transformer failure data for the period January 1994 to December 1999 were collected and analysed.

The reticulation transformer failures also affected the performance or reliability of supply of the region. Calculations showed that the transformer failures contributed an average of 5.3% per month of the overall Supply Loss Index (SLI). The SLI is an internal Eskom performance index that is a measure of unavailability of supply hours. A maximum contribution of 14.5% per month of the overall SLI was calculated for the months during the storm seasons. This was a substantial percentage of the overall SLI and was an area of concern for the business (Chatterton, 1999a).

Eskom initiated a research project during 1999. The objective of this research project was to undertake a practical and experimental study to determine the reasons for these transformer failures and implement practical methods to reduce the number of transformer failures. The project involved the establishment of an experimental program on existing Eskom reticulation networks. The purpose of the investigation was to test the effectiveness of the proposed practical solutions to attempt to reduce the transformer failures.

The practical implementation of the proposed solutions was completed at the end of October 1999. Monitoring of the equipment failures and measurement of the performance of the networks was performed. The collected project data and results for this dissertation are for the time period October 1999 to March 2002.

1.2 Failure Hypothesis and Proposed Solutions

The proposed failure hypothesis was as follows :
When the unshielded reticulation line is struck directly by lightning, the lightning current will flow along the conductors to earth. The majority of the reticulation networks are fully insulated with the line BIL of between 1MV and 2MV. The residual voltage on the line will not easily flashover due to the high pole insulation to ground. In addition, transformer installations that have a low earth electrode resistance, will act as current sinks for the lightning current.

Lightning current will then flow towards the transformer installations with low earth electrode resistances. The amount of current depends on voltage flashover and the resistance of the transformer electrode resistance. This results in a higher energy dissipation of the surge arrester. This energy dissipation may be high enough to destroy the surge arrester or for the surge arrester disconnector to blow away and prevent a permanent phase to earth fault on the network.

The transient impedance behaviour of the transformer earth electrode needs to be taken into account. If the voltage developed upon the earth electrode due to the injection of the lightning current is sufficiently large enough then the surrounding soil will ionise. This ionisation envelope increases the effective radius of the earth electrode. This results in the reduction of the earth electrode impedance. The reduction factors are in the order of 0.2 to 0.8 (Geldenhuys, 1992a).

The lightning parameters that may be responsible for high energy absorption levels leading to these transformer failures are :

- Large amplitude first stroke lightning currents (greater than 100kA to be discussed in chapter 3).
- Very fast first stroke rise times less than 1μs (Richter, 2001) and (Sakshaug, 1979).
- Very close strikes to transformer installations within a span (CIGRE, 1991).
- Long duration tail fall time currents (100-200A for a second) (Gaunt et al, 1989) and (Mata, 2000).
- Multiple lightning strokes (Darveniza et al, 1989) and (Darveniza et al, 1994).

The distribution class surge arresters are chosen to deal with energy absorption levels corresponding to induced surges. Higher energy absorption may lead to the failure of the arresters and leave the transformer unprotected. Subsequent lightning strikes subject the unprotected transformer to further overvoltages resulting in the failure of the transformer. The long term ageing effect or degradation due to power frequency voltages of the arresters is not considered as a contributor to the failures in this investigation due to the improved quality of the materials and the manufacturing process (Richter, 1999) and (Richter, 2001).

A possible solution is to provide additional lightning protection on the primary side of the transformer to adequately protect the transformer against surges conforming to the above lightning parameters. This could be achieved by the following proposed practical methods :

- Increase the energy rating of the surge arrester. This can be cost effectively achieved by installing two surge arresters in parallel. This effectively doubles the energy rating of the surge arresters.
- Create a discharge path before the surge arresters that will bypass the arresters under conditions of large lightning overvoltages.
- Lower the basic insulation level (BIL) of the line to allow multiple voltage flashovers along the line and so "dissipate" the lightning current before it reaches the arresters and causes damage.

The use of a single station class surge arrester is an alternative option but the costs and the availability of stock are disadvantages.

Three existing 11kV Eskom networks were chosen for the experimental project near the town of Glencoe in Northern Kwa-Zulu Natal. Two networks had practical methods implemented on them. A third network was used as a control or reference network.

The networks were selected on certain criteria including transformer population, line length and number of transformer failures per annum. An important factor was that the networks were similar in selection criteria and close to the town of Glencoe and nearby to each other. It was intended that similar lightning patterns would be experienced on all three networks. All three selected networks had transformer failure rates of more than 5% per annum (Chatterton, 1999b).

The following practical methods were implemented on each network :
(N/B means network breaker and is an Eskom network naming convention)
(1) Glencoe N/B 15 : An earthed down conductor was installed on every intermediate wood pole structure on the line to provide multiple discharge paths for the lightning surge. A 600mm wood path was inserted in series with the down conductor. The crossarms were bonded (electrically connected by the conductor). This provided a BIL of 300kV for the network.

(2) Glencoe N/B 13 : A double surge arrester arrangement was implemented on the line. There was an understrung conductor strung from the transformer installation to one span back to the prior structure. A 600mm wood path was created in series with the earthed down conductor on the prior structure. This structure acted as a "sparkgap" for lightning overvoltages to discharge to earth. The rest of the network was fully insulated (no wood path in series with an earthed down conductor on the intermediate structures) with a BIL of 1-2MV.

(3) Dundee N/B 18 : This was the control line and was used as a reference line for the two experimental lines. This line was not modified in any way and left in the normal operation mode. This line was fully insulated (no earthed down conductors on the intermediate structures) with a BIL of 1-2 MV.

1.3 Objectives of the Dissertation

The objective of the dissertation was to undertake experimental laboratory work and theoretical simulation studies of the proposed failure reduction methods.

Laboratory work was conducted in the high voltage laboratory at the University of Natal on various metal oxide varistor (MOV) blocks of surge arresters. This was done to determine the effect of MOV blocks in parallel under power frequency and current impulse conditions. The power frequency work looked at the voltage and current (V-I) characteristics and temperature dependence under alternating current (ac) conditions of new MOV block samples from different surge arrester manufacturers. A Fourier analysis of the harmonic content of the resistive component and capacitive component of the leakage current was performed.

This impulse experimental work was performed to simulate the behaviour of two surge arresters in parallel as implemented on the Glencoe N/B 13 network. To determine what the current sharing of arresters with different V-I characteristics would be under impulse conditions.

The experimental project networks were modelled using the Alternative Transients Program (ATP) simulation package and various parametric studies performed on the single conductor simulations. Each network component (such as the line, transformer and surge arresters) and phenomena (such as the effect of corona, transient earth electrode resistance and voltage flashover) were modelled.

The effect of surge arresters in parallel and the use of an understrung conductor arrangement was quantified. A current sharing factor (k-factor) was introduced to quantify the sharing of the lightning currents through surge arresters in parallel with different V-I curves.

The following key research questions are answered by the dissertation :

- To what extent can the transformer failures be reduced by the proposed practical methods ?

- What is the effect of the double surge arrester configuration on the energy absorbed by the individual surge arresters ?
- What is the effect of the understrung conductor on the energy absorbed by the surge arresters ?
- What is the influence of the present 300kV BIL insulation co-ordination practice in Eskom on the failure rates of pole mounted transformers ?
- What is the effect of the practical methods implemented on the performance of each experimental line ?
- What are the practical effects of mismatched surge arresters in terms of current sharing ?

1.4 Dissertation Outline

The dissertation is structured in the following way :

Chapter 2 Lightning protection of transformers research

In this chapter the history of lightning research in South Africa and other previous Eskom transformer investigations findings are summarised. The results of other similar international research work from the United States of America (USA), England, Columbia, Greece and Australia are presented. The use of surge arresters in parallel, especially in nuclear fusion applications is also discussed.

Chapter 3 Lightning interaction with networks

This chapter provides the background understanding of Eskom reticulation networks. The important topics such as the use of surge arresters and the earthing arrangement of the transformer installations in Eskom are discussed.

A brief explanation about the lightning phenomena and the return stroke is provided. The engineering parameters for lightning strokes and their application are provided.

Chapter 4 Surge arrester theory and application

This chapter provides an overview of the characteristics of metal oxide surge arresters. A proposed CIGRE equivalent circuit of the metal oxide disc is presented and the corresponding V-I characteristic curve is shown.

Typical failure modes of surge arresters such as thermal runaway, puncturing and cracking are discussed. Unique probabilistic failure curves based on energy absorption limits are presented.

Chapter 5 Transformer failure statistical analysis

This chapter provides the statistical analysis of the Eskom transformer failure data. The analysis provides important information about the cause of the pole mounted transformer failures.

From the data analysis it was clear that the failures were during lightning storm periods. The results of the initial field investigations are discussed and the random samples of transformer earth resistance measurements are presented.

Chapter 6 Experimental project and results

In this chapter the three experimental networks are discussed with accompanying photographs. The results of the three network audits and the results of the transformer earth resistance measurements are presented. An analysis of the lightning data obtained from the Eskom LPATS system is provided. The analysis of the measured performance of each network is presented.

Chapter 7 ATP modelling and simulation results

In this chapter of the dissertation, the different component models used in the ATP simulations are presented and discussed in detail. Some testing and verification of the individual models is performed.

The main focus of the individual model section is the proposed surge arrester model used in the ATP simulations. Two types of models are presented for use in the simulations; the CIGRE model and the modified IEEE arrester model. A comparison of and the results of the two models are presented.

The chapter provides the results of the many ATP simulations performed by modeling the three individual networks as used in the experimental project at Glencoe. A comparison study is performed between the three networks to determine which network configuration has the most impact of reducing the energy absorbed by the surge arresters.

Chapter 8 Laboratory work and results

This chapter contains the results of the laboratory work conducted by the author at the high voltage laboratory at the University of Natal. The purpose of the laboratory work was to conduct power frequency experiments on MOV blocks

The final component of the laboratory work consisted of impulse experiments of MOV blocks in parallel and the quantification of the current sharing between various types of manufacturer blocks. This was done to simulate the two surge arresters in parallel on the project lines out at Glencoe.

Chapter 9 Discussion

This chapter provides a summary and discussion of the results of the experimental project, the laboratory work and the ATP simulations.

Chapter 10 Conclusions

The main conclusions of the dissertation are presented.

Chapter 11 Future work

Possible future laboratory work and ATP simulation work is proposed. This additional work would expand on the findings and results presented in this dissertation.

CHAPTER 2
LIGHTNING PROTECTION OF TRANSFORMERS RESEARCH

This chapter presents a summary of the relevant history of lightning research in South Africa. The important findings from the research work conducted and the findings of various Eskom transformer failure investigations are outlined. Eskom Distribution has performed numerous investigations into the failures of pole mounted transformers. Possible solutions were recommended but not implemented on networks due to a lack of co-ordination and lack of funding. Later Eskom MV design standards did incorporate some of the proposed solutions such as mounting surge arresters directly on the transformer tank.

The findings of international transformer investigations are presented and discussed. The results of other similar research work from Australia, USA, England, Columbia and Greece are presented. The application of surge arresters in parallel as implemented in other countries is also discussed. It was found that the double surge arrester configuration was commonly used in nuclear fusion experiments.

2.1 History of Lightning Research in South Africa

The earliest mention of the influence of lightning on electrical networks in South Africa was by the author Ardendorff in a South African Institute of Electrical Engineers (SAIEE) paper presented in 1911. The major recommendations of this paper were the use of a regularly earthed shield wire, installation of arcing horn arresters and the earthing of the transformer neutrals (SAIEE, 1989).

From the period 1910 to 1930, various local South African mining groups experimented with lightning protection of their overhead and underground distribution networks. Most of the details of the experiments are unavailable due to the lack of a co-ordinated effort of the research projects (SAIEE, 1989).

From 1930 to the 1960's, small field studies were undertaken by individual Eskom distributors on their operational lines. These studies were primarily to mitigate the effects of lightning causing high network outages and equipment failure rates (SAIEE, 1989).

During the period 1951 to 1960, field studies were conducted by the Eskom Natal distributor on lightning related failures of pole mounted distribution transformers (Walter, 1960) and (Brady, 1976). The findings of the studies were :

- All transformer installations should be fitted with primary side surge arresters. The use of arcing horns was found to be inadequate for lightning protection.
- The MV surge arresters should be installed as close as possible to the transformer.
- The neutral of the transformer LV winding and the MV arrester earth should be joined in order to protect the LV winding from insulation failure.

The transformer failure rate of that time period was reduced from 7.3% per annum to between 0.7% to 1.5% per annum. It must be noted that the manufacturing quality of the transformers and surge arresters improved considerably during this time period. This resulted in a significant reduction of the number of transformer failures in the field (SAIEE, 1989).

During this period fully insulated woodpole constructions (woodpoles without earthed down leads) were introduced. The available data on the performance of these networks was inconclusive and only based on a small network sample.

The expansion of the Eskom distribution networks during the 1960's into the Rand area and Orange Free State area was accompanied by increased network outage rates during the storm periods. The majority of the causes of these outages were transformer failures and punctured porcelain pin insulators.

In 1973 the Council for Scientific and Industrial Research (CSIR) task force on lightning protection of distribution lines was established. The aim of the task force was to study the reasons for the high number of transformer and surge arrester failures and other network related equipment failures. The task force also evaluated the technical feasibility and benefits of shielded distribution lines (SAIEE, 1989).

In 1977 the CSIR and Eskom constructed a dedicated 10km long 11kV wood pole test line, 30km east of Pretoria. The test line was to be used for lightning research in South Africa. The following were studied on the NEERI line (SAIEE, 1989) and (Geldenhuys et al, 1992b) :

- Lightning induced surges
- Direct strikes and related phenomena
- Surge arrester performance
- The effect of a shield wire
- Protective relaying and fault clearance aspects
- Aerial bundle cable (ABC)

The results and findings of this important work are presented in (Gaunt et al, 1989).

As a result of the findings of the NEERI line and Eskom operational experiences, the discharge current ratings of surge arresters was increased from 5kA to 10kA in the early 1980's. The performance of metal oxide arresters was also evaluated on the test line. One of the results of the test line research was that induced voltage surges rarely exceed 300kV. This resulted in the introduction of the 300kV BIL for wood pole lines used in Eskom. The later part of the lightning research on the test line in 1987 concentrated on the refinement and optimisation of various wood pole designs (Gaunt et al, 1989) and (Geldenhuys et al, 1992b)

In 1994 a report by the South African Department of Mineral and Energy Affairs (DME, 1994), outlined the results of a two year project where performance data from overhead distribution lines was collected from throughout South Africa and analysed. The major results of the research project that are applicable to this dissertation are that :

- Lightning is the cause of approximately one third of all outages recorded.
- 2.5% of recorded outages were related to surge arrester damage.
- Attention to conductors, jumpers, conductor joints and transformers could probably improve distribution network performance.

2.2 Research into Transformer Failures

2.2.1 South African Investigations

In recent years some of the Eskom Distribution regions have conducted their own individual investigations into the causes continuing of pole mounted transformer failures.

The Eskom Southern Region (Eastern Cape area) had a transformer failure rate of about 3.3% per annum (Burger, 1998). The area is classified with a medium level lightning ground flash density. The major conclusions of the report were that :

- The transformer failures were due to insufficient lightning protection.
- Most of the failed transformers had their surge arresters mounted on the structure crossarms and not on the transformer tank.
- The surge arrester mounting leads were too long. This led to an inductive volt drop adding to the surge overvoltage and exceeding the BIL of the transformer.
- Failed transformers were to be audited (according to a provided audit sheet) before being replaced. This was to ensure that vital information about the transformer failure was recorded.

The excessive number of transformer failures in the Stella and Vryberg depots in the North West Region (Free State area) were investigated. All aspects of the 22kV networks were investigated including the method of earthing, surge arrester type and positioning, earth electrode resistance values, wood pole construction and the BIL of the line, as well as the design and manufacturing process of the transformers (Smit et al, 1993).

One interesting and beneficial aspect of this investigation was that 160 failed transformers were sent back to the manufacturers to be opened up and examined. Table 2.1 below provides a summary of the inspection findings. This was one of the first Eskom investigations in recent years that looked at the internal inspection of failed transformers in an attempt to identify the cause of the failures.

Table 2.1 Summary of failed transformer inspection findings (Smit et al, 1993)

Reason for failure	Frequency
Low oil level/bushing damage	24
No visible damage	20
MV winding fail	74
LV winding fail	4
Poor workmanship	9
MV line leads	23
Tapswitch failure	6

The data in Table 2.1 above indicated that 46% of the failed transformers had failed MV winding insulation and 14% had their line lead of the MV winding fail. The data suggested that the transformer failures were mainly MV side related. The data supported the failure dissertation that the transformer failures were mainly lightning related and that additional primary side lightning protection was required.

The transformer failures in the Eskom Central Region (Gauteng area) were investigated (Bavin, 1998). This investigation focused more on the larger power transformers found in substations. Some of the smaller pole mounted transformers were included in the investigation. No causes of the failures could be identified.

The use of single line surge arresters placed at certain points along a network to reduce the number of pole mounted transformer failures was looked at by (Van Schalkwyk, 2001). The position of the placement of the arresters is discussed in the dissertation. The added benefit of the line arresters was an improved performance of the network, especially with "rogue structures" or low insulation level structures.

The experiences and findings of transformer failures of Power Distribution Services (PDS), Rotek Engineering is presented in (Van Wyk, 1997) and (Van Wyk, 1999). PDS does most of the repair and refurbishment of Eskom's power transformers. Statistics are presented in Table 2.2 below for transformer failures of sizes less than 1 MVA.

The majority (44.4%) of the transformer failures can be attributed to internal electrical failures. Most of these failures were due to lightning and network through faults (faults not detected by the primary side circuit breaker protecting the transformer).

Table 2.2 Transformer failures in Sub-Sahara Africa < 1 MVA (Van Wyk, 1999)

Reason	1996	1997	1998	Total	Percentage
Bushing failure	132	180	190	502	3.4%
Tap changer failures	88	69	124	281	1.9%
Internal mechanical failures	1418	932	1606	3956	26.9%
Internal Electrical failures	1808	2099	2633	6540	44.4%
Age related Failures	576	721	1100	2397	16.3%
People related failures	310	52	432	794	5.4%
Externally related failures	100	62	93	255	1.7%

The transformer repair company, Revive Electrical Company in Rosherville, Gauteng was visited. The company manufactures and refurbishes transformers for Eskom and the local industry. The author collected records of over 870 failed transformers from this company and analysed the failures according to different failure groups. It was found that 97% of the failed transformers had at least one or more of their primary windings damaged (Chatterton, 2000a). This data also supported the transformer failure dissertation of this dissertation, that the transformer failures were mainly lightning related and that additional primary side lightning protection was required.

2.2.2 International Investigations

The utilities from Australia and the University of Queensland (UQ) have conducted numerous field investigations and laboratory experiments into the cause of pole mounted transformer failures.

The lightning protection of transformers was first implemented in Australia during 1965 and 1966. A major reduction in transformer failure rates was achieved by locating the surge arresters close to the MV terminals of the transformer and fitting LV arresters to the transformers (Darveniza et al, 1989).

The relocation of arresters to the transformer terminals eliminated both the distance effect and the voltage drop of the arrester leads. The installation of LV surge arresters protected the transformer from lightning surges entering the transformer from the LV side. There were occasions where damage to the LV and/or damage to the MV winding occurred. The "stepping up" action of the LV surge voltage to the MV side resulted in the MV voltage exceeding the BIL of the transformer.

Data was collected over twelve years of field experience to support these above ideas. In 1960 an Australian electric utility, the Southern Electric Authority of Queensland (SEAQ), commenced a joint investigation with the UQ. The investigation focused the causes of excessive failure rates of distribution transformers due to lightning (Darveniza et al, 1989).

Theoretical studies and experimental investigations in the laboratory were performed with detailed assessments of the field performance of SEAQ distribution transformers and surge arresters. Technical papers were published on the work performed (Darveniza et al, 1968), (Darveniza et al, 1989) and (Darveniza et al, 1999)

The most important probable causes of transformer failures identified were :

- Excessive lead lengths between the surge arresters and the MV terminals of the transformer.
- No overvoltage protection on the LV side of the transformer. Lightning surges were entering the transformers from the low voltage lines. The use of LV arresters was proposed.

A number of other laboratory testing and research areas and were looked at by UQ (Carter et al, 1976) and (Parnell et al, 1968) :

- Winding stresses due to surges entering on the MV and LV terminals.
- Statistical aspects of the impulse strength testing of transformer MV windings.
- Impulse strength testing and specification of the LV winding.
- Fault detection techniques for transformers.
- Response of surge arresters and insulation to non-standard waveshapes particularly steep fronted wave shapes typical of direct lightning strokes.

The findings of field inspections and laboratory tests of surge arresters withdrawn from service from the field are discussed in (Darveniza et al, 1999). The different failure modes due to laboratory multiphase lightning currents and high temporary voltages were discussed. Ten Australian surge arrester manufacturers participated in the research project and a total of 124 MOV arresters were tested. Roughly half of the samples were porcelain housed and half were polymer housed surge arresters. The arresters were recovered from 11kV and 22kV networks (3 wire systems, no neutral conductor).

The major findings and conclusions of (Darveniza et al, 1999) were :

- Internal inspections revealed moisture ingress through ineffective seals for the gapped metal oxide arresters. Laboratory tests showed degradation of the blocks.
- For the gapless metal oxide arresters their internal components showed the effects of power frequency fault currents which damaged the MOV blocks and their protective casings. The blocks had visible surface or near surface damage. For majority of the time the cause of the arrester failure was not obvious and unknown.
- A surprising portion of the failed arresters had been installed on line-to-cable potheads or associated with single-pole switching using disconnect links. These may have caused very high temporary overvoltages resulting in the arrester failure.
- Some of the field staff reported that the arresters had failed even when no lightning was present.
- Some of the arrester failures in the field were attributed to severe lightning. Such failures were mostly by surface or near-surface flashover of the arrester blocks.

- Information from the field suggested that MOV arresters on Single Wire Earth Return (SWER) lines are relatively vulnerable to damage by severe lightning. This was because the SWER lines are mounted on wood poles that have high impulse insulation levels and of the large spacing between the SWER transformers protected by surge arresters.

The effect of multiple lightning strikes on the surge arresters protecting the transformer was investigated in (Darveniza et al, 1991), (Darveniza et al, 1993) and (Darveniza et al, 1994). Multiple lightning strikes caused the surge arresters to experience higher energy absorption levels and resulted in thermal run away of the MOV blocks leading to failure of the arrester unit. The Eskom arrester energy rating specification takes into account the effect of multiple lightning strikes. A value of 1.2kJ/kV is suggested to allow for the multiple stroke duty (Ericksson et al, 1986b).

In 1978 the U.S. Department of Energy supported the lightning research work directed by Darveniza (University of Queensland) and Uman (University of Florida). The participating utilities in the research were Tampa Electric Company, Florida Power Corporation and Florida Power and Light Company. The view was that a new approach was required in lightning research for distribution systems. The increasing quantity of distribution equipment failure and the increasing demand of modern incentives for the development of improved lightning performance and reliability of supply of networks lead to the research work. The work was presented in (Darveniza et al, 1982) and (Darveniza et al, 1984).

The University of Florida (UF) is one of the few universities in the world conducting active lightning research. The International Centre for Lightning Research and Testing (ICLRT) is an outdoor facility occupying 100 acres of land at Camp Blanding about 45km Northeast of Gainesville, Florida. Lightning initiation from overhead clouds using the rocket-and-wire technique is used and the resulting triggered lightning studied. Triggered lightning experiments are studied and utility-based research projects are conducted at ICLRT.

The research conducted at ICLRT was sponsored by the Electric Power Research Institute (EPRI), The Federal Aviation Association (FAA) and local electrical utilities. The results of the research work performed at ICLRT are well published in numerous EPRI reports and various international Engineering and Physics journals.

Work at the ICLRT of interest and importance to Eskom Distribution includes :

- Lightning protection of distribution lines (current research focus)
- Testing of distribution MOV surge arresters
- Characteristics of lightning surges on distribution lines
- Effects of induced overvoltages on power lines
- Experiments on line surge arresters and their failure modes

The current research work at ICLRT includes :

- The effect of low level long duration currents on the energy absorbed by the surge arresters (these are characteristic initial currents of triggered lightning).
- The interaction of these low level long duration currents with the pole footing resistances.
- The effect of vertical versus horizontal line configurations on the lightning performance of a network.
- The effect of line surge arresters.

The high frequency current components of lightning flow down to ground nearest the strike point. It has still not been ascertained where the low level long duration currents flow to along the network. These low level long duration currents occur at the start of artificial triggered lightning and between flashes for natural lightning strokes (Mata, 2000). These types of lightning currents have not accurately been recorded or measured in South Africa (Gaunt et al, 1989). It must be noted that for American four wire networks, the neutral tends to be earthed at almost every pole and this results in a low network BIL. This is significantly different to the current fully insulated or 300kV BIL

From 1984 to 1990, EPRI funded tests to determine the characteristics of lightning caused voltage and current surges on distribution systems. The work tried to quantify the distribution system damage that occurred because of lightning (EPRI, 1990) and (EPRI, 1991). The work was similar to the research work conducted on the South African NEERI test line.

In 1995 and 1996, tests were performed on MOV arresters under actual triggered lightning conditions with a goal of improving lightning protection for equipment. The simultaneous arrester discharge currents and residual voltages were recorded and the energy absorption by the arresters was calculated (Mata, 2000), (EPRI, 1997) and (Fernandez et al, 1999).

Investigations were performed into the high number of transformer failures, fuse failures and lightning caused network outage rates in the St. Petersburg area of Florida Power and Light (FPL) distribution system (Parrish, 1991). Transformer failures in the Daytona Beach area of the FPL distribution were also investigated (Plummer, 1995). The proposed solutions were also to reduce the primary surge arrester lead length and the use of LV surge arresters on the transformer.

Some possible causes of transformer failures were reported as :

- Extreme lightning events such as high peak currents, very fast rise times, positive flashes and multiple stroke flashes. (Sakshaug, 1979) investigated the effect of lightning current rise times on arrester failures.
- Transformer ageing resulting in reduced insulation strength (BIL).
- Lightning surges entering from the secondary circuits or LV customer side. Refer to the relevant references below.
- Mechanical damage of the transformer winding during transportation and installation.
- Transformer core saturation from long duration lightning current or multiple stroke flashes (Darveniza, 1991).
- No overvoltage protection due to a failed arrester or blown arrester disconnector.

The entry of lightning surges at the LV terminals of the transformer and the application of LV arresters was further investigated. It was found that the low voltage surges consisted of two components; the natural frequency of the system and the inductive response of the system due to the lightning stroke current. The inductive response could be responsible for transformer failures (Goedde et al, 1991). The effect of multiple customers been supplied from the transformer and the effects of the pole grounding resistance were investigated (Dugan et al, 1988). The design of different single phase transformers and the effect of LV surges on specific transformer designs was investigated (McMillen et al, 1982).

Other countries have also investigated the lightning protection of transformers. In Norway (Huse, 1981) concluded that protection on the LV side of the transformer was needed as well as simple spark gaps on the MV side of the transformer for overvoltage protection.

In 1969 the Distribution Research panel of England set up Working Group No. 2 that dealt with the protection of distribution systems against lightning (ECR, 1973). The protection policy recommended the use of ground mounted circuit breakers, fuses, surge arresters and protective gaps for distribution systems.

Experiences from Ireland are reported in (Gallagher, 1989) where rod gaps are used to protect transformers against lightning overvoltages.

Distribution transformer failures were investigated in Columbia. CODENSA (The national Colombian utility) looked at the design, manufacturing, transportation, installation and protection of the transformers (Umana et al, 1999) and (Teorres et al, 1999). CODENSA investigated the installation of LV surge arresters on the transformer secondary. The possible implementation of line surge arresters was also discussed. The major disadvantage of this solution is the costs involved with installing line surge arresters along a network.

One interesting proposal that came out of CODENSA's work was that transformer installations should be relocated from mountain tops or high hills to lower ground and to where the ground had better soil resistivity (near rivers or dams) and better shielding from nearby trees and buildings.

Research conducted by the Public Power Corporation (PCC) of Greece indicated that the PPC had experienced an average transformer failure rate of 3.6% per annum for the period 1970 to 1990. The proposed solutions were the relocation of the MV arresters to the transformer tank and the use of LV arresters (Alexandri et al, 1998).

2.3 Use of Surge Arresters in Parallel

The use of surge arresters in parallel has been investigated by other researches from around the world.

The national utility CODENSA from Columbia did implement two surge arresters in parallel on each phase of the transformer but found that the double arrester configuration did not significantly reduce the number of transformer failures. No further explanation and information was given as to why the double arrester configuration did not work (Umana et al, 1999).

The results of using arresters in parallel from the Hokuriku Electric Power Corporation in Japan are presented in (Sugimoto et al, 1999). The intention was to use the parallel arresters to reduce the energy absorbed by the individual arresters and hence reduce the arrester failure rates. Two 2.5kA rated arresters were installed in parallel. It was found that the discharge voltages were similar for large peak lightning currents. A 2.5kA rated arrester and a 10 kA arrester were installed in parallel.

Parallel arresters have also been used in nuclear fusion experiments in Italy (De Lorenzi et al, 1987). Arresters were tested in parallel under pulsed conditions and the current sharing between the arresters quantified. A current sharing or K factor was introduced for the arrester currents. This will be discussed further in chapter 7 of the dissertation. It was found that the current sharing between arresters became better at higher currents.

Double surge arresters were also used in controlled fusion research experiments at the Los Alamos Laboratory in Mexico (Milton, 1989). The statistics of failure (using the method of incomplete failure data) and current sharing were also quantified. It was found that the double arrester arrangement provided increased reliability (low risk of failure) for the nuclear fusion related applications.

CHAPTER 3
LIGHTNING INTERACTION WITH NETWORKS

This chapter provides the background information about Eskom reticulation network. The use of surge arresters and the earthing arrangement of the transformer installations are discussed. An explanation of the lightning phenomena and the return stroke is provided. The engineering parameters for direct lightning strikes and indirect lightning strikes are discussed. These lightning parameters are important for the ATP simulations and the performance of the networks in the experimental project at Glencoe. The majority of the work is referenced from (Gaunt et al, 1989).

3.1 Insulation Co-ordination

Insulation co-ordination is the selection of the electrical strength of equipment and its application in conditions of normal and abnormal operating conditions within selected reliability margins. The normal stresses on electrical equipment include normal operating voltages and temporary overvoltages at supply frequency and overvoltages caused by switching or lightning. For a distribution system transient overvoltages caused by switching are not important as the voltage surges are below the voltage withstand levels of the equipment. Switching overvoltages are mainly caused by transformer and line switching operations on distribution networks. These voltage levels are much lower than lightning overvoltages in distribution networks (Gaunt et al, 1989) and (IEC, 1996).

In South Africa lightning is the most significant cause of surge overvoltages on the distribution networks. In Eskom Distribution the medium voltage networks of 11kV and 22kV are used extensively throughout South Africa. The preferred MV voltage level is 22kV due to the flexibility offered by this voltage at a marginal extra cost of insulation as compared to 11kV voltage level. The additional *basic insulation level (BIL)* given by the 22kV insulation level also greatly improves the general lightning performance of MV overhead lines.

The BIL of the line is defined as the "*peak value of a positive voltage surge having a 1.2/50μs waveform for which the probability of withstand is 90%*" (SCSASABE7, 2001).

Table 3.1 Rated lightning impulse withstand voltage
(Data taken from SABS 1019 and IEC 71-1)

Nominal system voltage kV rms	Highest system voltage kV rms	BIL SABS (kV)	BIL IEC (kV)
6.6	7.2	75	60
11	12	95	75
22	24	150	125
33	36	200	170

Table 3.1 above shows the rated lightning impulse withstand voltage according to SABS 1019 and the IEC 71-1 definitions (IEC, 1996). Due to the high lightning intensity in South Africa, the SABS BIL levels are higher. The South African standard takes into account the higher incidence of lightning, but some imported equipment may be rated for the IEC impulse withstand voltage. The BIL of 11kV rated transformers is 95kV and the BIL of 22kV rated transformers is 150kV.

3.2 Eskom Medium Voltage Networks

3.2.1 Reticulation Networks

The reticulation lines supply the pole mounted power transformers. The secondary or LV side of the transformer supplies the customer. The LV side normally comprises of aerial bundle conductor (ABC) or underground cable supplying the customer. Each phase of the primary or MV side of the transformer is fitted with a gapless metal oxide surge arrester to protect the transformer against temporary overvoltages (TOVs) and lightning overvoltages on the networks.

The current Eskom MV design standard does not use LV surge arresters to protect the secondary side of the transformer against lightning strikes on the LV conductor. There is a neutral surge arrester fitted between the transformer tank and the LV neutral bushing to protect the LV winding from overvoltages and insulation breakdown (SCSASABE7, 2001).

The most common transformer sizes used in the rural and electrification areas are the 25kVA, 50kVA and 100kVA transformer ratings. The 25kVA transformer size comprises roughly 50% of the population in the field. Pole mounted transformers less than 500 kVA may be mounted on a single vertical wood pole structure. Larger size transformers have to be mounted on a wooden H-pole structure. There are also single phase, dual phase and single wire earth return (SWER) transformers of 5kVA, 10kVA, 16kVA and 32 kVA power ratings used in Eskom.

The oil immersed, natural cooled distribution transformers in South Africa are built to the South African Bureau of Standards specification SABS 780. The SABS 780 specification covers constructional requirements, physical and electrical requirements, markings, sampling and methods of inspection and testing of all distribution transformers manufactured in South Africa (SABS, 1979).

The poles used for the MV structures may be either concrete or wood poles. Wood poles are predominantly used in the rural and electrification areas. Concrete poles are conductive to lightning surges and hence prone to lightning damage with the concrete splintering. The wood poles come in various lengths ranging from 5m to 18m. The standard transformer pole length used is 11m in length. The wood pole cross arms varying in lengths from 2.5m to 4.5m depending on the structure design and application. The most common type of structures used on the reticulation networks are vertical structures, staggered vertical structures, delta structures, T-frame structures and H-pole structures (SCSASABE7, 2001).

For reticulation networks, insulation co-ordination is obtained by the use of the wood itself as part of the phase-to-earth and phase-to-phase insulation of the structure. A 4mm diameter galvanised steel wire conductor and a 500mm wood path are used in series on the intermediate (no stay wires) pole structures. The 500mm wood path is placed near the top of the pole below the crossarm.

The top of the galvanised down conductor is secured by a circumferential stainless steel strapping around the pole that enhances the probability of lightning following the down conductor along the pole to earth. This prevents lightning damage such as wood splintering to the pole.

The down conductor is connected to a 1.5m copper earth spike that is inserted 500mm below the surface of the soil. The 1.5m earth spike is the most commonly used earth electrode configuration for wood poles.

On suspension type structures, the BIL of long rod insulators, BIL of the stay insulators and the position of the stay wire determines the BIL of the structure (SCSASABE7, 2001).

3.2.2 Surge Arresters

The surge arresters are fitted on the transformer tank (with the supplied brackets already installed on the transformer) in such a way that the leads between the surge arrester and the bushing and between the surge arrester and the tank are as short as possible. This is done to reduce any inductive volt drop due to the length of the conductors. The standard (NRS 039, 1995) and the Eskom specification (SCSSAAN5, 2000) provide the detailed required specifications of the surge arresters. The NRS 039 standard applies to distribution networks of voltages up to 44kV. The standard deals with the selection, testing and application of metal oxide surge arresters used to protect transformers and other electrical equipment in South Africa.

The Eskom surge arresters used are metal oxide gapless arresters. The surge arresters are connected to the earth stud of the transformer that is connected via a down conductor to the transformer earth electrode. The ratings specified by Eskom Distribution for 11kV and 22kV metal oxide surge arresters are shown in Table 3.2 below. The neutral surge arrester has a rated voltage of 6kV, MCOV of 5.1kV and a discharge current rating of 10kA.

Table 3.2 Eskom MV surge arrester specifications (SCSSCAAN5, 2000)

Specification	11kV surge arrester	22kV surge arrester
MCOV	10.2kV	19.2kV
Discharge current	10kA	10kA
Residual voltage	40kV	80kV
Energy absorption (per MCOV)	2.5kJ/kV	2.5kJ/kV

The maximum continuous overvoltage (MCOV) is the highest root mean square (r.m.s) power frequency voltage that an arrester can withstand continuously. After exposure to the specified tests as required by the relevant specifications, the surge arrester should be able to return to its normal operating temperature with this MCOV voltage rating applied continuously (NRS 039, 1995).

The residual voltage is the voltage that is maintained between the arrester terminals during the passage of a 10kA (8/20μs) discharge current (IEC 60099-4). The discharge current is the peak value of lightning current impulse that is used to classify an arrester (SABS IEC 99-4). The energy absorption capacity is the maximum amount of energy that an arrester can absorb without its thermal stability being adversely affected (SCSSCAAN5, 2000).

The distribution surge arresters are all fitted with disconnectors. The disconnector is a device that separates the earth lead from the arrester in the event of an arrester failure. This prevents a permanent earth fault on the network and loss of supply from occurring. The disconnector also provides a visible indication of a surge arrester failure (NRS 039, 1995).

3.2.3 Earthing Arrangement

The earthing arrangement for the pole mounted transformer consists of a multiple rod electrode (three point star) otherwise known as a "crows foot." The earthing lead conductor to the electrode is normally annealed stranded conductor or solid copper conductor.

The previous Eskom MV earthing standard specifies a combined MV and LV earth electrode at the transformer. The MV surge arresters, tank of the transformer and LV neutral were bonded to the combined MV and LV earth electrode. All of these transformer installations had to have their combined earth electrode resistance less than 1Ω.

The problem with this earthing arrangement is that any surge on the MV line side that causes the MV surge arresters to operate will cause the potential of the combined earth electrode to rise.

To reduce these large potential rises a low earth electrode resistance to ground was needed. In most practical situations this was not possible due to the high soil resistivities in South Africa.

A similar large potential rise will occur for any MV winding insulation failure to earth. More importantly the combined earth electrode produced a rise in the neutral voltage. This was experienced by the customer as a transfer of potential to his supply and possible equipment damage and safety risk.

The rise in potential can be avoided if the LV neutral does not share the same earth electrode as the MV surge arrester and the transformer tank. Two separate earth electrodes are used to achieve this. The MV surge arresters and the transformer tank are connected to the *MV earth electrode* and the LV neutral is connected to the *LV earth electrode*.

The current Eskom earthing standard specifies that the MV and LV earths be separated at the transformer installation. The MV and LV earths are separated by a minimum of 5m to prevent coupling between electrodes. The maximum resistance of the MV earth electrode is *30Ω*. This resistance limit is to ensure that for a MV line to transformer tank fault (SCSASAAL9, 1999) :

- No dangerous voltages are experienced on the LV neutral
- LV neutral surge arrester energy absorption limits are maintained

The LV earth resistance value of 70Ω was chosen so that the MV source substation earth fault protection will operate in the event of a breakdown between MV and LV windings of the transformer.

Figure A.1 of annex A in (NRS 016, 1995) shows a typical example of a transformer installation with separate MV and LV earthing arrangement.

The separate MV and LV earthing arrangement has its disadvantage. During a surge that causes the MV surge arresters to operate, the MV earth electrode rises in voltage while the LV earth electrode remains at ground potential.

This is neglecting the electrode coupling effect of the two electrodes. The relative rise in potential between the MV earth electrode and the LV earth electrode stresses the transformer insulation.

Two practical methods are able to prevent the transformer insulation from been stressed. One method is to over insulate the transformer but this is very expensive and the other method is to limit the differential voltage using a surge arrester connected between MV and LV earth electrodes. From a practical aspect this surge arrester is placed between the LV neutral bushing and the transformer tank.

3.3 The Lightning Phenomena

Lightning is a natural phenomenon that is usually produced in electrified cumulonimbus (thunderstorm) clouds. Electric fields are established which can lead to lightning discharges to occur within the cloud itself, between nearby clouds and between the cloud and earth. As negative charges build up in the lower part of the cloud, so the negative charges on the earth, below the cloud are repelled. Only positive charges exist on the earth directly below the cloud (Hart et al, 1979).

This electrical discharge is known as lightning. The return stroke produces the luminosity and the thunder noise commonly associated with lightning. The return stroke is a negative current flowing to ground. The return stroke acts to neutralise the charge at the base of the cloud. The lightning flash may consist of more than one stroke (Hart et al, 1979). Subsequent return strokes can also occur. These subsequent strokes carry a lower current than the first stroke but exhibit higher rate of rise of current than the first stroke.

In South Africa over 95% of the ground flashes transport negative charge to the ground in the first return stroke. The subsequent strokes have a medium time of 30ms and may be as much as 800ms. The total duration of a multiple stroke flash rarely exceeds 1 second. Fewer than 25% of lightning flashes have more than four strokes (Gaunt et al, 1989).

Figure 1 of (Gaunt et al, 1989) provides an example of a typical lightning flash. The continuous low level currents between the five successive strokes can be seen.

Return stroke modelling is of benefit as it provides a mechanism by which the return stroke currents at the ground can be determined individually or the statistical distributions of the lightning stroke currents can be obtained. The electric and magnetic fields can also be calculated to determine the lightning induced voltages appearing (Nucci et al, 1995).

There are numerous return stroke models such as the Bruce-Golde (BG) model, transmission line (TL) model, the travelling current source (TCS) model, the modified transmission line model (MTL) and the Diendorfer-Uman (DU) model. None of the above mentioned models seem to be able to reproduce the fine structure observed in the measured electric and magnetic fields (Nucci et al, 1995) and (De la Rosa et al, 1998).

In terms of this dissertation the modelling of the return stroke will not be looked at. The manner at which lightning is transferred onto the line is not important, but rather its engineering parameters and the effect of the lightning current on the transformers and surge arresters.

3.4 Lightning Performance and Parameters

3.4.1 Lightning Performance

The basic engineering characteristics of lightning have been studied by many researchers throughout the world in various different countries. Particular attention in this dissertation will be given to the research findings of work done by researchers in South Africa. Most of the lightning data and performance curves on lightning interaction on reticulation lines originate from the NEERI test line and are provided in (Gaunt et al, 1989).

Some of the more general international research work that is applicable to lightning studies in South Africa will also be discussed. The following engineering parameters are for understanding the basic principles of lightning interaction on reticulation lines and then applying them to the experimental project lines at Glencoe and the ATP simulations.

Networks need to be designed with acceptable lightning performance. The following lightning parameters are important of interest (Anderson et al, 1980) :

- Parameters of incidence
- Peak current amplitude parameters
- Impulse shape parameters

Lightning overvoltages on overhead reticulation lines can arise in two ways :

- Direct strike – the lightning strikes the conductor directly and injects current into the line resulting in an overvoltage.
- Indirect strike – the lightning strikes the ground close to the line and induces electromagnetically an overvoltage on the line.

The direct strikes to reticulation lines generally result in a high rate of voltage rise (100 to 2000 kV/μs) and high peak current values (1-200 kA). Indirect strikes produce lower rate of voltage rises (30 to 300 kV//μs) and low peak currents (less than 2kA) (CIRED, 1997).

The frequency of lightning incidence is called the ground flash density N_g and is measured by the average number of flashes to ground per square kilometre per year. This value can be obtained from recording instruments called lightning flash counters such as the CIGRE 500kHz counter (Anderson et al, 1980).

In South Africa the CSIR conducted an 11-year research project, to determine the lightning ground flash density throughout South Africa. A lightning map was produced providing different isokeraunic levels of lightning flash density in South Africa. Appendix A shows a copy of the South African lightning flash density map (Gaunt et al, 1989).

In the past where lightning flash counter measurements were not available a relationship between the ground flash density N_g and the known keraunic level T_d was established. The keraunic level T_d is defined as the number of counted thunderstorm days in a year.

In South Africa the following relationship was determined from directly measured data (Anderson et al, 1980) :

$$N_g = 0.023\ T_d^{\ 1.3} \qquad (3.1)$$

This relationship shows reasonable agreement with the trend of other collected global data. It must be noted that for larger values of T_d so the corresponding values of N_g have greater variations.

3.4.2 Direct Lightning Strikes

Almost every direct strike to an unshielded reticulation line and most direct strikes to a shielded line will cause flashover between the phase conductors and flashover to earth at the pole nearest the strike. If the lightning strikes in mid-span, the phenomenon of pre-discharge will cause currents to flow between the struck conductor and the other two conductors. The time to flashover is delayed and takes place at the nearest crossarm rather than at mid-span. The lightning current is shared between all phase conductors (Brown et al, 1976) and (Darveniza et al, 1979a).

If the insulation levels are low (less than 100kV) flashover will occur at several adjacent poles to the pole first struck by the lightning. If the insulation levels are high, 1MV to 2MV, then the line is fully insulated and flashover may take place at only one structure or not at all. In this case a large overvoltage may be transmitted to terminal equipment on the network resulting in damage.

When a conductor is struck by lightning the voltage on the conductor rises very rapidly due to the characteristic fast rise time of the lightning current. This voltage is limited by the discharge to earth. The maximum overvoltage depends on the peak current that is usually in the first stroke.

The voltages developed on the lines depend largely on the peak of the lightning current and the rate of rise of the current. Both lightning stroke current peaks and rate of rise times distributions are shown below in Figure 3.1 and Figure 3.2 respectively below.

It can be seen in Figure 3.1 that that on average the peak current amplitudes of first strokes exceed those current amplitudes of subsequent strokes. In Figure 3.2 it can be seen that on average the rate of rise of subsequent strokes are much faster than those of the first lightning strokes.

The lightning stroke current amplitude probability approximation by (Anderson, 1982) and applied in the IEEE Simplified Method (IEEE, 1985) may be used :

$$P(I) = \frac{1}{1+\left(\frac{I}{31}\right)^{2.6}} \qquad (3.2)$$

where P(I) is the probability that the current in any lightning flash will exceed peak current I
I is the peak current in kA

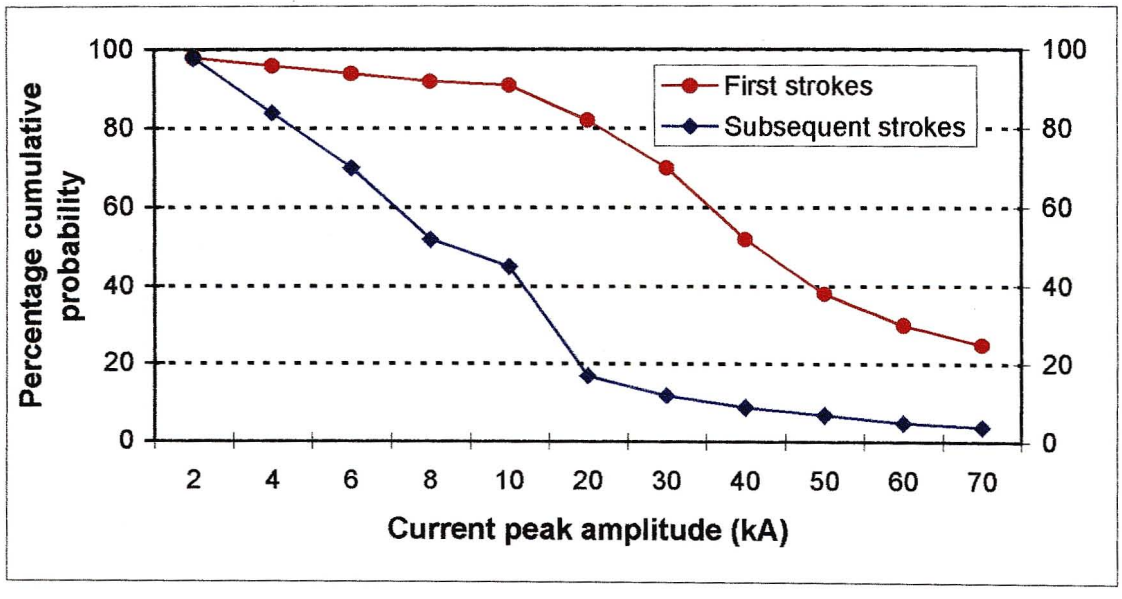

Figure 3.1 Cumulative frequency distribution of lightning current peak amplitudes representative values taken from (Gaunt et al, 1989)

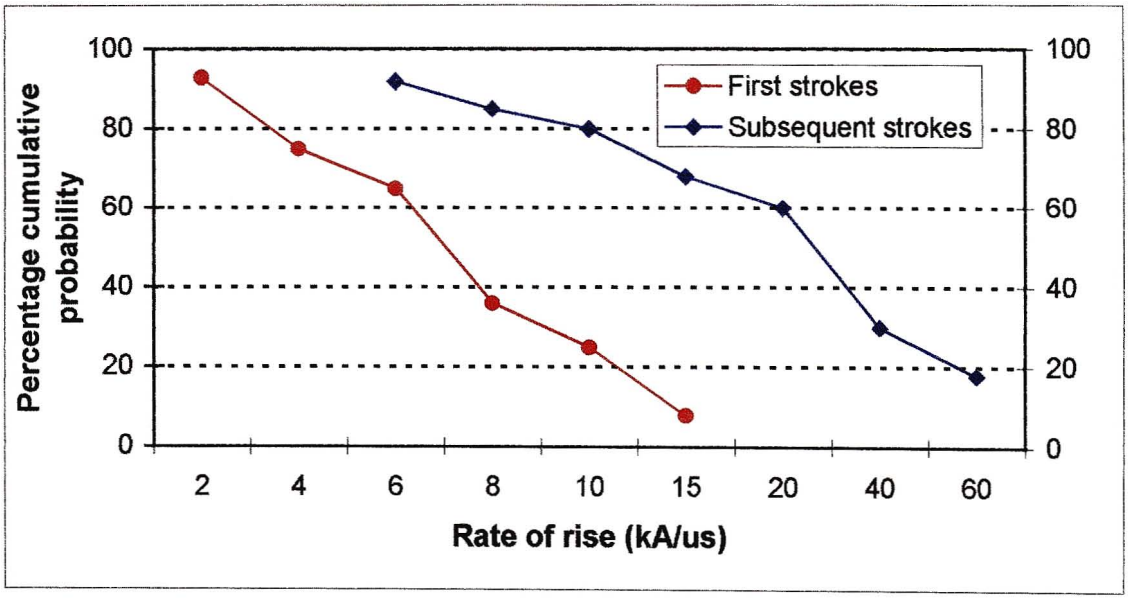

Figure 3.2 Cumulative frequency distribution of lightning current rate of rises representative values taken from (Gaunt et al, 1989)

Table 3.3 below provides the engineering parameters of the lightning first strokes. The information is important when setting protection relays and auto-reclose switchgear. Sufficient delay time should be allowed before reclosing of the network breaker is attempted. The reclose time should be at least longer than half a second and even up to two seconds long. Surge arresters should be capable of repetitive lightning discharges and reseal operations over short periods of time (Gaunt et al, 1989).

Ericksson collected a large data set on the average attractive radius of structures. The relationship below was derived in (Ericksson, 1987) :

$$R_a = 14\ H^{0.6} \qquad (3.3)$$

where R_a is the lightning attractive radius of the structure in m

H is the height of the structure above the ground in m

Table 3.3 Lightning first stroke probability parameters (Gaunt et al, 1989) and (Anderson et al, 1980)

Parameter	95%	50%	5%
Peak current (kA)	14.1	31.1	68.5
Rate of rise (kA/us) S(10/90)	1.7	5	14
Rise time (us) T(10-90)	2.2	5.6	14
Tail half times (us)	30	75	200
Number strokes per flash	1.2	2.4	10
Flash duration (us)	50	200	N/A
Inter stroke intervals	6	35	200

Using equation the (3.3), a typical 11m high reticulation line has a lightning attractive radius of 59m. This average attractive radius is larger than what one would expect of a reticulation line. Based on the formula in equation (3.3) above, the number of direct lightning strikes N_S to a line can be calculated from (Ericksson, 1986a) as follows :

$$N_S = N_g (28\ H^{0.6} + W) \times L \times 10^{-3} \qquad (3.4)$$

where Ng is the annual ground flash density

L is the line length in km

H is the average line height in m

W is the line width in m

Equation (3.4) may be simplified without significant loss of accuracy (Gaunt et al, 1989) :

$$N_S = 0.028\ N_g\ H^{0.6}\ L \qquad (3.5)$$

Equation (3.5) assumes that there is no shielding by other nearby Eskom networks, telephone lines, trees or buildings. An average shielding factor of 0.5 to 0.6 has been suggested by (Gaunt et al, 1989). For a typical reticulation network built in a high lightning area with Ng about 9 km^{-2} $yr.^{-1}$ of average line length of 50km and a structure height of 11m above ground receives 53 direct lightning strikes a year.

3.4.3 Power Frequency Arcs

When a transient overvoltage initiates an arc in air it usually develops into a power arc which is sustained by the power frequency voltage. An arc in air is characterised by a near zero arc voltage. The power arc may only be extinguished by disconnecting the supply. The wood path is used to prevent power arc follow through when a direct lightning strike does occur. The effectiveness depends on the arc current quenching properties of the wood used (Darveniza, 1980). This topic will be further discussed in chapter 7 of the dissertation.

3.4.4 Indirect Lightning Strikes

For indirect overvoltages the surge waveform comprises a relatively slow wavefront and wavetail. The waveform is typically a 5 to 10μs rise time and 20 to 40μs tail half time value (Gaunt et al, 1989).

There are many models used to calculate the magnitude of induced voltages on an open-wire line. One of the simplest and most useful for engineering applications is Rusk's equation (Rusk, 1977). The equation states that the peak induced voltage U_m is proportional to the peak lightning current I_{max} and the line height H and inversely proportional to the distance D between the lightning strike and the line. Records of lightning induced voltages on the NEERI line support this equation in principle.

$$U_m = Z_0 \cdot \frac{I_{max} \cdot H}{D} \cdot \left(1 + \frac{\beta}{\sqrt{2 - \beta^2}} \right) \qquad (3.6)$$

where Z_0 is the wave impulse impedance and can be approximated to 30Ω

I_{max} is the peak value of the lightning current in kA

H is the height of the line above ground in m

D is the distance of the lightning stroke from the line in m

β is the velocity of the return stroke as a ratio of the speed of light

Further work was done by Rusk to derive an empirical relationship for the velocity of the return stroke β and the lightning current I_0 (Ericksson et al, 1982) :

$$\beta = \left(1 + \frac{4.5\ x\ 10^5}{I_0}\right)^{-0.5} \tag{3.7}$$

The minimum distance D for an indirect lightning strike to the ground depends mainly on the height of the line H and the peak lightning current I_{max}. The greater the height and the larger the current so the greater the lateral interception distance D of the line.

For practical purposes (for average heights of reticulation lines between 5m and 15m), the following relationship can be used (CIRED, 1997) :

$$D = H + 0.27 H^{0.6} . I^{0.8} \tag{3.8}$$

For values of $D < H + 0.27\ H^{0.6}\ I^{0.8}$ results in a direct lightning strike to the line. For practical lightning scenarios in South Africa, taking average values of I_{max} = 35kA and H = 11m, the average lateral interception distance D for reticulation lines is 30.6m.

Equation (3.8) above does not take into account the effect of ground conductivity on the induced voltage on the line and assumes an ideal ground scenario. Depending on the location of the lightning stroke and the observation point along the effected line, the induced voltage may increase or decrease or produce an inversion polarity of the induced voltage (De la Rosa et al, 1998).

Recent work performed involving the shielding and coupling effect of three line conductors on the magnitude of the induced voltages showed that the magnitude of the voltages induced on each conductor was generally lower by 15% to 25% of the voltage magnitude corresponding to a single conductor. Using a shield wire generally results in 25% to 35% reduction in induced voltage magnitude (De la Rosa et al, 1998). The probability of induced overvoltages on a reticulation line can be seen in Figure 3.3 below (Gaunt et al, 1989).

As the ground stroke is usually negative, the corresponding induced overvoltage will be positive. Figure 3.3 shows that the number of induced voltage surges exceeding 100kV is approximately the same as the number of direct strikes to a line. For a line shielded from direct strikes by nearby trees or structures the induced surges will be of a higher voltage.

Figure 3.3 below shows that for a typical unshielded reticulation line 10m high, the induced voltage by indirect lightning strikes rarely exceed 250kV. The voltages are of similar waveshape and amplitude on all the phases. Flashovers between phases would not therefor be expected. The induced overvoltage is normally less than the phase to phase insulation of the conductors.

Flashovers to ground can occur at structures having an insulation level lower than the induced voltage or where reflection leads to the voltage doubling effect. Flashover of the line insulation may cause chopped voltage wave shapes with steep voltage changes.

An induced surge is not a true travelling wave. The induced surge is an injection of energy along the line. The amplitude attenuation of induced voltages are low. Structures with low insulation strength to ground (less than 100kV) may cause flashover for surges several kilometres away. Flashover of one phase reduces the induced voltages on the other phases (Gaunt et al, 1989).

A 300kV BIL for a network can reduce the number of flashovers due to indirect induced overvoltages. A theoretical analysis and statistical Monte Carlo simulation was performed by (Geldenhuys, 1984). The work conducted predicted that the magnitude of induced overvoltages was not directly proportional to the line height. The magnitude was found to be less sensitive to the line height at higher values of induced overvoltages.

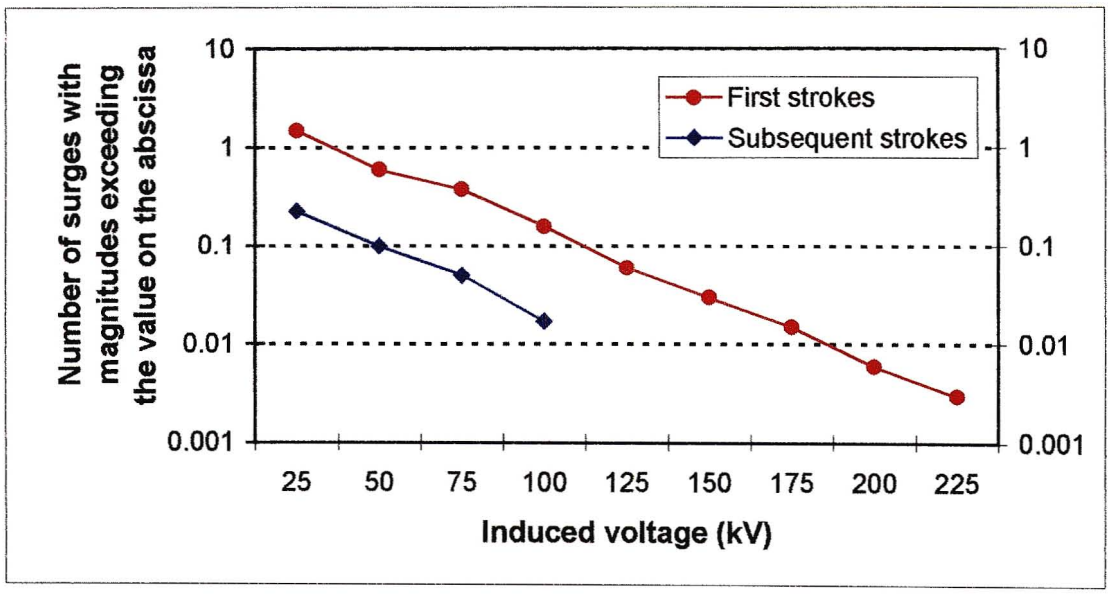

Figure 3.3 Incidence and magnitude of induced overvoltages produced on open NEERI test line representative values taken from (Gaunt et al, 1989)

This resulted in an increase in the number of direct strikes to a line that would otherwise have been responsible for inducing overvoltages on the line. This meant a decreasing insulation level was needed for decreasing tower heights.

As the withstand level is increased to 1 to 2 MV level of a fully insulated wood pole, the number of structures flashing over due to direct strikes decreases and the discharge current at each flashover increases. The impulse withstand level selected is a compromise between limiting flashover caused by direct strikes and limiting the effects of flashover caused by indirect strikes. From the findings of the work done by Eskom and the CSIR on the NEERI test line, a BIL of 300kV provided the best overall performance. A BIL of 300kV is maintained between all phases and between the phases and ground. The 300kV BIL limits the stresses on the surge arresters while avoiding line flashovers due to induced voltage surges (Gaunt et al, 1989).

CHAPTER 4
SURGE ARRESTER THEORY AND APPLICATION

The preceding chapter discussed the important engineering parameters of lightning and the effects of lightning on reticulation networks. This chapter provides an overview of the characteristics of metal oxide surge arresters used to protect equipment against overvoltages. An equivalent CIGRE proposed circuit of the metal oxide disc is presented and the corresponding V-I characteristic curve is shown. Typical failure modes of surge arresters such as thermal runaway, puncturing and cracking are discussed. A unique probability of failure curve for an 11kV of arrester in terms of the energy absorption limits are presented.

4.1 Background

Gapless metal oxide (MO) surge arresters comprising of ZnO blocks were first introduced in the USA in 1977. These arresters were used as station class arresters for the larger voltage networks but were later applied to the lower voltages in the distribution class arresters (Hileman, 1999). MO arresters have been used in South Africa for the past twenty-two years or so. Insulating materials such as silicone rubber and other polymeric insulating materials such as ethylene-propylene-diene monomer (EPDM) are now used for the surge arrester housing.

The new type MO arresters have numerous advantages over the old SiC type arresters (Hileman, 1999) :

- They are far less complex in design than SiC arresters. This improves the overall quality and decreases the chance of moisture ingress.
- Reduced peak voltage applied to the transformer during surge conditions.
- The MO arresters have low leakage currents.
- MO arresters have good energy dissipation characteristics.

The major disadvantage of a gapless MO arrester is that the power frequency voltage is continually resident across the arrester and produces a leakage current of about 1mA. This low magnitude leakage current is not detrimental but with higher leakage currents, due to temporary overvoltages (TOVs) or lightning overvoltages, can produce heating of the arrester. If the overvoltages are sufficiently large enough or long in duration, then the temperature may increase sufficiently so that thermal runaway and eventual failure of the arrester may occur (Hileman, 1999).

4.2 ZnO Material Characteristics

The ZnO blocks (also called "varistors") make up the MO arrester. The ZnO material used in the varistor blocks or discs is a ceramic comprising of a mixture of mostly ZnO (about 95% mol) and the rest of the constituents typically made up mainly from Bi_2O_3, Sb_2O_3 and Co_2O_3. The exact mixture of constituents and sintering process used influence the electrical properties of the resultant ZnO material. The mixture is dried, pressed into discs and finally sintered (Olsson, 1989). The ZnO grains (about 10μm diameter) have a low resistivity and are surrounded by a granular layer which is a highly resistive oxide (about 0.1μm thick) (Schei et al, 1990).

The MO disc can be represented by an equivalent circuit as shown in Figure 4.1 below. Ri represents the non-linear resistance of the granular layers. The resistivity of Ri changes from 10^8 Ω.m for a low electric field stress to about 0.01 Ω.m for a high electric field stress (Schei et al, 1990).

C represents the granular layer and has a dielectric constant of between 500 and 1200 depending on the manufacturing process used. In principle the capacitance of the disc is voltage and temperature dependent. Rz is the resistance of the ZnO grains with a resistivity of about 0.01 Ω.m. L represents the inductance of the MO disc and is determined by the geometry of the current flow path (Schei et al, 1990).

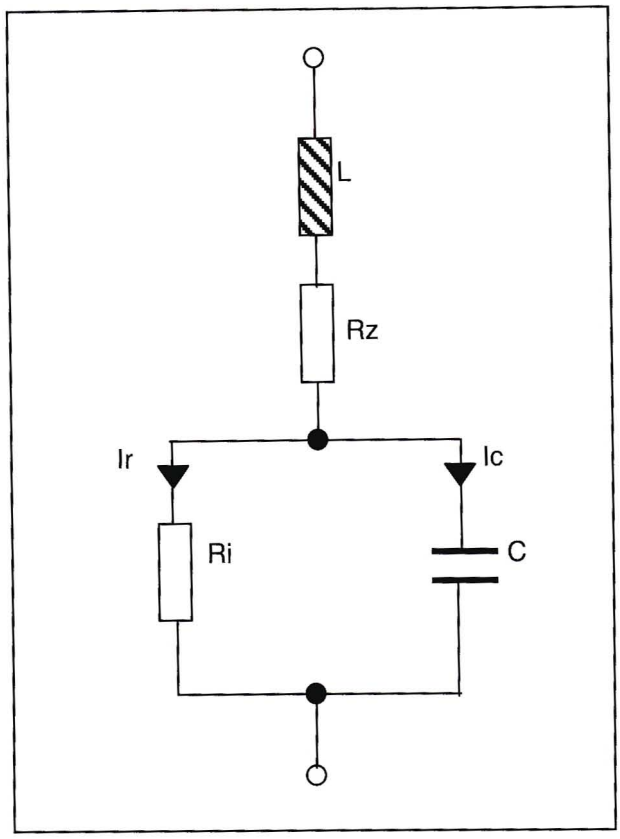

Figure 4.1 Equivalent circuit of a metal oxide disc taken from (Schei et al, 1990)

The basic non-linear voltage-current (V-I) relationship of MO disc is illustrated in Figure 4.2 below. The resistive current component Ir and the capacitive current component Ic of the total current through the MO disc are shown. Using the equivalent circuit in Figure 4.1 the characteristics of the current can be divided into three operating regions (Schei et al, 1990) and (Hileman, 1999) :

- Low electric field region (Region 1) : The conduction mechanism in this region can be explained by means of energy barriers in the granular layer. These barriers prevent electrons from moving from one grain to another. The typical Schottky emission effect (as found in semiconductor devices) is active in this region. This region is the alternating current (ac) region with typical leakage currents of less than 1mA. The disc behaves as a capacitor in this region and the current is predominantly capacitive. The resistive current component Ir in Region 1 depends on the granular layer and is heavily influenced by the manufacturers material used and the production techniques. The maximum continuous operating voltage (MCOV) of the arrester MCOV, is chosen in Region 1.

- Medium electric field region (Region 2) : This region is also referred to as the transition region. The electrons can move through the barriers by the tunnel effect. This is the TOV and switching surge operation region. The current is predominantly resistive current and ranges from about 1mA to 2kA.

- High electric field region (Region 3) : The volt drop across the resistance Rz of the ZnO grains dominates in this region. This is the lightning operation region for which very large discharge currents 2kA to 100kA occur.

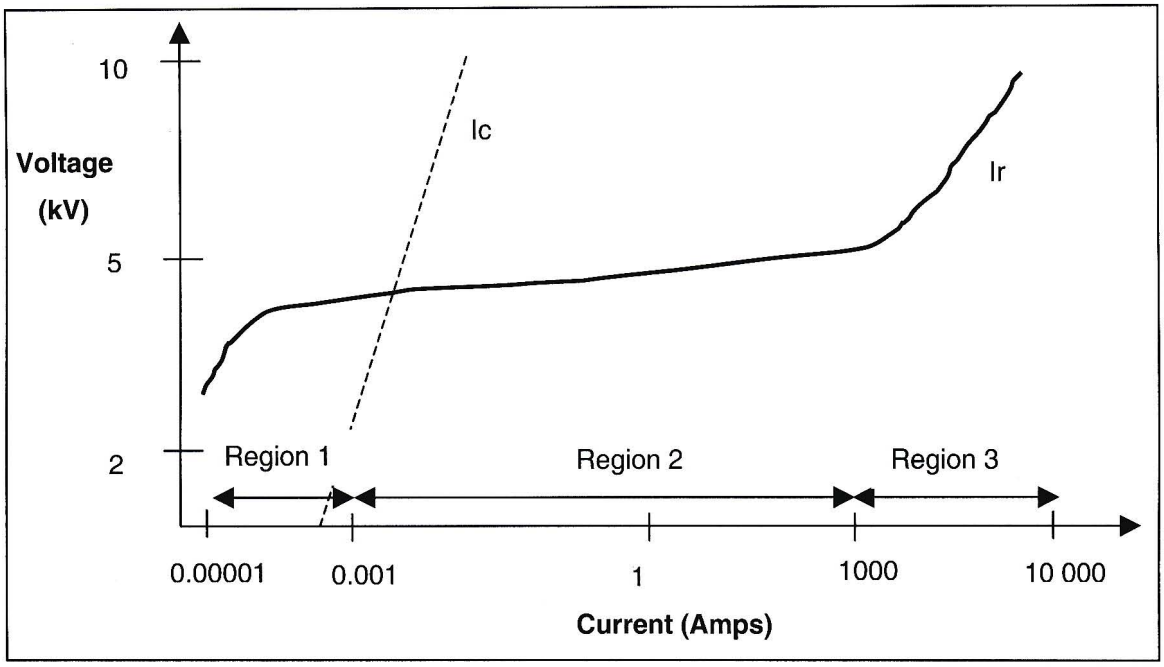

Figure 4.2 Representative typical V-I characteristic of metal oxide disc (taken from Schei et al, 1990)

The laboratory work conducted as part of this thesis looked at the effect of lightning currents on the V-I characteristic in Region 1 and Region 2. The ATP simulations looked at the current sharing between parallel arresters in Region 3.

An extensive discussion about the various different equivalent circuits that can be used to represent MO blocks for different applications is presented in (Van der Linde, 1999) and (Haddad et al, 1990). The different equivalent circuits could be frequency dependent or specifically applicable to alternating or direct current modelling.

An in depth discussion about the protection performance of MO arresters is provided by (Hileman et al, 1990). The protection characteristics of the arrester are determined by the voltage-current characteristic in Region 2 and Region 3. In these two regions the influences of temperature and capacitances have disappeared and the deviation from the linear voltage distribution along the arrester is only determined by the dispersion of the resistive V-I characteristic.

The following are important properties of ZnO blocks relevant to this dissertation are (Van der Linde, 1999) :

- The phenomenon of conduction in the transition region.
- The temperature dependence of conduction in the ohmic region as opposed to the temperature independence in the highly non-linear region.
- The temperature independence of the conduction in the transition region.
- The capacitance change in the transition region.

4.3 Failure Modes of Surge Arresters

The three main modes of surge arrester failures are thermal runaway, puncturing and cracking. The leakage current and consequently the joule heating of the MO arresters increases with temperature. If the temperature is raised above the thermal stability temperature, then the power input may exceed the heat dissipation and therefor thermal runway occurs of the metal oxide blocks (Tominaga et al, 1980) and (Bartkowiak et al, 1999).

Surge arresters can fail due to (Akbar et al, 1998) and (Bartkowiak et al, 1999) :

- Degradation of the ZnO blocks under continuous ac stress over time until the leakage power exceeds the thermal capacity of the arrester.
- Degradation of the blocks under continuous ac stress to the point where the ZnO blocks are heated so that they fail to recover from transient flow of charge.
- Thermal failure due to lightning (multiple strikes or long duration) or switching overvoltages.
- Radial electrical stresses within the arrester housing leading to failure of the block surface insulation.

- Extreme ambient conditions.
- Moisture ingress leading to internal discharges and possibly leading to internal flashovers.
- External contamination leading to surface discharges and possibly flashover.

One method to determine the condition of a surge arrester is to remove the arrester from service and compare its performance in a laboratory to the standards that the arrester should comply. An alternative method is on line monitoring of the ac characteristics and tracking the V-I characteristic changes. A harmonic analysis is performed on the resistive current component. This is further discussed and expanded on in chapter 8.3.

In terms of this dissertation lightning currents (as discussed in chapter 1) are considered as the major cause of the surge arrester failures. Lightning currents cause the following effects on MO blocks (Darveniza et al, 1993) :

- Changes to the V-I characteristic changes. Small changes in the characteristic are normal for 8/20μs currents magnitudes up to the rated discharge currents.
- Breakdown by internal puncture or external flashover of the MO block. This should not happen for 8/20μs currents up to twice the rated discharge current and should not happen for the high current withstand test of 4/10μs impulses of 100kA for 10kA rated arresters.
- Temperature rise of the MO block and heat transfer to other internal components.

The above three effects are not independent and are caused by a combination of current, voltage and thermal stresses on the block.

There have been numerous studies and laboratory work conducted by (Darveniza et al, 1991), (Darveniza et al, 1993) and (Darveniza et al, 1994) on the failure of surge arresters due to multiple lightning strikes. About 45% of typical lightning flashes have 3 or more strokes in a flash and about 20% of all flashes consist of more than 6 strokes. The time intervals between strokes have a median value of 35ms and may be as high as 200ms (Anderson et al, 1980). Table 3.3 provided the relevant engineering parameters of lightning.

These multiple flashes are vastly different to the testing of surge arresters by using impulse tests with either 1.2/50μs voltages or 8/20μs currents. Laboratory impulse generators use capacitors that are charged in parallel and then discharged in series to produce an impulse voltage or in parallel to produce an impulse current. Normally a single impulse is generated and then the capacitors have to be recharged. This recharging process takes about a minute. This time is much longer than the median inter stroke time of 35ms.

The IEC 99-4 standard has a conditioning test that comprises twenty 8/20μs impulses of nominal 10kA current and two 4/10μs high current impulses of 100kA magnitude. The nominal current impulses provide negligible energy while the high current impulses represent a considerable energy stress (Stenstrom et al, 1999).

4.4 Energy Absorption of Surge Arresters

It was reported that the residual voltage across an arrester could be normalised to the arrester power frequency voltage rating and plotted against the discharge current (Geldenhuys et al, 1986). The arrester discharge curves for arresters rated at 3kV to 24kV with a 10kA discharge current rating were found to coincide. Surge arresters of different sizes and different manufacturers can be described by equation (4.1) below which is valid for the 1kA to 65kA current range.

$$\frac{V}{V_{rms}} = 2.5\, I_0^{\alpha} \qquad (4.1)$$

where V is the residual voltage across the arrester in kV

V_{rms} is the nominal arrester power frequency voltage rating in kV

I_0 is the peak arrester discharge current in kA

α is the exponent of non-linearity ($0.1 \leq \alpha \leq 0.25$)

The current discharge rating of a surge arrester determines its energy absorption capability. If the current discharge rating is too low then an unacceptably high arrester failure rate may occur.

The price of an arrester is roughly proportional to the energy rating. The magnitudes of the arrester discharge currents were measured on the NEERI test line.

The energy E per arrester rating in Joules per kV could be calculated with the following equation (Geldenhuys et al, 1986) :

$$E = \left(\frac{3.6\tau}{1+\alpha} \cdot I_0^{1+\alpha} \right) \qquad (4.2)$$

where τ is the time to 50% of current peak in μs

α is the exponent of non-linearity ($0.1 \leq \alpha \leq 0.25$)

I_0 is the peak arrester discharge current in kA

The assumptions made for equation (4.2) are that the lightning current rises instantly to a peak value and then decays exponentially. It can be seen that the energy dissipated in the arrester is directly proportional to the arrester voltage rating. Data recorded from the NEERI test line provided an average energy absorption of 1.7kJ/kV by using equation (4.2) (Geldenhuys et al, 1986).

An equation based on equation (4.2) to calculate the energy absorbed W_a by a 12kV rated surge arrester is provided by (Ericksson et al, 1986b) :

$$W_a = 0.2\, I_a \qquad (4.3)$$

where W_a is the energy absorbed by the arrester in kJ

I_a is the peak current discharged kA

From (Ericksson et al, 1986b) it was noted that the observations made from experiments on the NEERI test line indicated that the current sharing of the three arresters protecting the transformer was not equal. It was found that about two thirds of the current was flowing through one arrester, about thirty percent through the second arrester and 5% of the current through the third arrester. A similar discussion about the probability of flashover between conductors and the amount of current sharing between arresters was presented in (Schei et al, 1978).

The curves provided in (Ericksson et al, 1986b) provided curves that indicated that an arrester discharge current of 20kA is equivalent to a 210-year return period (for Ng = 1 km^{-2}) and an arrester discharge current of 10kA was equivalent to a 65-year return period (for Ng = 1 km^{-2}).

Measured discharge currents from the NEERI test line showed that 10kA rated arresters had a failure rate of 1.5% per annum and 20kA rated arresters had a failure rate of 0.45% per annum. The assumption made was that a surge arrester would fail if the lightning peak current through the arrester exceeds the rated discharge current. The failure rate of 20kA rated surge arresters was less than 10kA rated arresters by a factor of less than three (Gaunt et al, 1989).

Information about the energy absorption limits in J/cm^3 of MO blocks used in station class arresters is provided in (Ringler et al, 1997). A time-to-failure curve obtained from testing the arresters to destruction was presented. It was found that there was a linear dependence between the logarithm of the mean time-to-failure and the logarithm of the mean MO block current.

Investigations were performed to determine the probabilistic energy rating of surge arresters (Martinez et al, 1997). The authors produced plots of discharge current as a function of energy capability for failure probabilities ranging from 0% to 50%. It was found that the standard deviation averages were about 13% and the zero probability of failure point was about 4 standard deviations below the mean. From this, it was concluded that the energy capability of surge arresters was probabilistic.

A Weibull cumulative distribution function may be used to model the energy characteristic of the surge arrester and setting the discharge energy for the standard tests at the mean minus 4 standard deviations, then probability of failure P_{FA} may be stated written as (Hileman, 1999) :

$$P_{FA}=1-0.5^{\left(\left(\frac{Z}{4}+1\right)^5\right)} \qquad (4.4)$$

The function Z can be written as

$$Z = \frac{W_c/W_R - 2.5}{0.375} \qquad (4.5)$$

where W_c is the energy capability for a probability of failure P_{FA}

W_R is the rated energy capability as specified by the manufacturer

Equation (4.5) assumes a standard deviation of 15% of the mean. Substituting equation (4.5) into equation (4.4) provides a typical probability curve of a surge arrester failing as shown in Figure 4.3 below.

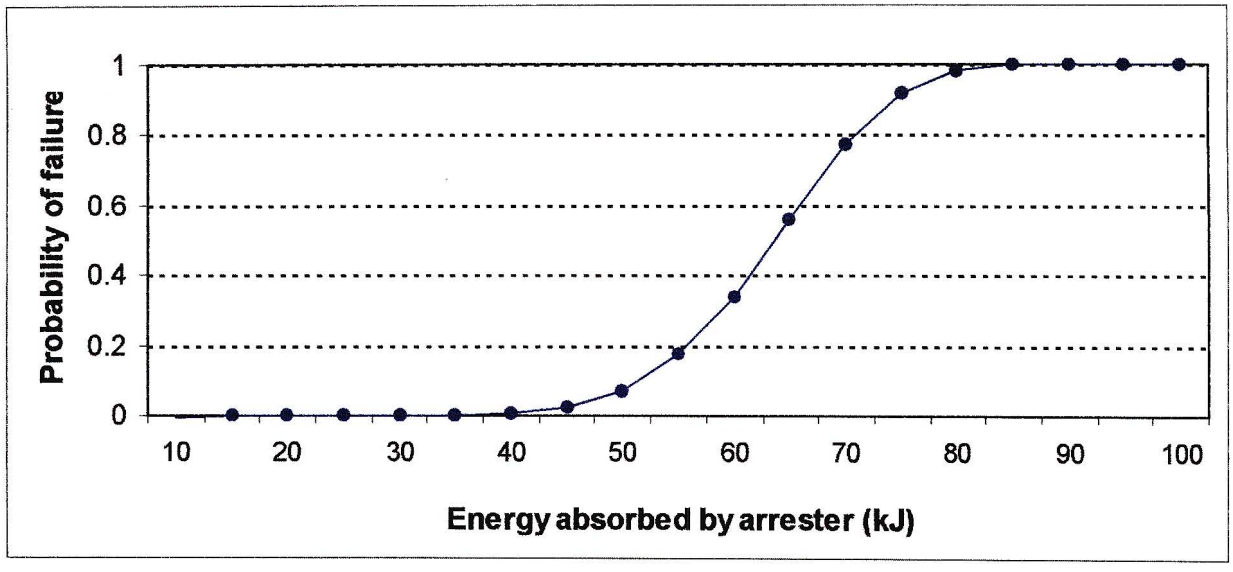

Figure 4.3 Energy probability of failure characteristic for an 11kV arrester modified from (Hileman, 1999)

The above curve in Figure 4.3 was modified from the curve in (Hileman, 1999). The author has plotted the energy probability of failure curve for an 11kV distribution class surge arrester. The Eskom distribution surge arresters are specified at 2.5kJ/kV (MCOV). The MCOV rating for an 11kV arrester is 10.2kV. This provides an energy capability of 25.5kJ for the arrester.

From Figure 4.3 above it can be seen that the energy absorption limit of 25.5kJ corresponds to almost a zero probability of failure. A 50% probability of failure corresponds to an energy absorption of 64kJ.

This was 2.5 times the rated energy rating of the surge arrester. It was proposed that the maximum energy that can be absorbed by an arrester was 4kJ/kV (rated voltage) (Greenwood, 1991). This provided an energy absorption limit of 48kJ for Eskom rated 12kV surge arresters. An energy level of 48kJ corresponds to a probability of failure of approximately 5%.

A point of reference was provided in (McDermott et al, 1994) that the simulated energy of a 100kA (4/10μs) test impulse was 4.7kJ per kV of MCOV rating. For an 11kV surge arrester this would be an energy absorption of 47.9kJ.

The probabilistic current capability has not been studied by researches. In the high current test, the arrester is required to withstand a 100kA 4/10μs current impulse. The current probabilistic capability may be simply stated as 100kA with zero probability of failure (Hileman, 1999).

4.5 Conclusions

An equivalent CIGRE proposed circuit of the metal oxide disc was presented and the corresponding V-I characteristic curve shown and discussed. The typical failure modes of surge arresters was discussed. A unique probability of failure curve for an 11kV of arrester in terms of the energy absorption limits was presented. For 11kV arresters as used in the experimental project, it was found that the energy absorption rating of 25.5kJ corresponded to almost a zero probability of failure. A 50% probability of failure for the 11kV arresters corresponded to an energy absorption level of 64kJ. This was 2.5 times greater than the rated energy level of the surge arrester. The current probabilistic capability could be simply stated as 100kA with a zero probability of failure. This current probabilistic capability was based on the required arrester high current test results.

CHAPTER 5
TRANSFORMER FAILURE STATISTICAL ANALYSIS

This chapter provides the statistical analysis of the transformer failure data. The analysis provides important information about the reason for the pole mounted transformer failures. From the data analysis performed it was clear that the failures were during the lightning storm periods. The results of the initial field investigations are discussed and the random samples of transformer earth resistance measurements are presented. A summary of the results of the network audits is discussed.

5.1 Transformer Failure Statistics

The Eskom Distribution Network Availability Performance Index (NAPI) database for the period of January 1994 to December 1998 was statistically analysed in detail (Chatterton, 1999b). The statistics presented below are a summary of the important statistical results from the comprehensive analysis conducted. The transformer data for 1999 was unavailable due to the implementation of a new performance measuring software program (NEPS) and difficulties with querying the records in the database in Eskom Distribution. For this dissertation only the transformer failure data for the period January 1994 to December 1998 was collected for the background investigation.

These presented results were used as part of the breakdown statistical analysis during the background investigation stage of the research project. The data analysis of the transformer failures grouped the failed transformers according to common failure factors. Factors such as location of transformer failure; reasons for the failure; make of the failed transformer; month and time of when the transformer failure occurred and the transformer's operating voltage.

The data analysis showed that the transformer failure in numbers was equal for the two operating voltages of 11kV and 22kV. The different BIL ratings of the transformers did not seem to have an effect on the failure rate.

The data summarised in Table 5.1 below indicated that 65% of all transformer failures could be attributed to lightning storm activity. In South Africa the most active lightning storm period is from October through to March the next year.

A large proportion of transformer failures were due to "unknown" reasons. These failures were classified as "unknown" because no identifiable cause of the failures could be seen by the Field Service staff. The reason for the failure was highly subjective and depended on the quality of information supplied by the Field Service staff. It must be noted that most unknown failures were attributed to lightning even if a storm was not visibly nearby.

Table 5.1 Reasons for transformer failures in the Eastern Region

Year	**1994**	**1995**	**1996**	**1997**	**1998**	**Total**
Storm/ Lightning	366	392	497	524	607	**2386**
Electrical	12	9	32	17	14	**84**
Mechanical	7	10	21	8	8	**54**
Human	3	3	9	4	3	**22**
Nature	3	3	9	4	3	**22**
Animals	4	2	16	19	12	**53**
Unknown	198	202	181	198	300	**1079**

It was suspected that most of the "unknown" component transformer failures could be attributed to lightning storms. This was confirmed in further statistical analysis of the data. The unknown failures were grouped according to month of failure and time of failure. An important finding was that the unknown failure component was not random and over 60% of all the unknown failures correlated strongly with periods of known lightning activity in Kwa-Zulu Natal (Chatterton, 1999b.

Figure 5.1 below shows the transformer failure trend per month. The seasonal trend peaks around the lightning storm months of December and January can be clearly seen. It can also be seen that the number of transformer failures was increasing as the installed population in the field increased each year due to load growth.

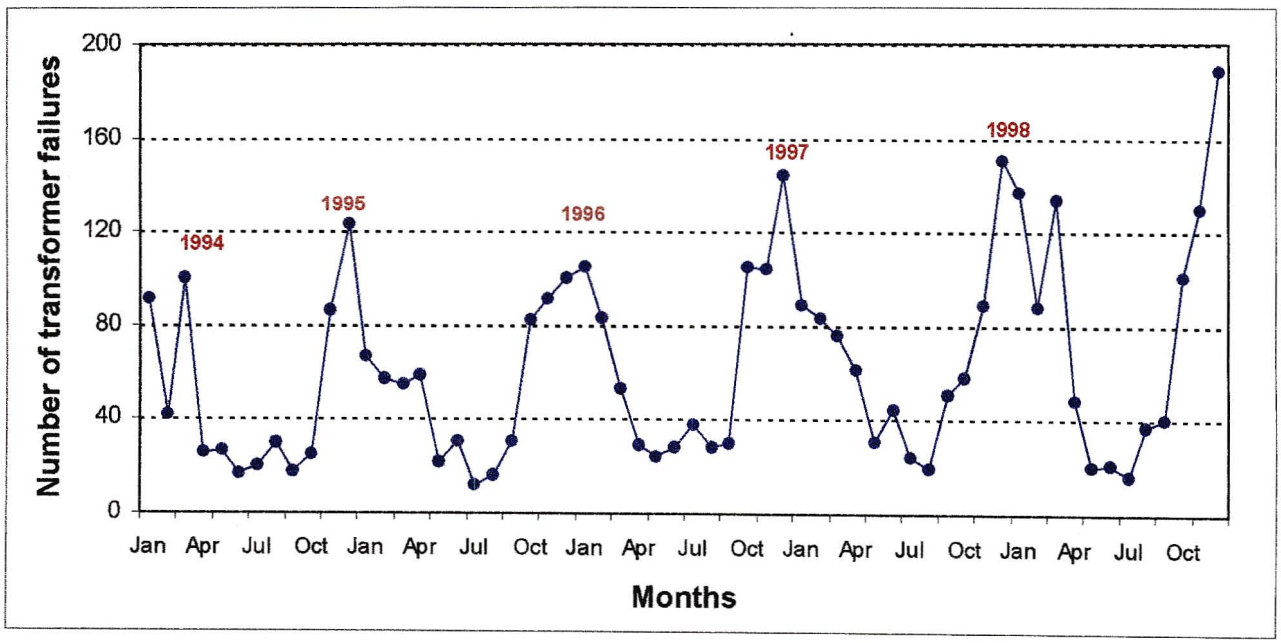

Figure 5.1 Transformer failure trend per month (1994 to 1988)

In Figure 5.2 below it can be seen that most of the transformer failures occurred between the months from October to March. This period comprised 76% of the total number of transformer failures and correlated with the lightning storm season in Kwa-Zulu Natal. For the period May to September, the number of transformer failures decreased as this period was during the autumn and winter seasons and lightning activity was at a minimum.

The NAPI data was grouped into various time periods in which the transformers were reported as having failed. The time periods were categorised as follows :

- Morning : 5h00 to 9h00
- Late morning : 9h00 to 11h00

- Afternoon : 11h00 to 15h00
- Evening : 15h00 to 20h00
- Night : 20h00 to 5h00

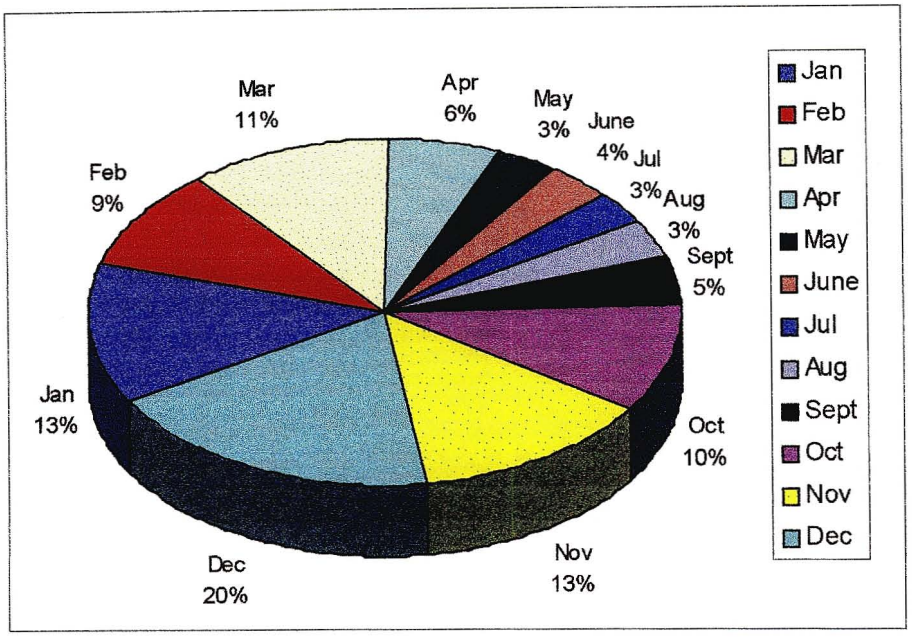

Figure 5.2 Transformer failures grouped per month

Most of the transformer failures occurred during the classified "evening" period from 3:00pm in the afternoon to 8:00pm at night. This evening period as can be seen in Figure 5.3 below, was also when most of the lightning storms occur in Kwa-Zulu Natal. From the above data analysis results it was clear that the transformer failures were occurring during lightning storm periods.

The impact of the transformer failures on the performance of the Distribution business was also analysed. In 1998 there were 990 recorded transformer failures out of an eastern region transformer population of 42 300. A total of 5504 MVA hours was lost due to these transformer failures. This resulted in a calculated loss of between R9 million and R13 million for 1998 (Chatterton, 1999a).

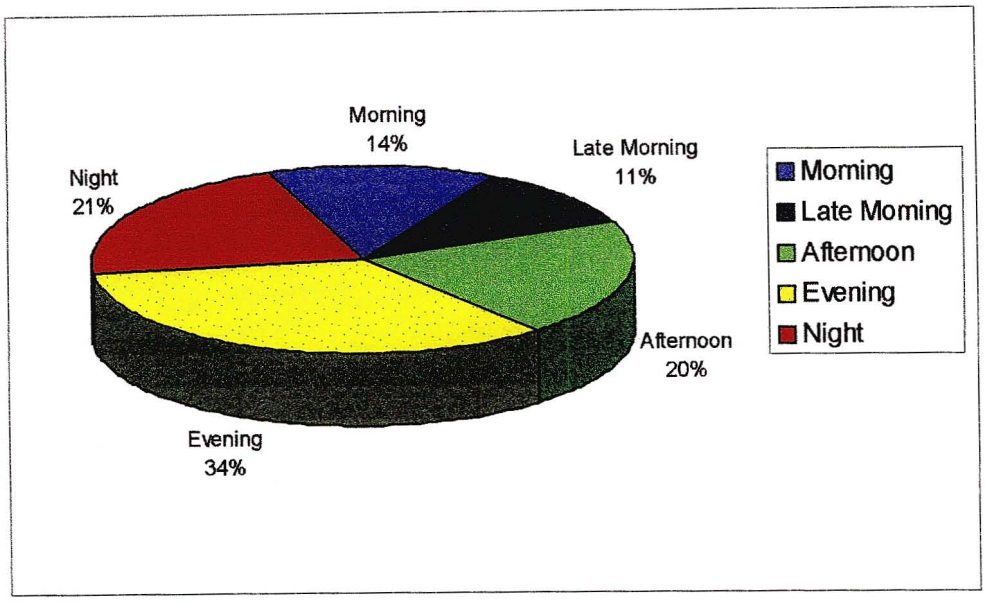

Figure 5.3 Transformer failures grouped per time

Distribution consists of seven regions (most of the regions are in high lightning areas), so the cost of these transformer failures was considerable to the business. It was found that the transformer failures also effected the performance or reliability of supply of the region. It was calculated that the transformer failures contributed an average of 5.3% per month of the overall Supply Loss Index (SLI). The SLI is an internal Eskom performance index that is a measure of unavailability of supply hours. A maximum contribution of 14.5% per month of the overall SLI was calculated for certain months during the storm season (Chatterton, 1999a). This was a substantial percentage of the overall SLI and was an area of concern for the business.

5.2 Initial Field Investigation Results

An initial investigation was conducted by the author to find the cause of the transformer failures. This consisted of field work and transformer earth resistance measurements.

5.2.1 Glencoe Data Analysis

From the data analysis it was found that the Newcastle Field Service Area (FSA) had the highest number of transformer failures per annum. This is shown in Figure 5.4 below. The Newcastle FSA is one of the four FSA's of Eastern Region. It was decided to analyse the Newcastle FSA transformer data in detail. It was calculated that the Newcastle FSA had an average transformer failure rate of 3.8% per annum. All the transformer failures for the Newcastle FSA were grouped according to Technical Service Centre (TSC) concerned. The TSC is an area of the FSA that is responsible for the maintenance and repair of the particular networks situated in that area. The Newcastle area comprises of ten TSCs.

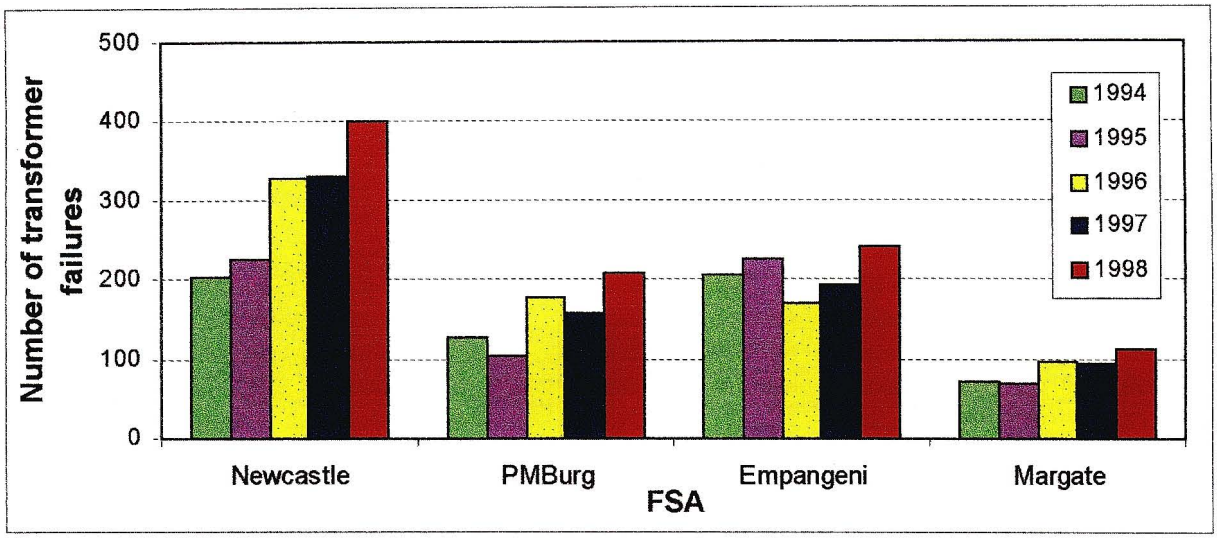

Figure 5.4 Transformer failures in each FSA of Eastern Region

It was found that the Glencoe TSC experienced the highest number of transformer failures in the Newcastle FSA. Glencoe TSC also experienced the highest transformer failure percentage i.e. the failures were normalised for the number of installed transformers.

The transformer failure data for Glencoe TSC was then analysed for each network in the TSC and the highest failure reticulation networks were then identified. Failure rates of up to 18.2% per annum were obtained for certain networks in the area. This was notably for networks in the Glencoe town area. The Glencoe area was known to historically have very frequent and severe lightning storms.

Data from the Eskom Lightning Position and Tracking System (LPATS) was collected and analysed. The lightning ground flash density around the Glencoe TSC area was found to be around 8 to 11 flashes per km^2 per year.

The woodpole lines studied were fully insulated with a BIL of 1MV to 2MV. Most of the networks in the Newcastle area were older than 25 years and built to the old Eskom construction standard with no earthed down conductor for insulation purposes.

5.2.2 Transformer Earth Electrode Resistance Measurements

The networks with high transformer failure rates in Glencoe TSC were identified and randomly chosen networks with low transformer failure rates were also selected. Multiple transformer failure installations were investigated. These were installations that had experienced two or more transformer failures since 1994. These networks were identified from the breakdown process described above.

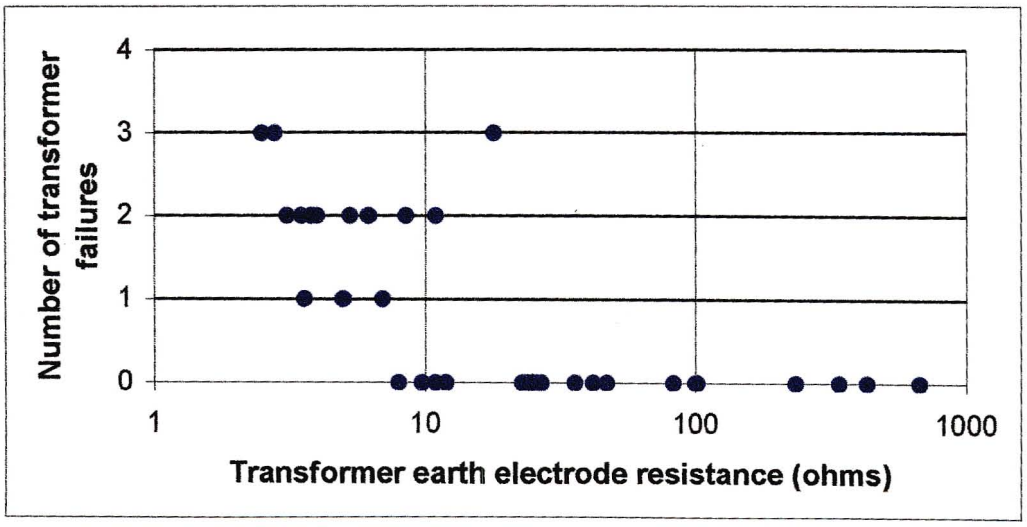

Figure 5.5 Results of initial field transformer resistance measurements

A hand driven generator using the null balance operating principle and an analogue Top Tronic T-1505 earth tester were used for these transformer earth resistance measurements. The data collected indicated that on average multiple failure installations (2 or more failures) had lower earth resistance measurements than single failure installations (1 or less failures).

The transformer resistance measurement results are shown in Figure 5.5 above and statistically summarised in Table 5.2 below. The most noticeable difference was in the sample mean of the two failure categories. There seemed to be a correlation (in the selected sample) between installations with multiple transformer failures and low transformer earth electrode resistances for the initial results. This was indicated by the upper left hand corner of Figure 5.5.

Table 5.2 Summary of transformer earth resistance measurements results

Statistical Indicator	Single failure installation earth resistance value (ohms)	Multiple failure installation earth resistance value (ohms)
Sample population	26	11
Sample mean	100.4	6.3
Sample standard deviation	160.7	4.7

Some of the transformer installations with low earth electrode resistances had some type of nearby industrial plant connected. Most of the transformer MV and plant LV earth electrodes were connected in parallel. This reduced the overall resistance of the transformer MV earth electrode been measured.

5.2.3 Failed Surge Arresters

The reticulation fault logbook from the Glencoe TSC was analysed. The following data pertaining to the failed transformers and surge arresters was obtained. The data provided information about the number of failures and condition of the failed transformers and surge arresters.

From the data collected, a "blown" transformer was classified as either a transformer that had the tank split open or was bulging. The physical damage of the transformer was clearly visible. Figure 5.6 below was an example of a blown transformer with blown porcelain surge arresters. A transformer failure classified as "internal" was a failed transformer where there was no external sign of damage. A surge arrester failure was classified as when there was visible sign of damage to the arrester or the disconnector had operated.

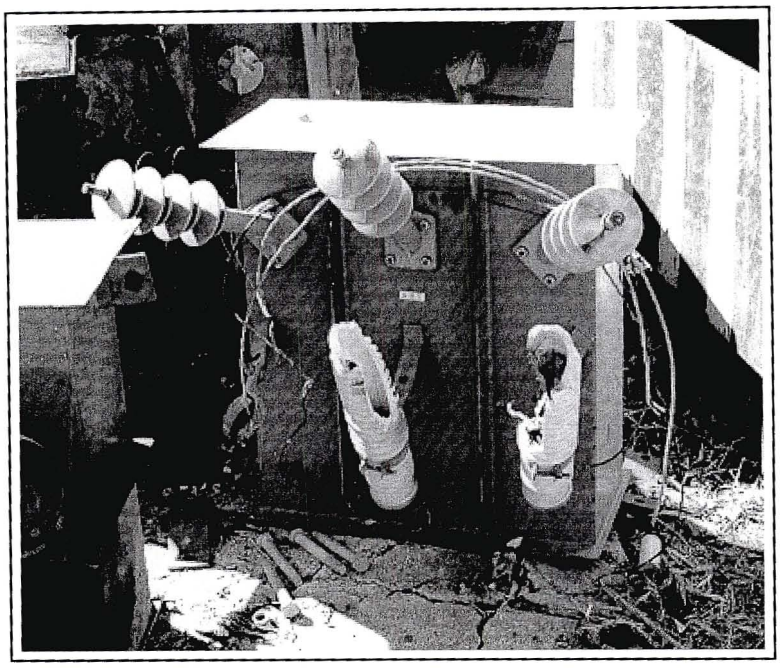

Figure 5.6 Failed transformer with blown surge arresters at Glencoe TSC

Figure 5.7 below showed that for all the transformer failures, 35% of the failures had all three arresters fail. The data also showed that 24% of all the transformer failures had no arrester failure. The information provided did not indicate whether the arrester had exploded or the disconnectors had operated.

It is debatable whether lightning or a power frequency fault would cause a transformer to explode. With the older gapped type arresters moisture ingress might cause the arrester to explode. The shattering effect may cause the other porcelain arresters to be damaged. A slow inter-winding fault is more likely to cause the transformer tank to expand and eventually split open due to the pressure build up inside. Most of the failed transformers had very dirty black oil remaining in them. This indicated carbon build up due to internal arcing.

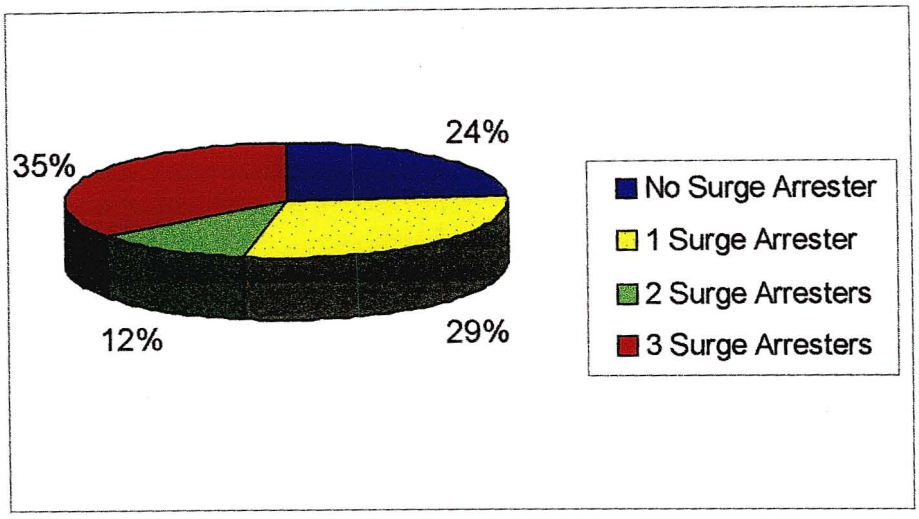

Figure 5.7 Number of surge arresters failing with a failed transformer.

Figure 5.8 below shows the condition of the failed transformer for when a number of arresters correspondingly also failed. For no failed arresters, the majority of the transformers had internal (no visible damage) failures. For all three surge arresters failing, the majority of the transformers were "blown" (ruptured). This could indicate a severe lightning strike or possible (as discussed above), the arresters were porcelain causing damage to the other arresters.

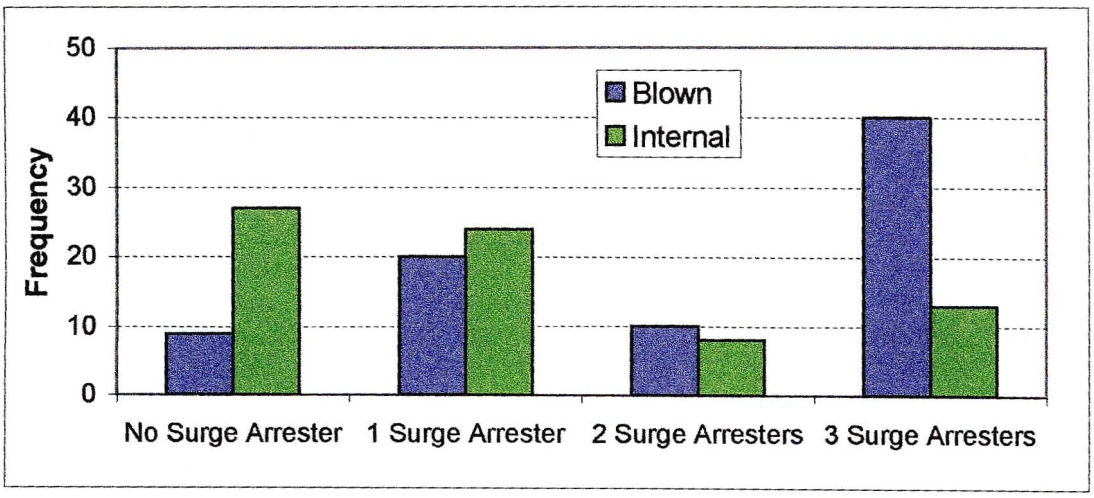

Figure 5.8 State of the failed transformer for number of failed arresters

Figure 5.7 and Figure 5.8 provide important information about the condition and number of arresters failing. This was discussed in chapter 4.4 and detailed in (Ericksson et al, 1986) and (Schei et al, 1978).

5.3 Conclusions

The transformer data analysis results indicated that the transformers and surge arresters had failed during periods of lightning storm activity. The results from the analysis of the Glencoe TSC fault logbook, indicated that for majority of the failed transformers with external signs of damage, all three associated arresters had also failed. The arrester failure mode was either that the arrester had visible damage or the disconnector had operated. The collected data could not provide information about whether both the transformers and arresters failed at the same time. There seemed to be a correlation (in the selected sample) between transformer installations with multiple transformer failures and low transformer earth electrode resistances for the initial results. The transformer earth electrode resistance is an important factor effecting the energy absorbed by the arresters. The analysed data also supported the dissertation that lightning was responsible for the majority of transformer failures.

CHAPTER 6

EXPERIMENTAL PROJECT AND RESULTS

The preceding chapter provided a summary of the statistical analysis of the transformer failures. The results of the analysis indicated that 65% of the transformers failed during lightning storm periods. In this chapter the practical methods implemented on the networks to protect the transformers against lightning are presented. The three experimental networks are discussed with accompanying photographs. The findings of the three network audits and the results of the transformer earth resistance measurements are presented. An analysis of the available lightning data obtained from the Eskom LPATS system is provided. Each network had a voltage dip recorder installed to measure the performance of each network. The analysis of the voltage dips and interruptions recorded for each network is summarised.

6.1 Experimental Networks

Three networks were chosen from the Glencoe TSC area. The existing reticulation networks were selected on certain criteria such as installed transformer population, line length and percentage of transformer failures per annum. It was ensured that the networks were similar in selection criteria and in close proximity to the town of Glencoe. It was intended that similar lightning patterns would be experienced on all three networks. An important factor was that the networks selected had not been identified for any refurbishment work or network expansion for the next three years. This meant that the networks in the Glencoe TSC with very high transformer failure rates could not always be selected.

All three networks selected had transformer failure rates of more than 5% per annum (double the regional average) and an installed transformer density of more than 0.8 transformers per km of line. All three networks were rated at 11kV and fully insulated.

N/B means network breaker. This is a standard Eskom naming convention of networks that assigns a network name to its network circuit breaker in the source substation.

6.1.1 Dundee N/B 18 Network

Dundee N/B 18 was used as a control line. This line was "left as is" and used as a reference line to compare the performance of the other two selected experimental lines to this line. Dundee N/B 18 was very similar in criteria to the other two experimental networks described below. The network was 43.3km long and had 33 pole mounted transformers installed on the network.

This network was fully insulated (no 600mm wood path in series with the earthed down conductor to provide a 300kV insulation level). The transformer installations all had the single surge arrester configuration installed on each phase. All the transformer installations had combined MV and LV earthing arrangements.

6.1.2 Glencoe N/B 15 Network

Glencoe N/B 15 was fitted with a 600mm wood path in series with an earthed down conductor on each intermediate woodpole structure (see Figure 6.1). This was to provide a BIL of 300kV for the network. The network was 67.3km long and had 54 transformers installed on the network. The transformer installations all had the single surge arrester configuration installed on each phase. The majority of the transformer installations had combined MV and LV earthing arrangements. There were a few of the newer transformer installations with separate MV and LV earthing arrangements.

The crossarms of the wood pole structures had been purposely bonded (phase-to-phase) to obtain the 300kV insulation level on the structure as shown in Figure 6.1 below. A 50mm gap was allowed between the post insulator and the circumferential stainless steel strap (bandit strap) on the crossarm to prevent small arcing occurring between the two components.

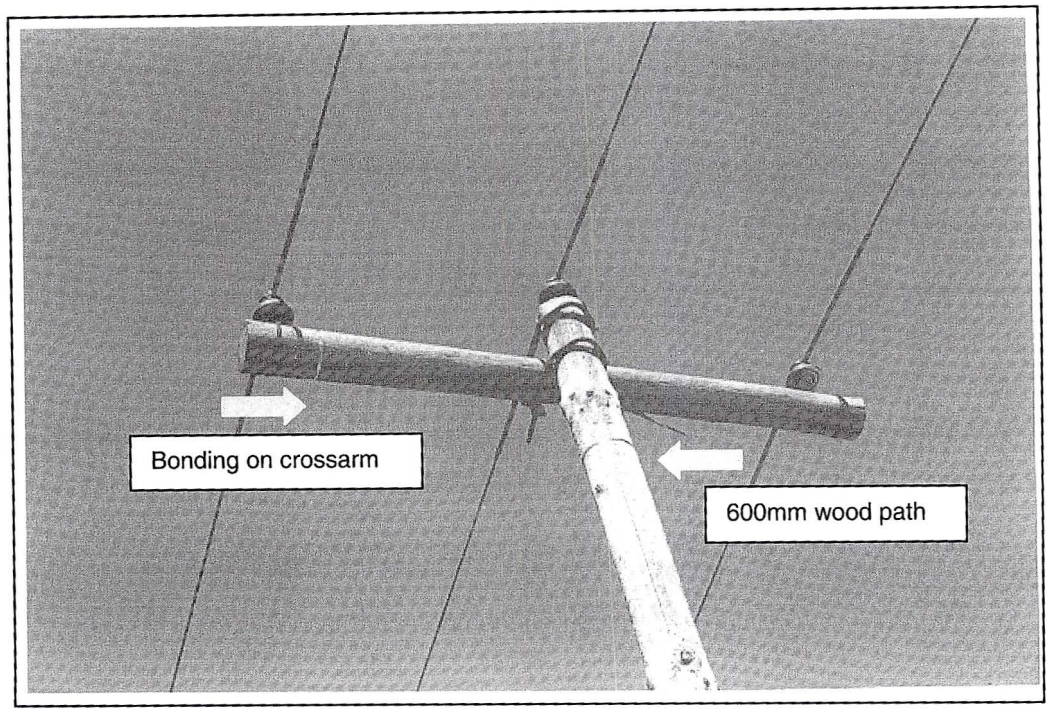

Figure 6.1 Bonding of crossarms and 600mm wood path on Glencoe N/B 15

6.1.3 Glencoe N/B 13 Network

Glencoe N/B 13 was fitted with two surge arresters in parallel per phase (double arrester configuration) on the transformer. In addition a voltage flashover point (BIL of about 300kV) was created at the first structure back from the transformer. This point was connected to the transformer earth electrode via an understrung conductor to the transformer structure. This effectively acted as a "spark gap" to discharge overvoltages larger than 300kV down to earth at the first structure away from the transformer. Smaller overvoltages would propagate harmlessly towards the transformer where the arresters would clamp the overvoltage and adequately protect the transformer. The network was 46.2km long and had 43 installed transformers. The network was fully insulated.

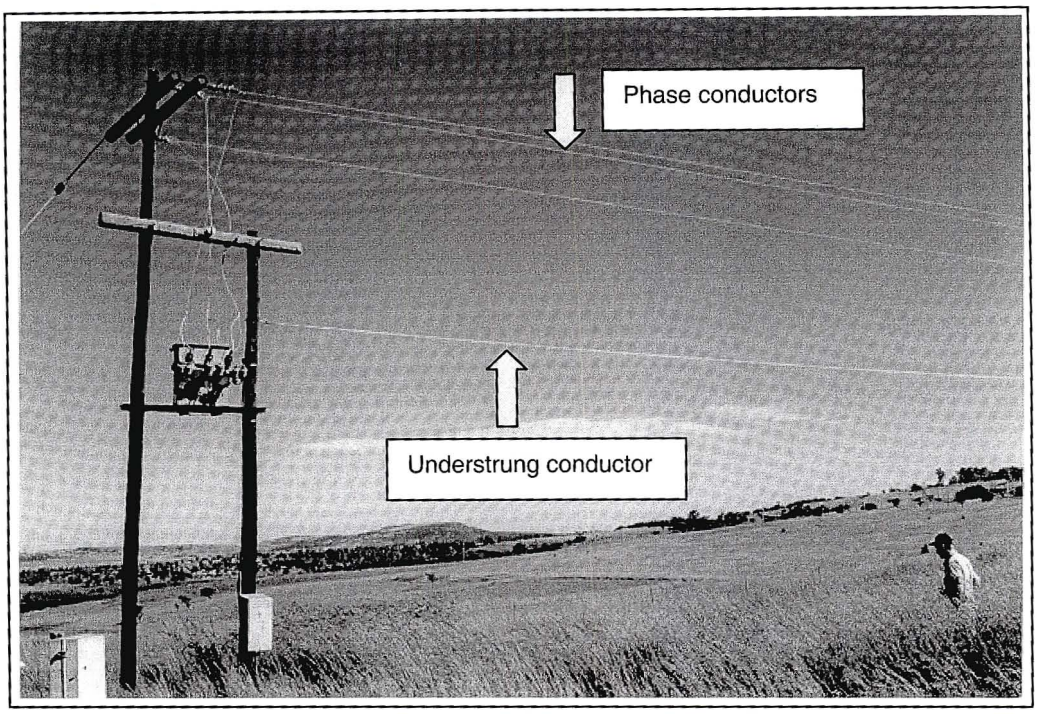

Figure 6.2 Typical transformer installation on Glencoe N/B 13

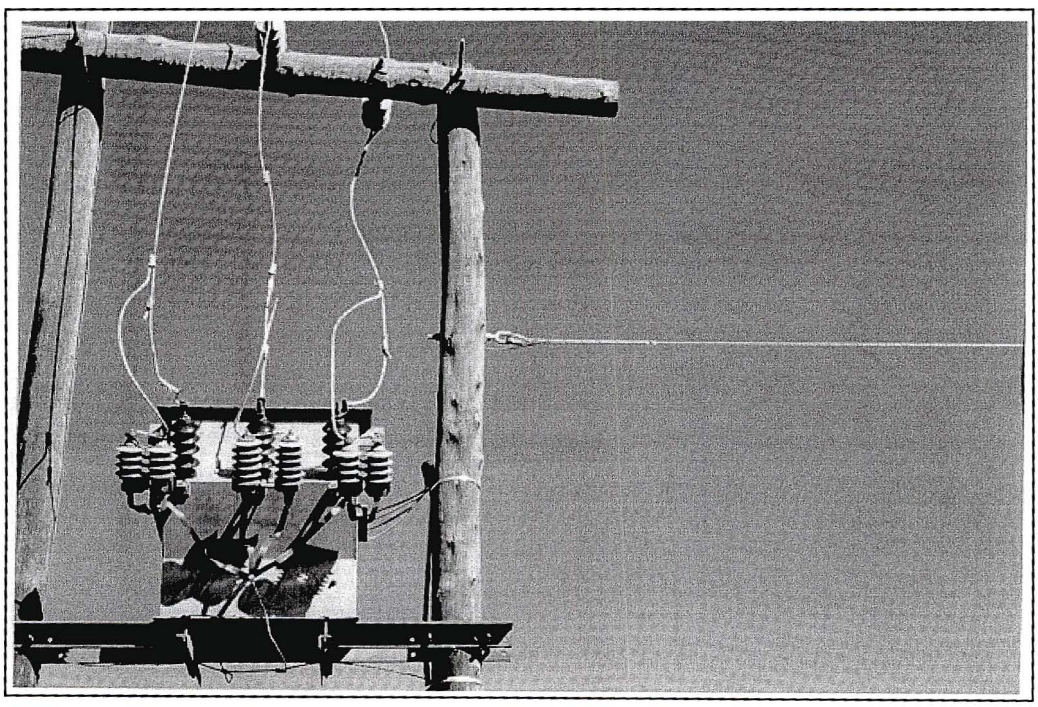

Figure 6.3 Double surge arrester configuration on Glencoe N/B 13

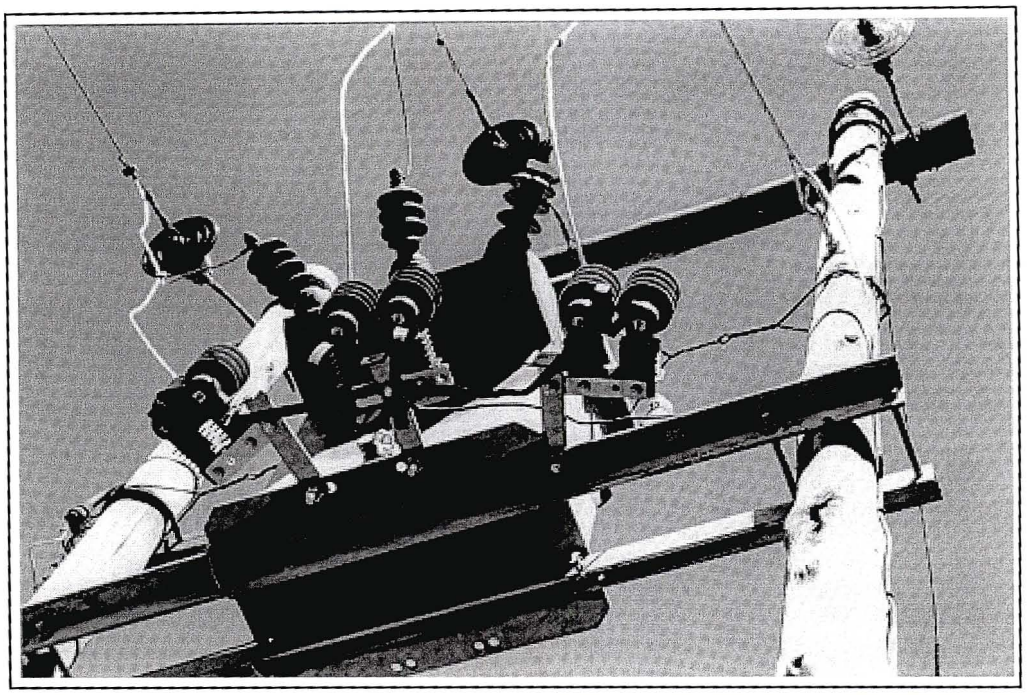

Figure 6.4 Close up view of double surge arrester configuration

6.2 Experimental Project Network Audits

Phase 1 of the research project was the implementation of the practical methods on Glencoe N/B 13 and Glencoe N/B 15 and was completed by the end of October 1999. The first network audit was conducted in November 1999 to obtain a reference condition of the three networks.

A network audit would typically consist of the following tasks :

- Establish the condition of the each transformer installation.
- Audit each transformer installation according to a supplied questionnaire as shown in Appendix B.
- Take photographs of each transformer installation (provide a visual history).
- Note the condition and position of the surge arresters (on crossarm or transformer tank).

- Perform transformer earth electrode resistance measurements at each transformer installation.
- Note any transformer or surge arrester failures.
- Note any woodpole splintering due to lightning flashover.
- Take the GPS co-ordinates of each transformer installation.
- Produce a detailed report of the findings for each network audit.

For the second network audits in September 2000, Duke Engineering were again contracted to conduct the audit work. The main purpose of the audit was to identify and quantify what equipment failures and lightning related damage had occurred on the networks during the period December 1999 through to August 2000.

Phase two of the experimental project was implemented on Glencoe N/B 15 and Dundee N/B 18 during April 2001. This phase of the project consisted of replacing all the old gapped SiC type surge arresters with the MOV type arresters. The existing surge arresters on the transformer structure crossarms were re-located to the transformer tanks. The double surge arrester configuration network, Glencoe N/B 13 was left alone.

A third network audit was also conducted in May 2001. The main purpose of the third audit was to identify and quantify what equipment failures and lightning damage had occurred on the networks during the period October 2000 to April 2001.

The following important findings were obtained from the third audit on each network :

Dundee N/B 18 : Control Line

- No surge arrester failures.
- No transformer failures.
- No pole damage was observed.

Glencoe N/B 15 : BIL Downwire

- Three surge arresters had failed at transformer installations GR169, GR165, GR200.
- Two transformer failures (GR135 and GR90) were found. These two transformers were identified in the second network audit.
- Nine poles had the circumferential stainless steel straps on the crossarms burnt off or there was evidence of woodpole. It was suggested that Distribution might need to re-examine the practise of using a circumferential stainless steel strap at both ends of the wood path.

Glencoe N/B 13 : Double surge arresters and understrung conductor

- No surge arrester failures.
- One transformer failure (installation IM 47). This transformer was more than 40 years old and there was a suspected LV fault that caused damage to the transformer.
- None of the understrung conductor spans had burnt off or been damaged by lightning.
- There was evidence of wood splintering on the wood path gap at some of the structures one span back from the transformer installation. This was expected as this demonstrated that the woodpath "sparkgap" was operating. Overvoltages of 300kV and greater were discharging to earth across the woodpath.

The transformer and surge arrester failures recorded in the third audit are summarised below in Table 6.1 below. Figure 6.5 and Figure 6.6 below show some examples of the wood pole splintering found during the audits.

Table 6.1 Summary of equipment failures on networks as found in the third audit

Network	Installation Number	Number of failed surge arresters or transformers	Earth resistance (ohms)	Type of arresters	Position of arresters	Type of MV/LV earthing
Glencoe N/B 15	GR 169	single arrester no transformer	1.3	SiC	transformer	combined
Glencoe N/B 15	GR 165	single arrester no transformer	156.9	SiC	transformer	combined
Glencoe N/B 15	GR 200	single arrester no transformer	5.2	MOV	transformer	combined
Glencoe N/B 15	GR 90	transformer fail no arrester	25.8	SiC	crossaram	combined
Glencoe N/B 15	GR 135	transformer fail no arrester	83.3	SiC	transformer	combined
Glencoe N/B 13	IM 47	transformer fail no arrester	2.2	MOV	transformer	combined

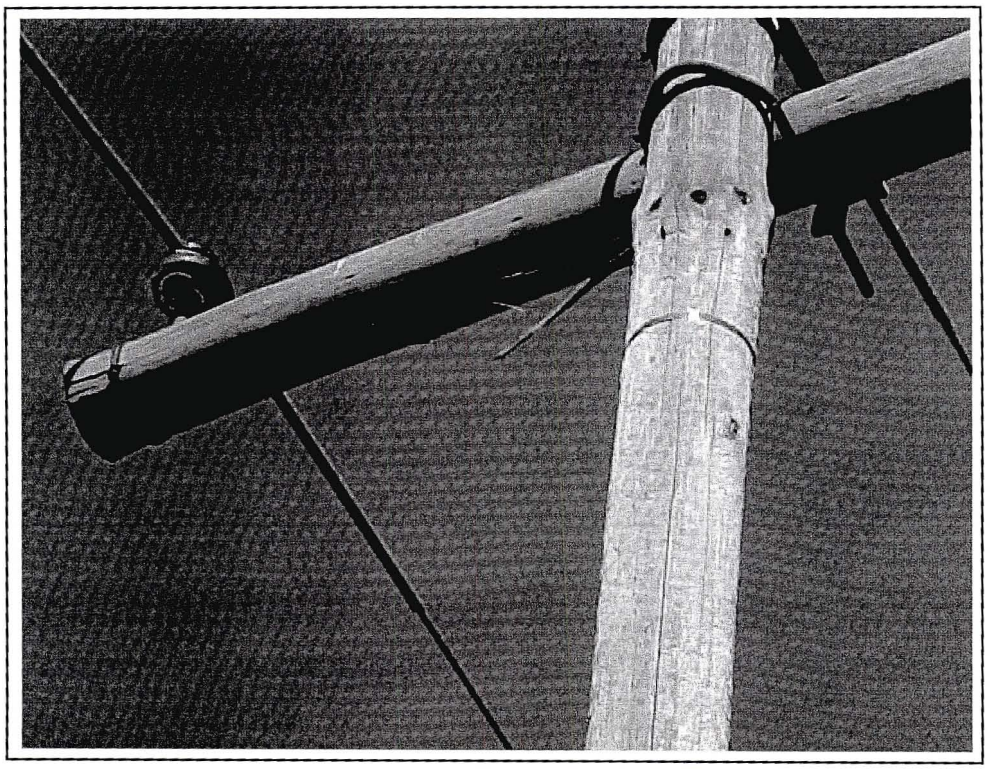

Figure 6.5 Example of wood pole splintering on Glencoe N/B 15

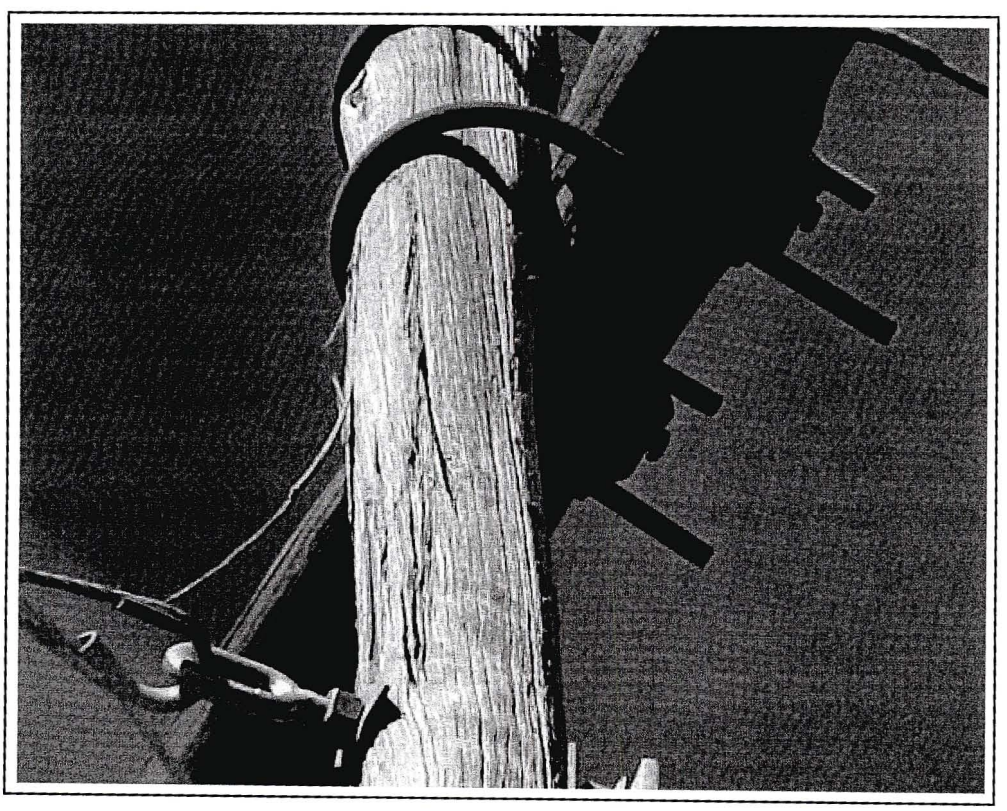

Figure 6.6 Example of wood pole splintering on Glencoe N/B 13

6.3 Results of Earth Resistance Measurements

A statistical summary of all the transformer resistance measurements conducted in the three audits are shown below in Table 6.2. The intention was to show the variation of resistance values for each year.

Table 6.2 Statistical summary of earth resistance measurements for all networks

Audit date	Dec 1999	Oct 2000	May 2001
Population	127	128	129
Mean	19.1 ohms	67.9 ohms	24.7 ohms
Std Dev	27.3 ohms	134.3 ohms	37.4 ohms
Less than 30 ohms	80.3%	61.7%	75.2%
Less than 10 ohms	56.7%	35.9%	58.1%
Less than 5 ohms	34.6%	18.0%	34.1%
Less than 2 ohms	12.6%	3.9%	11.6%

The standard deviation of the second network audit was much larger than that measured during the first and third network audits. It must be remembered that the second audit was conducted at the end of the Winter season of 2000. The winter season of 2000 was a particularly dry season as compared to previous years. The recorded variations in the resistance measurements are similar to those measured on the NEERI test line (Gaunt et al, 1989).

Table 6.3 below shows a summary of the earth resistance measurements results for Glencoe N/B 13 for the third network audit. As can be seen 53% of all the transformer installations on the networks had transformer earth resistances of less than 10 ohms.

Table 6.3 Summary of transformer resistance measurements on each network for 2001

Earth electrode resistance	Glencoe N/B 13	Glencoe N/B 15	Dundee N/B 18
Less than 10 ohms	23	25	27
Between 10 and 30 ohms	8	12	2
Between 30 and 100 ohms	10	12	3
Greater than 100 ohms	2	4	1
Total	**43**	**53**	**33**

Table 6.4 below shows the number of transformer failures recorded on each network for the period November 1999 to March 2002. It can be seen that Glencoe N/B 13 had not had a single transformer (or surge arrester) fail due to lightning since the project implementation. The indicated transformer failure at installation number IM 47 was regarded as failure due to old age. There have been recorded transformer failures on the other experimental line, Glencoe N/B 15 and the control line Dundee N/B 18.

Appendix C provides a summary of the experimental project timetable with activities to date.

Table 6.4 Number of transformer failures on each network
(1994 to March 2002)

Year	Glencoe N/B 13	Glencoe N/B 15	Dundee N/B 18
1994	3	2	1
1995	2	2	1
1996	4	3	2
1997	2	4	2
1998	3	3	3
1999	Unknown	Unknown	Unknown
2000	0	2	0
2001	1	2	0
2002	0	0	0

6.4 Results of LPATS Data Analysis

LPATS is a Lightning Position and Tracking System that monitors and records lightning activity in South Africa. Atmospheric Research Systems Inc. based in Florida, USA, developed the system. The current Eskom LPATS system was installed in 1993 with six remote receivers positioned around South Africa.

The recorded LPATS data for the period January 1994 to March 2002 was collected and then analysed by the author using a program called LPATS Workstation. The LPATS Workstation program is an Eskom customer designed program, that is a simple viewing program for the recorded LPATS data files.

The intention was to quantify and compare the lightning activity in the area around the three networks before the project implementation to that of after the project implementation. Only the lightning data for the storm season months of the year (January to March and October to December) were analysed. The data that was provided contained information about the lightning ground flash density and the lightning first stroke current probability distributions.

One of problems encountered with the existing LPATS Workstation, was that the lightning data was only analysed for the whole of South Africa. In other words, the lightning parameters for a specific area or town could not be obtained. The 'box" providing with the co-ordinates of analysis (of South Africa) was fixed in the program.

Modifications to the LPATS software by Engelbrecht (STRI, Sweden) allowed the user to calculate the lightning data of a specific area (box). The box whose co-ordinates were 28.36 to 28.06S and 30.08 to 30.28E contained all three networks of the project. The box had an area of 624 km^2. The data analysis results can be seen in the following tables below.

Table 6.5 Total number of strokes to ground per month in the project "box"

Year	Jan	Feb	Mar	Oct	Nov	Dec	Average number of strokes for storm season	Stroke density for storm season (strokes/km ^2/year)
1994	1112	138	2640	147	789	151	829.5	8.0
1995	767	674	329	365	588	332	509.2	4.9
1996	695	461	42	1387	675	1247	751.2	7.2
1997	1996	2007	304	954	1989	3140	1731.7	16.7
1998	2498	283	41	1129	N/A	297	849.6	6.8
1999	1539	107	2249	65	**655**	**1211**	971.0	9.3
2000	**259**	**913**	**888**	**1682**	**373**	**1875**	998.3	9.6
2001	**427**	**1768**	**415**	**609**	**1208**	**2584**	1168.5	11.2
2002	**2121**	**1219**	**1986**				1775.3	8.5

It must be noted that the data in Table 6.5 is only for recorded negative first and subsequent lightning strokes. The light grey coloured cells indicate the months of the project (November 1999 to March 2002).

The recorded lightning data that was observed by the LPATS system recorders and may not the true situation out in the field due to the lightning detection algorithm used by the system. For internal comparison purposes the data analysis is adequate.

The calculated lightning ground "stroke" density values (internal comparison) for each storm season are fairly relatively consistent values for each year. The mean is 9.1 strokes/km^2/year with a standard deviation of 3.4. Assuming a detection efficiency (DE) of the LPATS receivers at the time of 80% to 90%, these values are increased but the "edge effects" of the box have not been taken into account.

Table 6.6 below shows a statistical summary of the lightning stroke data before and after the project implementation. It can be seen that the average and standard deviation values per month are of similar magnitude.

Table 6.6 Summary of lightning activity before and after the project implementation

	Before project implementation	After project implementation
Number of months data	33	17
Size of area (sq km)	624	624
Average number strokes per month	915.8	1187.8
Standard deviation	865.3	707.1
Maximum number of strokes in any month	3140	2584
Minimum number of strokes in any month	41	259

Table 6.7 below shows the first stroke lightning current probability distributions. It must be noted that these values are derived current amplitudes from the LPATS system algorithm. The data per year is only for the storm season months.

This data is based on the following parameters as specified by the user in the LPATS Workstation (Acknowledgements to Michelle Redelinghuys, Eskom Transmission) :

- Maximum distance between strokes : 8km
- Maximum time between strokes : 0.2s

A 96% probability means that 96% of all the recorded lightning currents first strokes had current magnitudes larger than the indicated values in the table. It can be seen that the 96% and 50% probability currents are fairly consistent over the years.

The major conclusion of the LPATS data analysis, was that the lightning activity before the project implementation and after the project were similar. The improved situation of no transformer or surge arrester failures on Glencoe N/B 13 was not due to reduced lightning activity, but rather due to the practical methods implemented on the network.

Table 6.7 First stroke lightning current probability distribution

	First stroke current occurring probability (kA)		
	96%	50%	4%
1994 Storm Season	14	26	55
1995 Storm Season	17	27	56
1996 Storm Season	14	28	61
1997 Storm Season	13	28	69
1998 Storm Season	11	25	65
1999 Storm Season	13	24	58
2000 Storm Season	15	30	110
2001 Storm Season	14	29	75
2002 Storm Season (Jan to Mar)	13	26	72

6.5 Voltage Dip Recorder Results

Voltage dip recorders (Vectographs^{TM}) were installed on each of the three networks described above. The voltage dip recorders were installed on the LV side of the transformer installation near the relevant network circuit breaker protecting the network.

The purpose of these voltage recorders was to record the voltage loss incidents such as dips and interruptions experienced on the particular network. This data could be used to quantify the performance of each network.

A *voltage dip* was defined as a temporary loss of voltage level on one or more phases below 0.9 per unit of the declared voltage level for the time period 20ms to 3 seconds (NRS 048, 1996). A voltage dip threshold of 85% of nominal voltage and a voltage surge threshold of 110% of nominal voltage were used as recording parameters for the Vectographs™. The nominal voltage was 240V measured on the customer LV side.

A *sustained voltage interruption* was defined as a complete loss of the supply voltage on one or more phases for the time period longer than two minutes. These interruptions could be due to forced (unplanned) or planned work on the network (NRS 048, 1996).

There exists a grey area of recording times between three seconds and two minutes. In Eskom Distribution this time period has been defined as momentary interruptions. These would occur when the network breaker detected fault current and auto reclosed (ARC).

The voltage loss data was collected and analysed. The following information was obtained :

- Time of day
- Month of the voltage loss occurring
- Phases affected
- NRS 048 voltage dip classification
- Magnitude versus duration plots
- Frequency distribution of voltage dips and interruptions

Data presented below was for the period November 1999 to March 2002. This provided 25 months of recorded data. The data for May 2000 was discarded to a download error experienced with the recorders and the data for the months April, May, September and October 2001 were unfortunately not collected by the relevant Eskom staff.

The plot in Figure 6.7 below shows how many voltage dips and interruptions occurred on Glencoe N/B 13. The magnitude of the voltage loss versus the duration was plotted with the duration on a logarithmic scale.

The voltage losses of duration 0.0001 minutes to 0.1 minutes were due to the other reticulation networks connected to the 11kV substation busbar and possibly caused by other Sub-transmission (88kV and 132kV) networks feeding the Glencoe substation on the high voltage incoming side.

The voltage interruptions (100% voltage loss) of duration 0.1 minutes to 10 minutes were due to the successful breaker auto reclosers (ARCs) of the network breaker or by Network Control closing the breaker using telecontrol. The interruptions of duration 10 minutes and longer are network breaker lockouts (permanent faults).

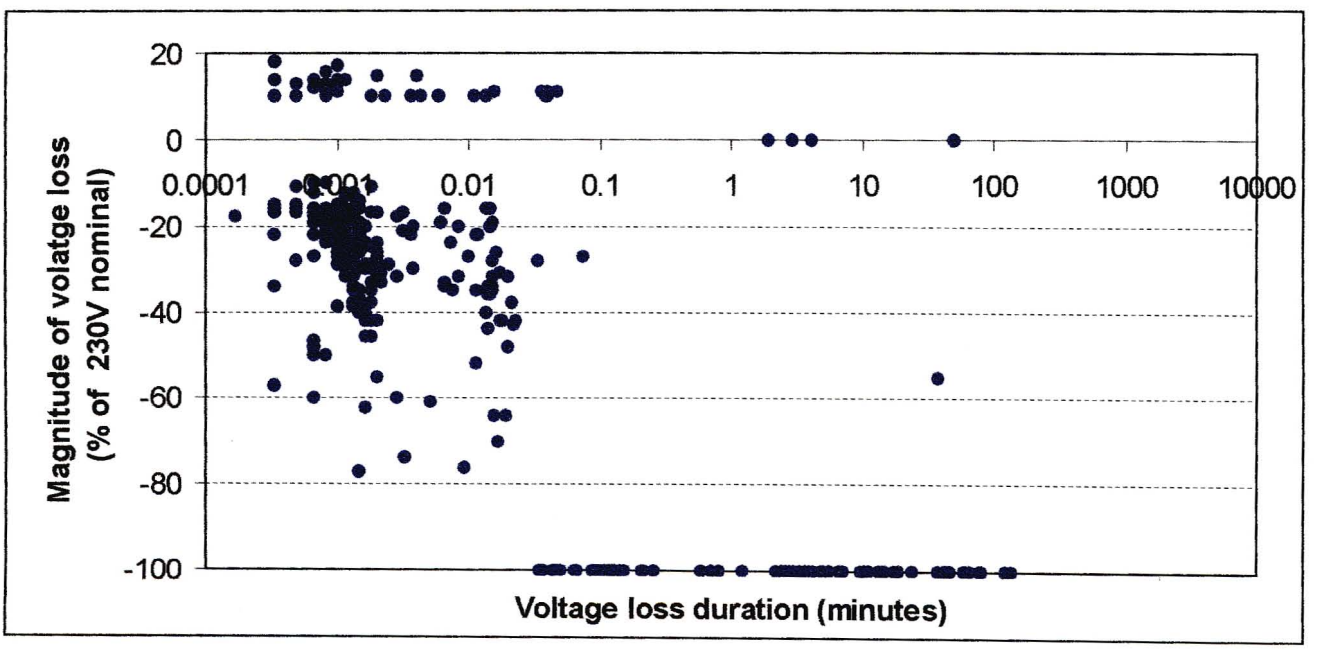

Figure 6.7 Glencoe N/B 13 magnitude of voltage loss versus duration plot (November 1999 to March 2002)

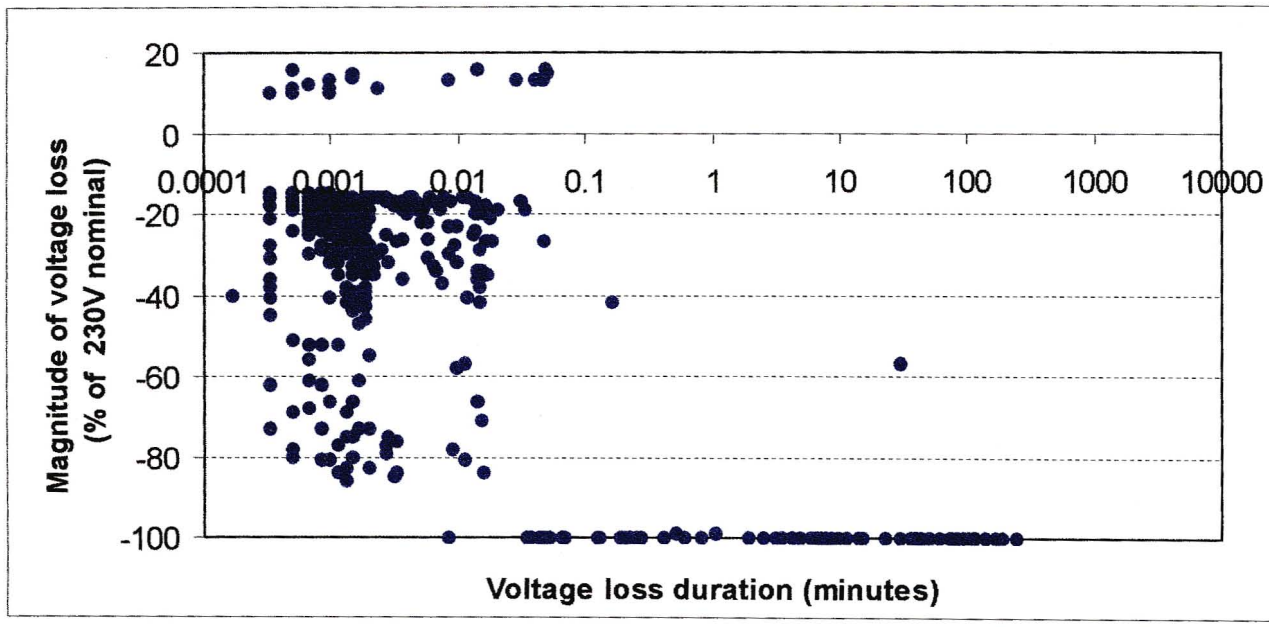

Figure 6.8 Glencoe N/B 15 magnitude of voltage loss versus duration plot (November 1999 to March 2002)

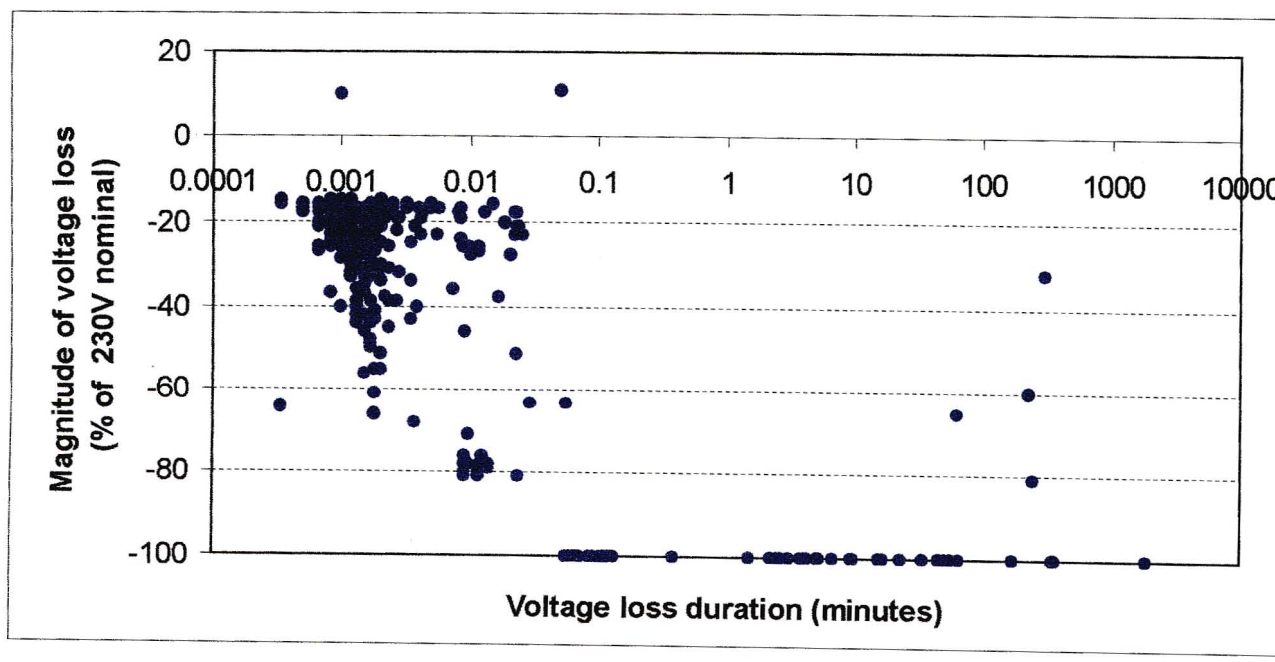

Figure 6.9 Dundee N/B 18 magnitude of voltage loss versus duration plot (November 1999 to March 2002)

In the above three figures, events of less than 100% voltage level loss with durations of between 100 and 1000 minutes can be seen. These events could be due to a single phasing scenario when one of phases is lost but the customer is still supplied with voltage from the other two phases. The voltage dip recorder would still record these types of events.

Table 6.8 below provides a frequency of voltage loss incidents comparison of the three networks. It can be seen that the number of voltage loss events of between 0.1 to 10 minute durations are very similar for Glencoe N/B 13 and Glencoe N/B 15. This time period would correspond to successful ARCs on the network.

Table 6.8 Comparison of voltage loss incidents for each network

	Number of voltage loss incidents		
Voltage loss duration	**Glencoe N/B 13**	**Glencoe N/B15**	**Dundee N/B18**
0.0001 to 0.1 mins	324	457	327
0.1 to 10 mins	71	70	31
10 to 500 mins	22	33	18
500 to 5000 mins	0	0	1
Total	**417**	**560**	**376**

The number of voltage dips and interruptions recorded on each network were normalised to 100km per year and were cumulatively plotted against the duration of the voltage loss. From Figure 6.10 below it can be seen that the two experimental measures implemented on Glencoe N/B 13 and Glencoe N/B 15 have not had a negative effect on the performance or reliability of the networks. The cumulative frequency distribution of voltage loss incidents for each network was similar.

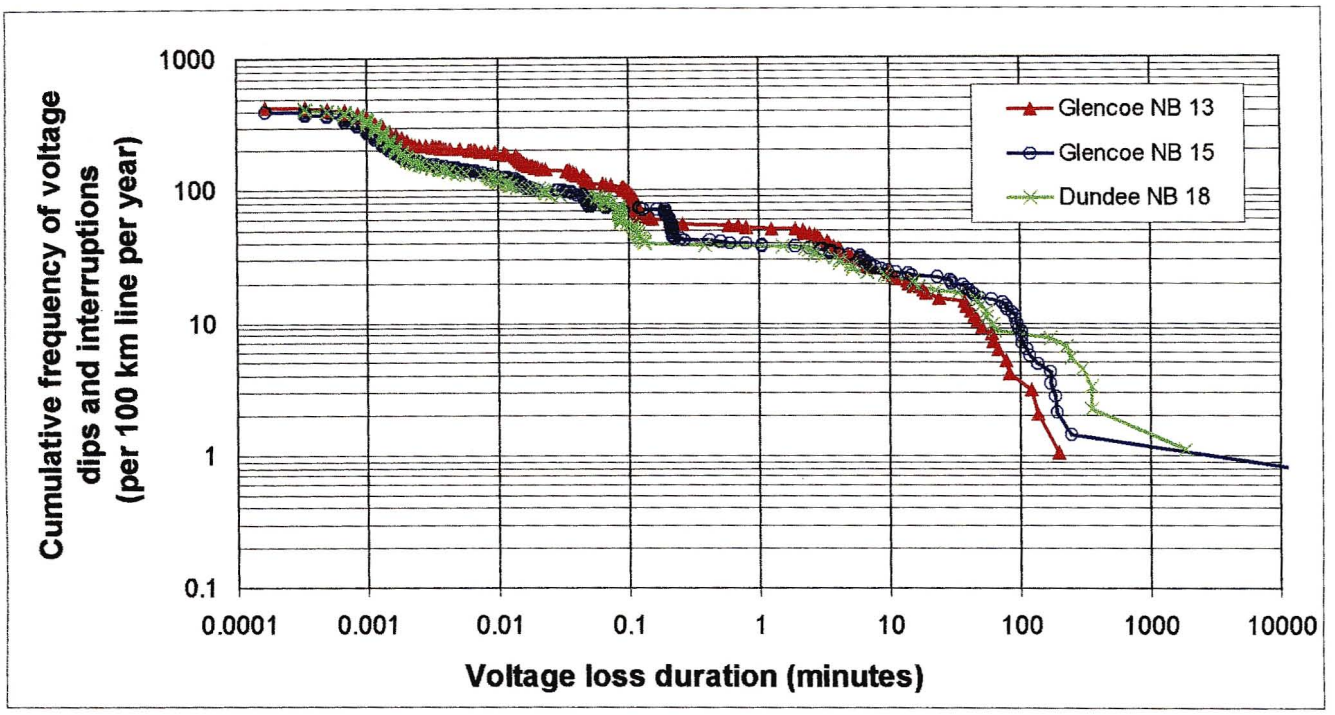

Figure 6.10 Cumulative frequency distribution of voltage loss incidents per 100km per year for each experimental network

From Figure 6.10 it was proposed to have a voltage loss incident benchmark or template for an 11kV rural network in a high lightning area. These values are proposed in Table 6.9 and plotted in Figure 6.11 below. The grey coloured cells in the table indicate the voltage interruptions.

Table 6.9 Frequency of voltage dips and interruptions benchmark table

Voltage dip and interruption duration	Frequency (per 100km per year)
0.0002	450
0.001	300
0.01	150
0.1	70
2	45
10	25
100	7
1000	1.5
5000	1

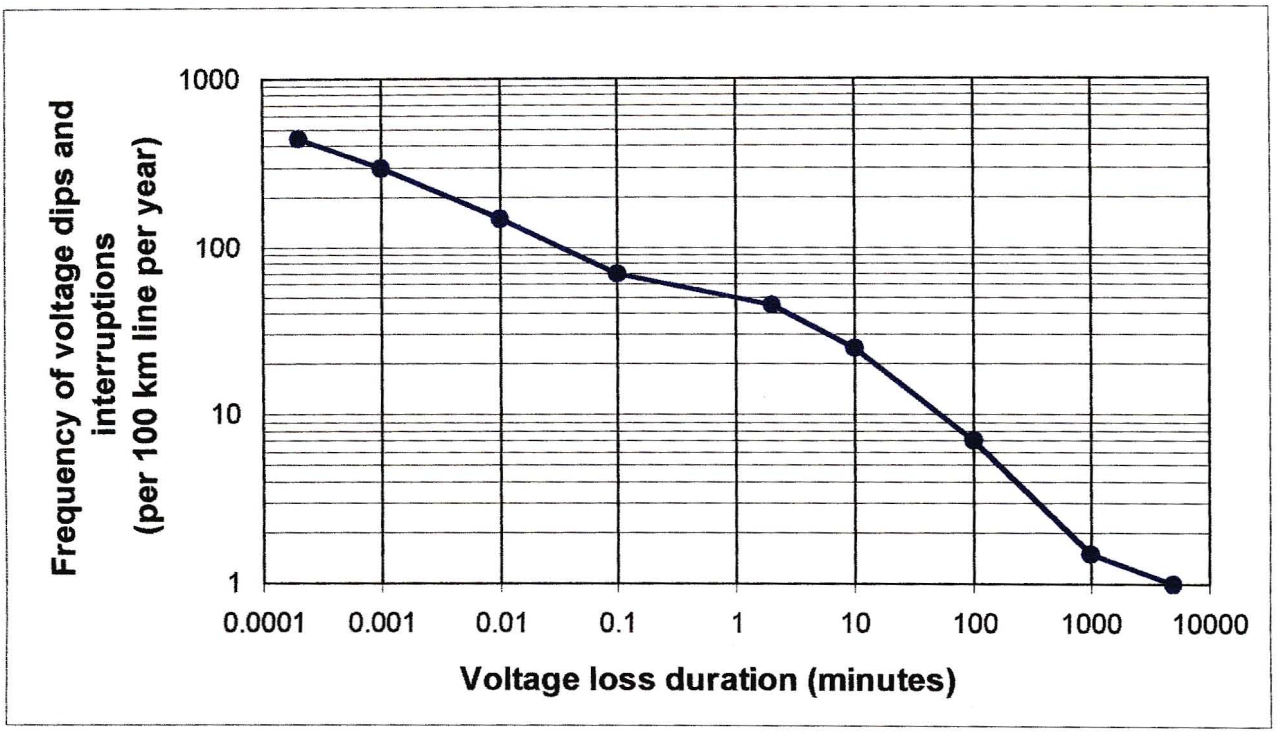

Figure 6.11 Proposed performance template for an 11kV reticulation line in a high lightning area

Using equation (3.5) and assuming an average line height H of 11m, line length L of 100km and ground flash density N_g of 9 flashes/km^2/year, yields a value for N_s of about 106 direct strikes a year to the line. Estimating a conservative shielding factor for the network of about 0.4, the number of network momentary interruptions (ARCs) should be 42 a year (Gaunt et al, 1989). Figure 6.10 (and the values averaged in Figure 6.11) provided an interruption value of 45. Figure 6.11 provides good agreement for the expected number of ARCs on the networks.

6.6 Conclusions

The experimental project consisted of three networks in the Glencoe area. The main emphasis of the lightning protection on Glencoe N/B 13 was the use of two distribution class arresters in parallel for each transformer and an understrung conductor arrangement.

The network Glencoe N/B 15 had single arresters installed on the transformers and a 600mm wood path in series with an earthed down conductor installed on each intermediate woodpole structure. This was to ensure a BIL of 300kV for the network.

For the period November 1999 to March 2002 not a single transformer or surge arrester had failed due to lightning on the double arrester and understrung conductor configuration experimental network. There were recorded transformer and surge arrester failures on the second experimental network and on the control network. This was a very positive result and indicated that the practical methods implemented on Glencoe N/B 13 did prevent transformer and arrester failures.

It was found that the practical methods implemented on Glencoe N/B 13 did not have a negative impact on the performance levels of the network. Each network was carefully monitored in terms of equipment failures and the performance levels of each network was measured with installed voltage dip recorders near the individual network circuit breakers. The Eskom Lightning Position and Tracking System (LPATS) data was collected and analysed to quantify the lightning activity before the project implementation to that of after project implementation. The analysis of the collected data showed that the lightning activity in the area surrounding the three networks before project implementation was similar to that activity after the project implementation. The conclusion could be made that the reduction in transformer failures was due to the practical methods implemented and not due to less lightning activity in the area surrounding the networks.

CHAPTER 7
ATP MODELLING AND SIMULATION RESULTS

In this chapter of the dissertation, the different component models used in the Alternative Transient Program (ATP) simulations are presented and discussed in detail. Some testing and verification of the individual models is performed. The main focus of the individual model section is the proposed surge arrester model used in all the ATP simulations. Two types of models are presented for use in the simulations; the CIGRE model and the modified IEEE arrester model. The results and a comparison of the two models are presented.

This chapter provides the results of the many ATP simulations performed by modeling the three individual networks as used in the experimental project at Glencoe. A comparative study is performed between the three networks to determine which network configuration reduces the energy absorbed by the individual surge arresters the most, and hence reduce the number of transformer failures.

7.1 ATP Software

Alternative Transients Program (ATP) is a software program used for the digital simulation of transient phenomena of electromagnetic and electromechanical nature in electric power systems. Complex networks of any arbitrary structure can be simulated in ATP. Analysis of control systems, power electronics equipment and components with nonlinear characteristics such as arcs and corona are possible as well (Prikler et al, 1998).

The ATP program was used to model the effect of lightning on the experimental networks at Glencoe. Suitable component models had to be chosen and set up so that the system (individual networks) could be simulated. The results of similar lightning and arrester operation simulations using the EMTP program at the University of Texas, USA are provided in (Mansoor et al, 1995). The results of modeling triggered lightning on distribution lines with EMTP at the University of Florida, USA are presented in (Mata, 2000).

For this dissertation, ATPDraw (version 2.4 with the relevant patch files) for Windows was used. ATPDraw is a graphical, mouse driven preprocessor to the ATP version of the Electromagnetic Transients Program (EMTP). ATPDraw can be used to create or edit a model of the electrical network to be simulated (Electrotek, 1999).

7.2 Component Models for ATP Simulations

Only single conductor ATP simulations were performed. This represents a "worst case" scenario for the surge arrester energy absorption limits, as the lightning current will not be shared between three arresters. It was reported in (Ericksson et al, 1986b) that observations based on the NEERI test line indicated that the current sharing of the three arresters protecting the transformer was not equal. It was found that about two thirds of the current was flowing through one arrester, about thirty percent through the second arrester and 5% through the third arrester.

The effect of induced voltages on the other two conductors and the coupling effect will not be taken into account. The effect of pre-discharge currents between phase conductors also will be ignored (Brown et al, 1976).

7.2.1 Lightning Current Source

For the ATP simulations, the lightning current was represented by a Heidler function (type 15 surge function) in ATP. The Heidler source function for ATP was introduced by Bernd Stein for ease of application for ATP lightning simulations (Leuven, 1992). The standard double exponential waveform that is commonly used to represent lightning current has some disadvantages.

For the ATP parametric simulations, the peak current values, rise times and tail half times were varied from a low value to a high value. Refer to Table 7.1 below. These lightning waveform parameter values correspond to the expected probabilities as presented in Table 3.3. The intention was to provide a range of parameters so that their effect in the simulations could be measured.

Although a deterministic approach has been adopted in the simulations, full account has been taken of the statistical variations in the lightning parameters in the simulations.

Table 7.1 Lightning parameter values for ATP simulations

	Lower value	Upper value
Peak current (kA)	10	80
Rise time (us)	1	10
Tail half time (us)	35	140

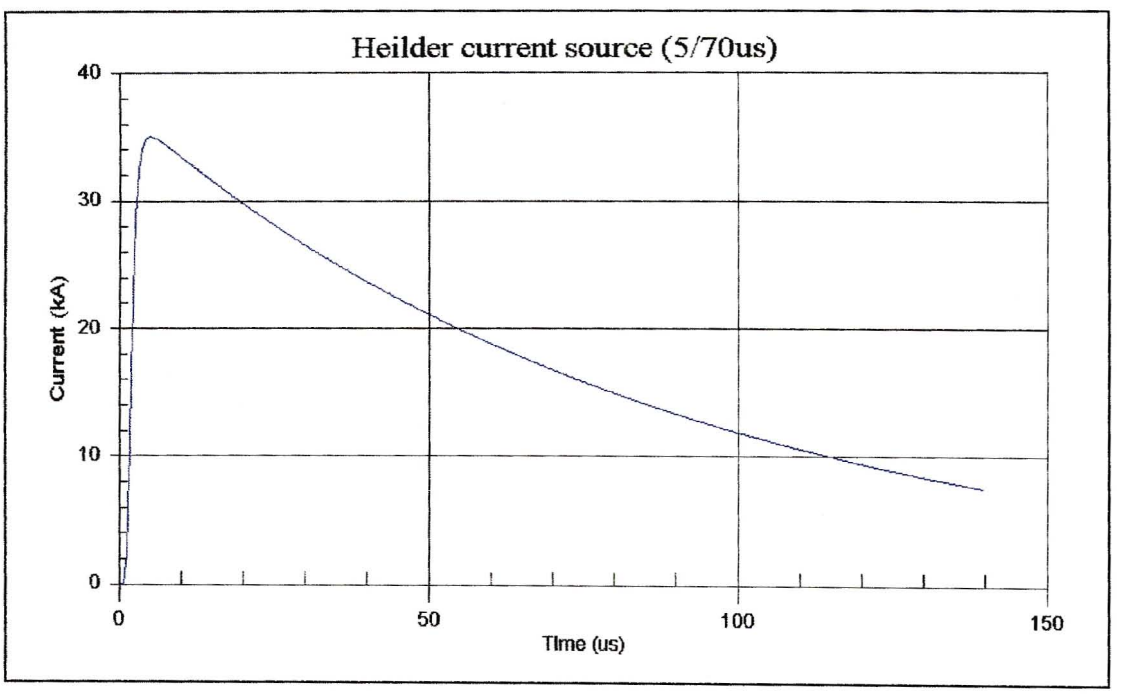

Figure 7.1 Example of a Heidler source in ATP (35kA 5/70μs lightning current waveform)

The positive correlation of peak currents with maximum steepness (rate-of-rise) and the concave wavefront characteristic as discussed in (Anderson et al, 1980) will not be taken into account due to the simulations being parametric.

In the ATP simulations the injection of current by the lightning return stroke onto the line is modeled as an ideal current source. The surge impedance of the stroke channel (which is connected in parallel to the current source) is considered to be at least ten times larger than the surge impedance of the struck point and can be neglected (Darveniza et al, 1979a). Only negative single flash strokes will be considered for practical lightning simulations in this dissertation (Anderson, 1982). The effect of two strokes (first stroke followed by a subsequent stroke with a low level continuing current in between) was evaluated by (Van Schalkwyk, 2001). Actual measured triggered lightning current waveforms for the current source was used in the simulations by (Mata, 2000).

7.2.2 Power Frequency Voltage

The effect of the 50Hz power frequency voltage was not taken into account in the single conductor simulations, as the effect of the steady state voltage is minimal on reticulation voltage level networks. Inclusion of the power frequency voltage effect may result in a slight increase in the number of flashovers in a three phase reticulation networks simulation (Borghetti et al, 1997). In (CIGRE, 1991) it was proposed to use the average positive polarity value of power frequency in estimating backflashover rates for simulations.

7.2.3 Reticulation Line Model

For the experimental project, the three networks consisted mainly of either Fox, Mink and Hare conductor type. These conductors are all bare Aluminum Conductor Steel Reinforced (ACSR). For the ATP simulations the Fox conductor was used for both the phase conductor and the understrung conductor. Fox conductor was chosen for experimental project as the understrung conductor due to its availability and its mechanical strength.

Table 7.2 ACSR conductors used on reticulation lines in Eskom (SCSASABE7, 2001)

Conductor	Overall diameter (mm)	Total Area (mm^2)	Mass (kg/km)	Breaking load (kg)	Current rating @ 75 deg C (Amps)
Fox	8.37	42.8	149	1340	155
Mink	10.98	73.65	257	2230	215
Hare	14.16	122.48	427	3670	290

7.2.4 Frequency Dependence and Voltage Attenuation

When performing lightning simulation studies it is important to take into account the frequency dependence of the electrical parameters and the distributed nature of the losses of the transmission line. Accurate modeling of this frequency dependence over the frequency range of the applied signal is essential for the correct simulation of the electromagnetic transient conditions. Closed mathematical solutions of the frequency dependent transmission line equations in the time domain are very difficult to solve and are susceptible to numerical instability (Carneiro et al, 1991) and (Marti, 1982).

Transmission line models which assume constant parameters at 50Hz cannot adequately simulate the response of the transmission line over the wide range of frequencies that are present during transient conditions such as lightning. It was found that in most cases, that the constant parameter models produced magnification of the higher harmonics of the signals and in general a distortion of the waveshape and the higher magnitude peaks (Marti, 1982).

Different types of transmission line models for transient studies are available in ATP (Leuven, 1992) :

- Nominal PI RLC models for short lines called the PI model.
- Constant parameter models like the KC Lee (untransposed) or Clark (transposed) models called the Bergeron model.
- Frequency dependent models with constant transformation matrix called the JMarti model.
- Second order recursive convolution model called the Semlyen model.

For the JMarti model both the characteristic impedance and propagation function are obtained using the modal characteristics calculated over the user defined frequency range using the assumption of a constant transformation matrix. The method is accurate in the frequency range 0 Hz (dc conditions) to 1 MHz (Marti, 1982). The JMarti model was chosen for the transmission line model for all the ATP simulations due to its accuracy over a wide frequency range and ease of application in ATP.

The frequencies of the lightning stroke depend on the crest or rise time of the waveform. The AIEE WG selected a 4μs crest time as a best representative value for transient simulations (AIEE, 1950). This proposed rise time corresponds to a frequency of 250 kHz. In (Leuven, 1992) a frequency of 250kHz is also recommended as the default value for lightning simulations using the JMarti model.

In the ATP simulations, span lengths of 100m Fox conductor were used and the simulation step time was decreased accordingly. The radius of the conductor and dc resistance/km were entered by the user. The JMarti model was used with a calculation frequency of 250kHz and a data fit of eight decades with ten points per decade was used for all the simulations. A soil resistivity of 500Ω.m was used assuming a homogeneous earth model. The Carson theory of frequency dependent earth return impedance was used (CIGRE, 1991). The JMarti model also used to model the understrung conductor.

The JMarti model was evaluated by using a 1kV surge voltage with a 50/100μs waveform over 100km of Fox conductor. The line model was left open on one side so that the voltage reflection could be clearly seen. Figure 7.2 below provides the evaluation circuit of the JMarti transmission line model. The resulting voltage and reflection can be seen in Figure 7.3 below.

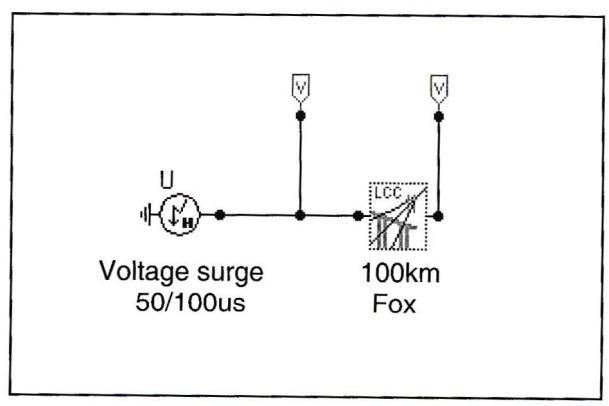

Figure 7.2 Evaluation circuit of JMarti transmission line model

A second voltage surge of also 1kV peak but with a 1/100μs waveform was simulated to demonstrate the effect of different rise times on the JMarti transmission line model.

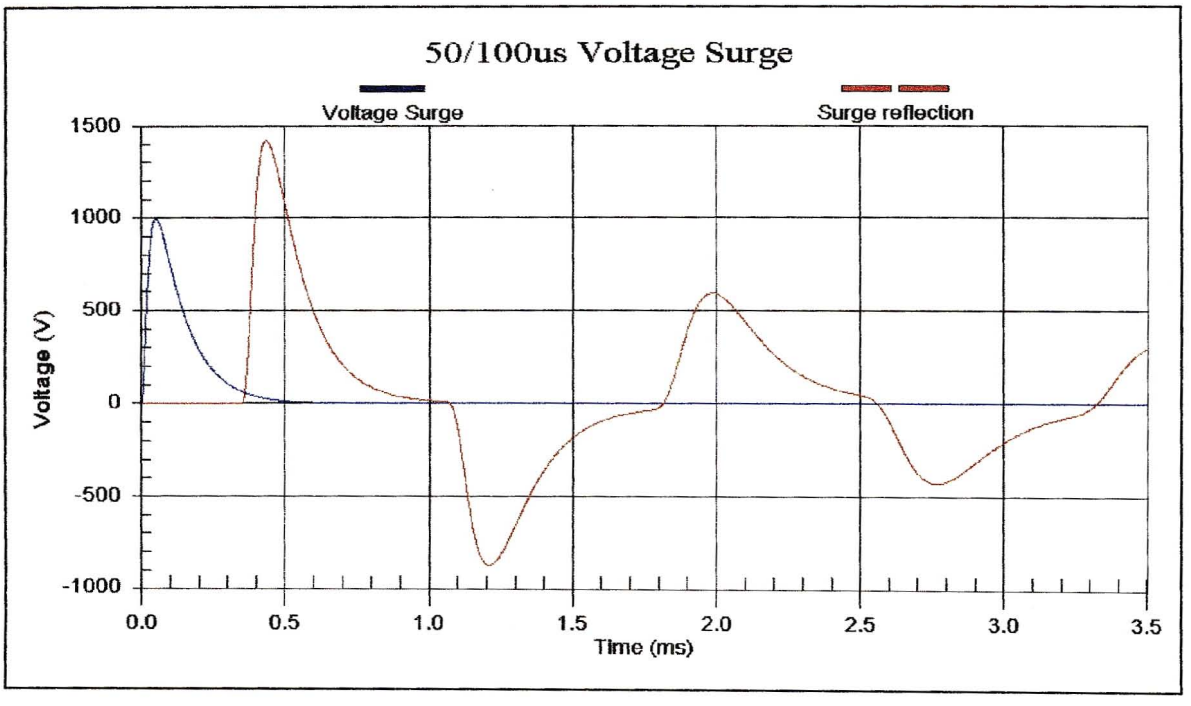

Figure 7.3 Voltage surge on JMarti line (50/100μs waveform)

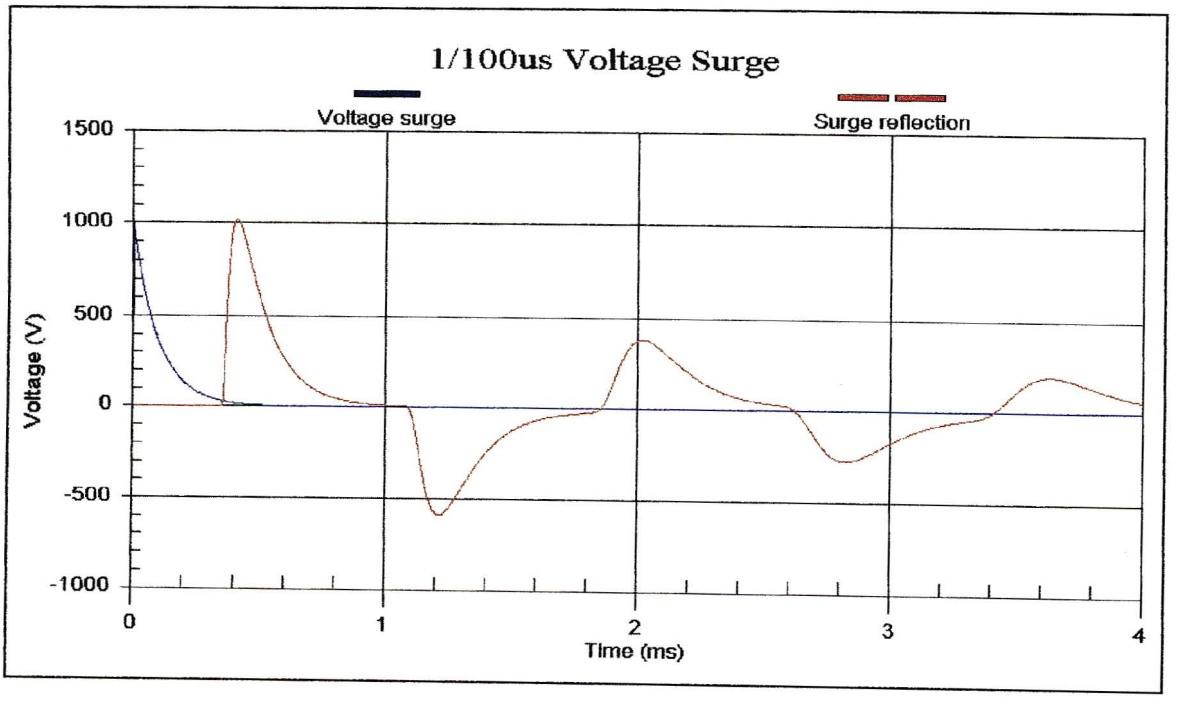

Figure 7.4 Voltage surge on JMarti line (1/100μs waveform)

Figure 7.3 and Figure 7.4 above show the effect of different wave front times. For the 50/100μs surge the peak voltage is 1.4kV and for the 1/100μs surge the peak voltage is 1.1kV.

Based on the assumption that the speed of the travelling voltage surge is approximately 300 x 10^6 m/s (speed of light), then the time taken for the surge voltage to reach the open end of the 100km line should be about 0.33ms. This can be seen by the delay time of the voltage reflection Figure 7.3 and Figure 7.4 above.

The characteristic impedance Z of the transmission line is given by (Grainger et al, 1994) :

$$Z = \sqrt{\frac{L}{C}} \quad (\Omega) \qquad (7.1)$$

where

$$L = 2 \times 10^{-7} \, \mathrm{Ln} \frac{d}{r} \quad (\mathrm{H/m}) \qquad (7.2)$$

and

$$C = \frac{2\pi\varepsilon}{Ln(d/r)} \quad (\mathrm{F/m}) \qquad (7.3)$$

For the phase Fox conductor as in the experimental project, the average distance d above ground is 9.2m and the radius r of the conductor is 0.42cm and ε is 8.85 x10^{-12} (assuming a relative permittivity of dry air equal to 1). Substituting these values into equation (7.1) and equation (7.2) provides L = 1.54 x 10^{-6} H/m and C = 7.23x 10^{-12} F/m respectively. Substituting these values for L and C into equation (7.1), provides a surge impedance of the line equal to 461Ω.

The amplitude of the voltage surge gets attenuated exponentially while travelling over the 100km section of line. The voltage *V* at a point *x* km away from source is given by (Grainger et al, 1994) :

$$V = V_0 e^{-0.5(R/Z + GZ)x} \qquad (7.4)$$

where V_0 is the initial magnitude of the surge voltage in volts

R the line resistance per km in ohms/km

G the leakage per km

Z the surge impedance in ohms

Substituting V_0 = 1 kV, R = 0.78 Ω/km, G = 0 (when assuming a lossless line) and x = 100km into equation (7.4) above yields V = 0.92 kV. For a lossless line the surge voltage will double at the end of the open circuit and will therefor be 0.92 kV x 2 = 1.84kV (Wadhwa, 1995).

In Figure 7.3 above it can be seen that for a 50/100μs voltage surge the peak voltage at the end of the line is only 1.4kV. The difference in amplitude is due to the skin effect on R and L, which the JMarti model in ATP does take into account. This is done by flagging the skin effect field in the JMarti model in ATP.

From (Kraus, 1992) the skin depth δ or depth of penetration of a conductor is given by :

$$\delta = \frac{1}{\sqrt{\pi f \mu \sigma}} \qquad (7.5)$$

where f is the frequency of calculation in Hz

μ is the permeability in H/m

σ is the conductivity in Ω^{-1}/m

Taking the values of f = 20kHz (50/100μs waveform) and using the average values for Aluminum of $\mu = 4\pi \times 10^{-7}$ H/m and $\sigma = 3.5 \times 10^{7}$ Ω^{-1}/m (Kraus, 1992); substituting these values into equation (7.5), we obtain that the skin depth at 20kHz is 601.5μm. Similarly for f = 1MHz (1/100μs waveform) we obtain a skin depth of 85.1μm. It can be seen that as the frequency increases (or the crest time decreases) so the skin depth decreases. The current flows closer to the surface of the conductor at higher frequencies.

The resistance R for the 1km of Aluminum conductor is given by (Hayt, 1994) :

$$R = \frac{L}{2\pi r \sigma \delta} \tag{7.6}$$

where L is the length of conductor in m

r is the radius of the conductor in m

σ is the conductivity in Ω^{-1}/m

δ is the skin depth in m

Substituting the relevant values into equation (7.6), the resistance of 1km Aluminum conductor for a 50/100μs surge is 1.8Ω and the resistance of 1km Aluminum conductor for a 1/100μs surge is 12.7Ω. It can be seen that the resistance increases as the skin depth decreases. This means that the resistance of the conductor increases for decreasing surge rise times. This explains the lower peak voltage of a 1/100μs surge than a 50/100μs surge.

7.2.5 Effect of Coupling and Corona

As discussed earlier, for the ATP simulations only single phase studies will be performed. In a practical three phase system there will be coupling between the phase conductors. Voltages will be induced in the other two phases due to coupling between the phase conductors. The effect of coupling is discussed in depth and equations presented to calculate the induced voltages in (Hileman, 1999) and (CIGRE, 1991).

Corona is the partial discharge that occurs when the electric field strength exceeds the ionization threshold for the air surrounding the conductor. When a large voltage surge appears on a transmission line due to lightning (direct or induced), then corona can occur on the line. Streamers emanate from the conductor increasing the effective radius of the conductor that increases the capacitance to earth. This results in a decrease in the velocity of propagation and the surge impedance of the conductor. The wave front is pushed back so that the steepness of the surge is decreased (Hileman, 1999).

From (Anderson, 1982), (CIGRE, 1991) and (Carneiro et al, 1991) the major effects of corona on a transmission line are :

- The corona sheath around the conductor increases the effective radius of the conductor and hence the capacitance of the line. This leads to a reduction in the steepness of the voltage surge.
- Corona (increase in resistance) does not effect the inductance of the line.
- Weather conditions have no significant influence on corona distortion.
- The tail of voltage surges is not influenced by corona.

It was found that only for severe direct lightning strikes would corona have to be taken into account for simulations (Nucci et al, 1995). Studies have been performed to investigate the influence of corona on induced voltages by describing the corona macroscopically as a charge-voltage diagram.. Work has also been performed to describe the effect of corona of induced voltages on distribution lines. For indirect voltages, the amplitude of the voltage may theoretically increase due to corona. It was found that the influence of corona was less important than the effect of ground resistivity if a linear charge-voltage diagram was used (De la Rosa, 1998).

The critical field strength E_0 for when corona starts is given by (Hileman, 1999) and is based on a CIGRE definition :

$$E_0 = 23\left(1+\frac{1.22}{d^{0.37}}\right) \quad \text{(kV/cm)} \qquad (7.7)$$

where d is the diameter of the conductor in cm.

Substituting d = 0.84cm for Fox conductor into equation (7.7) yields that E_0 = 52.9kV/cm. The corona inception voltage V_i for a single conductor can be estimated by (Hileman, 1999) :

$$V_i = \frac{Z_0 r E_0}{60} \qquad (7.8)$$

where Z_0 is the natural surge impedance of the conductor in Ω

r is the radius of the conductor in cm

E_0 is the critical field strength kV/cm

The natural surge impedance Z_0 of a single conductor radius r and at height h above the ground plane can be estimated by using the following equations (Hileman, 1999) :

$$Z_0 = \sqrt{\frac{L}{C}} \quad (\Omega) \tag{7.9}$$

where

$$L = 0.2 \, \mathrm{Ln}\frac{2h}{r} \tag{7.10}$$

and

$$C = \frac{10^{-3}}{18 \, \mathrm{Ln}\frac{2h}{r}} \tag{7.11}$$

Substituting r = 0.42cm and h = 920cm into equation (7.10) and equation (7.11) and then substituting the resultant values for L and C into equation (7.9), provides a surge impedance of 503Ω. Substituting the relevant values into equation (7.8) provides a corona inception voltage of 186kV for Fox conductor 9.2m above ground.

The corona radius envelope for a single conductor was estimated in (Anderson, 1982) by a simple derivation of Gauss's law. The corona radius R_C can be estimated by :

$$R_c \, \mathrm{Ln}\frac{2h}{R_c} = \frac{V}{E_0} \tag{7.12}$$

where h is the height of the conductor above ground in m

V is the voltage applied to the conductor in kV

E_0 is the critical field strength in kV/cm

In (Anderson, 1982) Figure 12.5.3 provides a graph of corona diameter d versus V/E_0 for different conductor heights h above ground curves are shown. For the ATP simulations the 10m curve was chosen and a set of (V/E_0, d) co-ordinates chosen.

The value for E_0 = 52.9kV/cm was used as calculated in equation (7.7). From this available data the curve for a conductor 10m above ground was plotted in Figure 7.5 below.

The diameter of Fox conductor with no corona onset is 0.0084m. The rapid increase in diameter due to corona for increasing line voltages can clearly be seen in Figure 7.5. A critical corona gradient E_0 = 15kV/cm was proposed as a reasonable representative value for use in lightning performance simulations (Anderson, 1982).

For the ATP simulations the effect of corona is simulated by increasing the conductor diameter. This is done through an iterative process where the simulation is run and the line voltage is measured. The curve in Figure 7.5 below is then used to calculate the effective corona envelope diameter and the radius of the conductor in the JMarti model in ATP is increased accordingly.

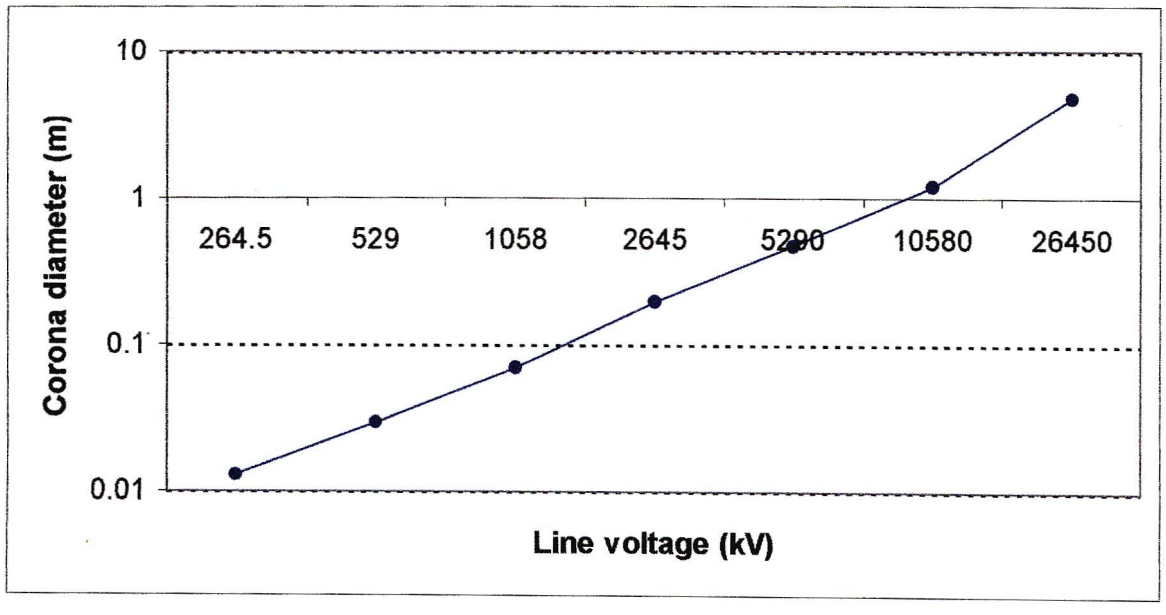

Figure 7.5 Graph of corona envelope diameter for various line surge voltages
Conductor 10m above ground modified for this exercise taken from (Anderson, 1982)

The effect of corona is simulated by using a simple ATP circuit as in Figure 7.2 for a conductor length of 500m. Figure 7.6 below shows the effect of corona on the line voltage. The voltage is less with corona due to the increased effective resistance of the conductor. The simulation results in (Van Schalkwyk, 2001) show that the effect of corona on a 300kV BIL reticulation line can be ignored and that the longer the duration of a voltage surge, the less the influence that corona has on the surge.

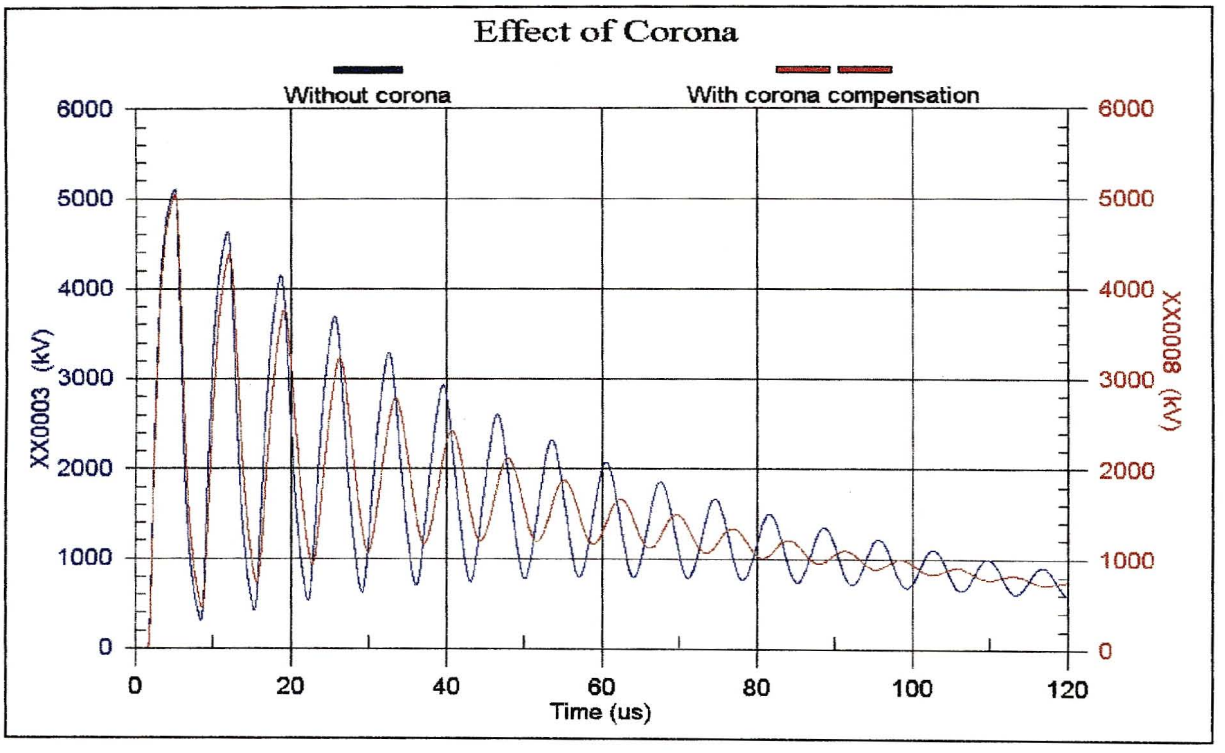

Figure 7.6 Effect of corona on the voltage of a 500m line
(with and without corona compensation)

7.2.6 Woodpole Structure Insulation

The insulation co-ordination philosophy applied by Eskom on its reticulation woodpole lines is to use the wood itself as part of the overall phase-to-phase and phase-to-earth insulation. As discussed in chapter 3 a BIL of about 300kV phase to earth is obtained by a 600mm wood path gap in series with the crossarm insulator and an earthed down lead of the pole. For the experimental project at Glencoe the crossarms were bonded. The 600mm wood path was on the main vertical pole.

The insulation strength of the wood depends on factors such as (Darveniza, 1980) and (Britten, 1992) :

- Moisture content of wood and the presence of rain
- Type of creosote treatment used for the wood
- Age of the wood
- Type of wood species
- Length of wood gap

The most important factor influencing the insulation strength of the wood is the moisture content of the wood. The impulse strength of wood under wet or rain conditions is on average 40% lower than dry wood (Geldenhuys, 1992b). The total impulse strength U_T of a insulator wood path combination is discussed in (Britten, 1992) and is based on the comprehensive work of (Darveniza, 1980) :

$$U_T = \sqrt{U_W^2 + U_I^2} \qquad (7.13)$$

where U_W is the U50 flashover voltage of the wood path for given length in kV
U_I is the U50 flashover voltage of the insulator in kV

The impulse strengths are given as U50 values (voltage for which there is 50% probability of flashover). Usually the U50 for an 11kV insulator is about 150kV and the average impulse strength of dry wood is about 500kV/m for Pine and Eucalyptus (Britten, 1992).

Substituting these values into equation (7.13) above and solving for U_W provides a value of U_W = 260kV which means that a dry wood path of 520mm is required. The specified 600mm wood path would cater for rain and wet conditions when the insulation strength of the wood is reduced by 30 to 40% (Gaunt et al, 1989).

Figure 7.7 below shows a simple impedance model of the insulator wood path combination subjected to lightning impulses proposed by (Darveniza, 1980). Such a model can be used to determine the relative distribution of voltage across the wood path and the insulator.

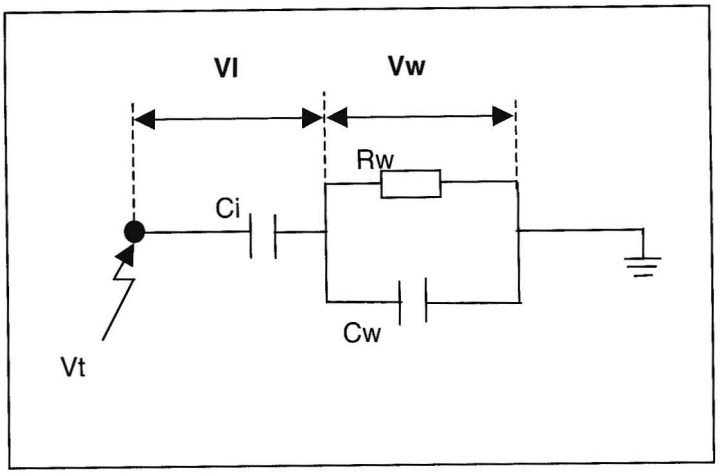

Figure 7.7 Simple impedance model of insulator wood path combination phase-to-ground model taken from (Darveniza, 1980)

C_i = 15pF/m to 30pF/m per disc

C_W = 4pF/m (dry) to 30pF/m (wet)

$R_W = 10^5$ Ω/m (wet) to 10^7 Ω/m (dry)

The flashover voltage V_T of the total combination is given by the following relationship (Darveniza, 1980) :

$$V_T = V_I . (C_I + C_W) / C_W \qquad (7.14)$$

Equation (7.14) only holds if $R_W(C_I + C_W) > 250\mu s$ (for dry or seasoned wood). Research has shown that voltage breakdown occurs mainly along the surface of the wood and not through air flashover (Darveniza, 1980). When a lightning impulse flashover occurs across the surface of the wood path then the resulting discharge of arc causes a residual voltage to be developed along the wood. This arc voltage can prevent the flow of power frequency fault current to ground or between phases. The flow of power frequency current may cause the network breaker to auto-reclose (ARC). This is not part of the scope of the dissertation but detailed information can be found in (Gaunt et al, 1989) and (Van Niekerk, 1987).

Various papers deal with the simulation of the voltage flashover of the insulator wood path combination. These papers provide modelling the voltage flashover via either the integration method or the leader development model (Darveniza et al, 1979b), (Funabashi, 1997) and (CIGRE, 1991).

For the ATP simulations a simple voltage controlled switch with a flashover voltage of 300kV was used as suggested in (Darveniza et al, 1979b). The switch is initially open and will close whenever the flashover voltage of 300kV is reached. The switch will stay closed for a preset length of time. The length of time is discussed in (Darveniza, 1980) and (Leuven, 1992).

Figure 7.8 below shows the ATP circuit used to demonstrate the 300kV BIL effect. The 500m of Fox conductor is modeled with the JMarti frequency dependent transmission line model. The 5Ω lumped resistance represents the sum of the resistance of the down lead conductor and the transient resistance of the earth electrode resistance for a 1.5m Copper rod. The chapter 7.3.2 deals with this subject in more detail.

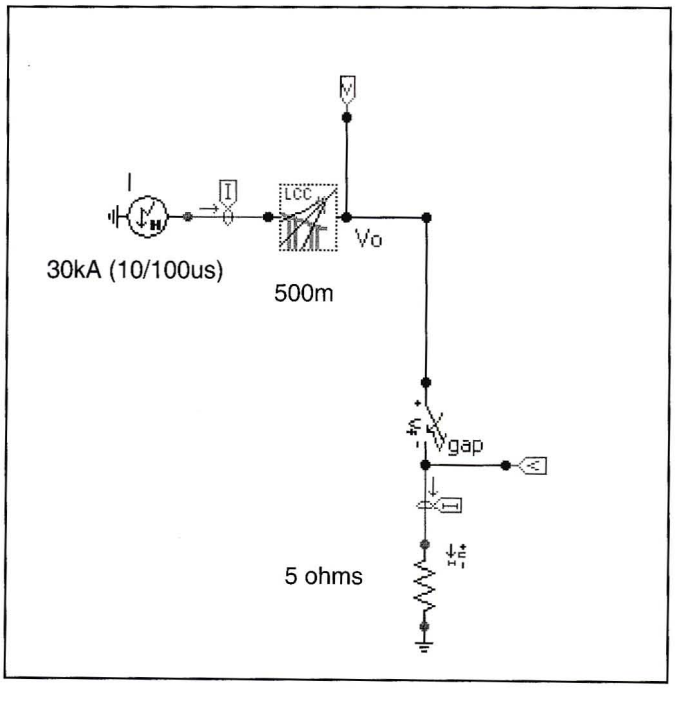

Figure 7.8 ATP circuit to simulate 300kV BIL of woodpole structures

In Figure 7.9 below it can be seen that the resistance of down conductor and earth electrode only comes into effect once voltage flashover occurs (300kV voltage controlled switch closes). The current flows to ground and the effect of reflections come into effect.

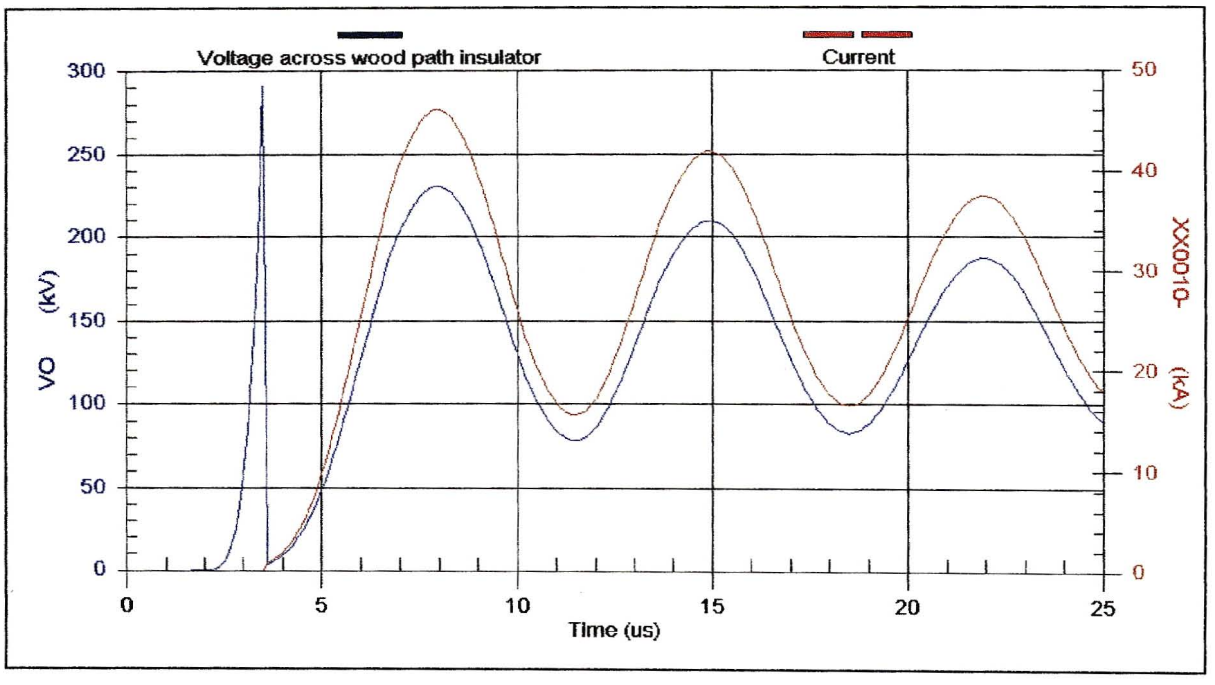

Figure 7.9 Voltage flashover of 300kV BIL woodpole

7.3 Down Conductors and Earth Electrodes

7.3.1 Down Conductors

If a standard Eskom woodpole length of 11m is assumed with a ground plant depth of 1.8m and 600mm for the woodpath gap, then a BIL down conductor average length of 8.8m may be assumed for calculations.

A 4mm diameter galvanised steel wire conductor is used as the down lead to the copper rod. The down conductor is secured at the top of the pole with a circumferential stainless steel strapping. Due to the relatively short length of the down conductor, it is not necessary to model the conductor as a single phase transmission line with a characteristic impedance and propagation velocity as the travel time τ is very short. Assuming the speed of light of 3 x 10^8 m/s, then the τ for the 8.8m down conductor is 29.3ns.

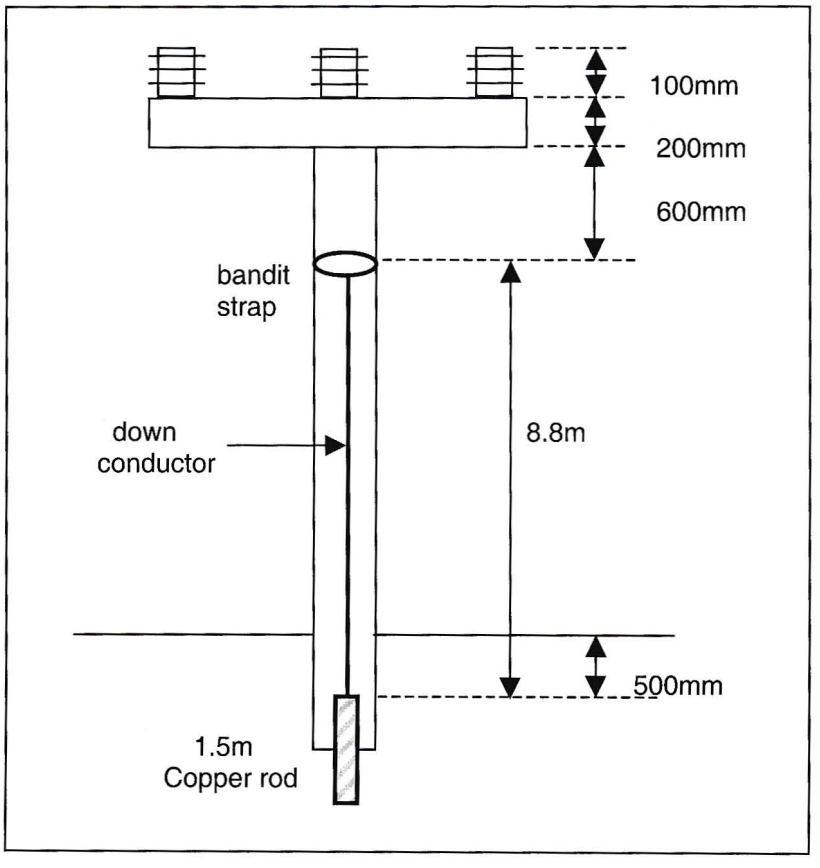

Figure 7.10 Typical Eskom 11m woodpole T-structure

The paper by (Chisholm et al, 1989) provides an equation for surge impedance between two parallel plates based on the cylindrical waveguide model as discussed in (Marcuvitz, 1951) :

$$Z=60\frac{h}{r} \qquad (7.15)$$

where h is the distance between the ground planes in m

r is the radius of the wavefront in m

For lightning calculations, the ground-plane surge impedance can be modelled as a lumped component. In this case an inductance L with the representation as non-causal may be used. In other words, the far end of the inductor "knows" that a current has been injected immediately, rather after a propagation delay.

This approximation is adequate when the rise time of the current is slow relative to the propagation delay. The inductance L can be obtained by (Chisholm et al, 1989) :

$$L = \int_{\tau}^{T_C} Z(t)\,dt \qquad (7.16)$$

where Z(t) is the surge impedance in Ω

T_C is the time to crest of the current in μs

τ is the propagation delay or travel time in μs

Substituting equation (7.16) into equation (7.15) and re-arranging allows that L can be written as (Chisholm et al, 1989) :

$$L = 60\,\tau\,Ln\left(\frac{T_C}{\tau}\right) \qquad (7.17)$$

The above equation provides the inductance L of the down conductor varying with the crest time of the current. Equation (7.17) shows that the inductance increases non-linearly with the time to crest of the current. The voltage produced will be a product of L and dI/dt. The down conductor impedance can be obtained by dividing the value for L by the crest time. Figure 7.11 below shows how the 8.8m down conductor's impedance varies with time to crest values.

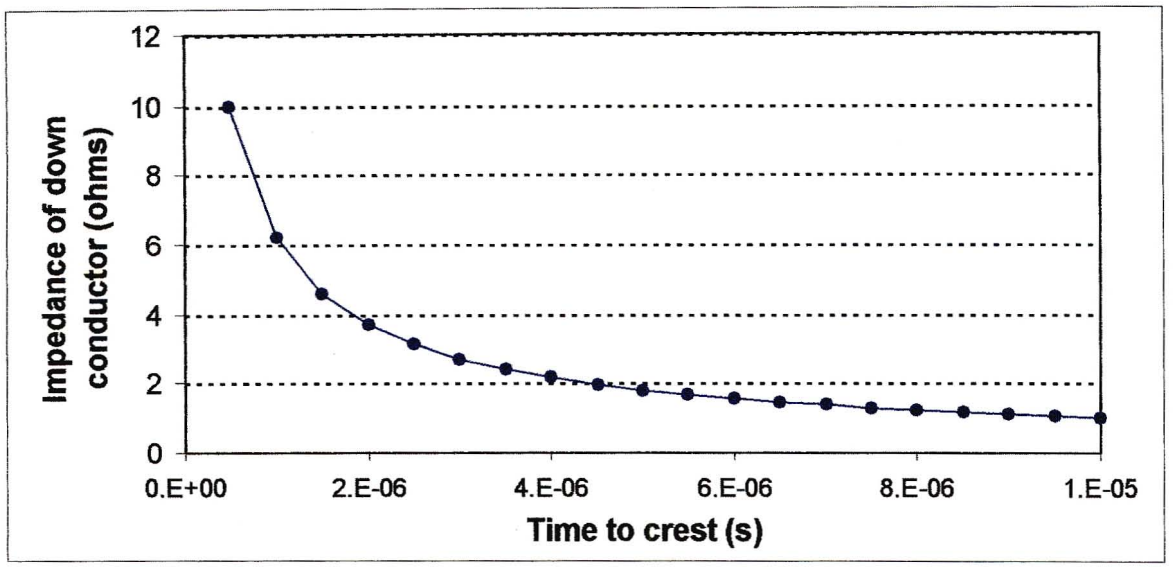

Figure 7.11 Non-linear impedance of down conductor modified from (Chisholm et al, 1989)

For the ATP simulations the down conductor will be represented as a lumped resistance varying with rise times based on the curve in Figure 7.11 above. For example, a typical rise time in the simulations will be 5μs which will result in a resistance of 1.8Ω for the down conductor.

7.3.2 Earth Electrodes

Normal earthing of wood pole structures and transformer installations is designed around the power frequency resistance and is normally below 100Hz. These earth electrodes are concentrated electrodes (Nixon et al, 1998). This earth electrode resistance is termed the low frequency, low current resistance R_0 or leakage resistance. This is the resistance that can be measured by the Fall of Potential method and that is usually referred to during normal power frequency operation of the network.

A 1.5m Copper rod with diameter 16mm is used as the earth electrode for the typical wood pole structures. The leakage resistance R_0 can be calculated by (Hilemann, 1999) :

$$R_0 = \frac{\rho}{2\pi L}\left[Ln\frac{4L}{r} - 1 \right] \qquad (7.18)$$

where ρ is the soil resistivity in Ω.m

L is the length of the rod in m

r is the radius of the rod in m

The effect of soil resistivity on the leakage resistance of the 16mm diameter rod can be seen in Figure 7.12 below. As the soil resistivity increases so the leakage resistance of the electrode also increases.

For transformer installations with separate MV and LV earthing arrangement, the electrode of the MV earth is a three point star (TPS) electrode configuration or otherwise commonly referred to as a "crows foot". This is also the electrode of the surge arrester as the arrester is connected to the earth stud of the transformer.

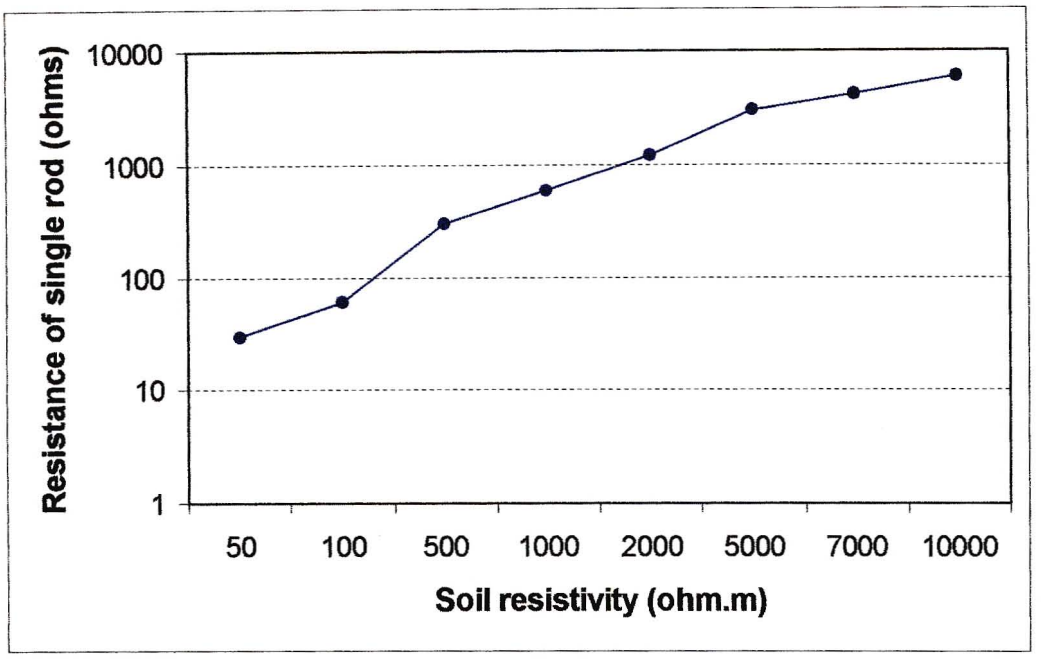

Figure 7.12 Resistance of 1.5m Copper rod for different soil resistivities (based on equation (7.18))

In (Geldenhuys, 1992a) the resistance curve R of a 5m crows foot electrode for different soil resistivities ρ is plotted. Some of the (ρ, R) co-ordinate sets were sampled and a trend line with the corresponding equation fitted to the sampled points in Figure 7.13 below.

It is well established that an earth electrode behaves differently under transient conditions such as lightning surges than a power frequency fault. The principal factors effecting the transient behaviour are (Nixon et al, 1998) :

- Geometry and arrangement of the earth electrode
- Dielectric nature of the soil
- Electromagnetic interaction with adjacent conductors
- Non-linear time varying effects of soil ionisation

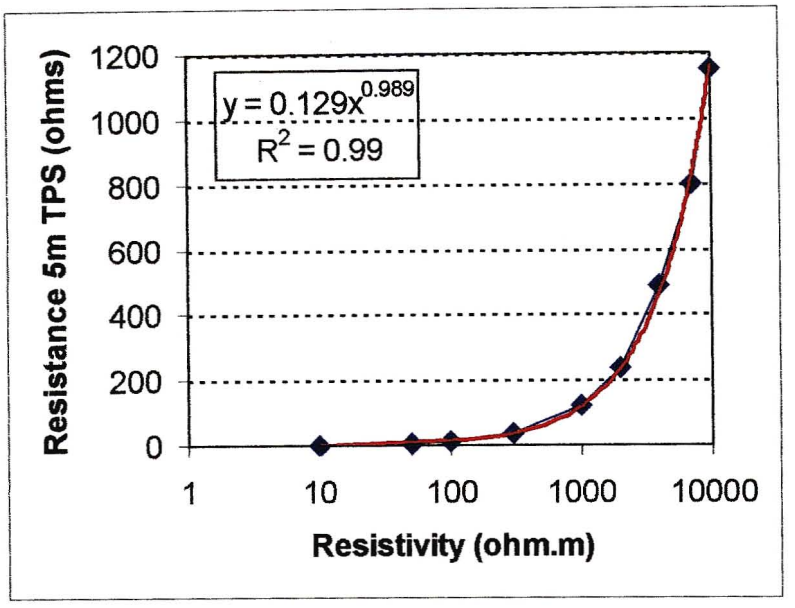

Figure 7.13 Resistance of a 5m crows foot earth electrode taken from (Geldenhuys, 1992a)

One of the significant effects of an earth electrode under transient conditions is that the surge impedance of the electrode can be higher or lower than the leakage resistance. The resistivity of the soil has a profound effect on whether or not soil ionisation occurs. Due to the high average soil resistivities in South Africa (500-5000Ω.m) it is essential that the non-linear effects caused by soil ionisation under transient conditions are included when performing lightning studies (Nixon et al, 1998)

Experimental and analytical evidence shows that lightning surge currents ionise the air in the soil. This ionisation process tends to increase the contact area of the earth electrode with the surrounding material. This larger contact area results in a lower resistance and less voltage stress per unit current. It is important to model the electrode under transient conditions (Chisholm et al, 1989) and (Menter et al, 1994).

The Korsuncev Similarirty Method (KSM) is presented in (Chisholm et al, 1989). This approach provides a general method for calculating the surge impedance of any earth electrode or footing resistance configuration. The soil is assumed to be homogeneous for the calculations.

Footing resistances of different electrode geometries can be represented by two dimensionless parameters Π_1 and Π_2 :

$$\Pi_1 = \frac{s R_f}{\rho} \tag{7.19}$$

$$\Pi_2 = \frac{\rho I}{E_0 s^2} \tag{7.20}$$

where s is the characteristic distance from the centre to the outermost point of the electrode in m

ρ is the soil resistivity in Ω.m

E_0 is the critical breakdown gradient (300 to 1500kV/m)

I is the instantaneous value of current in kA

R_f is the footing resistance in Ω

For each electrode geometry a value Π_1^0 is defined in terms of its low frequency, low current resistance. The characteristic distance s and surface area A are calculated and the value obtained for Π_1^0 from equation (7.21) below is substituted into equation (7.19) to obtain the R_g value of the earth electrode.

$$\Pi_1^0 = 0.4517 + \frac{1}{2\pi} Ln\left(\frac{s^2}{A}\right) \tag{7.21}$$

All electrodes behave like a hemisphere once ionised beyond a critical distance. The ionisation gradient in the Korsuncev model represents the average field intensity within this hemispherical ionised region. The transition between low current and ionised response occurs at the intersection of the electrode dependent value Π_1^0 and the independent portion of the (Π_1 - Π_2) criteria curve. A least fit of the (Π_1 - Π_2) curve (in the restricted range of 0.3 to 10) provides the following power law relation (Chisholm et al, 1989) :

$$\Pi_1 = 0.2631 \Pi_2^{-0.3082} \tag{7.22}$$

For higher currents equation (7.20) provides a value for Π_2 using E_0 = 1000kV/m as a median value in the KSM. As long as the Π_1 value from equation (7.22) is lower than the Π_1^0 value, then the ionisation zone has spread beyond the characteristic distance s and the surge reduced resistance can be calculated from equation (7.19).

A power law regression between the soil resistivity ρ and the critical breakdown gradient E_0 was proposed by (Oettle, 1987) :

$$E_0 = 241\rho^{0.215} \qquad (7.23)$$

In (Geldenhuys et al, 1987) a sensitivity analysis of the parameters of the KSM (equation (7.19) and equation (7.20)) was performed. It was found that E_0 had the smallest effect on the impulse impedance of the earth electrode.

The KSM does not take into account the time effects. This problem is addressed by (Geldenhuys et al, 1987) with the introduction of an instantaneous impedance equation at 6μs after impulse inception. This time dependency will not be looked at in the ATP simulations. A dynamic model which includes soil ionisation and de-ionisation time constants and a critical spark over voltage gradient so that both current and time dependency can be taken into account was proposed by (Liew et al, 1974). A more in depth discussion on detailed transient electrode modelling is provided by (Nixon, 1999).

The KSM was implemented in an Microsoft Excel ™ Spreadsheet and a parametric study performed for a 1.5m single rod and a 5m three point star earth electrode configurations. The results are shown in Figure 7.14 and Figure 7.15 below. The curves show the effect of different soil resistivity values on the transient resistance of the two types of electrodes.

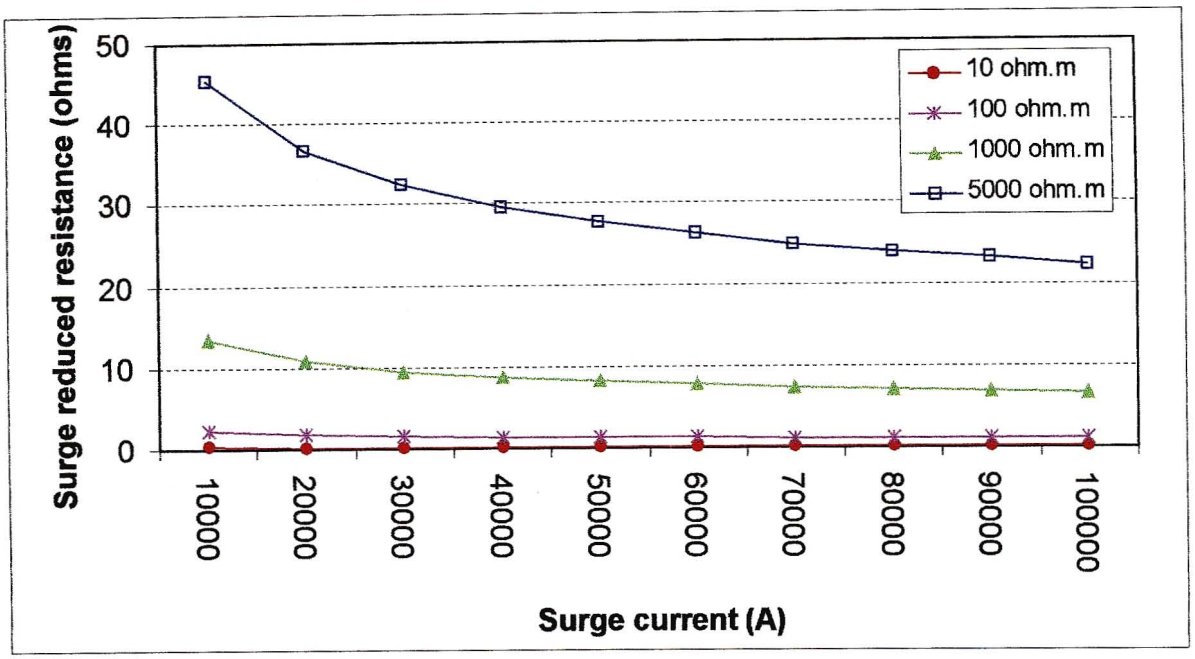

Figure 7.14 Surge reduced resistance of single 1.5m rod based on KSM

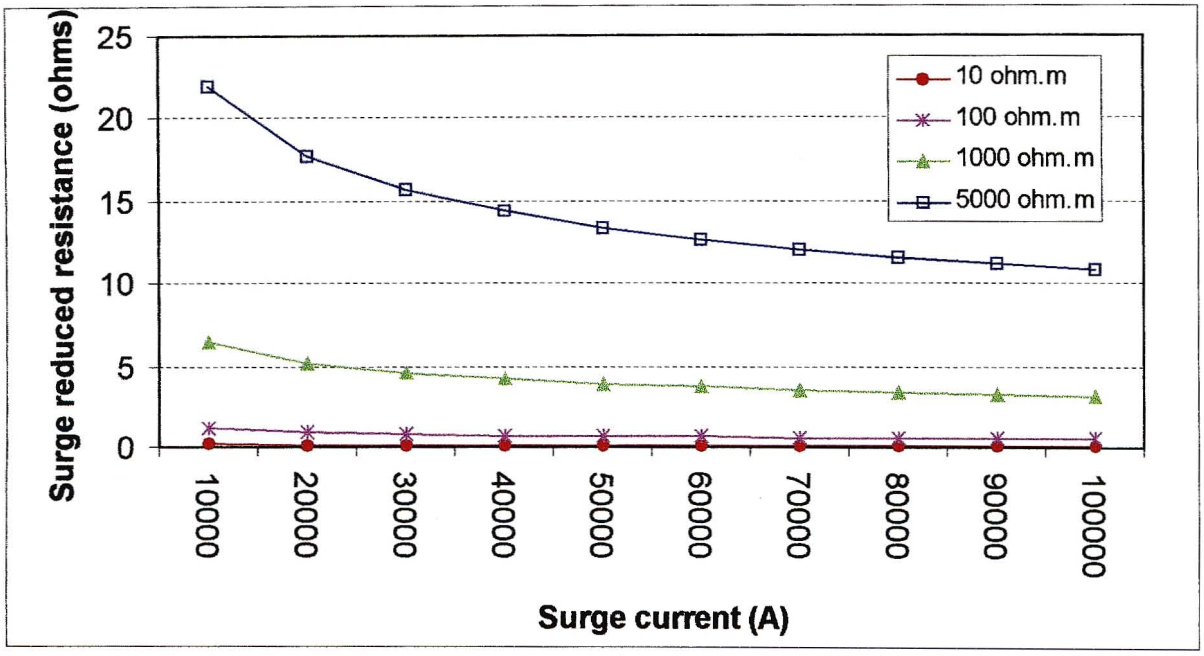

Figure 7.15 Surge reduced resistance of 5m crows foot based on KSM

The difference between the surge reduced resistance of a single vertical rod and a crows foot configuration can be seen below in Figure 7.16.

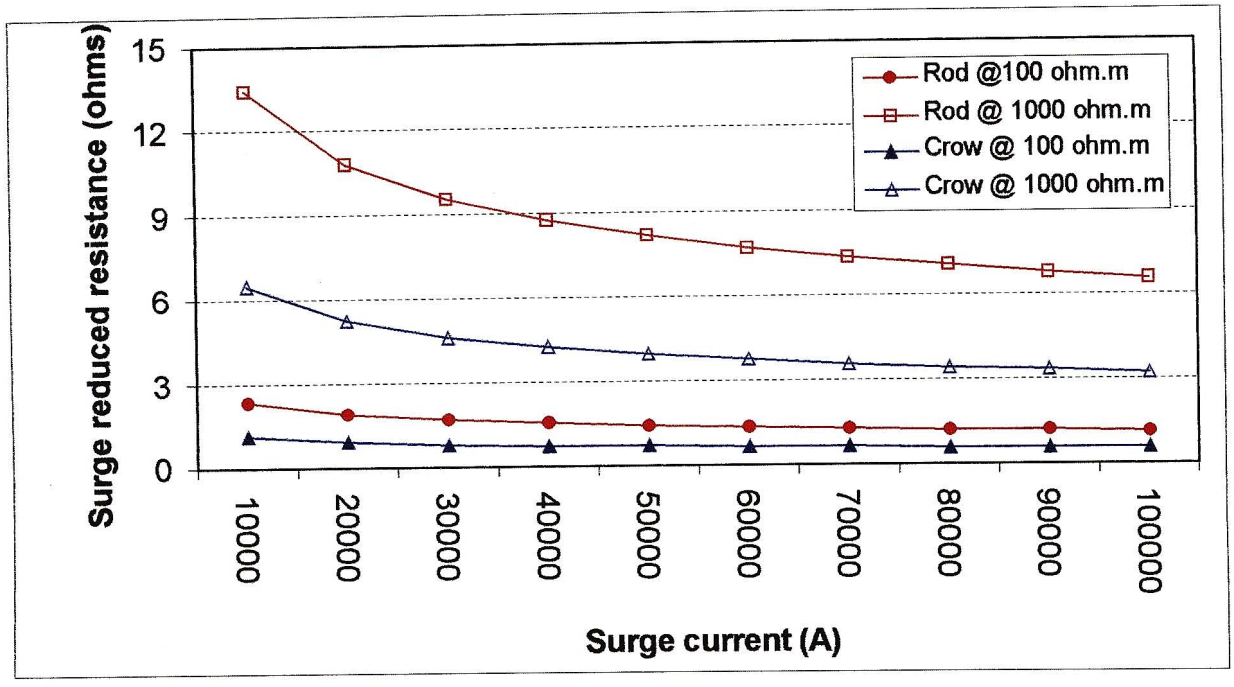

Figure 7.16 Comparison of transient impedance of single rod and crows foot electrode based on KSM

In the ATP simulations a parametric study was performed by varying the pole electrode resistances from 5Ω to 80Ω and the transformer earth electrode resistance from 2Ω to 20Ω. These values were the surge reduced resistances (based on the KSM) that were assumed to stay constant during the each lightning incident (Darveniza et al, 1979). This was to take into account the initial low frequency low current resistances with effects of soil resistivity and surge current. Refer to Chapter 6 for typical measured transformer earth electrode resistances.

It was proposed in (Anderson, 1982) that if the standard deviation of measured pole footing resistances was less than half the average value, then an average value of pole footing resistance may be used with an acceptable error in the simulations. In (Hileman, 1999) it was proposed that the average resistance value plus one or two standard deviations should be used to provide more conservative results for the simulations.

The soil was assumed to be homogeneous in the ATP simulations to simplify the modelling and if layered then average resistivity of the various layers was assumed. The model is valid for typical lightning impulse current frequencies and will loose accuracy above 1 MHz since the frequency dependent electrical properties of soil are ignored in the model (Nixon, 1999). The frequency dependent properties of soil are not taken into account in the simulations. provides A summary of the important issues when taking into account the frequency dependent effects of soil is discussed in (Van Schalkwyk, 2001).

7.4 Pole Mounted Transformer

To accurately model the behaviour of the pole mounted power transformer under lightning conditions, a detailed high frequency (HF) transformer model is required. The non-linear behaviour and the frequency dependent effects must be taken into account at high frequencies. The basic transformer representation in ATP (BCTRAN) does not take into account the HF behaviour of a transformer. The BCTRAN model can only reproduce the response of the transformer at the frequency (usually 50Hz) at which the short circuit and open circuit tests are conducted.

The effect of the frequency dependent copper and iron losses and the effect of stray capacitances are not taken into account by the ATP transformer model (Leuven, 1992).

The transformer is a complex arrangement of closely spaced coils around an iron core. This arrangement introduces capacitances (inter winding and winding to ground) and inductances. At high frequencies the capacitance of the winding comes into effect. Transformers have a number of resonant frequencies, with one dominant frequency in the 5-30kHz range and other resonances at other frequencies. Lightning surges may excite these resonances and cause voltage amplification inside the windings (Woivre et al, 1993).

A comprehensive background literature survey of the high frequency modelling of transformers is provided by (Kelly, 1996). The work provides information on the HF transformer model (based on measurements performed in the laboratory, mathematical processing in Matlab® and EMTP simulation results) for the transfer of overvoltages from primary to the secondary side of the transformer. The HF model presented could be used as an add on module or a stand alone module of a transformer. A high frequency model of a transformer based on the coupled coils level representation to be implemented in EMTP is provided by (Chimklai et al, 1995).

It was proved that for shell type transformers that the windings behave as a linear system without saturation effects in the period of time immediately following the beginning of the impulse (Woivre et al, 1993). A simple capacitive model is used to demonstrate that the lower the capacitance of the winding, the higher the resultant overvoltage.

It was found in (Morched et al, 1993) that the modelling of the distributed stray capacitances along the windings with lumped capacitances connected across the terminals of the transformer could not reproduce the behaviour of the transformer beyond the first resonance frequency.

When modelling a transformer for lightning surge studies on a network, a lumped capacitance may be used to represent the transformer. This only applies when the voltage transfer from the MV to LV side is not important. The constraints of using a lumped capacitance value representation of a transformer as discussed in (Woivre et al, 1993) and (Morched et al, 1993) are important. A lumped capacitance value of between 1nF and 2nF representing the pole mounted transformer is proposed by (Richter, 1999). A capacitance value of 1nF was used by (Holdalen, 1993) to represent the transformer.

For the ATP simulations a lumped capacitance was used to represent the pole mounted transformer. The drop out fuse links that are normally found on the transformer structure to isolate a faulty transformer from the network was not modeled. The fuse has a very low impedance. The down conductor used to earth the transformer, typically 12mm^2 solid copper conductor was modeled.

A similar model as used for the woodpole down conductors may be used in the simulations. A lumped resistance representing the sum of the transient earth electrode resistance (based on the work in chapter 7.3.2) and the non-linear impedance of the down conductor was used in the ATP simulations.

Figure 7.17 shows an ATP circuit used to simulate the effect of various lumped capacitor values representing the transformer. It must be noted that for this exercise the down conductors and earth electrode resistance was not modelled. The intention was to perform a simple simulation exercise based on the work in (Richter, 1999) to look at the effect of the transformer capacitance values.

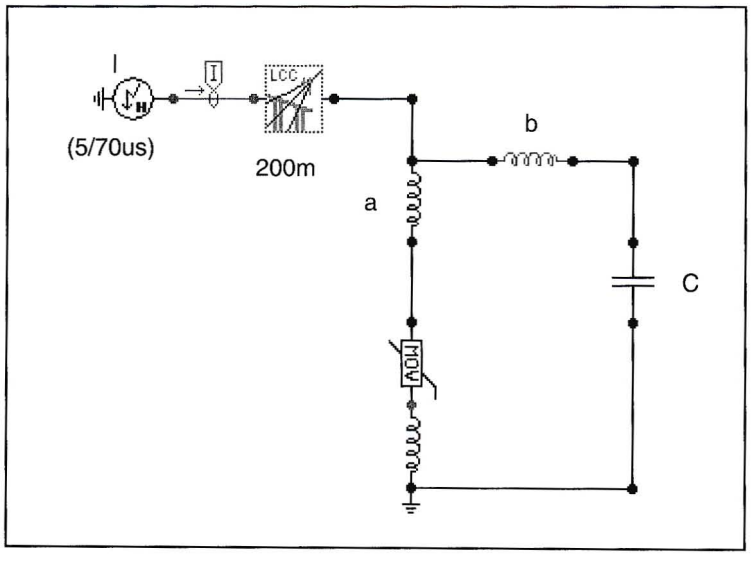

Figure 7.17 ATP circuit to measure the effect of various capacitor C values

a is the connection between the phase conductor and surge arrester. For this exercise a was assumed to be an average length of 2m.
b is the separation distance between the transformer and arrester and was assumed to be small (< 0.5m) as the majority of the surge arresters are mounted on the transformer tank. For this exercise b was assumed to be 0.5m.
C is the capacitance value representing the capacitance to ground of the primary winding

An inductance of 1μH/m as a general rule of thumb was used to calculate the inductance of the connection. The voltage to ground U_C was measured for various values of capacitance C.

It was found that the effect of the capacitance C was to cause voltage oscillations in conductors a and b (Richter, 1999).

From the results in Figure 7.18 it was decided to choose a capacitance C value of 2nF to represent the pole mounted transformer for future ATP simulations.

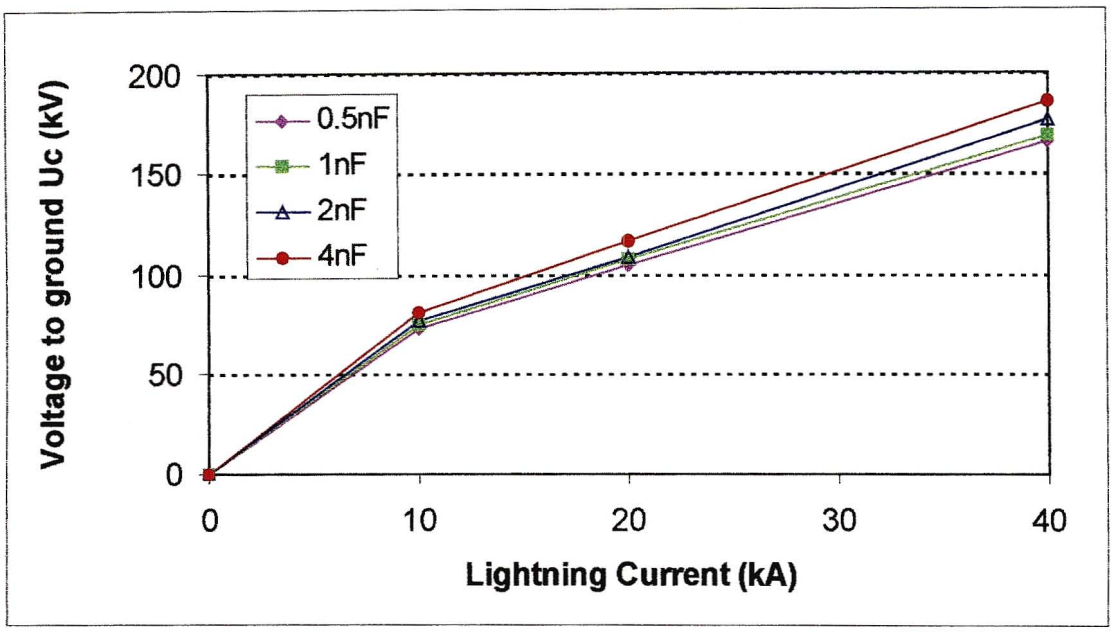

Figure 7.18 Effect of various capacitance C values on the voltage to ground Uc

The margin of protection (MP) for insulation co-ordination studies is defined (based on Figure 7.17) as (IEEE, 1991) :

$$\% MP = \left(\frac{BIL}{V_D + V_A} - 1 \right) x\ 100 \qquad (7.24)$$

where BIL is the insulation level of an 11kV transformer (95kV according to Table 3.1)

V_D is the discharge voltage of the surge arrester in kV

V_A is the inductive volt drop due to connection a in kV

Typically for high lightning density countries such as South Africa, a MP of 20% is recommended (IEEE, 1991). This can be expressed as :

$$V_D + V_A \leq 0.8 \times BIL \qquad (7.25)$$

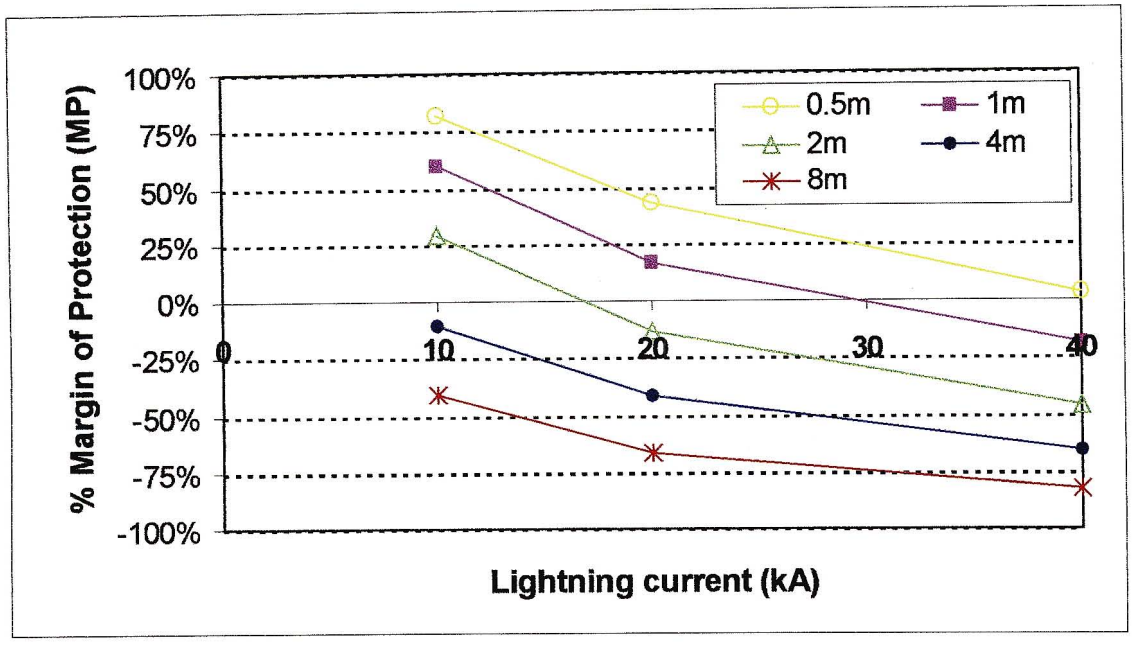

Figure 7.19 Effect of conductor length a on the margin of protection (MP)

ATP simulations were performed based on the circuit in Figure 7.17. In Figure 7.19 above it can be seen that the recommended MP may be very easily exceeded for conductor a lengths of 2m and more. This indicates that the tap off conductor to the surge arrester should be as short as possible. The separation distance b between the transformer and arrester should also be kept as small as possible (IEEE, 1991).

7.5 Surge Arresters

There are two main types of surge arrester models used to represent an arrester in transient simulation studies. Both the CIGRE and IEEE models produce the desired V-I characteristics and are both sensitive to the effect of increase in crest voltage.

7.5.1 CIGRE Surge Arrester Model

The WG 06 of CIGRE SC 33 proposed a simple equivalent circuit of a surge arrester for protection performance as in Figure 7.20 below.

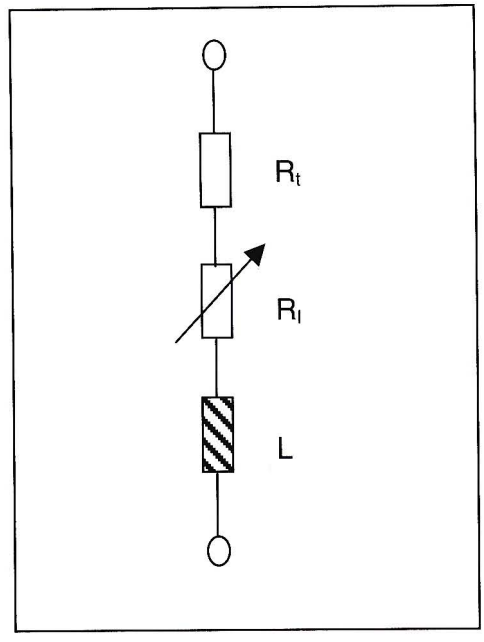

Figure 7.20 Simplified equivalent circuit of a surge arrester for protection performance taken from (Hileman et al, 1990)

where R_t is the turn on resistance. This resistance represents the conduction time delay. which results in a voltage spike or overshoot in the residual voltage.

R_l is the steady state resistance. This resistance can be determined from residual voltage measurements at different current amplitudes from the manufacturer data sheets.

L is represents the inductance of the current path through the surge arrester.

For the ATP simulations the turn on resistance R_t of the arrester model was ignored as most of the simulations occurred very high up in the non-linear range (Region 3) of the V-I curve of the arrester. It was assumed that the inductance L of the arrester defined the overshoot of the residual voltage and not the time delay in the conduction mechanism (Hileman et al, 1990).

The V-I characteristic curve was obtained from measured discharge voltage data for an 8/20μs current waveform from an 11kV surge arrester manufacturer A data sheet. An inductance of 1μH/m of arrester length was suggested by (Hilemann et al, 1990).

7.5.2 IEEE Surge Arrester Model

The IEEE WG 3.4.11 proposed a frequency dependent model for a surge arrester based on measured data. The arrester model took into account that the discharge voltage was a function of both rate of rise and magnitude of the current conducted by the arrester. The advantage of the model was that the parameters of the components were generated from the arrester's manufacturer published data sheet. The voltage response of the model was accurate for current surges with front times of 0.5μs to 45μs (IEEE, 1992).

The discharge voltage peak for a 1μs rise time current surge is about 8-12% greater than for a 8/20μs waveform with the same current magnitude. The discharge voltage peak for a 45-60μs rise time current surge is about 2-4% greater than for a 8/20μs waveform with the same current magnitude (IEEE, 1991). A more sophisticated model is required than the simple static non-linear resistance (V-I curves) normally used in transient simulations.

The arrester model as proposed in (IEEE, 1992) was implemented by (Ikmo et al, 1996) and (Fernadez et al, 2001) with slight modifications based on the required application and actual measured data of the particular arrester under study. Both papers claim to have achieved accurate simulation results using their modified model.

A frequency dependent surge arrester model based on the IEEE WG model was proposed by (Pinceti et al, 1999). The model is shown in Figure 7.21 below and is a simplified form of proposed model in (IEEE, 1992). The advantage of this model is that no iterative correction is necessary to identify the parameters of the model.

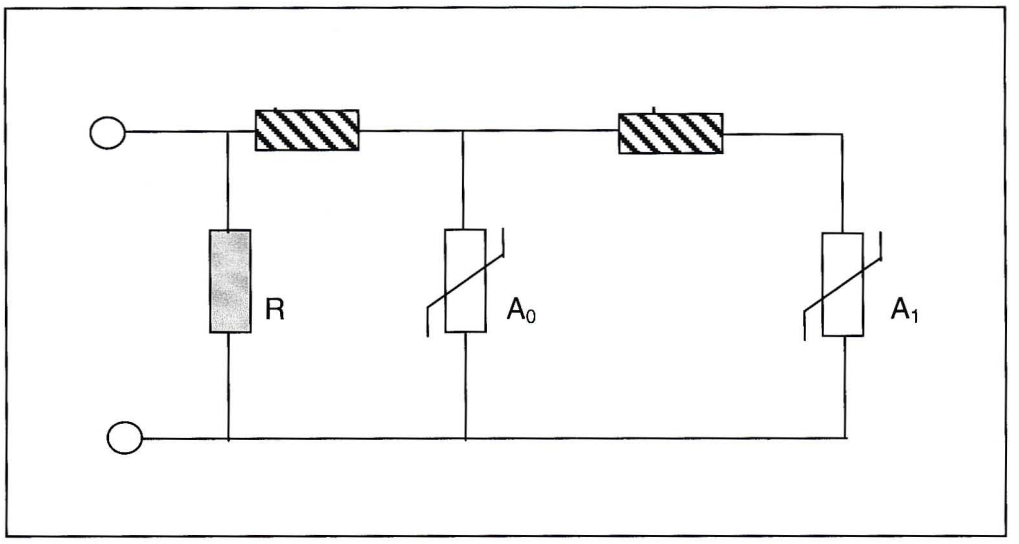

Figure 7.21 Frequency dependent model of surge arrester taken from (Pinceti et al, 1999)

R is the convergence resistor and is recommended to be about 1MΩ to prevent numerical oscillations in a digital transient program.

L_0 and L_1 in μH are inductive elements based on the residual voltage test results from the arrester data sheet.

$$L_0 = \frac{1}{12} \cdot \frac{V_{r1/T2} - V_{r8/20}}{V_{r8/20}} \cdot V_n \qquad (7.26)$$

$$L_1 = \frac{1}{4} \cdot \frac{V_{r1/T2} - V_{r8/20}}{V_{r8/20}} \cdot V_n \qquad (7.27)$$

V_n is the arrester rated voltage which is 12kV for the arrester used in the ATP simulations.

$V_{r1/T2}$ is the residual voltage for a 10kA fast front current waveform (1/T2μs). This is obtained from the arrester data sheet. The decay time T_2 is not explicitly written because different manufacturers may use different values. This is not a problem as the peak value of the residual voltage appears on the rising front of the impulse. For Eskom distribution class arrester specification, the fast front current is defined with a (1/5μs) waveform (SCSSCAAN5, 2000). An average value from various manufacturer data sheets of 44kV was used.

$V_{r8/20}$ is the residual voltage for a 10kA (8/20μs) current waveform. An average value of 40kV was used from different manufacturers.

Solving for equation (7.26) and equation (7.27) above provides the values for $L_0 = 0.1\mu H$ and $L_1 = 0.3\mu H$.

A_0 and A_1 represent the non-linear characteristics based on the normalised curves in per unit values from (Pinceti et al, 1999). These curves were proposed by IEEE WG 3.4.11 and are referred to the peak value of the residual voltage measured during a discharge test with various amplitude (8/20μs) lightning current waveforms. The resistance of A_0 is greater than the A_1 resistance for any given current. The faster the current surge, the higher the residual voltage. This is because high frequency currents are forced by the L_1 inductance to flow more in the A_0 resistance than in the A_1 resistance.

Table 7.3 A_0 and A_1 p.u values used in arrester model taken from (Pinceti et al, 1999)

Current (kA)	A0 (p.u)	A1 (p.u)
0.002	0.81	0.623
0.1	0.974	0.788
1	1.052	0.866
3	1.108	0.922
10	1.195	1.009
20	1.277	1.091

From now on the modified IEEE WG surge arrester model will be referred to as the Pinceti and Giannettoni (P&G) arrester model.

For the proposed P&G model, the relative errors between the calculated and measured discharge voltages are low for discharge currents with rise times between 1 to 30μs. The error decreases when the current rise times are not greater than 8μs. The accuracy of the model can be improved by adjusting the A_0 and A_1 curve profile to fit a specific make of surge arrester (Pinceti et al, 1999).

7.5.3 Comparison of Surge Arrester Models

Both the proposed CIGRE arrester model and P&G model were verified in ATP simulations by comparing the discharge voltage test results with the arrester manufacturer data sheet results.

The discharge voltage results for arrester manufacturer A and the average discharge voltage values for another three arresters are presented Table 7.4 below. The V-I curve of the non-linear resistance R_I in the CIGRE arrester model was based on the residual voltage measurements at different (8/20μs) current waveform amplitudes of arrester manufacturer A.

Table 7.4 Comparison of CIGRE 11kV arrester model and P&G arrester model for discharge voltage test results

Applied lightning impulse	Arrester A discharge voltage (kV)	Average values discharge voltage (3 types)	CIGRE model discharge voltage (kV)	P&G model discharge voltage (kV)	% difference CIGRE model compared to P&G model
10kA(8/20us)	42	40.2	40.4	42.2	-4.3%
10kA(1/20us)	47.9	40.4	47.1	51.7	-8.9%
20kA(8/20us)	47.7	42.8	42.8	45.5	-5.9%
60kA(5/70us)	N/A	N/A	54	57.5	-6.1%
40kA(1/20us)	N/A	N/A	84.5	77.3	9.3%
30kA(0.5/35us)	N/A	N/A	164	125	31.2%

It must be noted that for the CIGRE model used in the ATP simulations, the inductance per meter was changed to 0.5μH/m instead of the proposed 1μH/m by CIGRE (Hileman et al, 1990). This inductance per meter was changed by a manual iterative correction process to obtain better results comparable to the P&G model results.

This process provided an inductance L of 0.23μH for an arrester of average length of 0.45m. The rise time of 0.5μs produced the highest error of the CIGRE model as compared to the more sophisticated P&G arrester mode. For ATP simulations only rise times of 1μs and slower will be performed as discussed in Table 7.1. All simulations will be run for 2 x tail half times to optimise the simulation time of the ATP studies.

It was found that the simulation time of the P&G model took a long time due to the very small step size that was required to simulate the model. The connection of two P&G arrester models in parallel led to simulation difficulties. For this reason it was attempted to correct the proposed CIGRE arrester model so that the simulation results were close to those of the more detailed and accurate P&G arrester model. Table 7.4 and Table 7.5 demonstrate that the CIGRE arrester model (with L = 0.23μH) has comparable results to the P&G model.

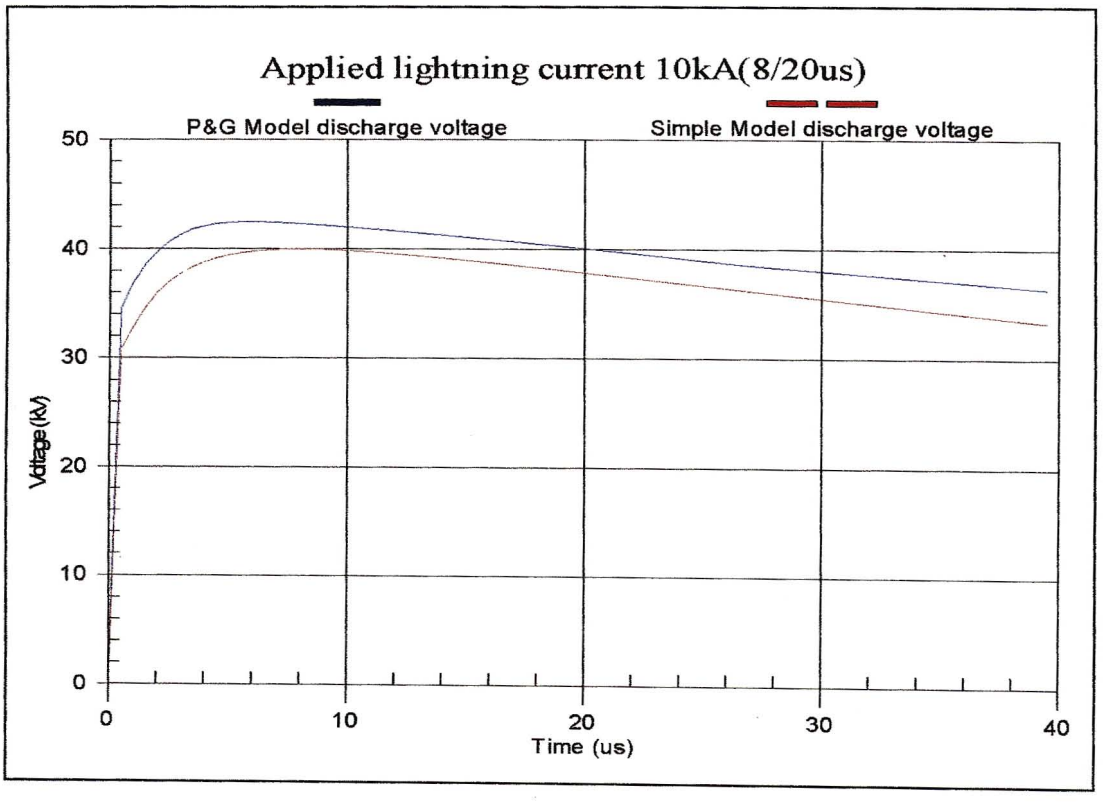

Figure 7.22 Comparison of discharge voltage of CIGRE model and P&G model for 10kA (8/20μs) current waveform

7.6 ATP Simulation Results

7.6.1 Surge Arresters in Parallel

The effect of two surge arresters in parallel was investigated with a few simple ATP simulations. The CIGRE surge arrester model as discussed in chapter 7.5.1 was used to represent each of the two arrester units in parallel. As discussed in chapter 7.5.1, the V-I characteristic curve of the first arrester A (default) was obtained from measured data for from manufacturer A. The V-I characteristic of the second arrester in parallel, was based on the first default arrester A curve with increasing discharge voltages. The increases were from 0.25% to 10%. Figure 7.23 below shows the various proposed curves.

The intention of these different V-I curves for the second arrester was to quantify the effect of different tolerances between arresters on the current sharing. The tolerances could be between arresters from the same batch or even from different manufacturers. The tolerances could also be due to the different materials used for the MOV blocks or different manufacturing techniques.

The following surge arrester names and corresponding tolerances were used in the simulations :

A : default
AAA : 0.25%
BBB : 0.5%
CCC : 1%
DDD : 2%
EEE : 5%
FFF : 10%

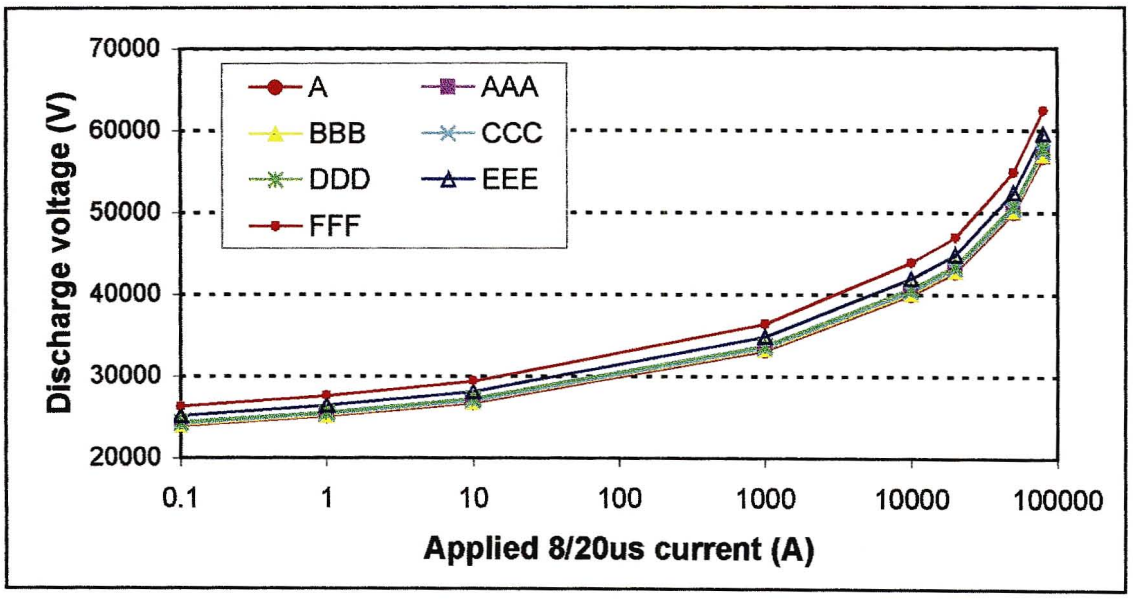

Figure 7.23 Different V-I characteristics of arresters (A to FFF)

A lightning current of 5/70μs waveform with varying magnitudes of current was applied to both ends of the two arresters in parallel and the corresponding discharge currents measured for each arrester. The exercise was intended to simulate the laboratory environment of testing two arrester units in parallel.

The current sharing or variation between two parallel surge arresters was quantified by the introduction of a K factor or current sharing factor of the two arrester discharge currents (De Lorenzi et al, 1987) :

$$K = \frac{I_{max} - I_{min}}{I_{ave}} \qquad (7.28)$$

I_{max} and I_{min} refer to the magnitudes (maximum and minimum) of the two discharge currents of the respective arresters.

I_{ave} is the average value of the two discharge currents

A factor K = 0 means that there is equal current sharing and a factor K = 2 means that one of the arresters discharges the full current and the other arrester discharges no current. The effect of the tolerances (0.25% to 10%) can be seen in the Figure 7.24 below.

The curves below show that at higher lightning currents the sharing of current between two arresters is better i.e. K factor decreases to zero. The large variance in K factor between the 10% tolerance (arrester FFF) and the other smaller tolerances can be seen clearly. The tolerance curves (0.25%, 0.5% and 1%) provide a current sharing factor of less than 0.2.

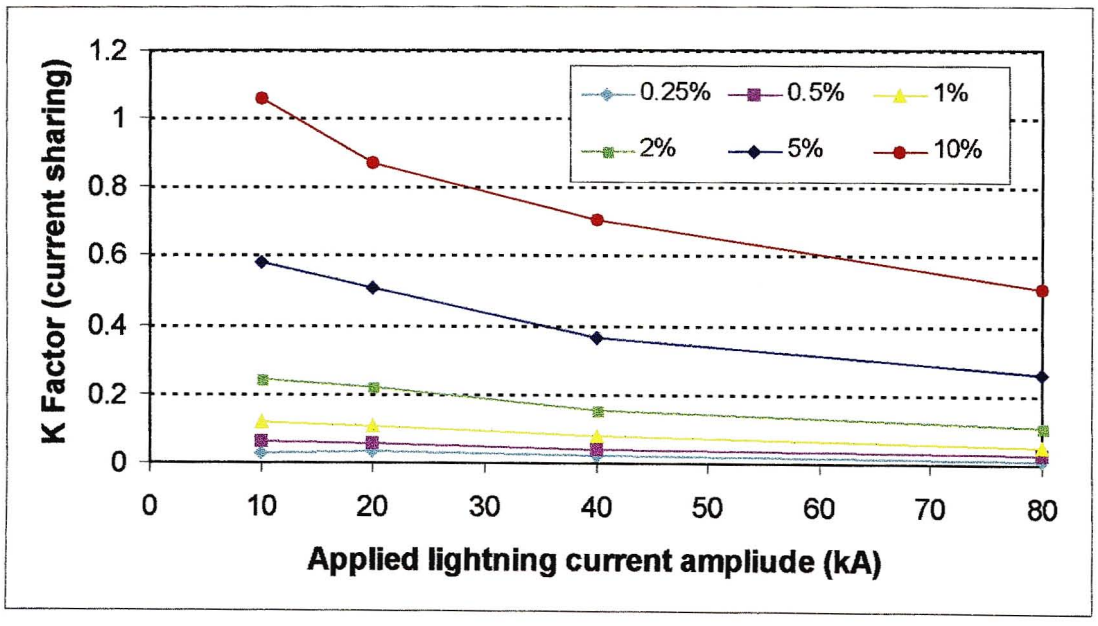

Figure 7.24 K factor for parallel arresters with different V-I characteristics

Figure 7.25 below shows the result from the same simulation exercise but now only the energy absorbed by the default arrester A is shown. The 5% and 10% tolerance curves have a significant effect as compared to the smaller tolerance curves on the energy absorbed by the arrester A. Figure 7.26 and Figure 7.27 below show the effect of the lightning current rise times and tail half times on the energy absorbed by arrester A, when arrester A and arrester EEE (5% tolerance) are in parallel.

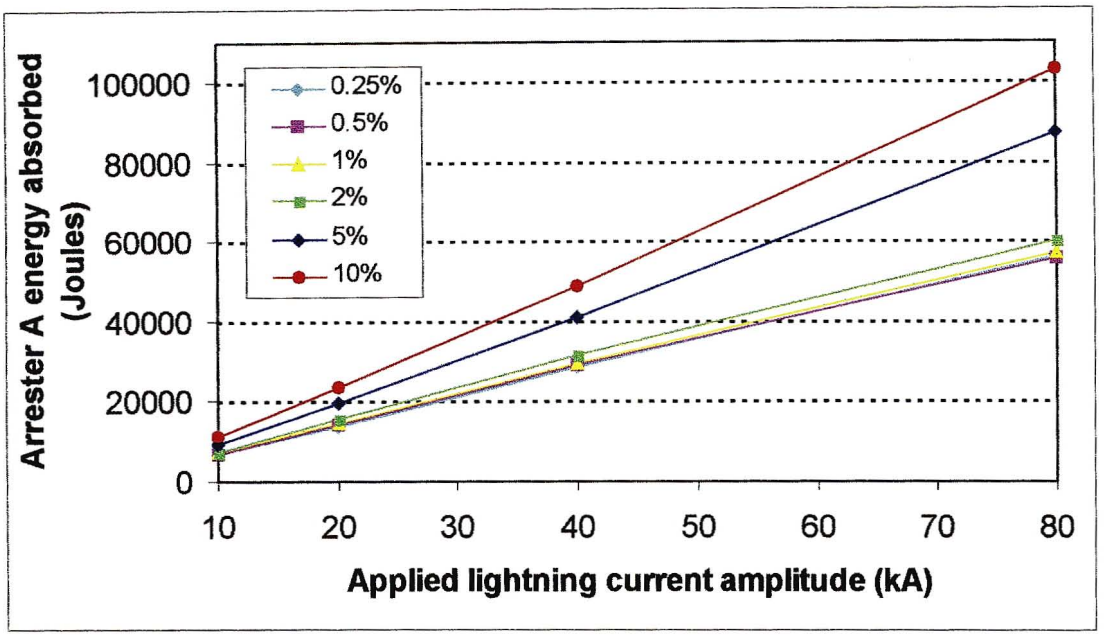

Figure 7.25 Energy absorption of arresters in parallel with different V-I characteristics

It can be seen in Figure 7.26 below, that the current rise time has a negligible effect on the energy absorbed by arrester A. The tail half time of the current has the most effect on the energy absorbed by arrester A. In Figure 7.27 below it can be seen that a doubling of the tail half time leads to approximately a doubling of the energy absorbed by arrester A. This was discussed in (Geldenhuys et al, 1986).

A similar parallel arrester exercise was performed using the more sophisticated P&G surge arrester model. Three different surge arrester manufacturer data sheets (manufacturer A, manufacturer J and manufacturer C) were used to obtain the component values for the model. The current sharing factor was quantified in Figure 7.28 below.

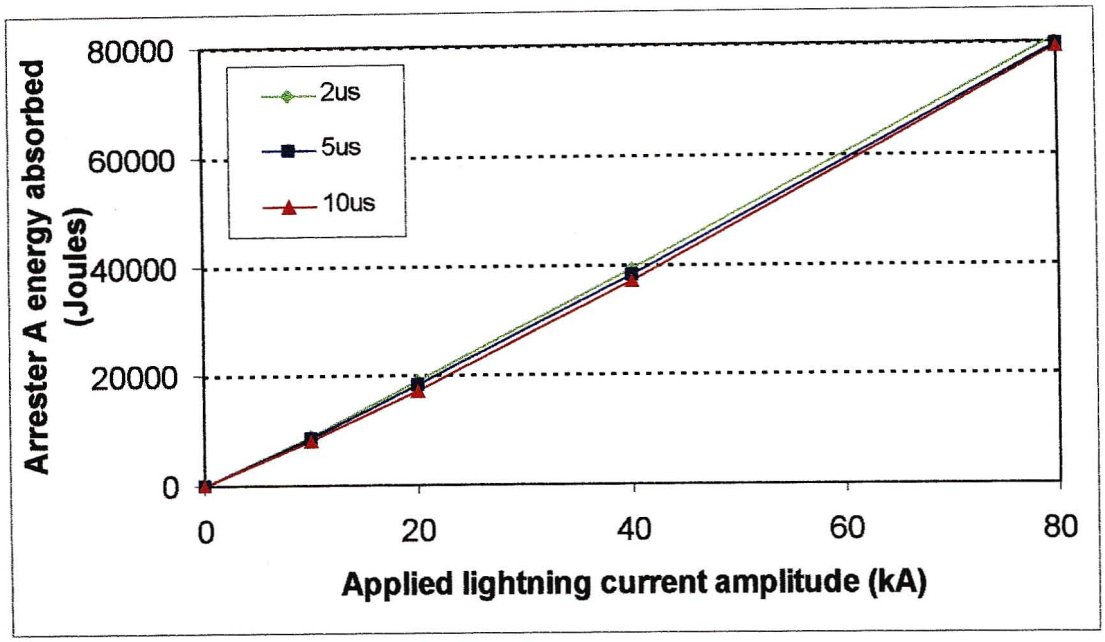

Figure 7.26 Effect of current rise time on the energy absorbed by arrester A when in parallel with arrester EEE (tail half time fixed at 70μs)

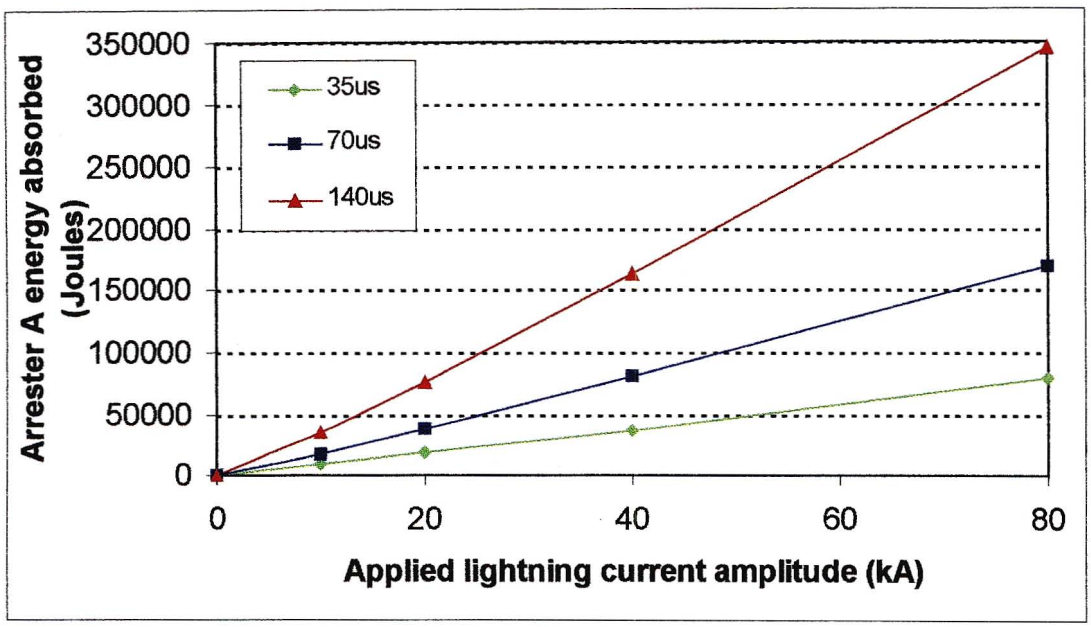

Figure 7.27 Effect of current tail half time on the energy absorbed by arrester A when in parallel with arrester EEE (rise time fixed at 5μs)

It can be seen in Figure 7.28 below that at larger lightning currents the sharing of current between the two arresters was better i.e. K factor decreased to zero (similar to Figure 7.24).

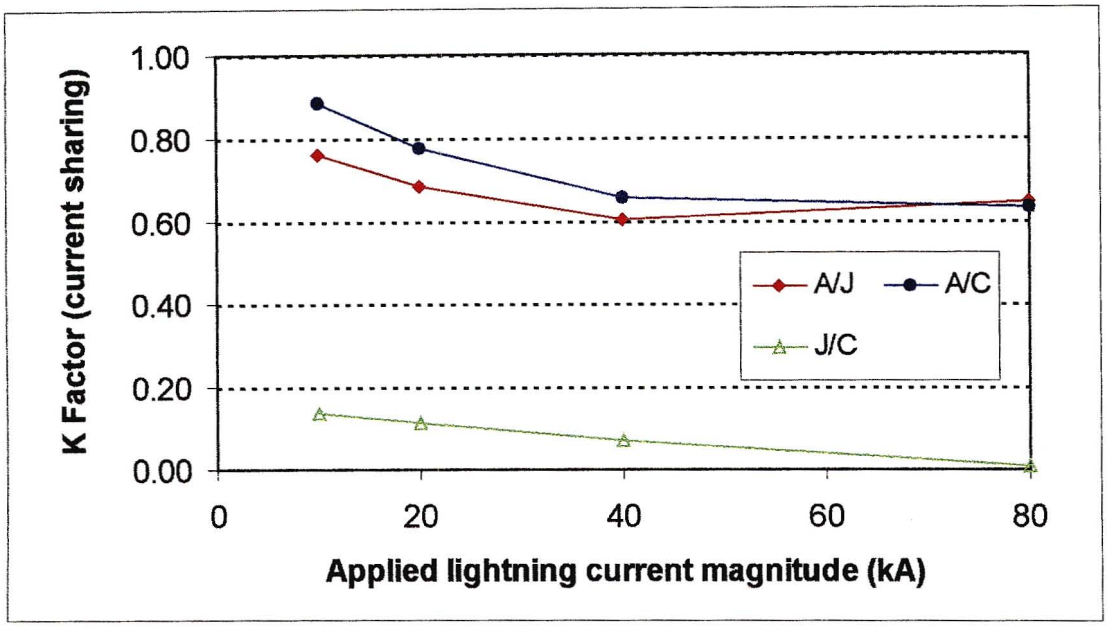

Figure 7.28 K factor for parallel arresters from different manufacturers using the P&G model (5/70μs current waveform)

Figure 7.29 and Figure 7.30 below show the effect of the lightning current rise time and tail half time on the current sharing between the A and C and J arresters in parallel. Figure 7.29 shows that the current rise time does slightly effect the current sharing between parallel arresters. The current sharing seems to be slightly better for faster rise times. Figure 7.30 below shows that the current tail half time has little effect on the current sharing of two parallel arresters.

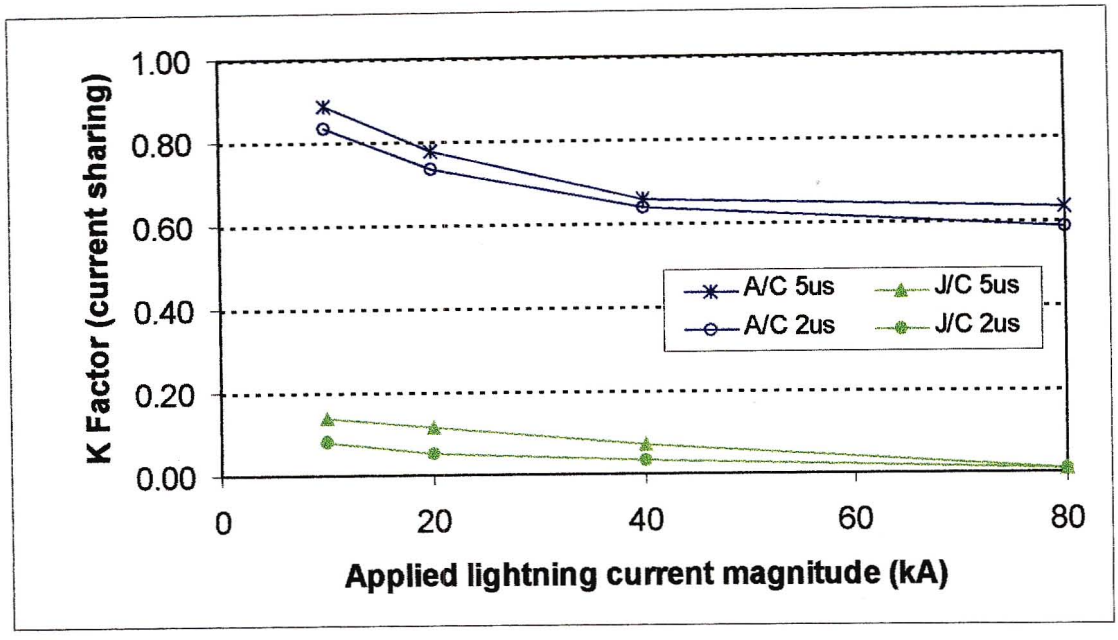

Figure 7.29 Effect of rise time on current sharing of parallel arresters using the P&G arrester model (tail half time fixed at 70μs)

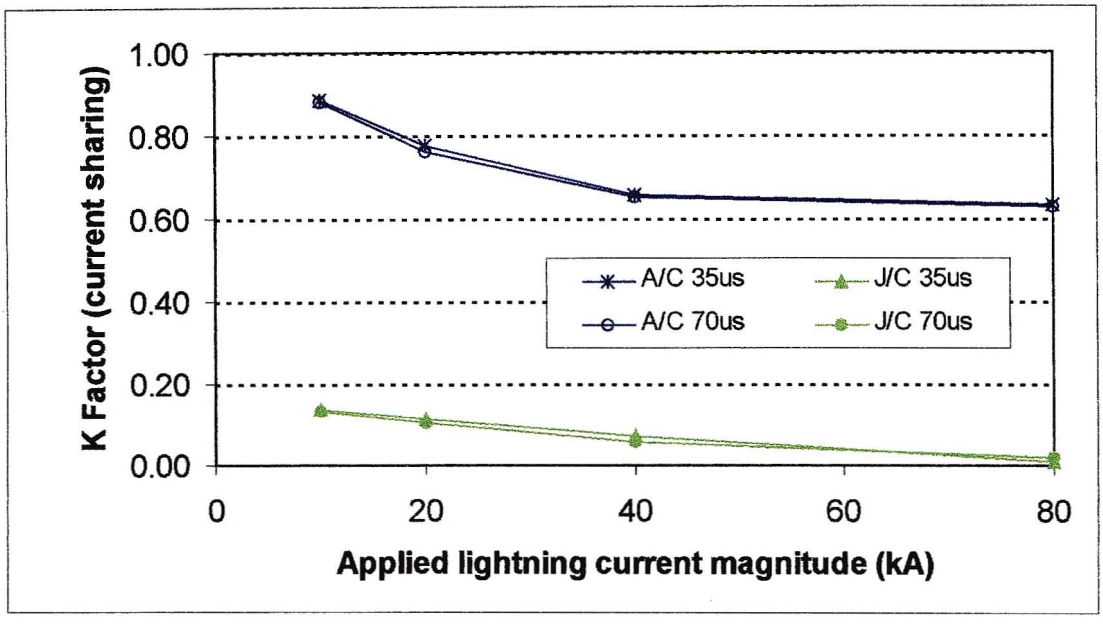

Figure 7.30 Effect of current tail half time on current sharing of parallel arresters using the P&G arrester model used (rise time fixed at 5μs)

Table 7.5 below shows a comparison of the energy absorption values for the two different arrester models (CIGRE and P&G model) and the results of using equation (4.2) and equation (4.3).

Table 7.5 Comparison results of energy values from simulations and calculations

Applied lightning current to arrester	ATP simulations (CIGRE Model)	ATP simulations (P&G Model)	Equation (4.2) using alpha = 0.2 Energy results	Erquation (4.3) Energy results
15.9kA (12/70us)	5.1kJ	5.2kJ	5.8kJ	12.7kJ
4.1kA (2.8/10us)	1.6kJ	1.7kJ	1.6kJ	1.7kJ
4.1kA (0.8/5.6us)	1kJ	0.9kJ	0.91kJ	1.7kJ
7.7kA (2.8/36us)	12.6kJ	12.1kJ	12.5kJ	4.3kJ
32kA (8/20us)	22.3kJ	27.9kJ	29.6kJ (alpha=0.1)	36.2kJ
50kA (5/70us)	188.2kJ	195.9kJ	169.4kJ (alpha=0.1)	70.7kJ

7.6.2 Effect of Understrung Conductor

The effect of the type of conductor used for the understrung arrangement as used on Glencoe N/B 13 was simulated in ATP. The purpose of this exercise was to determine what the effect of different diameter conductors with different DC resistance values would have on reducing the energy absorbed by the arresters. The understrung conductor was represented as a phase conductor using the JMarti transmission line model. The coupling effect between the phase conductor and understrung conductor was not included (Darveniza et al, 1979a) and (De la Rosa, 1998). This exercise also included the effect of having no understrung conductor but still having the 300kV BIL one structure back. The type of conductor used and its parameters and are shown in Table 7.6 below.

Table 7.6 Type of conductor used for understrung arrangement (SCSASABE7, 2001)

Conductor	Overall diameter (cm)	DC resistance @ 20 deg C (ohms/km)
Hare	1.42	0.2733
Fox	0.84	0.7822
Magpie	0.64	2.707
Steel (3/3.35)	0.74	7.4

The ATP circuit model used for this exercise is shown below in Figure 7.31.

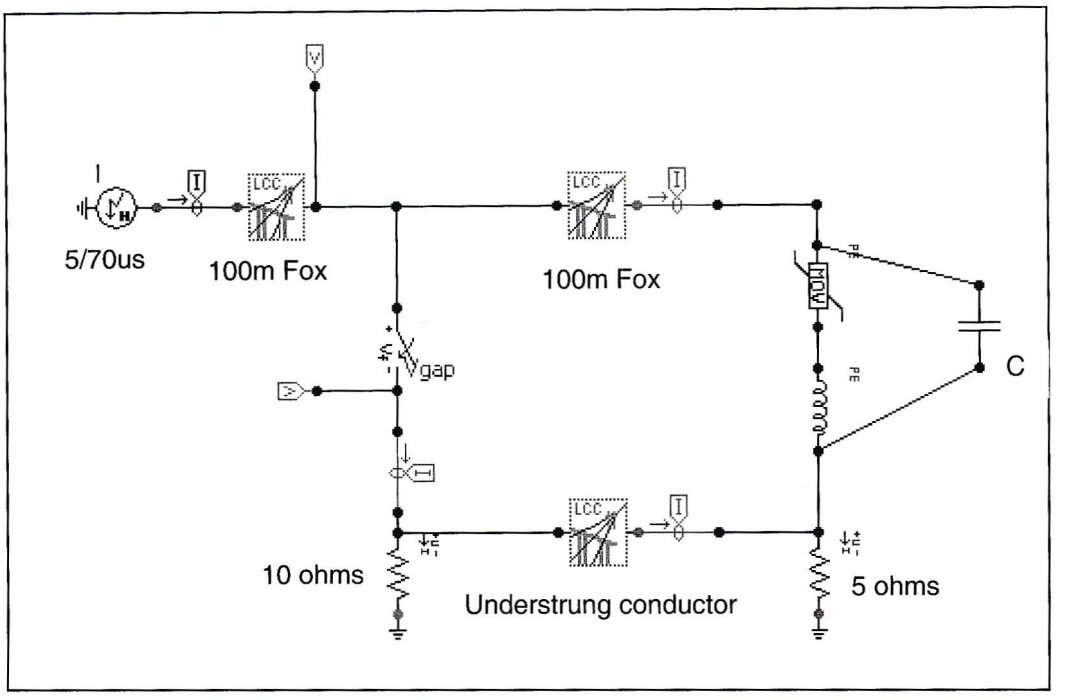

Figure 7.31 ATP circuit model of understrung conductor arrangement (single arrester scenario)

The following assumptions were made for the above ATP circuit :

- Span length : 100m
- Phase conductor : Fox
- Lightning current : 5/70μs waveform
- Transient pole footing resistance plus impedance of down conductor : 10 ohms (1.5m copper rod electrode)
- Transient transformer electrode resistance : 5 ohms (5m Crows foot electrode)
- Soil resistivity 500 to 1000 Ω.m
- 300kV voltage controlled switch (insulator wood path combination)
- Capacitance representing transformer : 2nF
- No corona (inception voltage for Fox is about 187kV)
- Understrung conductor : Fox (represented as a phase conductor using the JMarti transmission line model with no coupling effect with the above phase conductor)

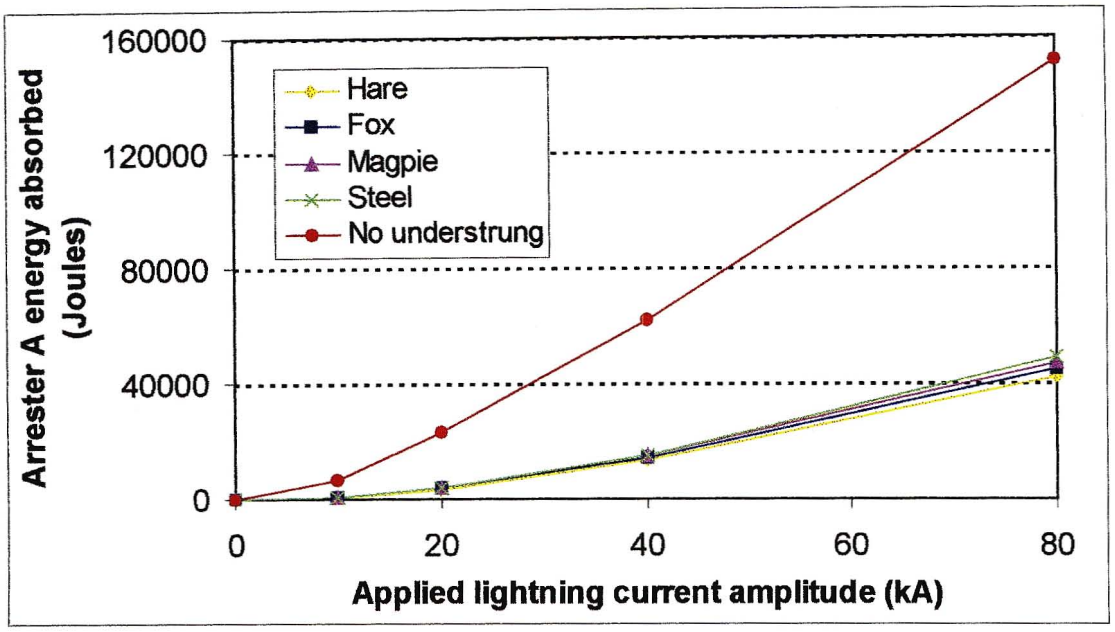

Figure 7.32 Effect of type of conductor used for understrung conductor arrangement on the energy absorbed by arrester A

Figure 7.32 above shows that the type of conductor used has negligible effect the energy absorbed by the arrester A. The current flowing to earth at the wood pole one structure back and along the understrung conductor does not vary. It can be seen that the use of an understrung conductor does significantly reduce the energy absorbed by the arrester as compared to not using the understrung conductor.

Figure 7.33 below shows what effect the tail half time of the lightning current has on the energy absorbed by the arrester. For this exercise Fox conductor was used as the understrung conductor (as used as on Glencoe N/B 13). It can be seen that there is not a doubling of energy absorbed by the arrester from a tail half time of 35μs to 70μs as would be expected.

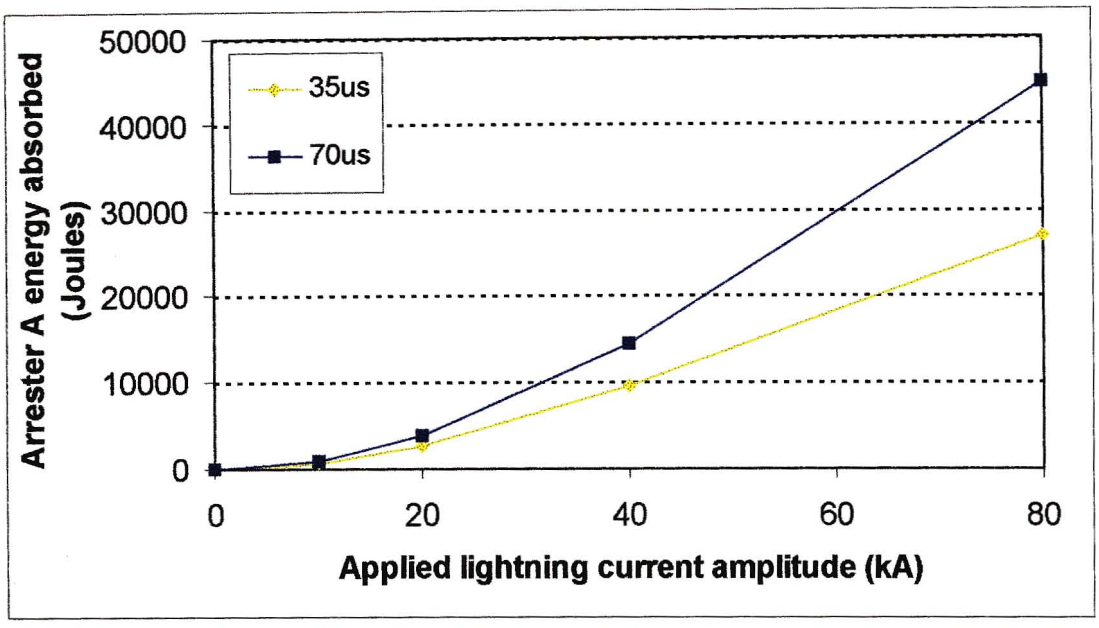

Figure 7.33 Effect of current tail half time on the energy absorbed by arrester A using the understrung conductor arrangement

Figure 7.34 and Figure 7.35 below show what the effect of varying the *transient* transformer electrode resistance and pole footing resistance has on the energy absorbed by the single arrester. No understrung conductor was used in this exercise. It is well known that these two parameters are very important in lightning simulation studies (Anderson, 1982).

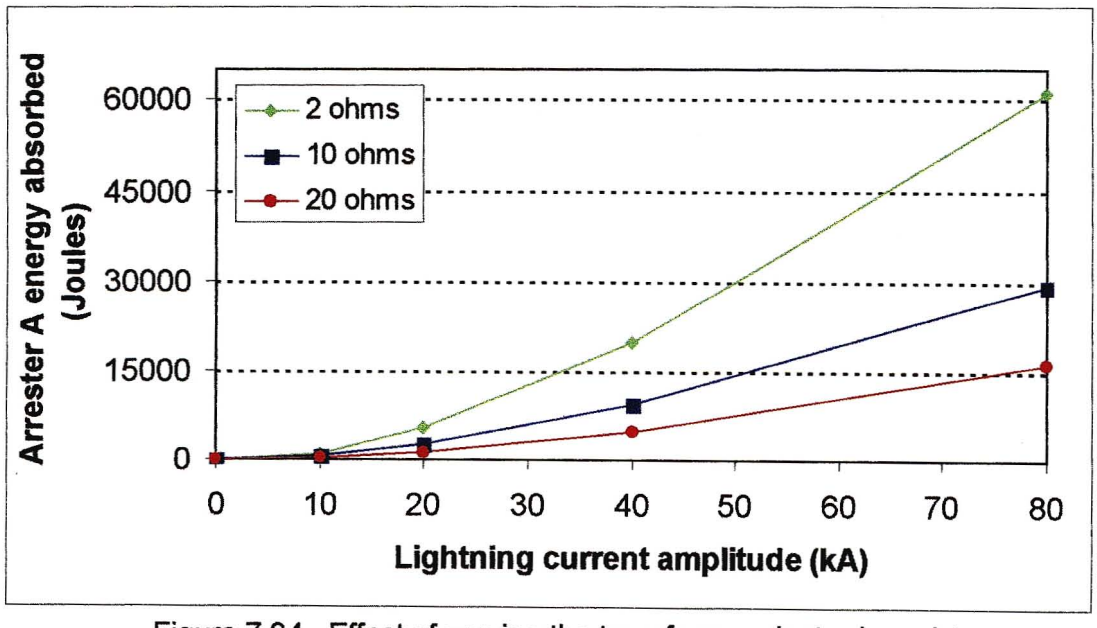

Figure 7.34 Effect of varying the transformer electrode resistance on the energy absorbed by arrester A (pole footing resistance = 10Ω)

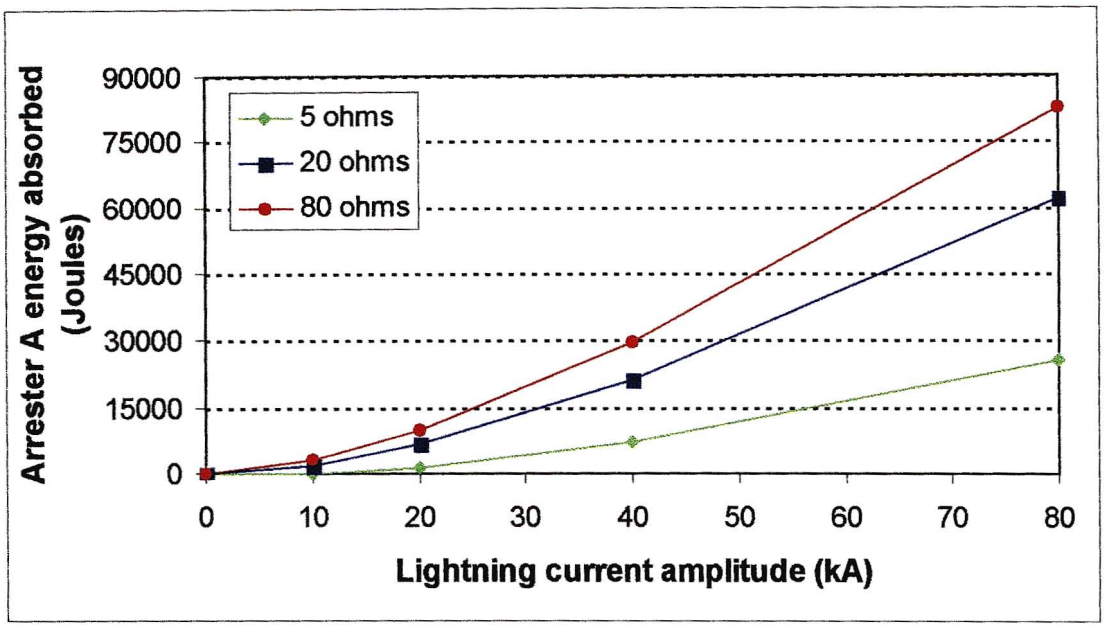

Figure 7.35 Effect of varying the transformer pole footing resistance on the energy absorbed by arrester A (transformer resistance = 5Ω)

Figure 7.34 shows that the variation of the transformer resistance has the most effect of reducing the energy absorbed by the arrester. The compromise is that the resistance can not be too low otherwise too much current flows to ground and the surge arrester energy absorption limits are exceeded.

Figure 7.36 below shows how the different practical methods implemented to reduce the energy absorbed by the arresters compare. It can be seen that the understrung conductor arrangement reduces the energy absorbed by the surge arrester more than the double arrester configuration. The combination of both the understrung conductor and double arrester configuration provides the best results.

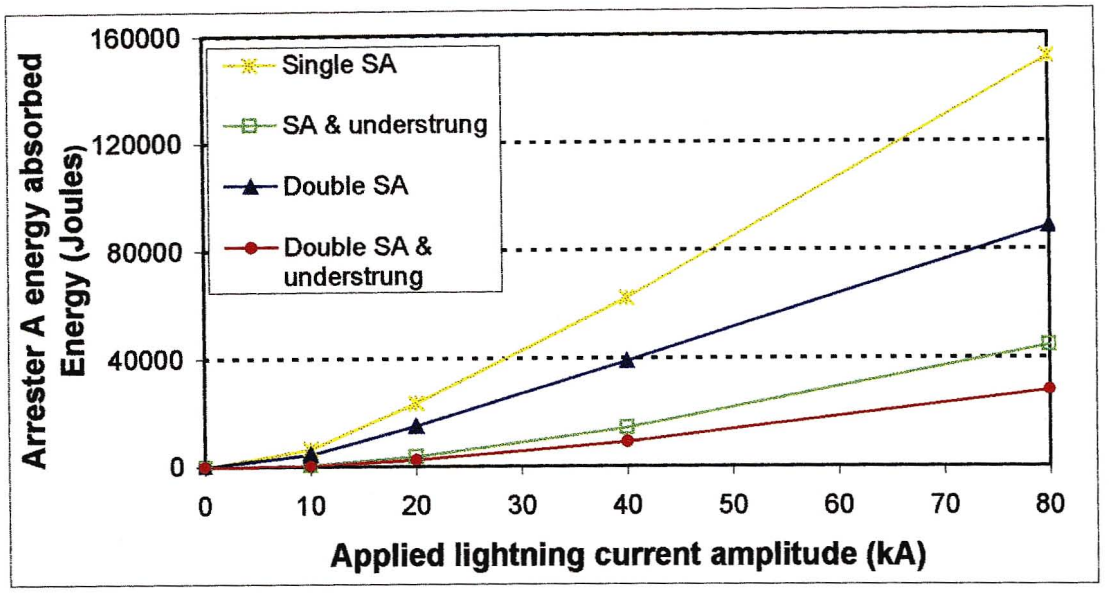

Figure 7.36 Comparison of the different practical methods implemented on the energy absorbed by arrester A

7.7 Detailed Simulation Results

7.7.1 Overall Comparison

A similar ATP circuit model as in Figure 7.31 was used with the same parameters for the circuit model. An overall comparison of the different practical methods implemented was performed. For this simulation exercise two spans before the transformer installation and one span behind the lightning struck pole were simulated to take into account the effect of the 300kV BIL structures. From (Van Schalkwyk, 2001) it was found that only two poles were required to adequately simulate the voltage flashover to ground phenomena on the line. Figure 7.37 below shows the comparison results of the three experimental networks. The intention was to have similar simulation configurations and parameters for all three networks.

The following information is for Figure 7.37 below :

Glen 13 single SA : Glencoe N/B 13 with only a single arrester instead of the double arrester configuration.

Glen 13 spark gap : Glencoe N/B 13 with the double arrester configuration and 300kV spark gap one span back. No understrung conductor arrangement was used.

Dun 18 double SA : Dundee N/B 18 with double arrester configuration.

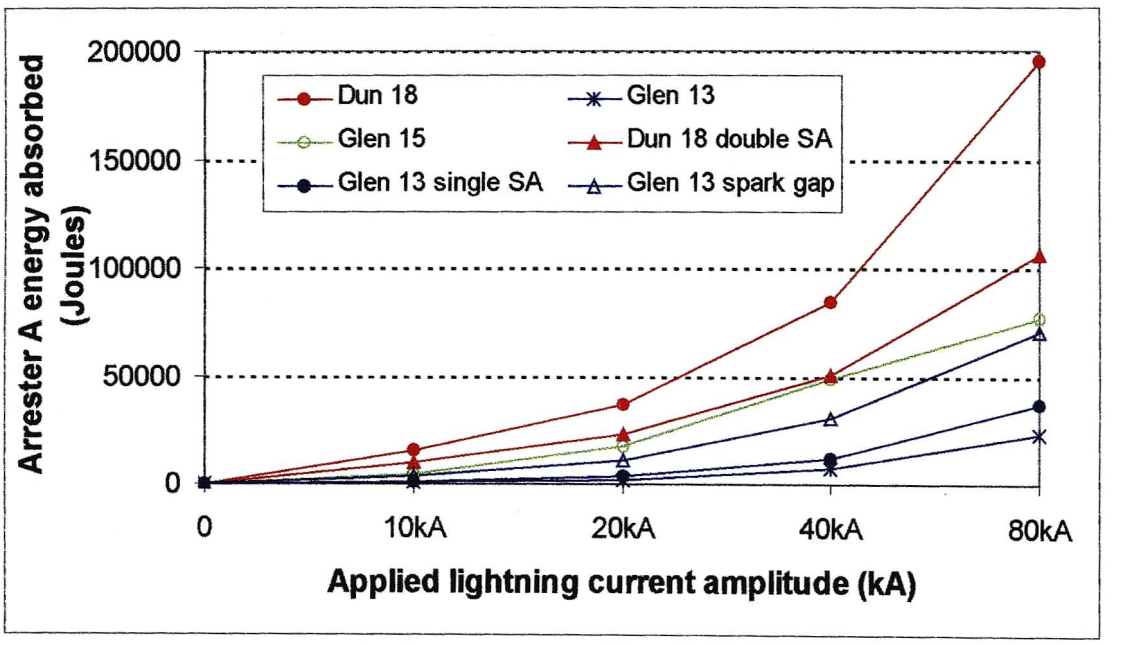

Figure 7.37 Overall comparison of the effect of the experimental lines on the energy absorbed by arrester A

Figure 7.37 shows that Glencoe N/B 18 (fully insulated line) results in the highest energy absorption by the arrester A. Even with the double arrester configuration for Glencoe N/B 18, the arrester energy absorption is still more than the other network configurations. The lowest energy absorption is with Glencoe N/B 13 (double arrester and understrung conductor arrangement). Glencoe N/B 13 with only a single arrester used provides the second lowest energy absorption levels.

The double surge arrester configuration would be more applicable to existing Eskom networks with high arrester or transformer failure rates. The understrung conductor arrangement is a more expensive option due to the large labour component of the total cost. It would be more advantageous to use the double arrester configuration.

7.7.2 Dundee N/B 18 Simulations

The parametric simulation results for Dundee N/B 18 are shown below. The transformer earth resistance was held constant at 5Ω.

Figure 7.38 below shows the effect of the lightning current rise time and tail half time on the energy absorbed by the arrester on Dundee N/B 18. It can be seen that the decrease in rise time has a negligible effect on the energy absorbed by the arrester (Schei et al, 1990). The increase in tail half time has the most significant effect on the energy absorbed by the arrester. The energy absorbed is proportional to the tail half time as discussed in Chapter 4.4.

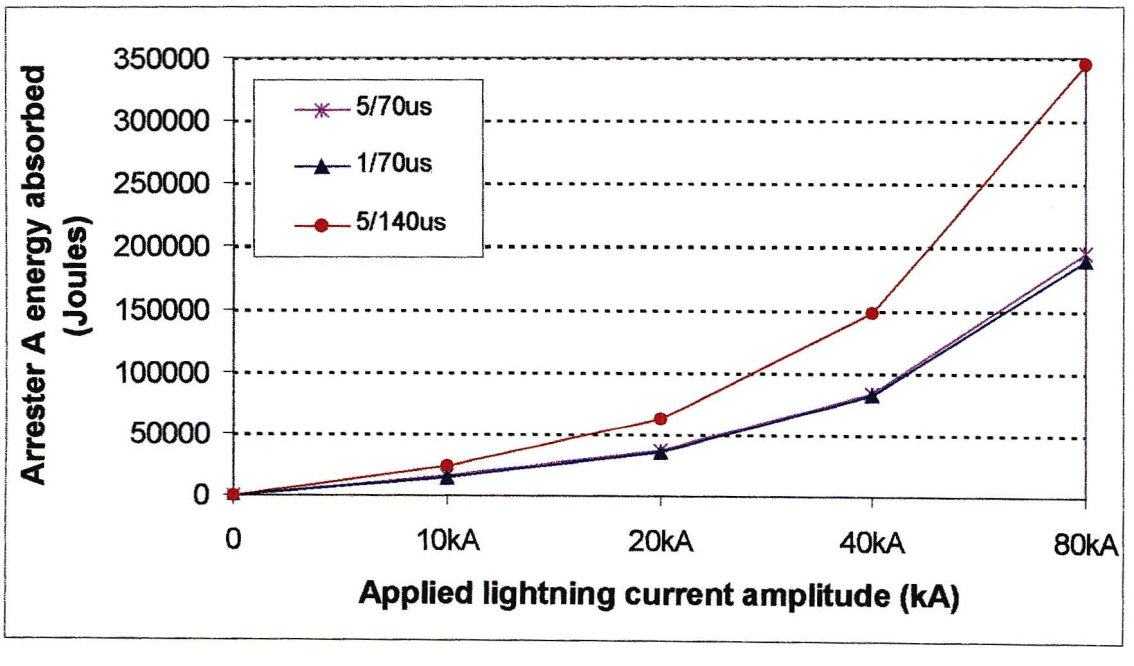

Figure 7.38 Effect of lightning current waveform on the energy absorbed by arrester A on Dundee N/B 18

Figure 7.39 below shows the effect of the transient transformer earth electrode resistance on the energy absorbed by the arrester. A decrease in earth resistance increases the current discharged by the arrester and hence the energy absorbed by the arrester.

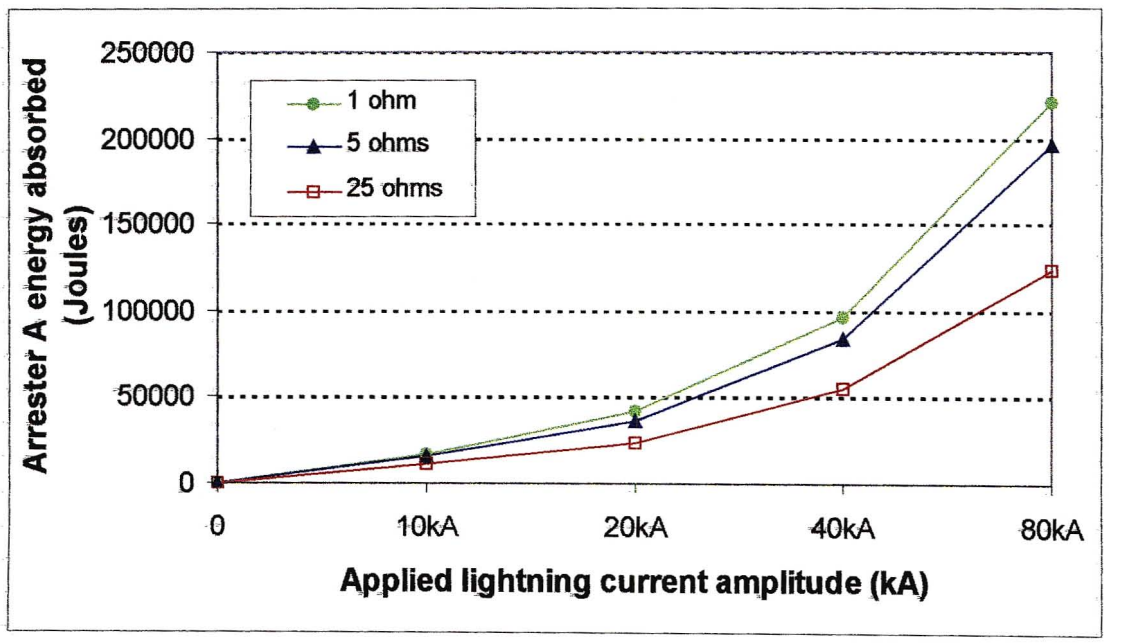

Figure 7.39 Effect of transformer earth resistance on the energy absorbed by arrester A on Dundee N/B 18

Figure 7.40 below shows the effect of the simulated lightning strike a certain distance away from the transformer installation. For larger peak currents the difference is more notable due to attenuation and corona effects on the network (Schei et al, 1990).

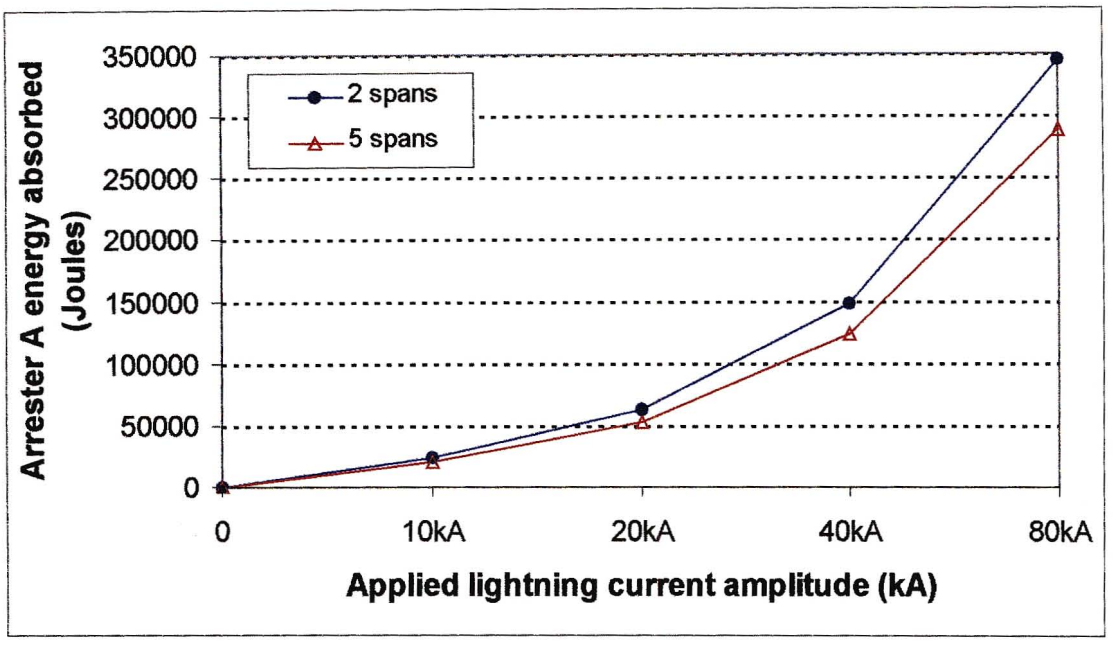

Figure 7.40 Effect of lightning striking a distance away on the energy absorbed by arrester A on Dundee N/B 18

7.7.3 Glencoe N/B 15 Simulations

Figure 7.41 below shows the effect of the lightning current rise time and tail half time on the energy absorbed by the arresters on Glencoe N/B 15. It can be seen that the decrease in rise time has a small effect on the energy absorbed by the arrester (Schei et al, 1990). The difference is more distinguishable than in Figure 7.38 for Dundee N/B 18. The increase in tail half time has the most significant effect on the energy absorbed by the arrester.

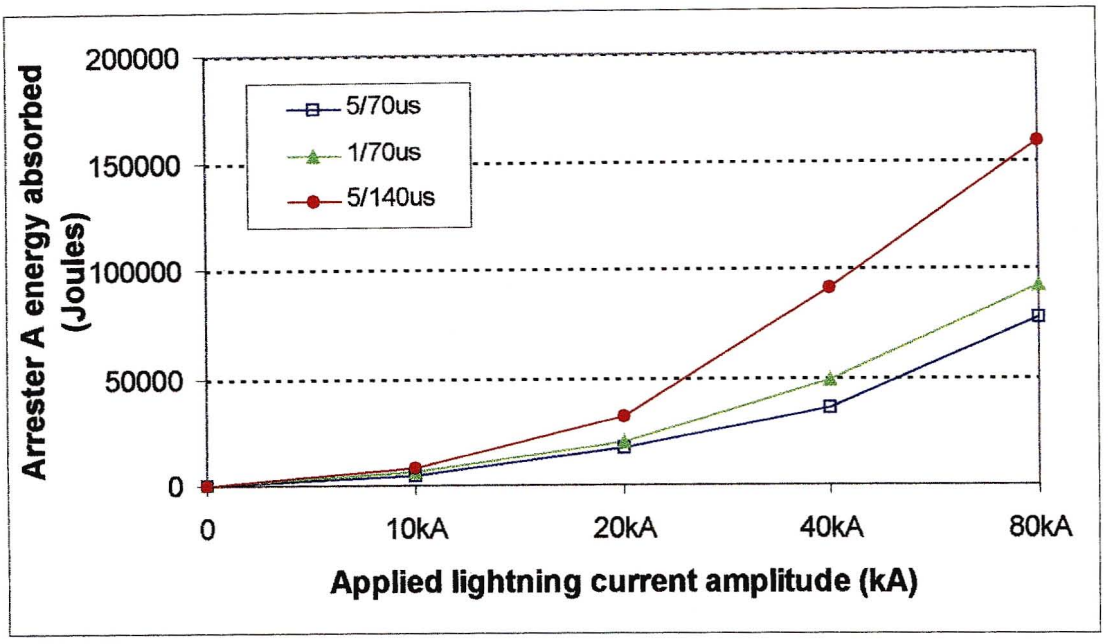

Figure 7.41 Effect of lightning current waveform on the energy absorbed by arrester A on Glencoe N/B 15

Figure 7.42 below shows the effect of the pole footing resistance on energy absorbed by the arresters on Glencoe N/B 15. This resistance can be the parallel combination of a number of woodpoles. The pole footing resistance only has an effect once voltage flashover across the porcelain insulator and 600mm wood path has occurred. The effect in Figure 7.42 is the ratio of the pole footing resistance and the transformer earth resistance (fixed at 5Ω). The simulation was for pole footing resistance values five times larger, equal to and five times less than the transformer earth resistance. The results show that the pole footing resistance should be as low as possible (Schei et al, 1990).

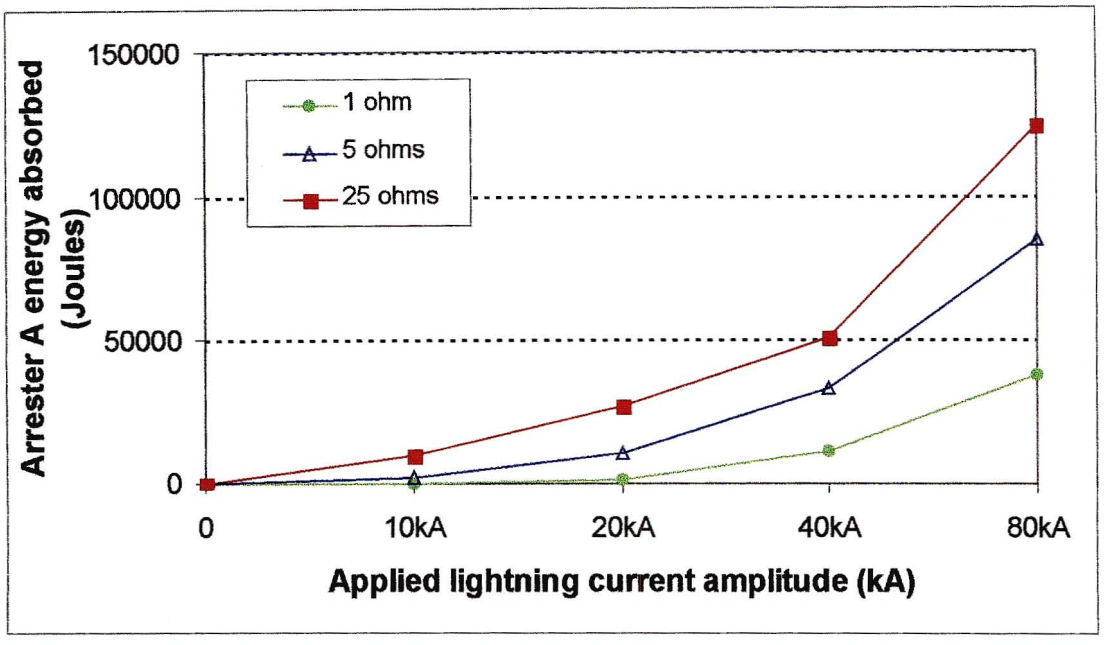

Figure 7.42 Effect of pole footing resistance on the energy absorbed by arrester A on for Glencoe N/B 15

7.7.4 Glencoe N/B 13 Simulations

Figure 7.43 below shows the effect of the lightning current rise time and tail half time on the energy absorbed by the arresters on Glencoe N/B 13. It can be seen that the decrease in rise time has a small effect on the energy absorbed by the arresters. The difference is similar as for Glencoe N/B 15. The increase in tail half time has the most significant effect on the energy absorbed by the arrester.

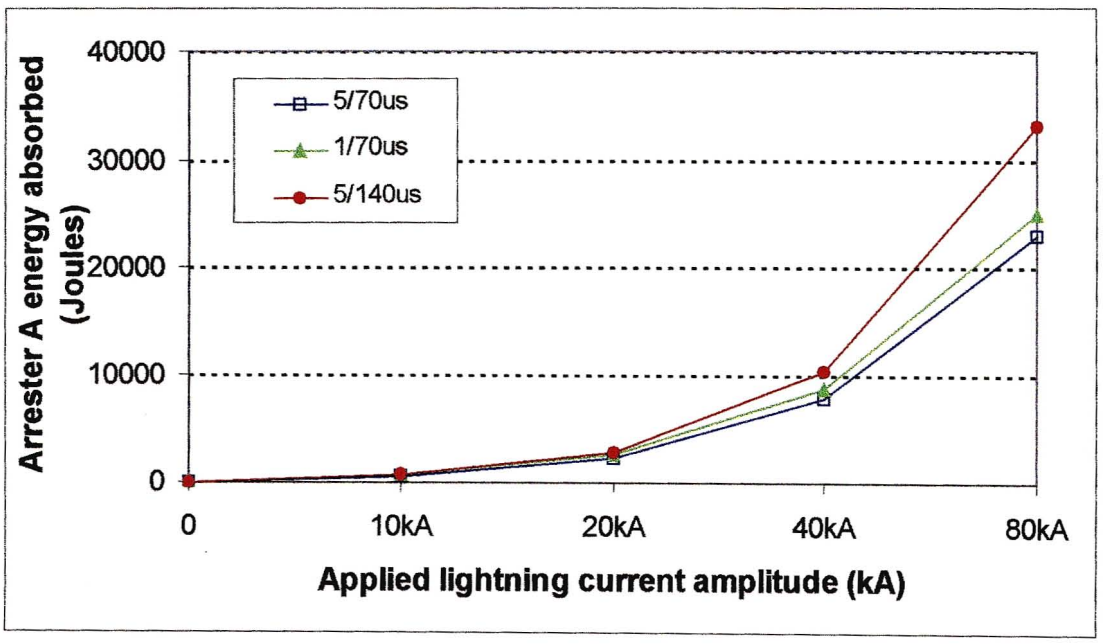

Figure 7.43 Effect of lightning current waveform on the energy absorbed by arrester A on Glencoe N/B 13

Figure 7.44 below shows the effect of the pole footing resistance on Glencoe N/B 13. The pole footing resistance only has an effect once voltage flashover across the porcelain insulator and 600mm wood path has occurred. The effect in Figure 7.44 is the ratio of the pole footing resistance and the transformer earth resistance (fixed at 5Ω). The simulation was for pole footing resistance values five times larger, equal to and five times less than the transformer earth resistance.

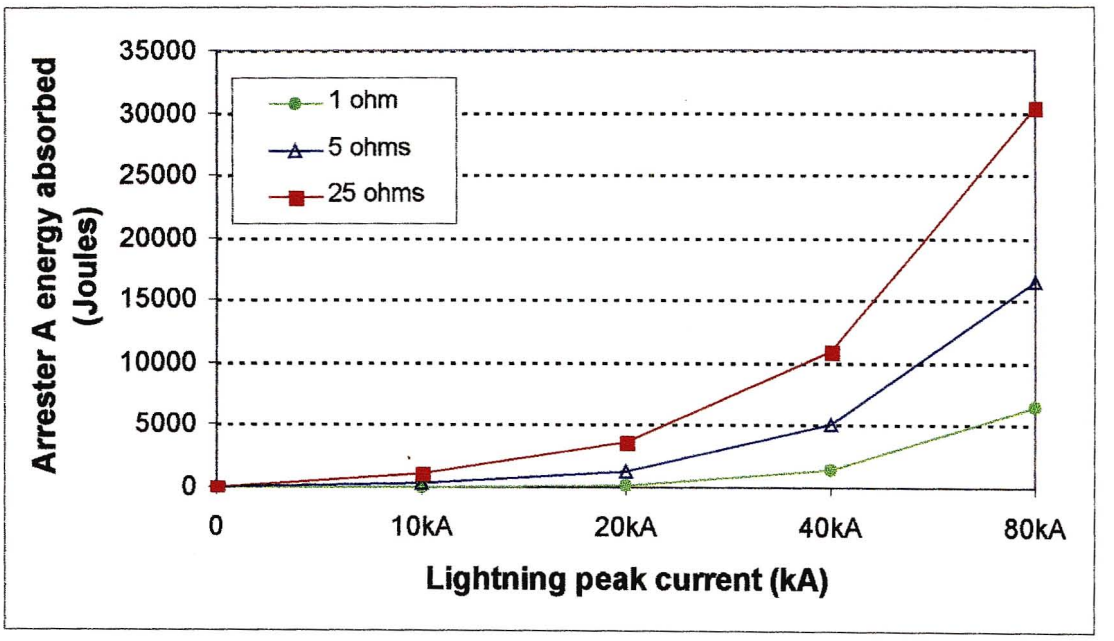

Figure 7.44 Effect of pole footing resistance on the energy absorbed by arrester A on Glencoe N/B 13

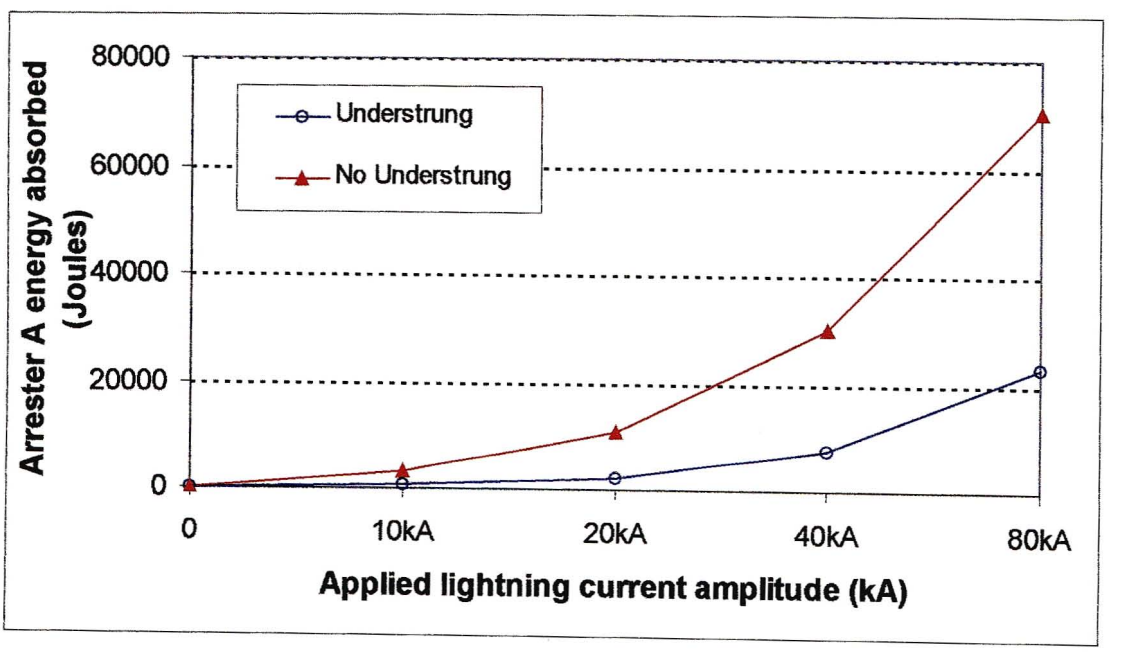

Figure 7.45 Effect of understrung conductor on the energy absorbed by arrester A on Glencoe N/B 13

Figure 7.45 above shows the effect using an understrung conductor and no understrung conductor.

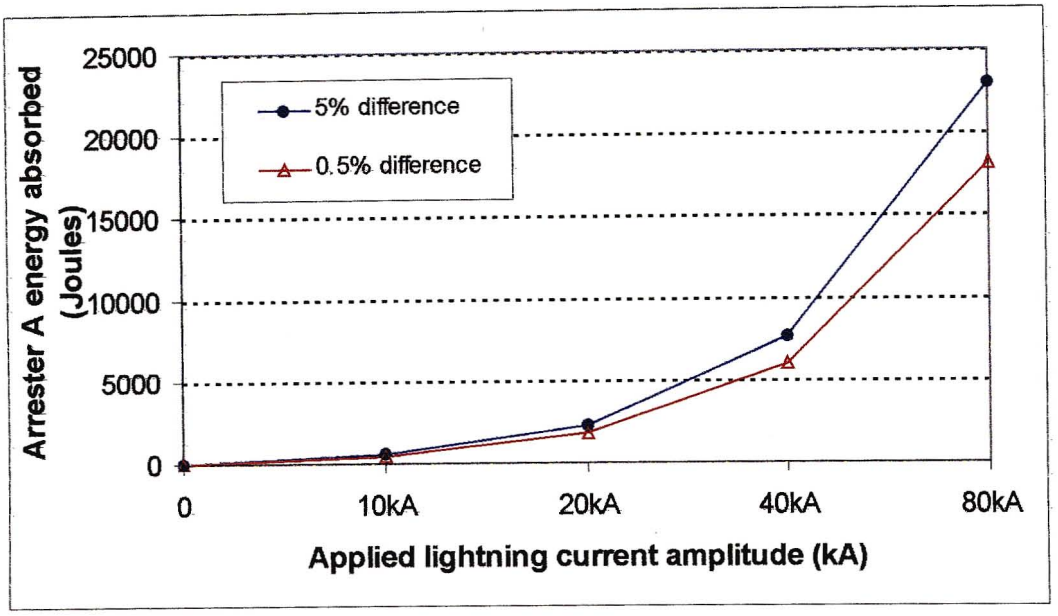

Figure 7.46 Effect of unmatched arresters on the energy absorbed by arrester A on Glencoe N/B 13

Figure 7.46 above shows the effect of "unmatched" surge arresters on the energy absorbed by arrester A. The more closely matched the lower the energy absorbed by arrester A.

7.8 Conclusions

The conclusions from the results and findings of the ATP simulations are :

The Glencoe N/B 13 network with the parallel arrester configuration and understrung conductor arrangement considerably reduced the energy absorbed by the individual arresters. The effect of the double surge arrester configuration was to reduce the energy absorbed by the individual arresters even with arresters with different V-I characteristics.

The understrung conductor arrangement was the major contributor towards the reduction of the energy absorbed by the arresters. The type of conductor used had negligible effect on the energy absorbed by the arresters.

The pole footing electrode resistance and transformer earth electrode resistance were found to be important factors effecting the energy absorbed by the arresters. The pole footing resistance had to be as low as possible. Practically this would be difficult as the transient impedance of a 1.5m copper rod would always be larger than the transient impedance of a crows foot electrode used to earth the transformer. This would be assuming both electrodes were in similar soil resistivities.

The tail half time of the lightning current also had a significant effect on the energy absorbed by the arresters. This was not a parameter that can be controlled by the line designer.

Dundee N/B 18 had the least effect of reducing the energy absorbed by the single arresters. This was due to the network been fully insulated with no discharge path along the network for lightning overvoltages.

CHAPTER 8
LABORATORY WORK AND RESULTS

In this chapter the alternating current (AC) behaviour and the impulse behaviour of ZnO material will be discussed. This chapter contains the results of the laboratory work performed by the student at the high voltage laboratory, University of Natal. The purpose of the laboratory work was to familiarise the author with the AC behaviour characteristics of metal oxide varistor (MOV) blocks used in surge arresters, and to conduct some simple AC experiments. The final component of the laboratory work consisted of impulse experiments of MOV blocks in parallel and the quantification of the current sharing between various types of manufacturer blocks. This was done to simulate the two surge arresters in parallel on Glencoe N/B 13.

The voltage and current (V-I) characteristics and temperature dependence under AC conditions of new MOV block samples from three different surge arrester manufacturers were compared to each other. The purpose was to also see how the different V-I characteristics of MOV blocks from different manufacturers were. A Fourier analysis of the harmonic content of the resistive and capacitive components of the leakage current was performed.

For the impulse experiments the energy absorbed by each block was calculated from the recorded applied impulse voltage and the corresponding discharge currents. The current sharing between two blocks in parallel was quantified by a current sharing factor K. The MOV block was modeled in ATP using a proposed equivalent circuit and the measured current waveforms compared to the simulated current waveforms. A good agreement between the modeled and measured waveforms was obtained.

8.1 AC Experimental Arrangement

The AC experimental arrangement layout used in the high voltage laboratory is shown below in Figure 8.1.

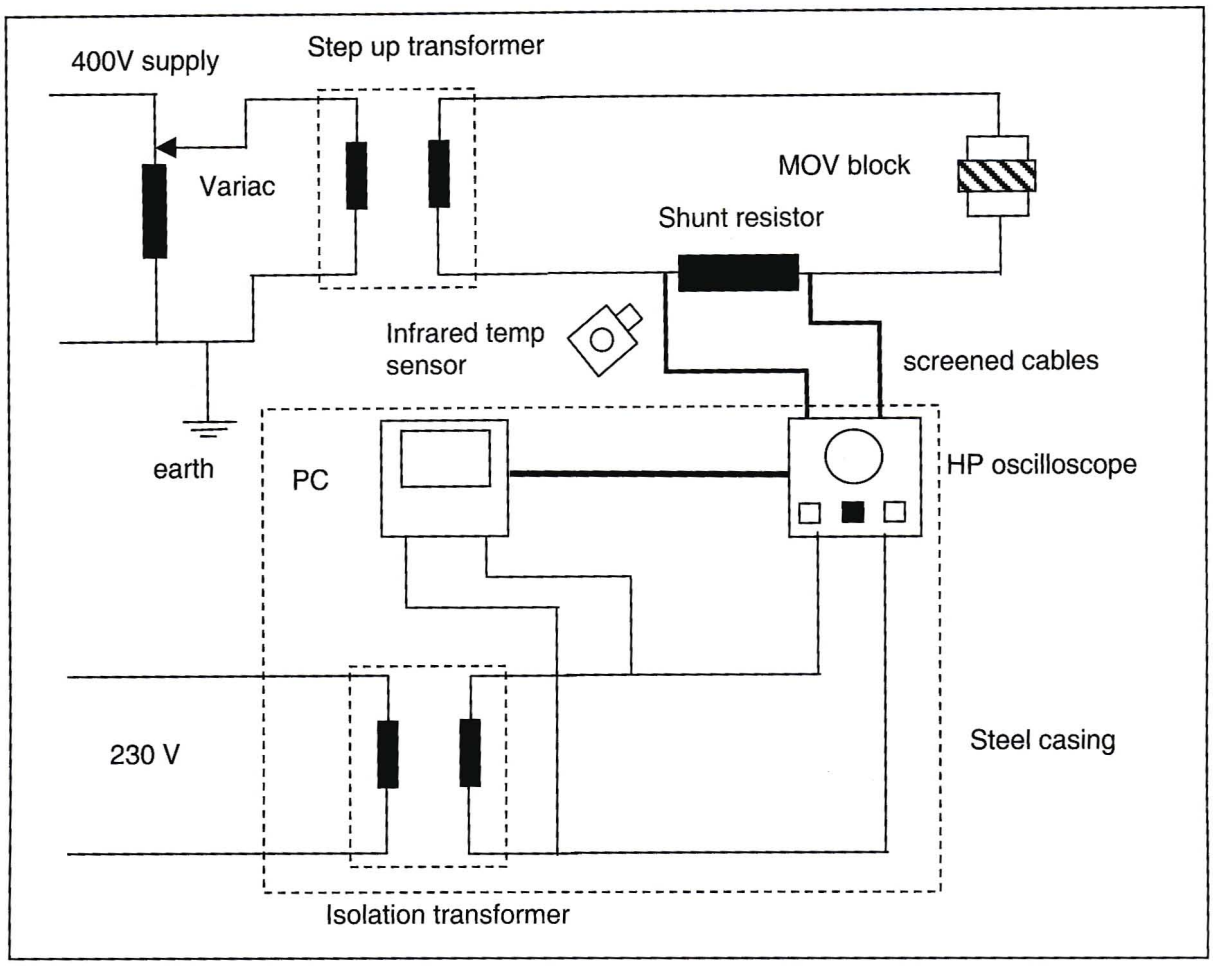

Figure 8.1 AC experimental laboratory layout diagram

A variable transformer supply (variac) of rating 0-260V 10A was used to vary the input voltage to a 10kV 150mA 50-60Hz step up voltage transformer. The variable voltage from the step up transformer was applied to one side of the MOV block. The MOV block was housed in a specially constructed single MOV block rig used by (Van der Linde, 1999). The rig provided adequate clamping force on the MOV block and minimized the heat loss from the block during energy absorption experiments. A similar experimental set up was discussed in (Ringler et al, 1997).

The other end of the block was connected to a shunt resistor of resistance 100Ω and power rating of 5W. This shunt resistor was used to measure the leakage current of the MOV block for different magnitudes of applied power frequency voltages. The power rating chosen was sufficient for the resistor not to overheat during the AC experiments.

All the voltage measurements were conducted using a Tektronix P6015A high voltage probe with 1000 times attenuation. The output of the transformer was also measured with a Fluke high voltage probe (rated up to 40kV peak). The voltage was displayed on a Fluke 8010A digital multimeter. The purpose of this arrangement was to provide a quick reference of the applied voltage to the MOV block.

The oscilloscope used was a Hewlett-Packard HP 54510A 250MHz 1Ga Sa/s with a HPIB interface card (HP, 1990). The HP 10441A probes used had ratios of 10:1. The data was downloaded onto a personal computer (PC) for viewing and storage. The PC was only used for data acquisition and data file storage. The Scopelink version 2 oscilloscope data analysis program was used to record the data. The supply to the PC and the oscilloscope was fed from the mains off an isolation transformer.

The temperature of the MOV blocks was measured by a Minolta Cyclops Compac 3-S infra red temperature sensor. A Tecpel™ 305 thermometer was also used as an additional rough check of the surface temperature of the block.

Each measurement comprised of recording the voltage and current waveforms as a function of time. The waveforms were sampled at 5kHz for a 50Hz power frequency voltage. The Scopelink program was used to record the waveforms.

The data was stored as individual voltage or current waveform and time files. Each file consisted of a 2 x 4000 element ASCII file. This file was then loaded into the MATLAB® current workspace and the relevant graphs plotted using the relevant MATLAB® program commands. The MATLAB® version 5.3 student edition was used to process the data and printing of the relevant graphs. The student version was limited to matrices of size 16 348 elements (128 by 128). The limitations of the student version are further discussed in (Hahn, 1997).

8.2 Results of the AC Experiments on Different MOV Blocks

8.2.1 Surge Arrester Voltage Specifications

Surge arresters are designed to satisfy a number of operating criteria. Arresters designed for identical purposes by different manufacturers can differ in their characteristics. This makes selection of a surge arrester a compromise between its protective levels, temporary overvoltage (TOV) capability and energy handling ability.

When comparing arresters of similar application but from different manufacturers, it is useful to have a reference voltage to work with. This selected voltage can be used as a common reference for all the arresters (Stenstrom, 1990). The two voltage ratings are specified by the IEC 99-4 specification for arresters are the continuous operating voltage (COV) and the rated voltage (U_r).

The COV or MCOV is defined by the South African (NRS 039, 1995) and the Eskom standard (SCSSCAAN5, 2000) as the *"maximum designated permissible r.m.s value of power frequency voltage that may be applied continuously between the arrester's terminals*". When specifying this voltage the earthing configuration of the electrical network and the harmonic content of the waveform needs to be taken into account. The MCOV is usually specified as 105-110% of the system phase-to-phase voltage U_m (Stenstrom, 1990). For Eskom reticulation systems the MCOV is specified as $U_m/\sqrt{3}$ times 1.73 for non-solidly earthed systems (NRS 039, 1995).

The rated voltage (U_r) is defined as the *"maximum permissible r.m.s value of power frequency voltage between its terminals at which it is designed to operate correctly under temporary overvoltage conditions"* (NRS 039, 1995). In case of the distribution class arresters used in Eskom, the arrester must be able to withstand TOV's for 10s. A detailed discussion of the selection of the rated voltage of distribution class arresters is provided by (Stenstrom, 1990).

For the laboratory work conducted, the MCOV was selected as the reference voltage to compare the characteristics of different arresters. The MCOV of an arrester is effected by the protective level and the thermal stability. The protective level is defined by the residual voltage of the arrester (Stenstrom, 1990).

The residual voltage or discharge voltage is the *"voltage that is maintained between the arrester terminals during the passage of discharge current"* (NRS 039, 1995). The Eskom distribution arresters are rated at 40kV discharge voltage for a nominal discharge current of 10kA of 8/20μs waveform. The MCOV is linked to the system voltage whereas the rated voltage is related to the residual voltage.

8.2.2 Single MOV Blocks Under AC Conditions

The electrical measurements were performed on six new MOV blocks. These blocks had been removed from three different types of arresters of manufacturer J, C and R. Each arrester unit consisted of four MOV blocks. The arresters were carefully cut open and two blocks from each arrester were randomly removed and used for the laboratory experiments. The blocks were designated as C1, C2, J1, J2, R1 and R2. The blocks with the same alpha prefix were from the same manufacturer. The blocks were all approximately 35mm in diameter and 20mm in height. Refer to Figure 105 for an example of block J1 (failed block). During the later impulse experiments block J1 was physically damaged and replaced by block J3.

Two of the arresters were commercial arresters that were used on the Eskom 11kV reticulation networks. The other type of arrester was also a commercial arrester used in the Electricity Supply Industry (ESI), but not used by Eskom. All the arresters had rated discharge currents of 10kA, MCOV of 10.2kV and rated voltages of 12kV. Each block had a COV of 2.6kV.

The V-I characteristics were measured for all six MOV blocks. Voltage and current waveforms were measured for 40 cycles of the 50Hz waveform. Effectively 100 samples per 50Hz waveform were taken. This provided a sampling frequency of 5kHz for each of the recorded channels. The applied 50Hz voltage was increased in steps of 0.5kV rms and the corresponding leakage current through the shunt resistor was measured. The voltage was increased until the leakage current reached approximately 26mA rms. This current value was used as an upper limit for all the blocks that were tested.

This proved to be a sufficient current range to compare the characteristics of the blocks mainly in the low electric field region and the start of the medium electric field region (Schei et al, 1990).

The low field region is where the leakage current increases linearly with the applied voltage. In the medium field region or transition region the V-I characteristic becomes non-linear. This non linearity started after approximately 1mA rms current for all the tested blocks. Increments between the voltage steps were decreased when taking measurements in the non-linear region to take into account the large increases in leakage current for small increases in applied voltages of the block. Refer to Appendix D for a sample of the V-I measurements taken for block J1 and J2.

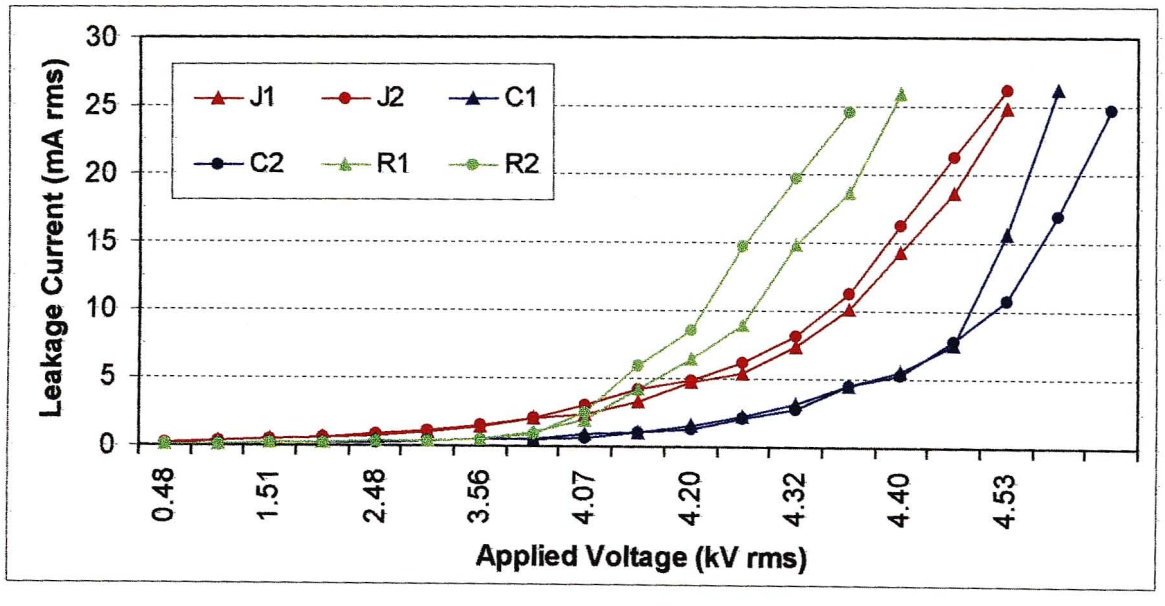

Figure 8.2 V-I measurements curves of tested MOV blocks

Figure 8.2 above shows the difference in V-I characteristic curves amongst the various arrester manufacturers. The characteristics of all the blocks in the low electric field region (less than 1mA rms) were similar. There was a notable difference in the characteristics of the R blocks (green curves) and C blocks (blue curves). The blocks R1 and R2 proceed into the transition region much earlier than the other four blocks. The characteristics of the R and C blocks start to diverge at about 150% COV.

Figure 8.3 below shows a complete set of measured applied voltage and corresponding leakage current waveforms for sample block J1. The change in the current waveforms for increasing applied voltage can be seen in the waveforms below. The applied voltage (peak to peak) increases from the top to the bottom of the page for the various plots.

Initially the leakage current magnitude increases linearly with the applied voltage. In the plot Wave 2 the 50% COV level was reached. In the plot Wave 4, the COV of the block was reached. The current was still purely capacitive and the block was still operating in the low electric field region of the characteristic curve (Schei et al, 1980). In the plots Wave 1 to Wave 4 noise spikes can be seen effecting the current waveforms. The noise was measured to be 2.82mV rms. No proper explanation can be offered as to the source of the noise as all possible electromagnetic interference (EMI) measures and shielding were taken.

The measurements were performed over several cycles so some of the noise component was statistically eliminated. In the plot Wave 7 150% COV was reached. Both the increase in the resistive component and the asymmetrical effect of the capacitive component of the total current can be clearly seen. This asymmetry of the current waveform is attributed to the passage of DC current through the material or the pulses during routine testing of the blocks after they have been manufactured (Eda et al, 1980) and (Hayashi et al, 1982). The magnitude of this displacement is a function of previously applied mono-polar impulse currents.

In the plots Wave 9 and Wave 10 the resistive current component is dominant. The block is now operating at the start of the transition region of the characteristic curve. The distortion of the current waveform can be clearly seen in these later plots (Wave 8 to Wave 10).

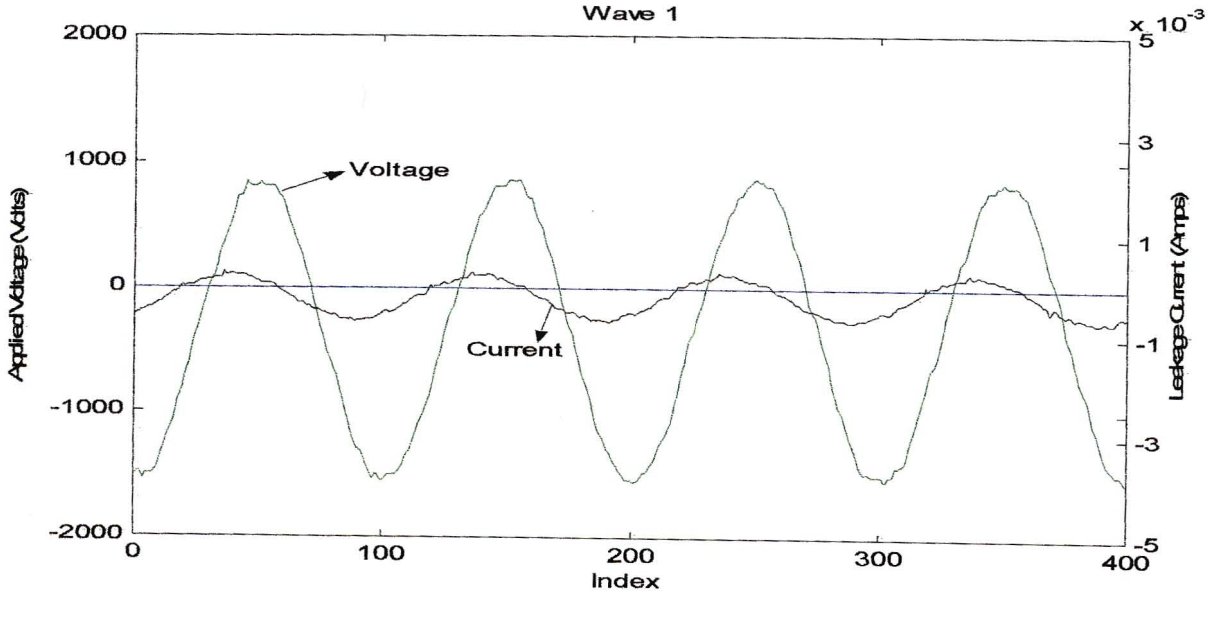

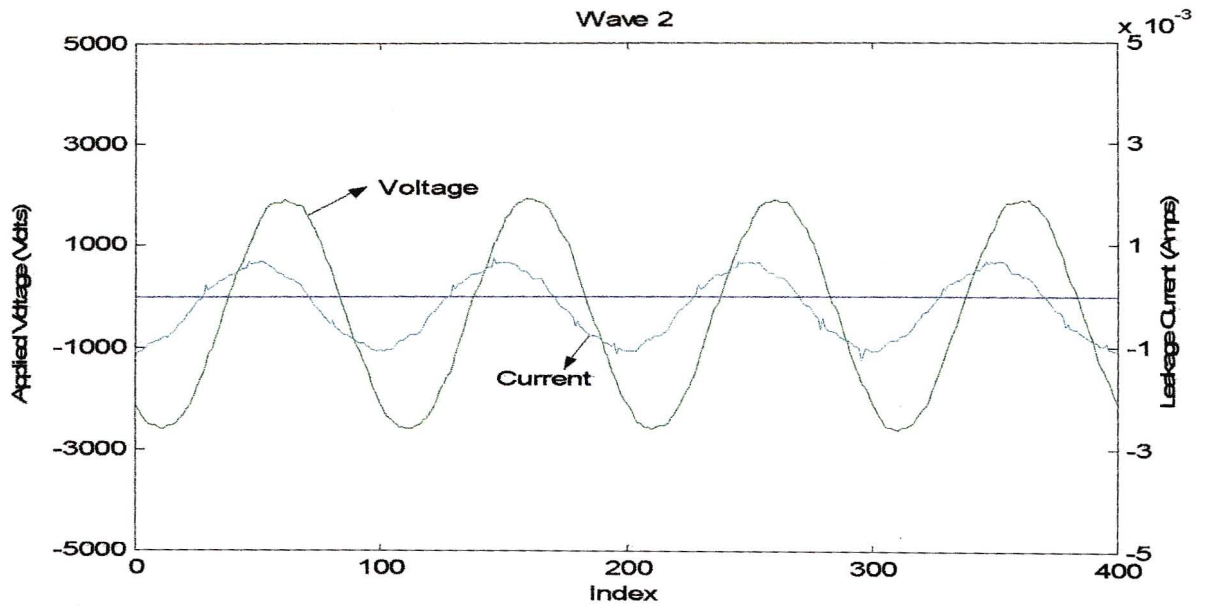
Wave 2
x 10^-3
5000
3000
1000
-1000
-3000
-5000
5
3
1
-1
-3
-5
Voltage
Current
Applied Voltage (Volts)
Leakage Current (Amps)
0
100
200
300
400
Index

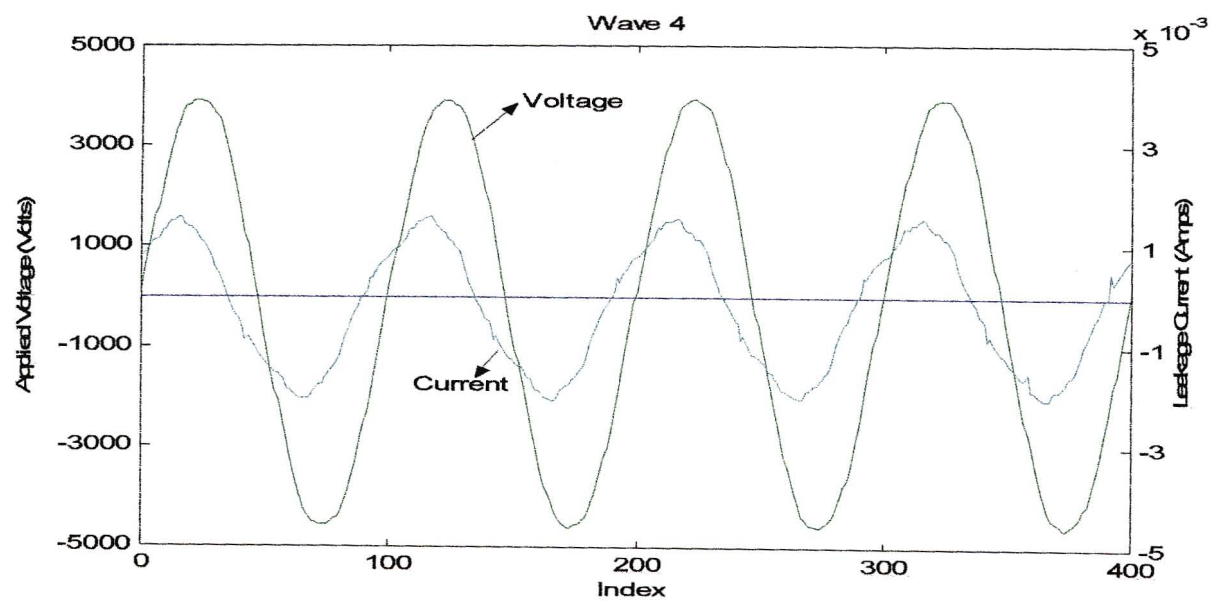
Wave 4
x 10^-3
5000
3000
1000
-1000
-3000
-5000
5
3
1
-1
-3
-5
Voltage
Current
Applied Voltage (Volts)
Leakage Current (Amps)
0
100
200
300
400
Index

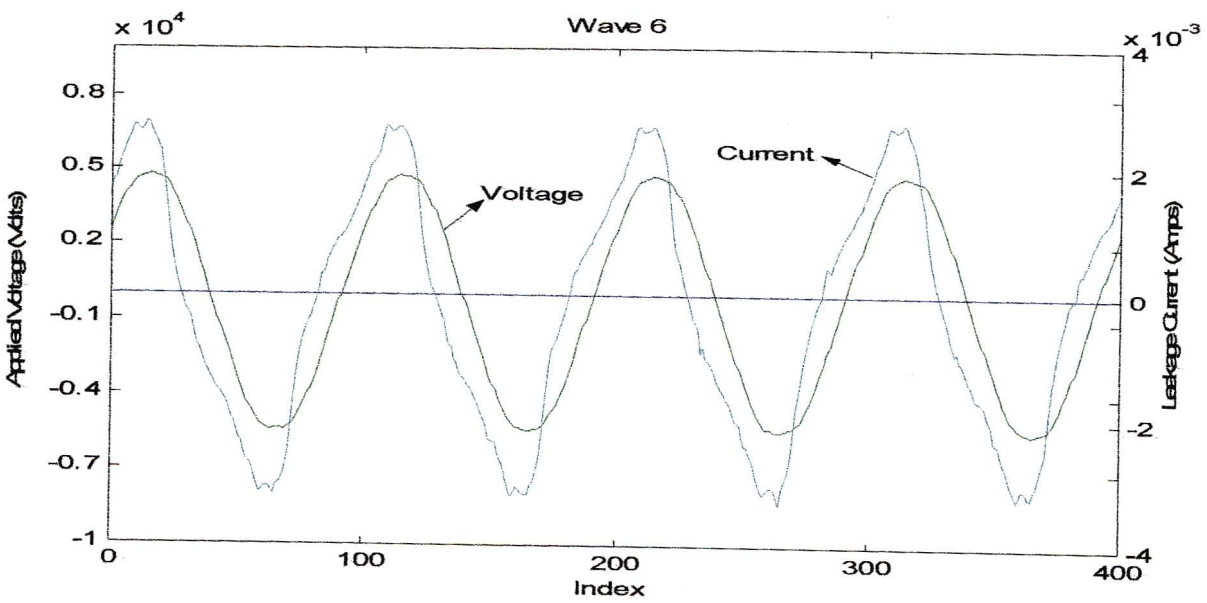
Wave 6
x 10^4
x 10^-3
0.8
0.5
0.2
-0.1
-0.4
-0.7
-1
4
2
0
-2
-4
Current
Voltage
Applied Voltage (Volts)
Leakage Current (Amps)
0
100
200
300
400
Index

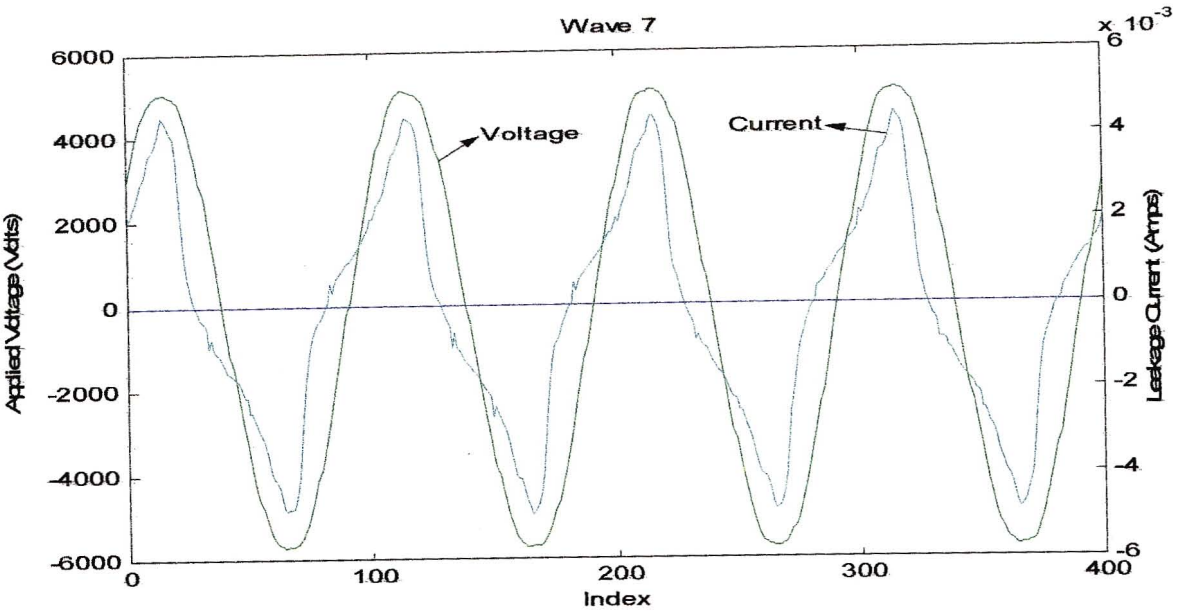
Wave 7
x 10^-3
Voltage
Current
Applied Voltage (Volts)
Leakage Current (Amps)
Index

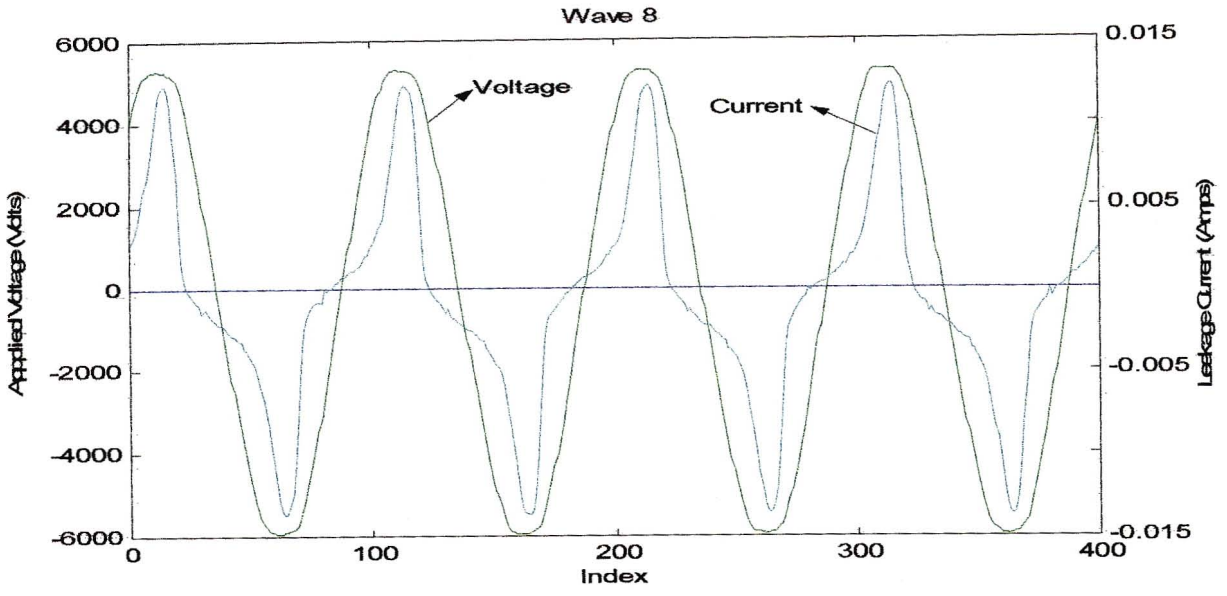
Wave 8
Voltage
Current
Applied Voltage (Volts)
Leakage Current (Amps)
Index

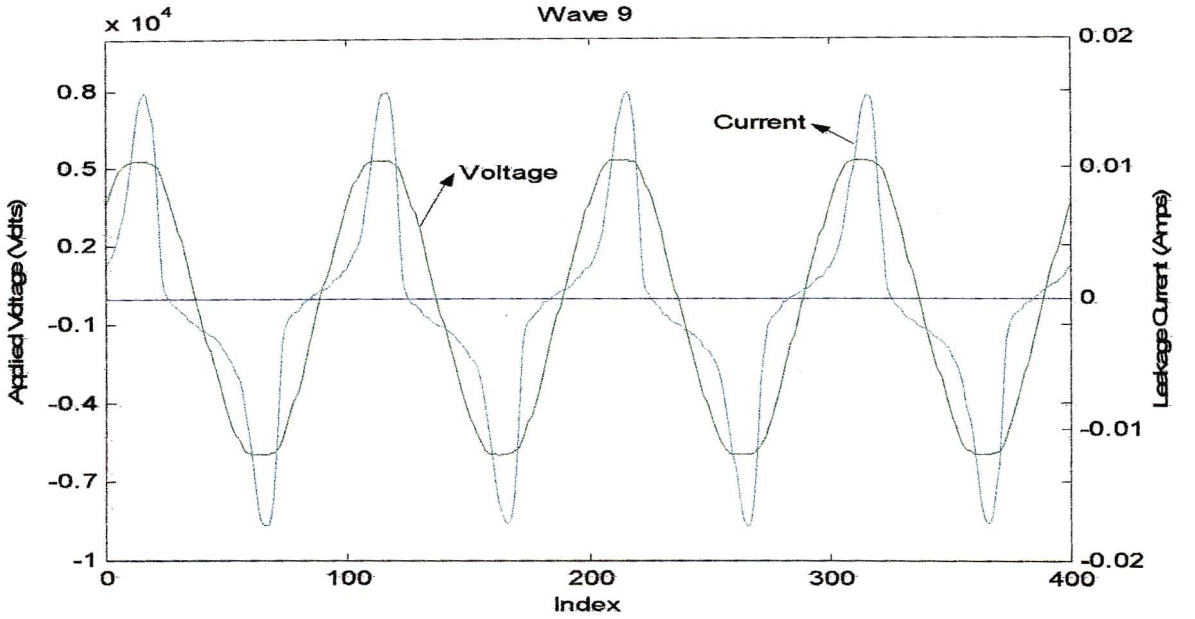
Wave 9
x 10^4
Current
Voltage
Applied Voltage (Volts)
Leakage Current (Amps)
Index

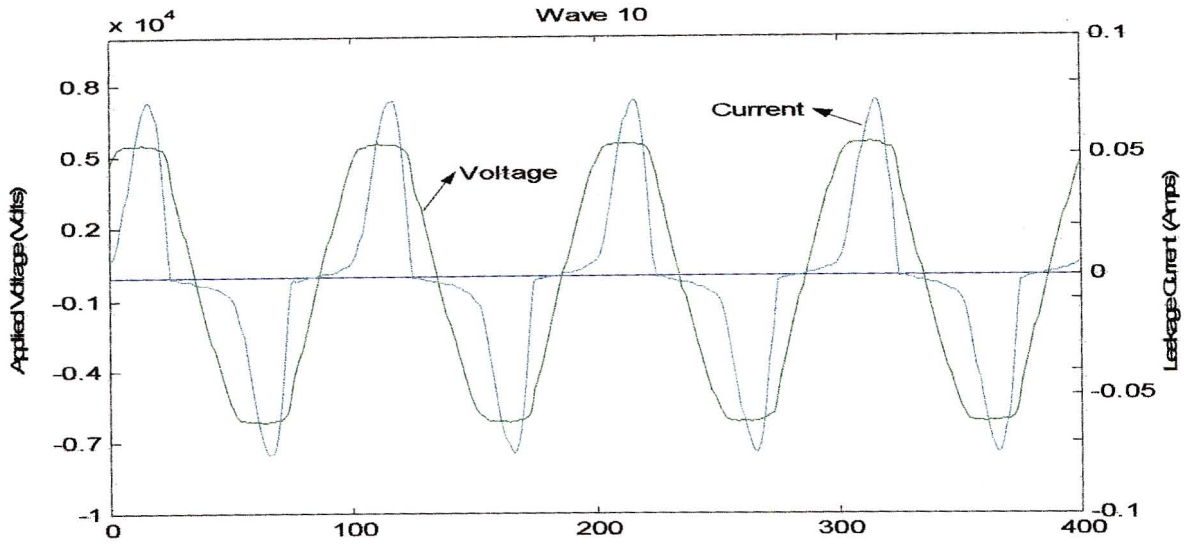

Figure 8.3 Applied voltage and resultant leakage current waveforms of block J1 (increasing applied voltage from Wave 1 to Wave 10)
(100 index points is equivalent to 20ms on the time scale)

8.2.3 Multiple MOV Blocks In Series

Two MOV blocks were placed in series and the V-I characteristic for the double block configuration was measured. The V-I characteristics were measured for three double varistor blocks J1 and J2, C1 and C2 and R1 and R2. Refer to Appendix E for a sample of the V-I measurements taken for the blocks J1 and J2 in double arrangement.

Voltage and current waveforms were measured for 40 cycles of 50Hz. The applied voltage was increased in steps of 0.5kV rms and the corresponding leakage current through the shunt resistor was measured. The applied voltage was increased until the voltage limit of the step up transformer was reached. Most of the measurements were made up until about 8.5kV rms applied voltage.

In Figure 8.4 below the V-I characteristics are shown from 10% COV to approximately 170% COV for two blocks in series. Effectively the COV of two blocks is double the COV of a single MOV block from the same arrester. This means that the applied voltage needs to be doubled in order to produce the similar magnitude leakage currents as for a single block.

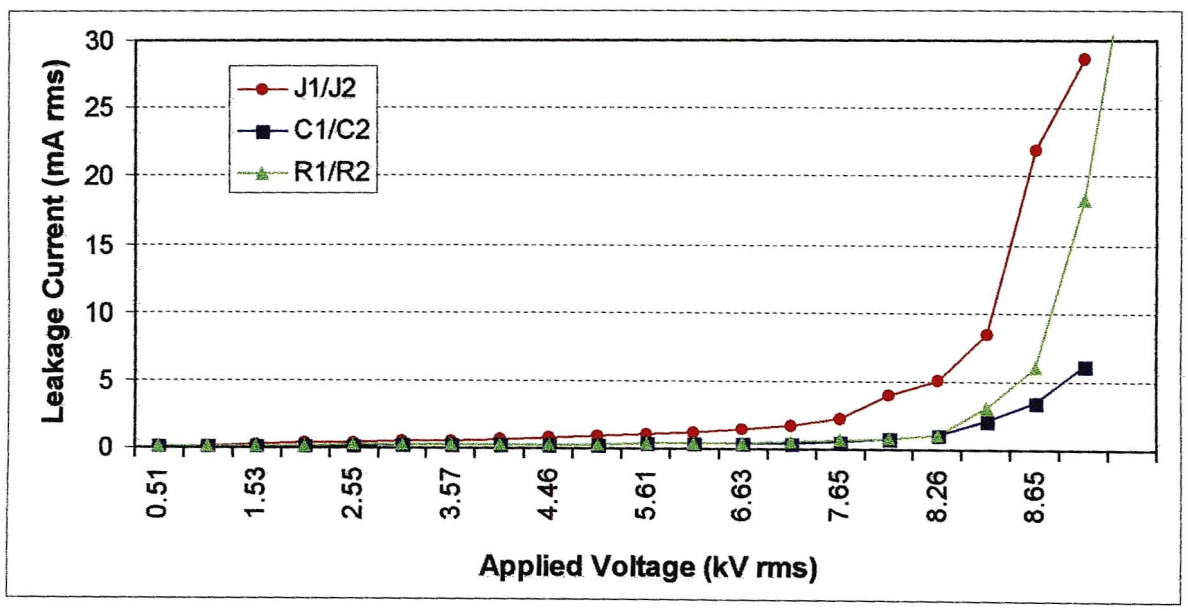

Figure 8.4 V-I measurements of two MOV blocks in series

Three blocks were also inserted in series J1, J2 and J3. Refer to Appendix E for the measured voltage and current values. Figure 8.5 below shows the characteristic curve for one to three blocks in series of manufacturer J. The difference between curves J1 and J1/J2 in series can be clearly seen. The curve J1/J2/J3 (green curve) cannot be clearly seen due to the low measured magnitudes of leakage current.

This was expected as the effective COV of J1/J2/J3 block arrangement is 7.65kV rms and the applied voltage of the transformer had an upper limit of 10kV rms. The measurements were only performed up until 8.7kV rms applied voltage.

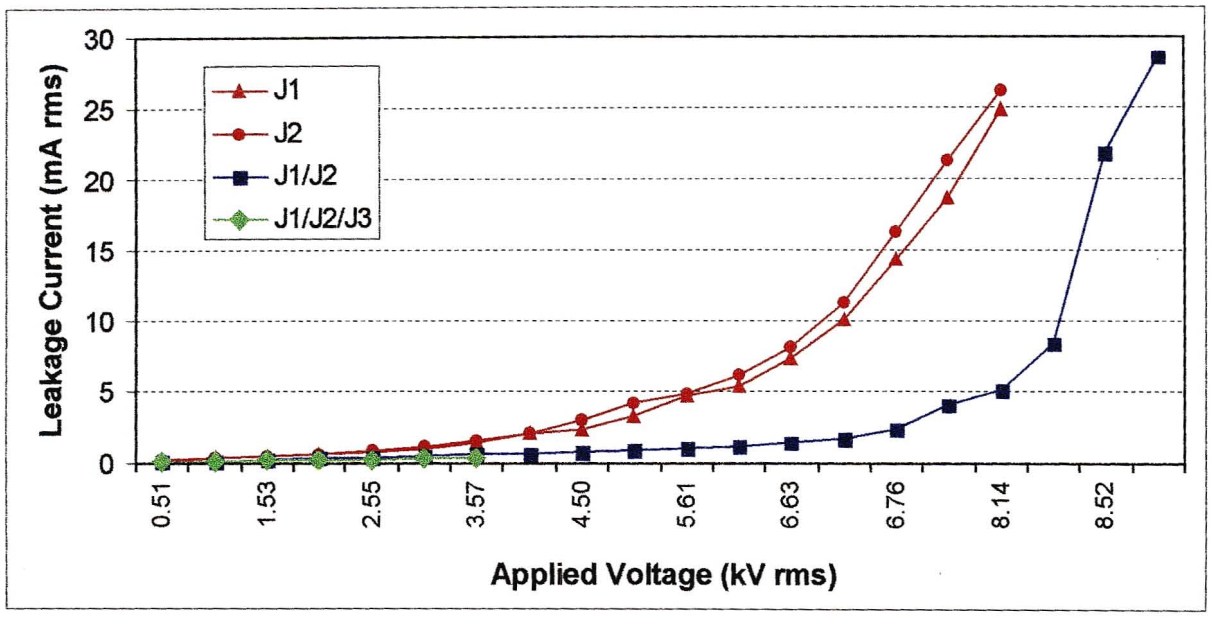

Figure 8.5 Characteristic curves of J blocks in a series arrangement

8.2.4 Failed MOV Blocks

Four MOV blocks were removed from failed arresters from manufacturer J. These blocks were designated as JF1, JF2, JF3 and JF4. The failed arresters had visible signs of physical damage. The cause of the arrester failure and details about the failure were not known. The V-I characteristics were measured for the four failed MOV blocks. Figure 8.6 below shows the V-I characteristics of four failed blocks.

As there can be seen there are two types of failed V-I characteristic curves. One V-I curve is very flat (JF2 and JF4) and the other V-I curve is very steep (JF1 and JF3). For the steep curves the leakage current values were much higher (1.5 to 3 times) than for the healthy tested blocks as shown in Figure 8.2.

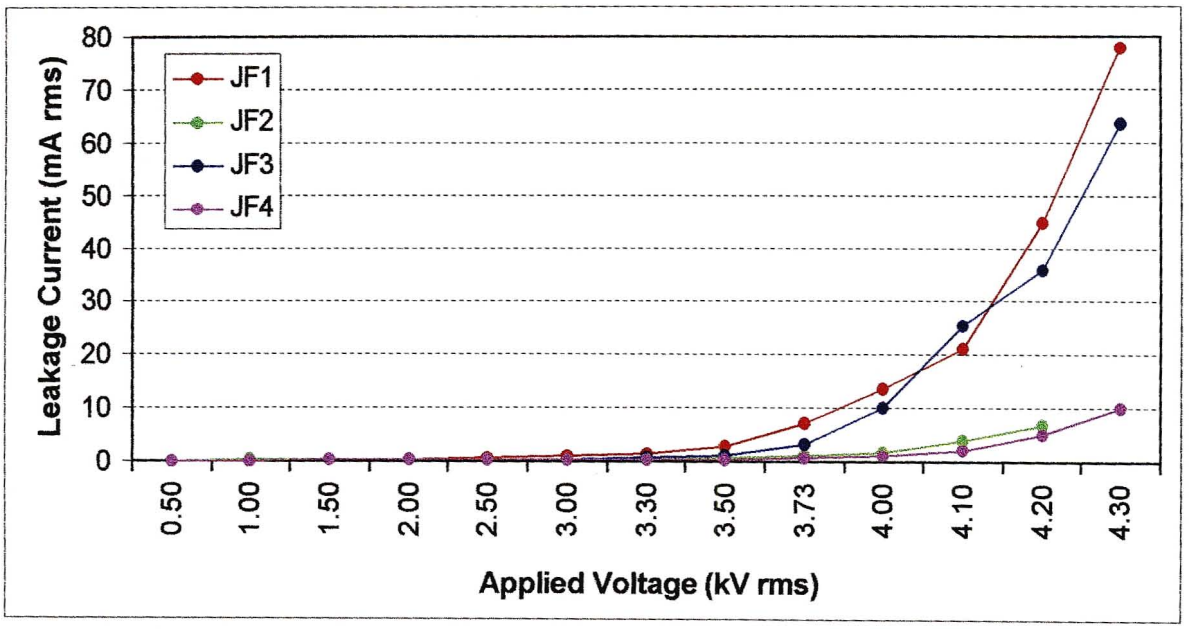

Figure 8.6 V-I characteristic curves of blocks removed from a failed arrester of manufacturer J

8.2.5 MOV Blocks in Parallel under AC Conditions

Various MOV blocks were connected in parallel under AC conditions. The voltage was applied to both blocks and the leakage currents for each block measured separately. The current sharing between the two parallel blocks was quantified by the introduction of a K factor or current sharing factor (De Lorenzi et al, 1987). Equation (7.28) was used to quantify the current sharing.

In (De Lorenzi et al, 1987) it was found that under impulse conditions the current sharing was better at higher currents. Figure 8.7 below shows that under the measured AC conditions the current sharing between two MOV blocks in parallel was worse as the current increased (K factor increased towards two).

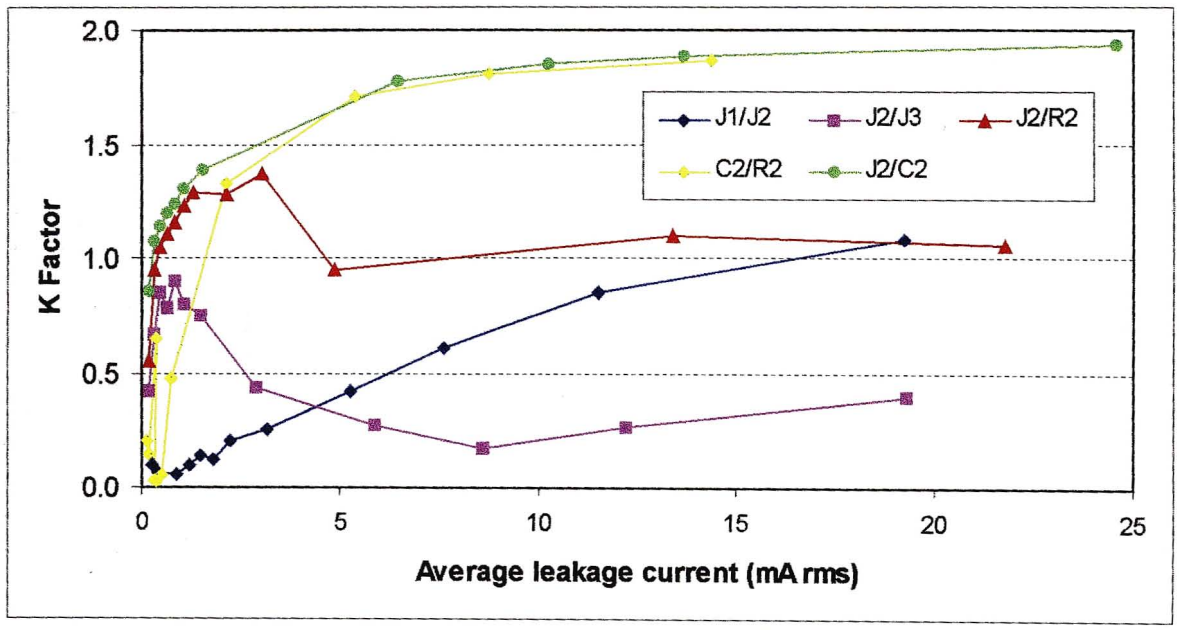

Figure 8.7 Current sharing of MOV blocks under AC conditions

The reason for this may be that under the measured AC conditions only measurements in the medium field region of the V-I curves were performed. This region is highly non-linear and very dependent on the materials used and manufacturing process. Temperature plays a big role on the leakage currents in these region (Schei et al, 1990) and (Schei, 2000).

In (De Lorenzi et al, 1987) the measurements of the arrester units were performed in the high field region where the V-I curve is more linear. The current sharing would become better at higher discharge currents with the impedance of the two blocks approaching similar magnitudes of resistance.

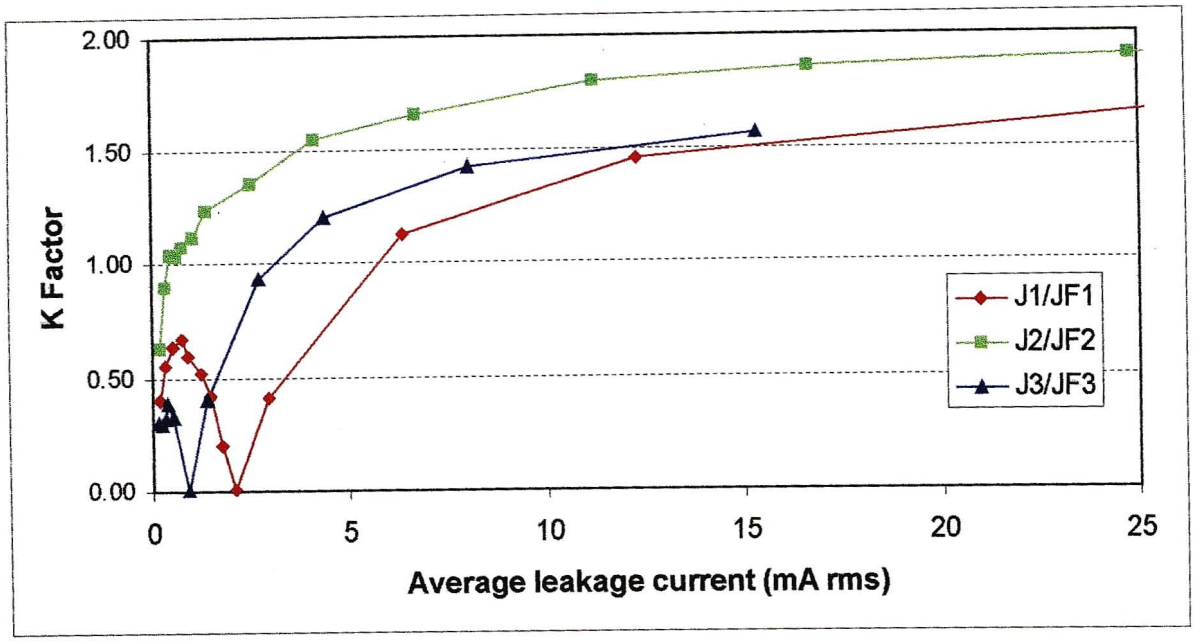

Figure 8.8 Current sharing of healthy and failed blocks in a series arrangement under AC conditions

Figure 8.8 shows what type of current sharing takes place between a healthy and failed block in parallel. This exercise was conducted to test the effect of the two type of different failure curves as discussed earlier. It was found that the type of failure V-I curve had no effect on the current sharing as one of the blocks (either healthy or failed) would draw most of the current in either scenario. Once again it can be seen that under the measured AC conditions the current sharing between two MOV blocks in parallel became worse as the current increased (K factor increased towards two).

8.3 Harmonic Analysis of Waveforms

8.3.1 Harmonic Content of the Leakage Current

Due to the non-linear resistance of the MOV block, the leakage current contains harmonics when the arrester is energised with a sinusoidal voltage. The harmonic content depends on the magnitude of the resistive current and the degree of non-linearity which is a function of voltage and temperature.

In the low electric field region the peak value of the resistive component is usually less than 1mA and the capacitive component is dominant. The voltage distribution at the operating voltage is capacitive and is influenced by stray and grading capacitances. The resistive component in the low field region depends on the granular layer and is influenced by the material used during manufacture and production techniques. The resistive component current can vary a lot from different arresters (Schei et al, 1990).

The capacitive component of the leakage current of an arrester is caused by the permittivity of the non-linear MOV blocks and stray capacitances. The specific capacitance of a MOV block is typically 60 to 150 pF.kV/cm^2. This results in a capacitive leakage current of about 0.2 to 3mA (Schei, 2000). At given values of voltage and temperature the resisitive component of the leakage current is a sensitive indicator of the V-I characteristic of the arrester. The resistive component current can be used as a diagnostic tool to measure the condition of the arrester. The resistive component current is in the order 5-20% of the capacitive current under normal operating conditions. This corresponds to about 10 to 600μA peak resistive current at a temperature of 20 deg C (Schei, 2000).

A harmonic analysis was performed on the leakage current of block J1. The analysis refers to Figure 8.3 with the ten different waveforms of leakage current and applied voltage. A harmonic analysis was performed on the leakage current of plots Wave 2, Wave 4, Wave 6 and Wave 9. This provided a wide range of applied COVs and corresponding leakage currents of the MOV block.

It was possible to separate the capacitive and resistive components of the total leakage current. This allowed one to perform a harmonic analysis on the leakage current. When a Discrete Fourier Transform (DFT) operates on a set of continuous data x(t), a complex value C_n is obtained. The data is transformed to X(f) such that (Orfanidis, 1996) and (Wood, 1988) :

$$C_n = \frac{1}{M} \sum_{U=0}^{M-1} Y_U \, e^{i 2\pi n u / M} \qquad (8.1)$$

where Y_u is the u-th sample value of a total number of M+1 samples and C_n is the n-th factor for the n-th harmonic.

In terms of complex number theory, equation (8.1) may be written in a high level form (Wood, 1988) :

$$C_n = \frac{1}{2}(A_n - iB_n) \tag{8.2}$$

where A_n is the real part of the complex number C_n and B_n is the imaginary part of C_n.

Using Eulers formula, equation (8.2) can be re-written out as the sum of a sine and cosine series each with the same angle for each harmonic calculated.

$$x(t) = \sum_{-(M-1)/2}^{(M-1)/2} C_n e^{-i2\pi nt/T_p} \tag{8.3}$$

Expanding equation (8.3) out

$$x(t) = \sum_{-(M-1)/2}^{(M-1)/2} A_n \cos(\frac{2\pi nt}{T_p}) + B_n \sin(\frac{2\pi nt}{T_p}) \tag{8.4}$$

where T_p is the time period. The equation (8.4) also allows the original function x(t) to be re-constructed from the real and imaginary parts from the DFT transformation.

It can be seen that the DFT operation produces a function that is the sum of two series. The magnitude of the real and imaginary parts of the DFT can be separated. These parts correspond to the capacitive and resistive components respectively of the leakage current.

The above discussed procedure was used to obtain the resistive component of the current in order to measure the harmonic content of the leakage current measured. A MATLAB script M-file was written by the student to obtain the harmonic content of the resistive component of the leakage current.

The M-file had to read in the relevant data file, extract the time and voltage recordings for 4000 samples of 40 cycles and determine the sampling frequency used to record the data.

Refer to Appendix F for the MATLAB™ software code with relevant comments to analyse the current and the voltage waveforms for the harmonic analysis.

From the sampling frequency the Nyquist frequency was calculated for the data. A one dimensional Fast Fourier Transform (FFT) was used to extract the frequency components of the voltage waveforms (Orfanidis, 1996) and (Oppenheim et al, 1989). This was expressed as a percentage of the fundamental frequency magnitude. Refer to Appendix G for a a table of the frequency content of the voltage waveform at the three different currents

The one dimensional MATLAB™ FFT function employs two transforms depending on the length of the sequence (MATLAB, 1997) :

- If the length of the sequence is a power of two then a high speed radix-2 fast Fourier transform algorithm is used.
- If the length is not a power of two, then a slower mixed-radix algorithm is used based on the prime numbers of the sequence length.

The complete data file of forty 50Hz cycles (4000 sample points) was analysed for block J1 at the measured applied voltage. The magnitudes up to the fifteenth harmonic (750Hz) were recorded. These magnitudes were expressed as a percentage of the fundamental frequency. This results can be seen in Figure 8.9 below.

It can be seen that the amplitudes of the harmonic currents generally increase with the applied voltage. The lower part of the V-I characteristic in the low field region is rich in harmonics. The odd harmonics are of interest in a harmonic analysis of the leakage current. Most traditional methods of trying to measure the condition of surge arresters whilst in service look at the third and fifth harmonic of the leakage current, Further detailed discussion about the harmonic analysis can be found in (Lundquist et al, 1990) and (Shirakawa et al, 1988).

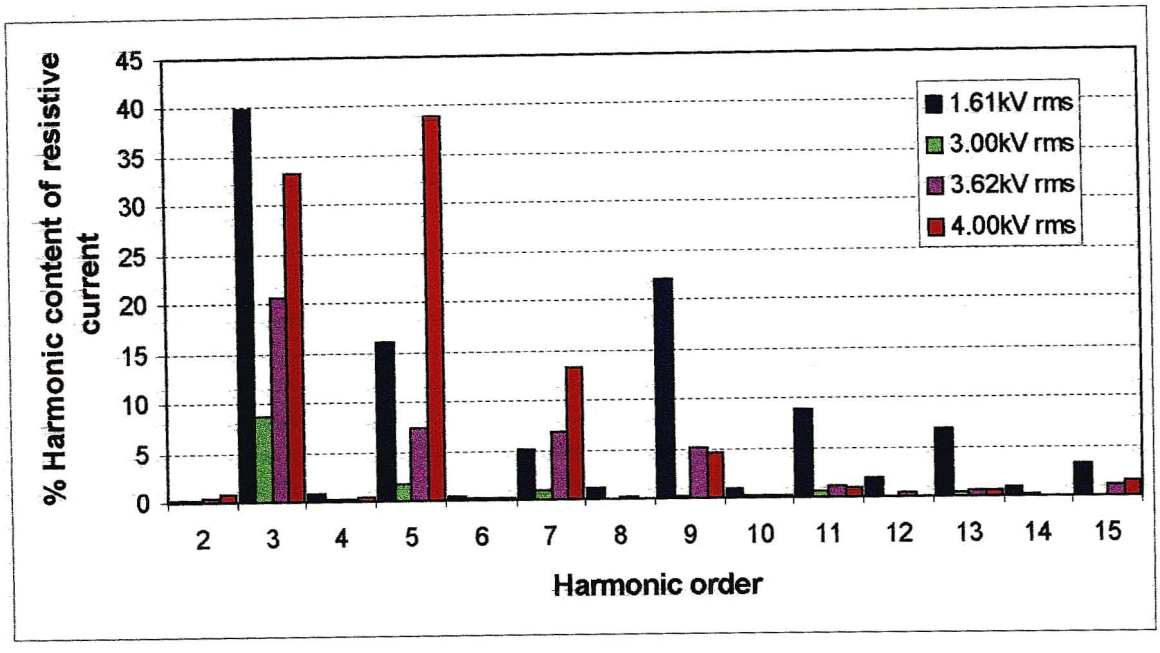

Figure 8.9 Harmonic analysis of the resistive component leakage current of block J1

In Figure 8.9 above and Figure 8.10 below, the high harmonics measured at 1.61kV rms could be due to the high noise-to-signal ratio for the low magnitude measured leakage currents.

The magnitude of the third harmonics recorded was compared to those measured by other researches. It was found that the magnitude of the third harmonics to be 20% to 25% (Van der Linde, 1999) and about 5% to 30% (Lundquist, 1990) of the total resistive component current in the leakage region. A range of 10% to 40% for the third harmonic magnitude was proposed by (Schei, 2000). This compare favourably with those measured by the author. The even harmonics are similar in magnitude (1% to 20%) to those obtained by (Van der Linde, 1999).

The even harmonics have been shown for completeness and additional interest but are not part of the scope of this dissertation. In (Van der Linde, 1999) it was found that that there was a even harmonic component in the capacitive component of the leakage current for the higher field strengths. This indicated that there was a difference in the value of di/dt of the positive and negative slopes. This might indicate that there was a degree of hysteresis in the high field capacitive AC behaviour of a MOV block.

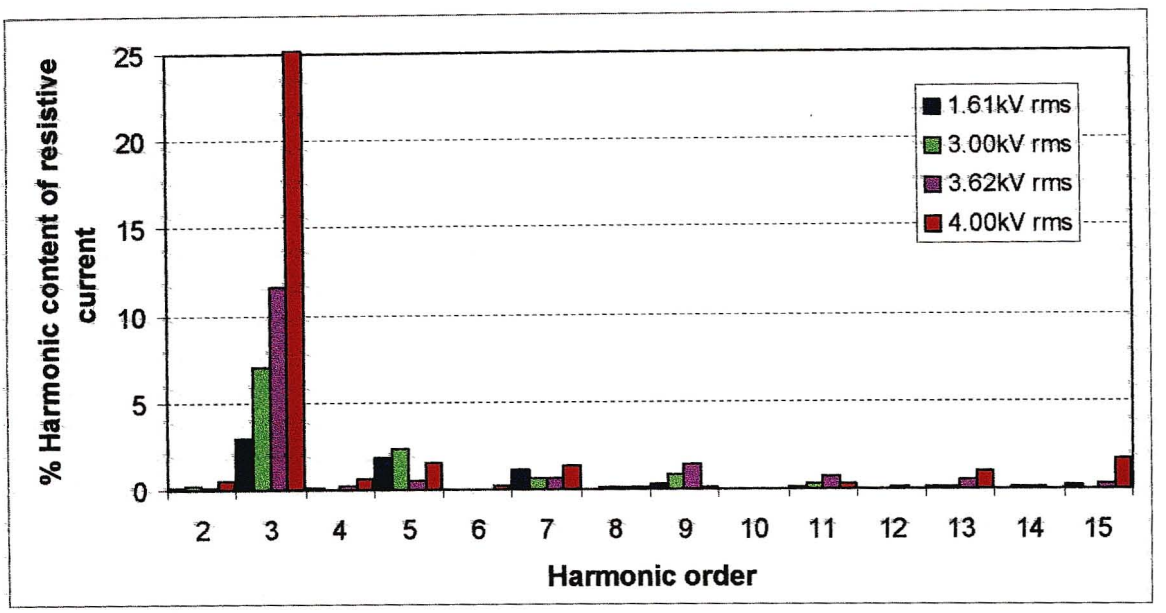

Figure 8.10 Harmonic analysis of the resistive component leakage current of block J2

A harmonic analysis was also performed on the two blocks J1 and J2 in parallel. The total leakage current (sum of currents from each block) was analysed. The results are shown in Figure 8.11 below.

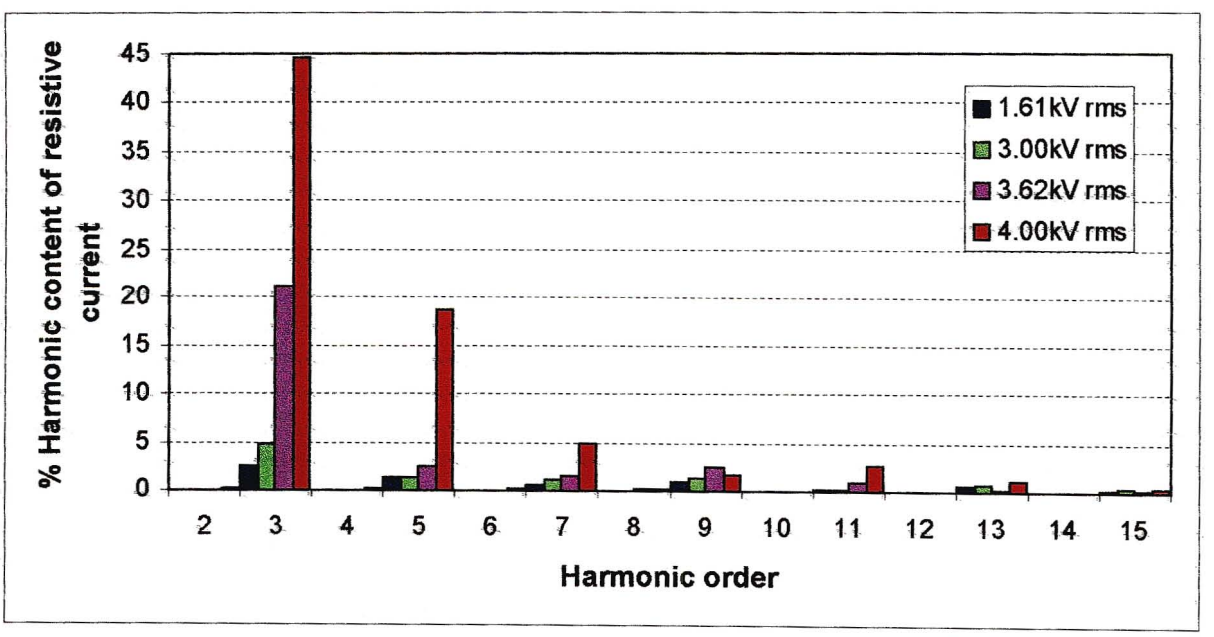

Figure 8.11 Harmonic analysis of the resistive component total leakage current of blocks J1 and J2 in parallel

A harmonic analysis was also performed on the two failed blocks JF1 and JF2. These two blocks had the steep and flat V-I curves respectively.

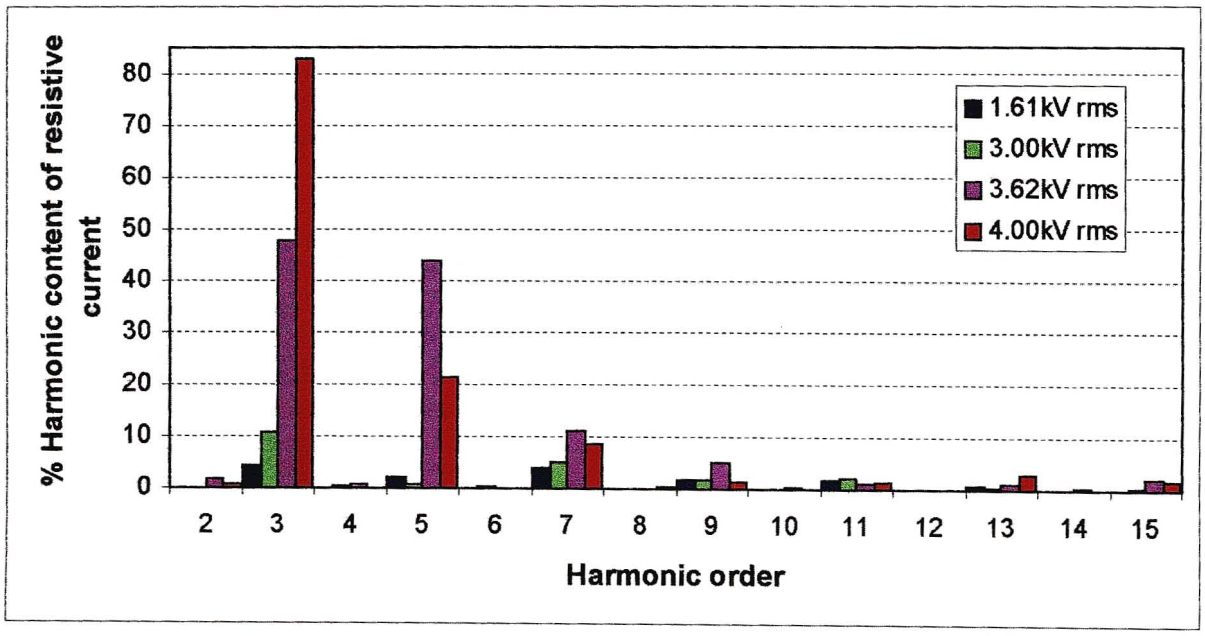

Figure 8.12 Harmonic analysis of the resistive component leakage current of failed block JF1 (steep V-I curve)

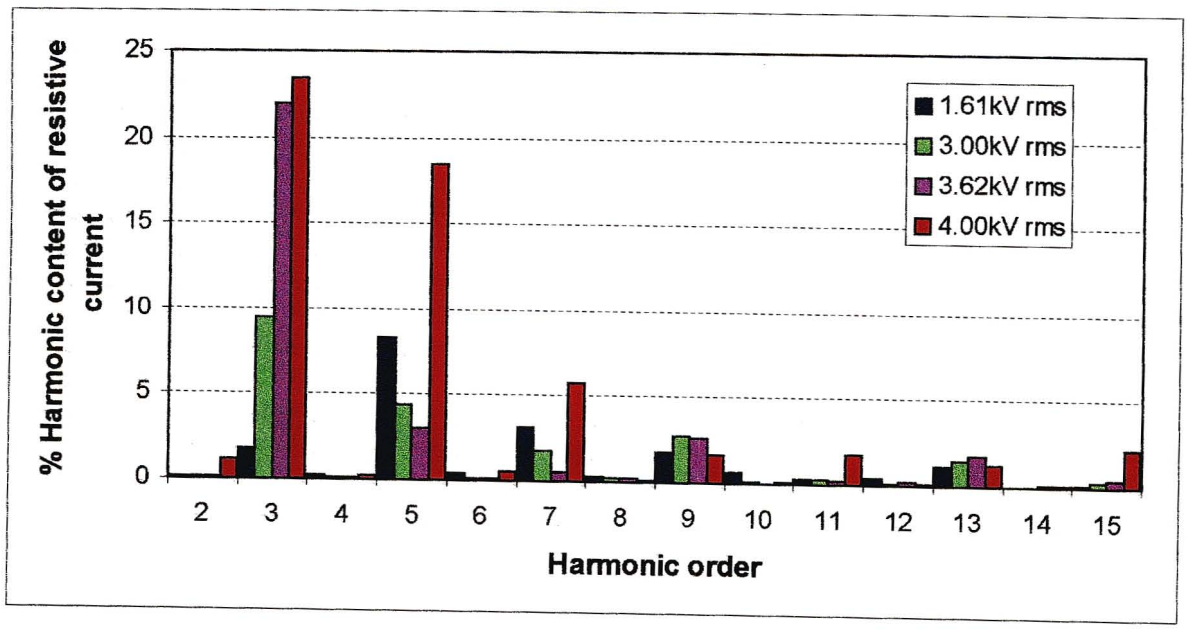

Figure 8.13 Harmonic analysis of the resistive component leakage current of failed block JF2 (flat V-I curve)

The magnitude of the third harmonics in Figure 8.12 and Figure 8.13 above were compared to those obtained in (Van der Linde, 1999). Van der Linde tested several failed blocks and found magnitudes from 2% to 43% for the third harmonic of failed blocks. An interesting point made in (Van der Linde, 1999) was that the failed blocks may not have actually failed but the abnormalities may be related to the insulation.

8.3.2 Resistive and Capacitive Component Current Waveforms

Figure 8.14 below shows the plots of the total current, resistive component (blue curve) and the capacitive component (green curve) currents of block J1. The total current (red and yellow curves) is the original measured leakage current and the re-constructed current. Equation (8.14) was used to separate the two current component waveforms. The software code used can be found in Appendix F. There was a visible overlay of the total current waveforms confirming the correctness of equation (8.14). At low applied voltages, the capacitive component current dominates as in the plot Wave 2. There is a significant DC offset between the measured total current and the derived capacitive component that has not been removed.

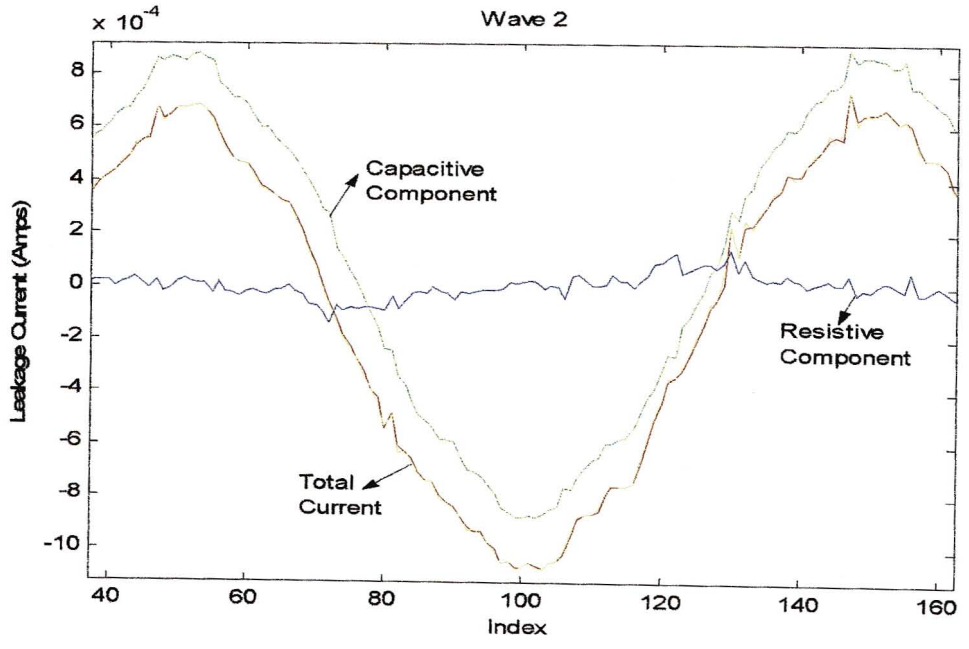

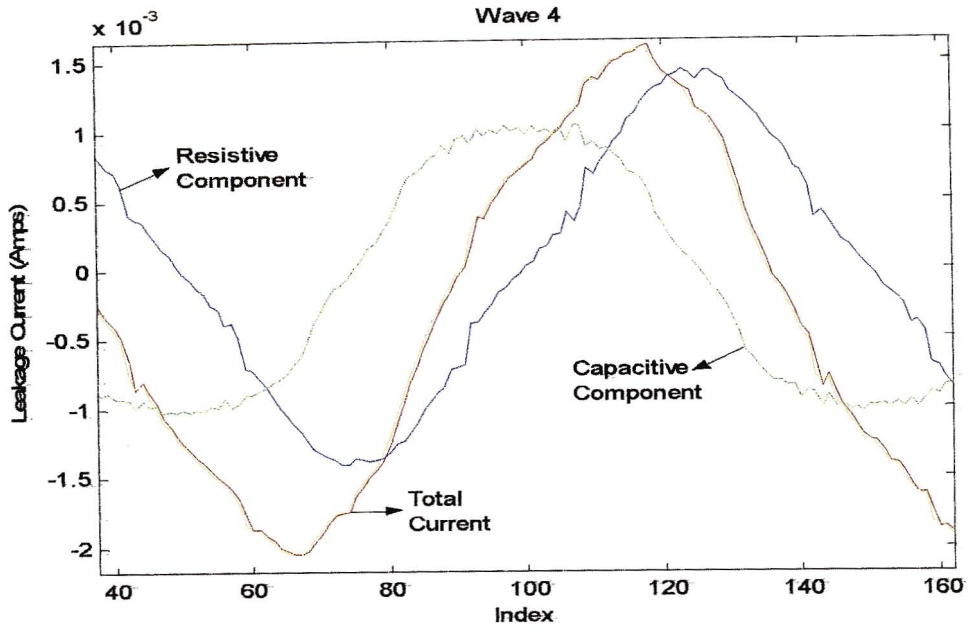

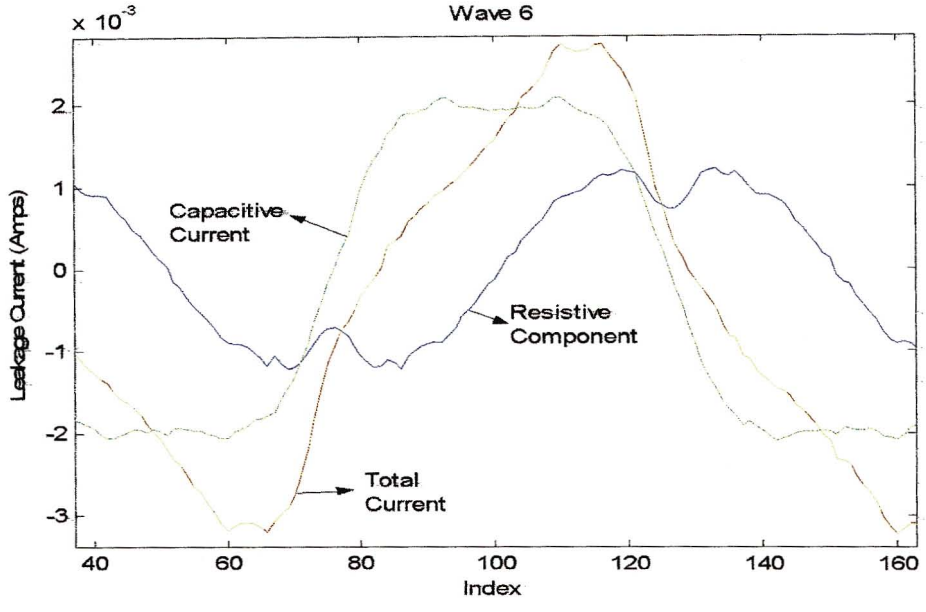

At higher applied voltages the non-linear resistive component current starts to dominate as in plot Wave 4. In plots Wave 6 and Wave 9 the resistive component is dominant. The block is now operating at the start of the transition region of the V-I curve. An advantage of this method was that the DFT used was measured over 40 cycles.

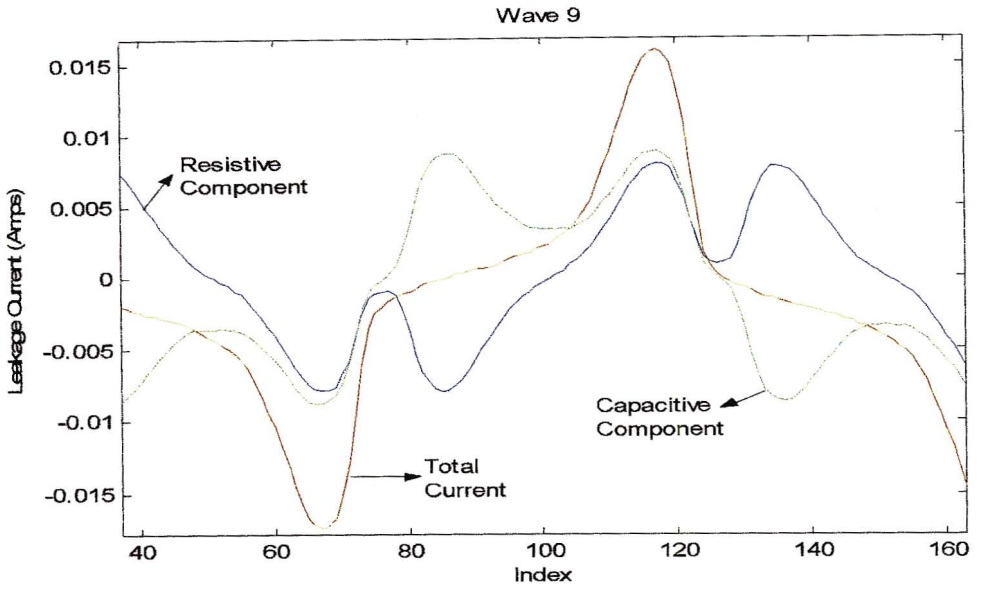

Figure 8.14 Plots of current components of leakage current of block J1 increasing applied voltage from top to bottom pages
(100 index points is equivalent to 20ms on a time scale)

8.3.3 Voltage Distortion with Resistor Load

In (Van der Linde, 1999) it was reported that distortion of the voltage waveform occurred for leakage currents greater than 2mA rms. The distortion was in the form of a slight flattening of the negative and positive half cycle peaks of the voltage waveform. The rest of the waveform was still sinusoidal. The three possible causes identified were :

- The varistor block limits the voltage
- Clipping due to the measurement circuit
- Poor voltage regulation

Van der Linde concluded that the voltage distortion was due to poor voltage regulation. The distortion of the voltage waveform caused oscillations of the current waveform that the value of current could not always be reliably measured at the voltage crossing if the current was larger than 2mA rms. The source could only be used for loads up to 2mA rms.

This conclusion of Van der Linde was tested in the laboratory. Eight 4kΩ wire-wound resistors were used in series as the load in the measurement circuit. The overall resistance was measured to be 31.63kΩ. The inductance of each resistor was measured to be 1.75mH at 1kHz. At 50Hz frequency this equals an inductive reactance of 0.55Ω.

The resistors were tested in the circuit for applied voltages from the source for increasing measurements of currents 32mA, 85mA and 130mA peak to peak respectively. There was no voltage distortion (waveform clipping) observed even at 130mA p-p load (4.18kV rms applied voltage). Refer the corresponding plots in Figure 8.15 below.

The applied voltage increases from top to the bottom in the plots. The visible distortion at 32.17mA seems to be due to the low signal to noise ratio at these levels. The harmonic analysis seems to confirm that there was no distortion of the voltage waveform.

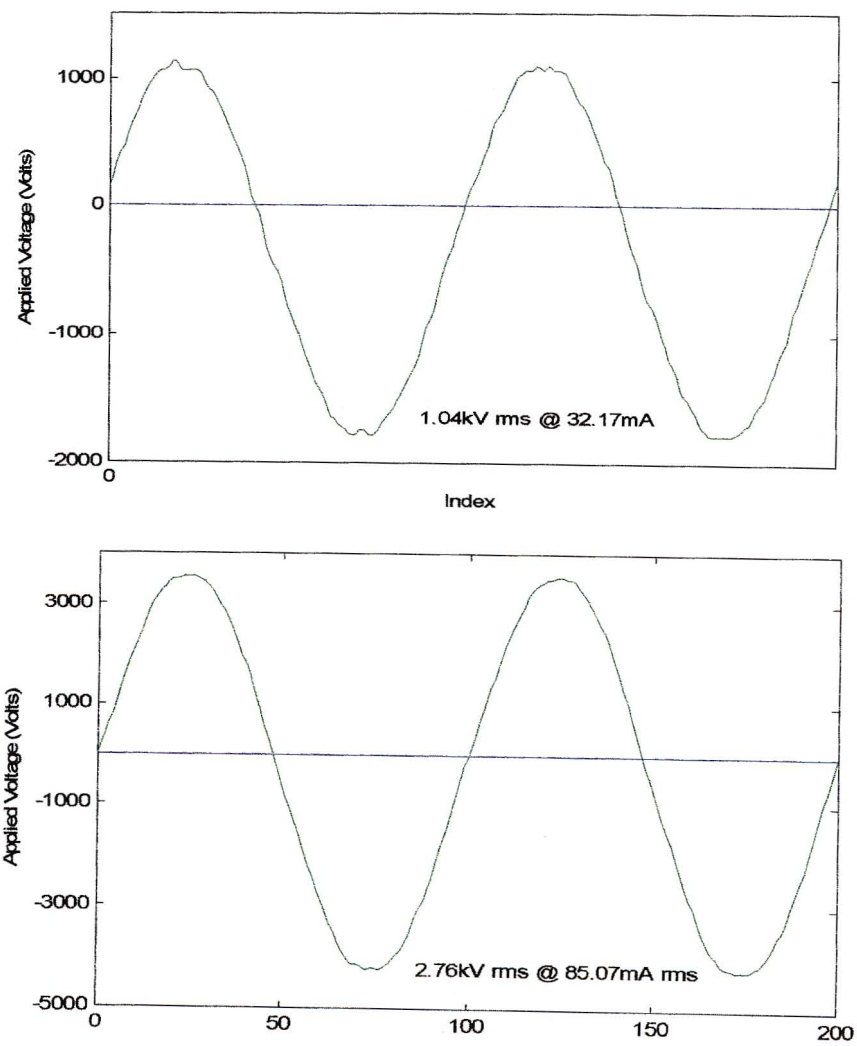

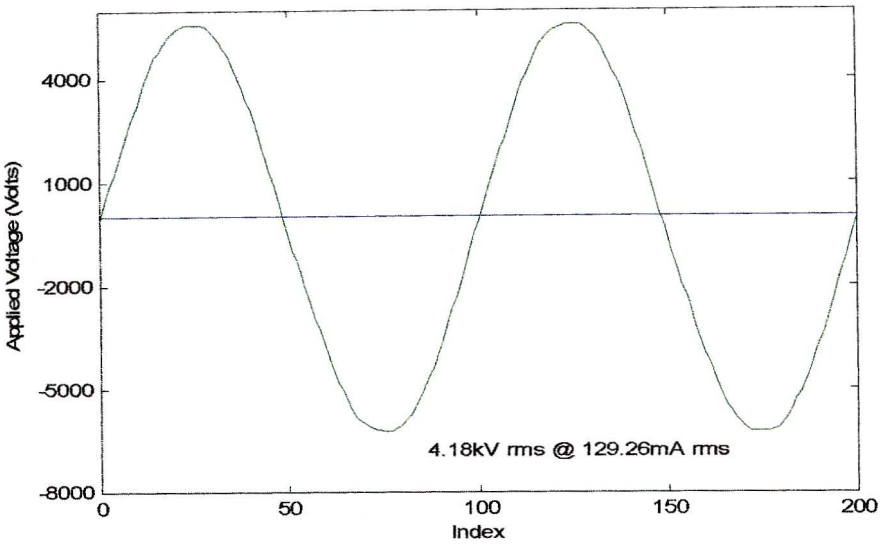

Figure 8.15 Different applied voltages with resistor load

A Discrete Fourier Transform (DFT) was performed on each recorded voltage waveform. A MATLAB script M-file was written to obtain the harmonic content of the voltage waveform. The harmonic order was calculated up to the 10^{th} order (500Hz). Beyond the 10^{th} order the percentage components became very small and were there for regarded as negligible for this particular exercise. Refer to Appendix G for the results.

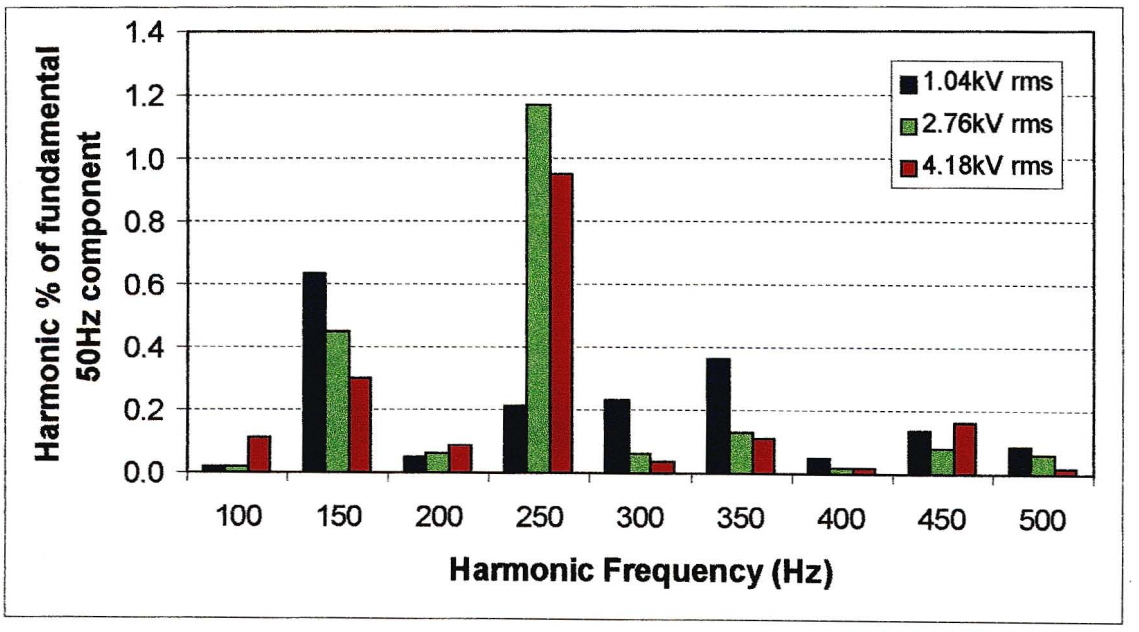

Figure 8.16 Harmonic analysis of applied voltage waveforms

It can be seen in Figure 8.18 above that the 250Hz component (5^{th} order component) is the major harmonic component with a calculated peak of 1.17%. The distortion level of the voltage waveform is very small and the voltage waveform can be regarded as pure sinusoidal waveform with no distortion.

8.3.4 Voltage Distortion by MOV Blocks

It was decided to also experiment on single MOV blocks to determine if a MOV block could result in clipping of the applied waveform. The voltage was applied to blocks J1 and C1. The applied voltage was increased to just before the corresponding 2mA rms clipping limit and just after 2mA rms limit as defined by (Van der Linde, 1999). Figure 8.17 below shows the harmonic content of the voltage waveforms at 1.8mA rms and at 2.35mA rms current limits. Refer to Appendix G for the measured results.

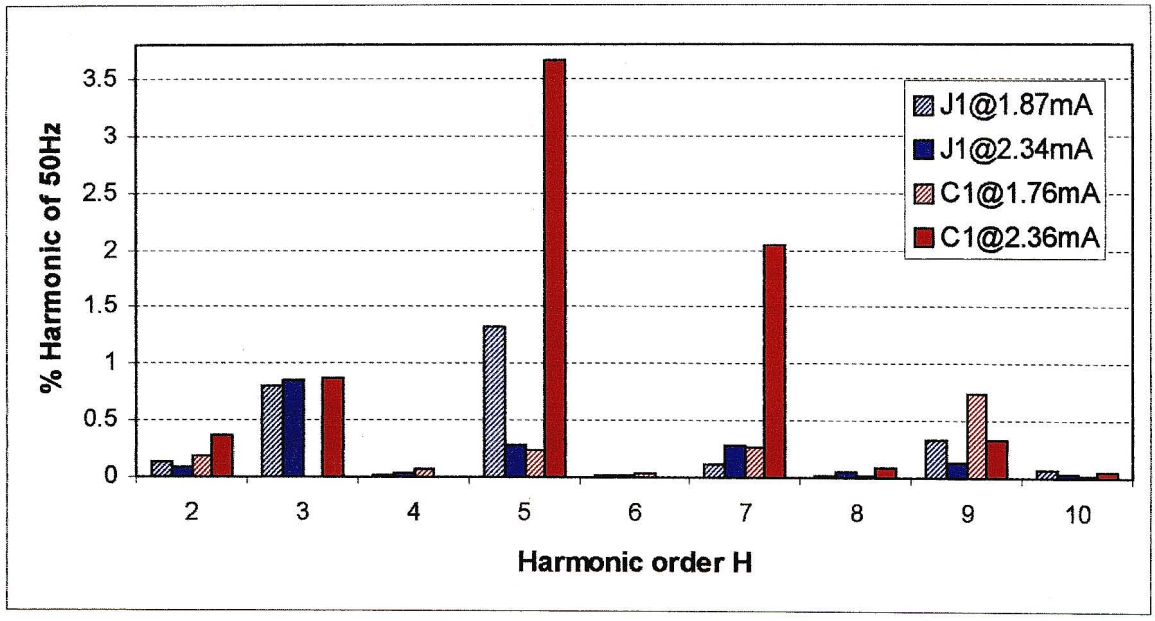

Figure 8.17 Harmonic content of voltage waveform for blocks J1 and C1

There was observed distortion of the voltage waveform for block C1 above 2mA rms load for the fifth and seventh harmonic. Table 8.1 below compares the Total Harmonic Distortion (THD) of each waveform for Figure 8.16 and Figure 8.17.

The THD is given by (NRS 048, 1996) :

$$THD = \sqrt{\sum_{h=1}^{N} V_h^2} \qquad (8.5)$$

where V_h is the per cent value of the fundamental frequency of the h^{th} harmonic

N is the highest harmonic considered (N<=40)

The maximum THD specified by the NRS 048 is 8%. A comparison of the THD's for the above waveforms is given in Table 8.1.

Table 8.1 THD of each voltage waveform

Load (mA rms)	% THD OF 50Hz
Resistor@32.17mA	0.82
Resistor@85.07mA	1.27
Resistor@129.26mA	1.02
J1@1.87mA	1.59
J1@2.34mA	0.96
C1@1.76mA	0.84
C1@2.36mA	4.31

It can be seen that block C1 has a THD of 4.3% at a current of 2.36mA. One can conclude that the MOV block does clip or distort the voltage waveform.

8.4 Temperature Dependence of MOV Blocks

The temperature dependence of the MOV block was determined by varying the block's temperature and keeping the applied voltage fixed. The block was heated in the oven and then inserted into the measurement circuit. A voltage was applied and the corresponding leakage current measured. The block was sometimes allowed to cool down to the specific target temperature and then the voltage applied and the leakage current measured. The temperature tests were performed on one block per manufacturer. The blocks J2, C2 and R2 were tested and graphs of the results are plotted below.

The temperature was increased from 30 °C to 110 °C. The applied voltage was increased from 50% COV to 150% COV to provide a wide range of operating temperatures and continuous operating voltages. Appendix H provides a full set of the measurements for the temperature dependence tests on blocks.

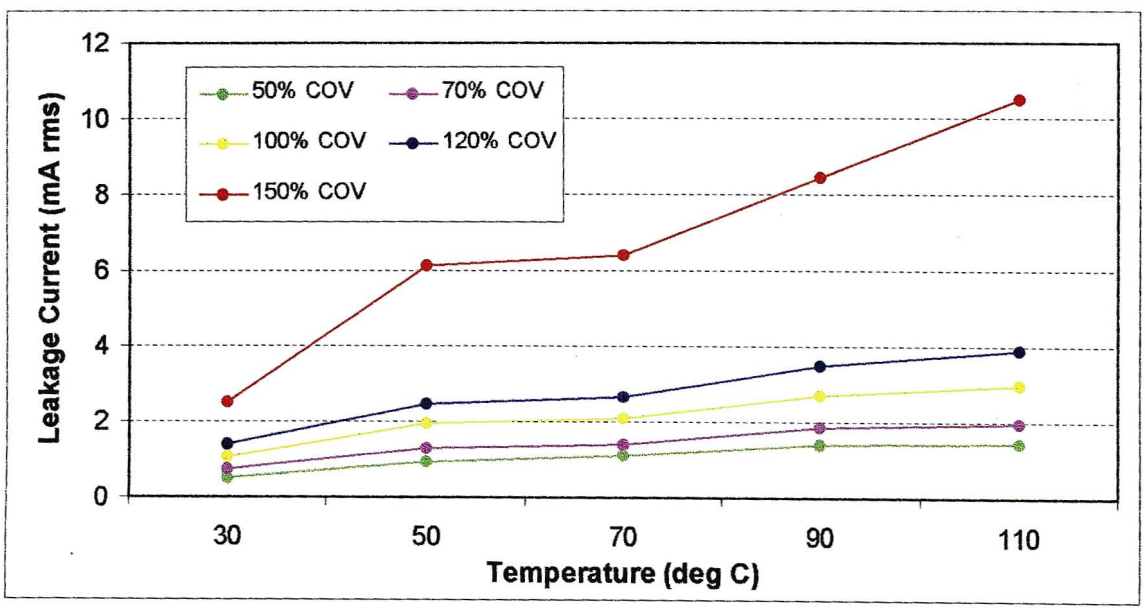

Figure 8.18 Temperature dependence results of block J2

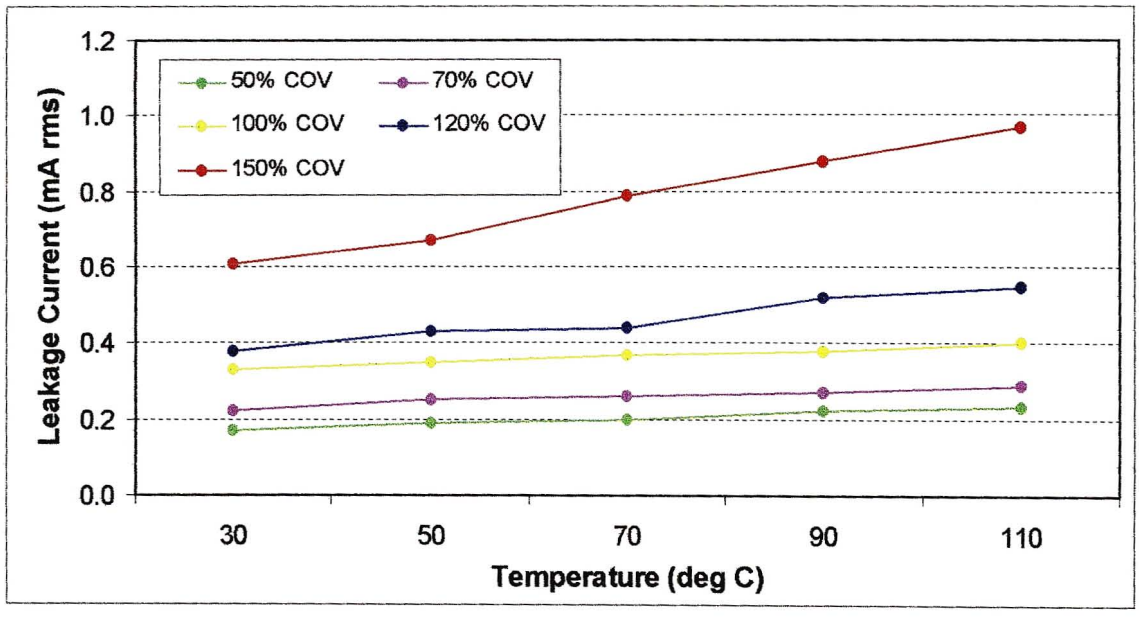

Figure 8.19 Temperature dependence results of block C2

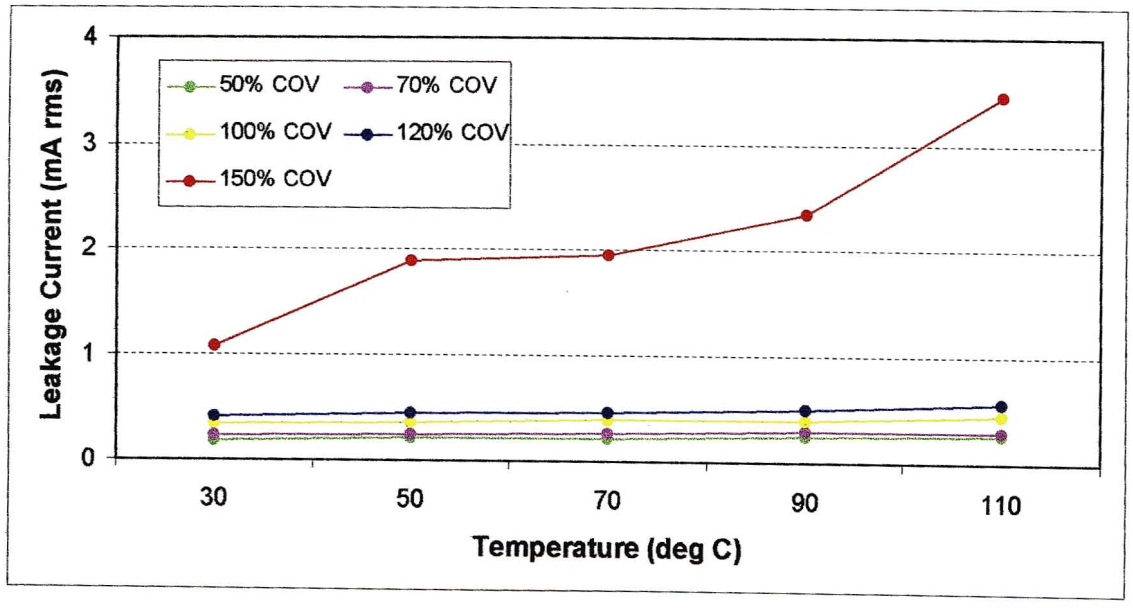

Figure 8.20 Temperature dependence results of block R2

The temperature dependence of the leakage current is well documented in (Schei et al, 1990), (Spellman et al, 1997) and (Bronikowski et al, 1982). It is the temperature dependence of the ZnO material that causes the well known phenomenon of thermal run away.

At 50% and 70% COV, the leakage currents were found to be linear for the temperature range 30 °C to 70 °C. The capacitive current component is dominant and changes accordingly with an increase in temperature. At 70% COV and 100% COV the resistive component was seen to be measurable. The variation with temperature in this operating region is the combined behaviour of the capacitive and resistive current.

The 120% COV and 150% COV V-I characteristic of the sample blocks is highly non linear. The magnitude of leakage currents of 150% COV is several orders of magnitude higher. Block R2 in Figure 8.20 has the most notable difference, refer to the red 150% COV curve. The resistive component of the R blocks can be assumed to have a temperature characteristic that is of a higher degree of non-linearity than the other two blocks. Small changes in applied voltage effect the leakage current significantly.

The behaviour of the different type blocks varies significantly with temperature. Most of the temperature dependence measurements are limited to 135 °C, above this thermal runaway could result (Van der Linde, 1999).

Experiments were also conducted on parallel block arrangements where the temperature dependence of the total leakage current was studied. Figure 8.21 and Figure 8.22 below show the study of healthy blocks in parallel and the effect of temperature.

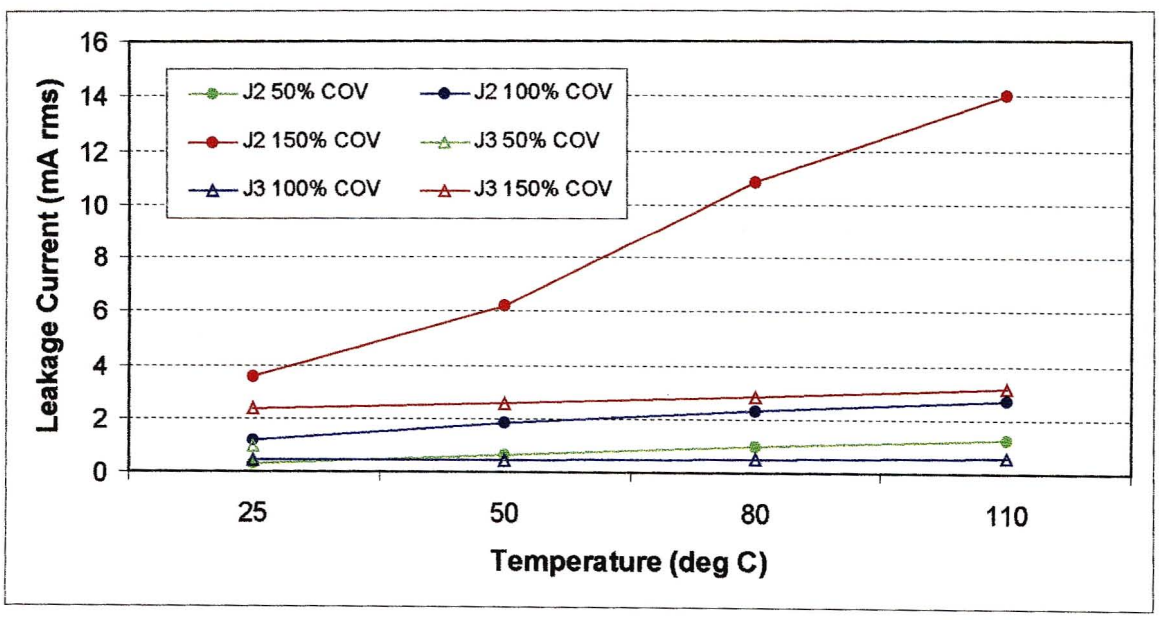

Figure 8.21 Temperature dependence results of blocks J2 and J3 in parallel

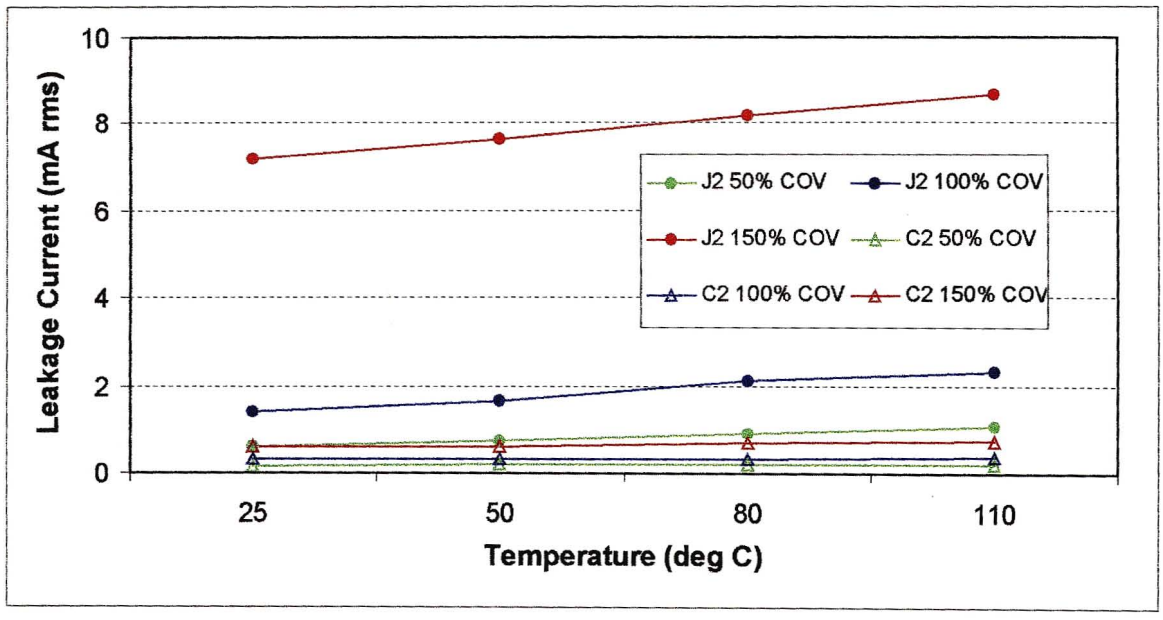

Figure 8.22 Temperature dependence results of blocks J2 and C2 in parallel

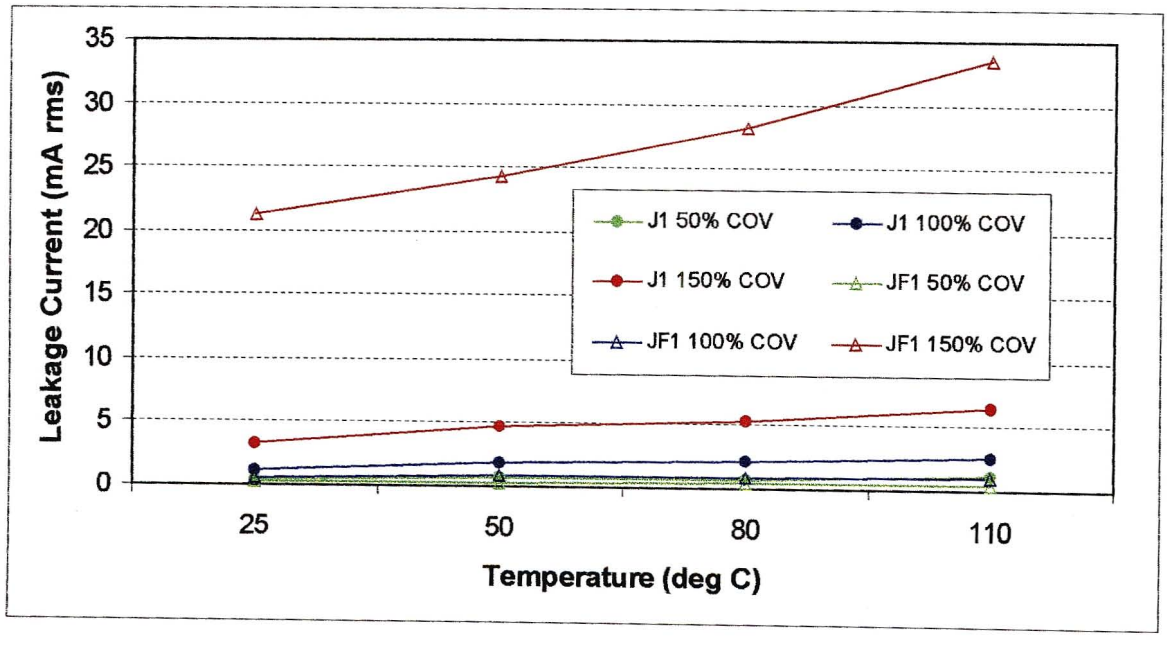

Figure 8.23 Temperature dependence results of blocks J1 and JF1 in parallel

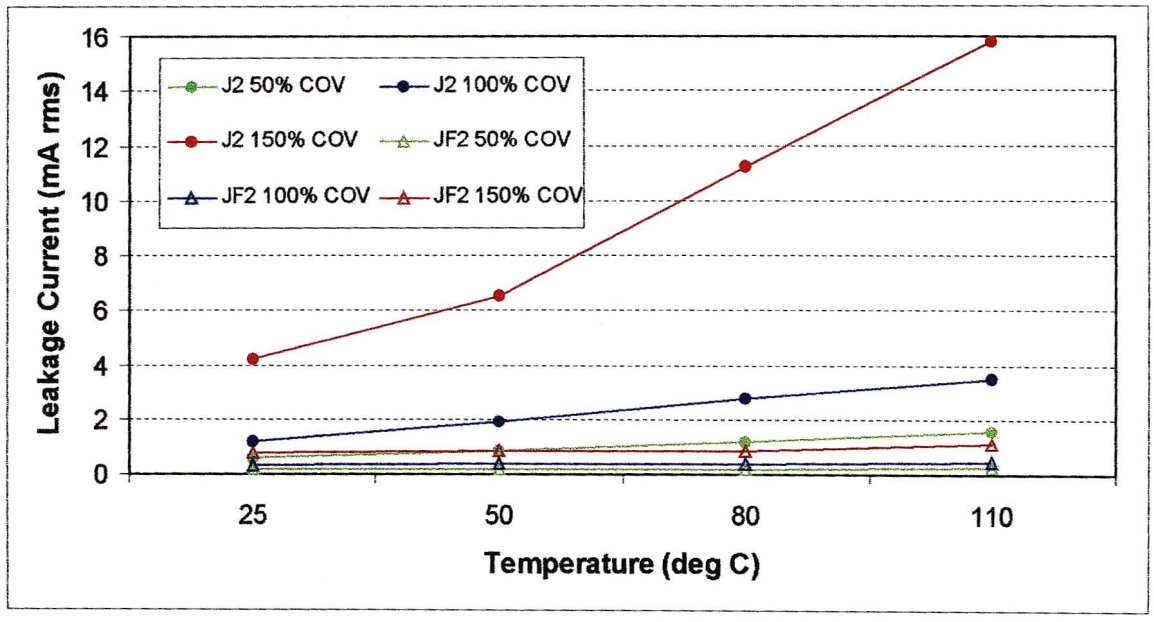

Figure 8.24 Temperature dependence results of blocks J2 and JF2 in parallel

The temperature effects the linear current range (currents less < 1mA) of the V-I characteristic curve whereas the non-linear region (current > 1mA) does not vary as a function of temperature. The influence of temperature on the response characteristics of ZnO elements is not that clearly understood (Asokan et al, 2000).

An in depth discussion about the arrester degradation under AC voltage and a theoretical analysis of the thermal stability and the effect of degradation on the performance of the MOV block is presented in (Mizuno et al, 1990).

8.5 Impulse Testing of MOV Blocks

8.5.1 Laboratory Set Up

In the laboratory, an impulse voltage with a rise time of approximately 200ns was generated by the capacitor bank and applied to the various MOV blocks (as used in the earlier power frequency experiments). The applied peak impulse voltage was increased in steps and the corresponding discharge current of the MOV block was measured and the waveform recorded by using the HP Scopelink program.

The capacitor bank consisted of six 33μF capacitors in parallel. A DC supply provided charging voltages up to 10kV at a maximum charging current of 5A. A high voltage ignitron (English Electric BK 472 with a stainless steel anode) was used as the main switch.

A Pearson current transformer (CT), model number 4160 (0.01V/A ratio) was used to measure the discharge current for the single MOV blocks. It was found from the data sheet that the 4160 model Pearson had a usable rise time of only 200ns. A smaller second clip on type Pearson CT model number 3525 (0.1V/A ratio) was obtained. This CT had a usable rise time of 25ns. The disadvantage of this CT was that the rated current time product was only 0.5 A.s. This meant that the larger Pearson (model 4160) with a rated current time product was 2.5 A.s. was used for the larger discharge current measurements and the smaller Pearson (model 3525) was used for the smaller discharge current measurements.

For the parallel MOV block experiments the larger Pearson CT (model 4160) and a wideband width (200MHz) co-axial current shunt (0.01Ω) was used. Only discharge currents for applied impulse voltages of 6.5kV rms and greater were looked at.

This was due to the better signal to nose ratio with the current shunt at these discharge currents. The current shunt was found to be very noisy at the lower discharge currents.

8.5.2 Recorded Discharge Waveforms

Below is a set discharge current waveforms of block J2 for various magnitude applied impulse voltages. One can see how initially the capacitive component current (short duration spike) in Figure 8.26 is dominant and later on the resistive component current in Figure 8.27 becomes more dominant.

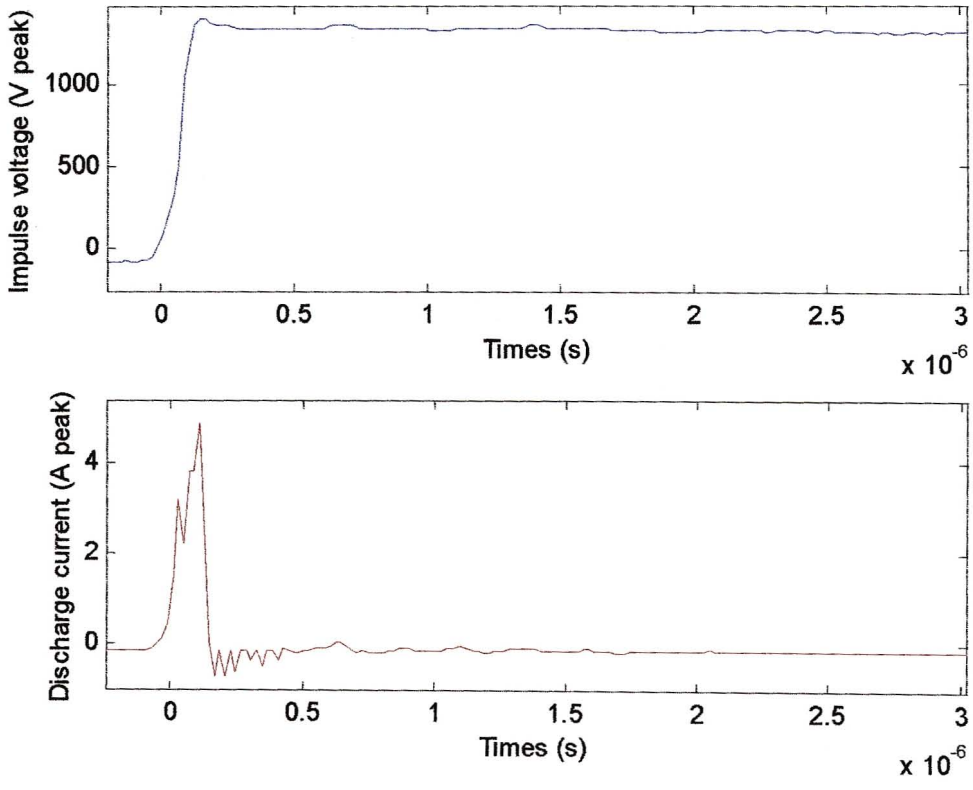

Figure 8.25 Example of a recorded applied impulse voltage and corresponding discharge current of MOV block J2 (notice the capacitive current)

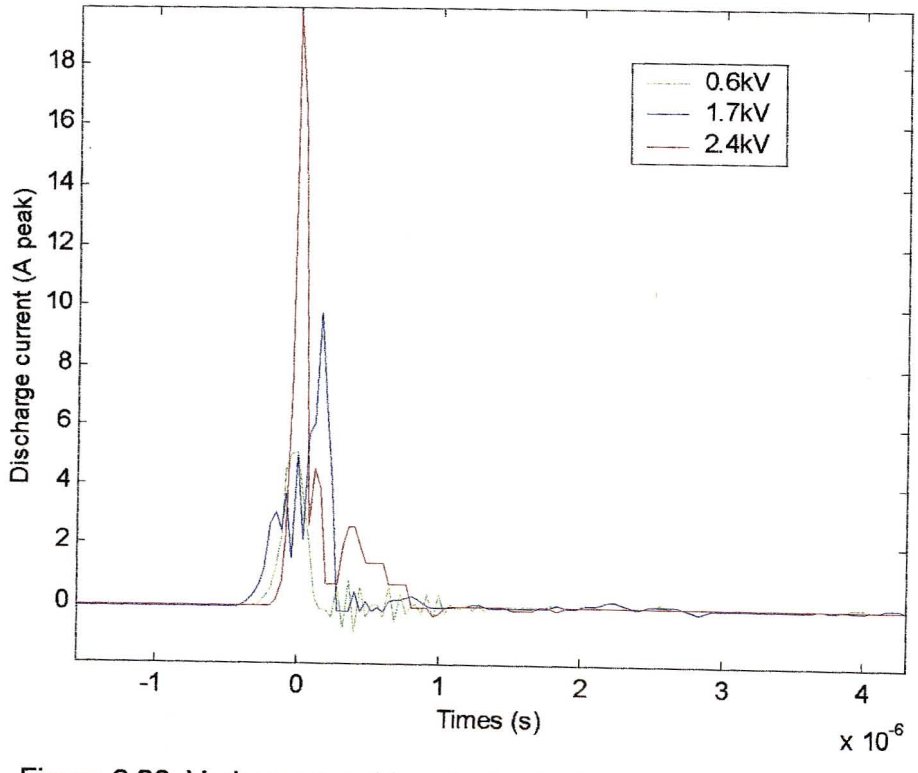

Figure 8.26 Various capacitive discharge currents for block R1 for Increasing applied impulse voltages

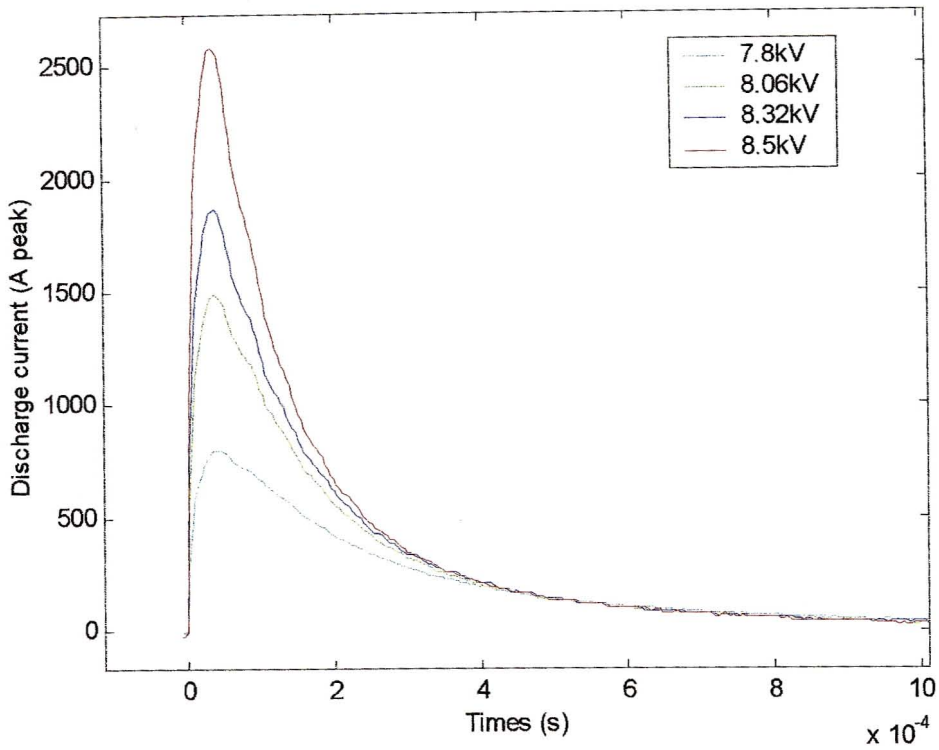

Figure 8.27 Various resistive discharge currents for block R1 for Increasing applied impulse voltages

8.5.3 Energy Absorbed by MOV Blocks

The energy absorbed by each MOV block was calculated by using a written MATLAB M-file. This file used the recorded discharge current and impulse voltage waveforms and calculated the energy absorbed by the block. Refer to Table 8.2 and Table 8.3 below.

The electrical energy absorbed W is the integral of the product of the voltage and current with respect to time. In the discrete domain this can be re-written as :

$$W = \sum_{t=0}^{\infty} v_n . i_n \Delta t \qquad (8.6)$$

Where V_n and i_n are the voltage and current samples at time t respectively and Δt is the sampling interval.

Table 8.2 Example of energy and impedance calculations for block J2

Impulse Voltage (kV peak)	Discharge Current (A peak)	Energy Absorbed (J)	Impedance V/I (ohms)
1.40	4.94	0.0078	283
3.90	15.1	0.0660	258
4.80	23.1	0.1300	208
7.68	146.5	2452	52
8.06	501.0	3188	16
8.21	879.6	3629	9
8.38	1250.0	4002	7
8.48	1687.0	4365	5
8.60	2265.0	4689	4

Table 8.3 Example of energy and impedance calculations for block C2

Impulse Voltage (kV peak)	Discharge Current (A peak)	Energy Absorbed (J)	Impedance V/I (ohms)
1.53	4.50	0.0081	340
2.84	9.80	0.0491	290
4.10	15.93	0.10	257
6.81	30.0	0.32	227
7.56	40.6	634	186
8.06	259.0	1499	31
8.43	638.0	2830	13
8.50	813.0	3729	10
8.80	1640.0	4539	5
8.90	1984.0	4780	4

The 11kV distribution class surge arresters are rated at 2.5kJ/kV (MCOV). The MCOV for 12kV rated surge arresters is 10.2kV. The total energy rating for an arrester is 25.5kJ. Each block has an energy rating of 6.4kJ. Figure 8.28 provides a plot of the energy absorption values for each block. A discussion about energy absorption and time to failure of station class MOV blocks is provided by (Ringler et al, 1997).

Figure 8.29 and Figure 8.30 below show the impedance values obtained for the healthy and failed J blocks. It can be seen that for the low current impedance of a failed block (390 to 530Ω) is greater than the impedance (280 to 330Ω) for a healthy block.

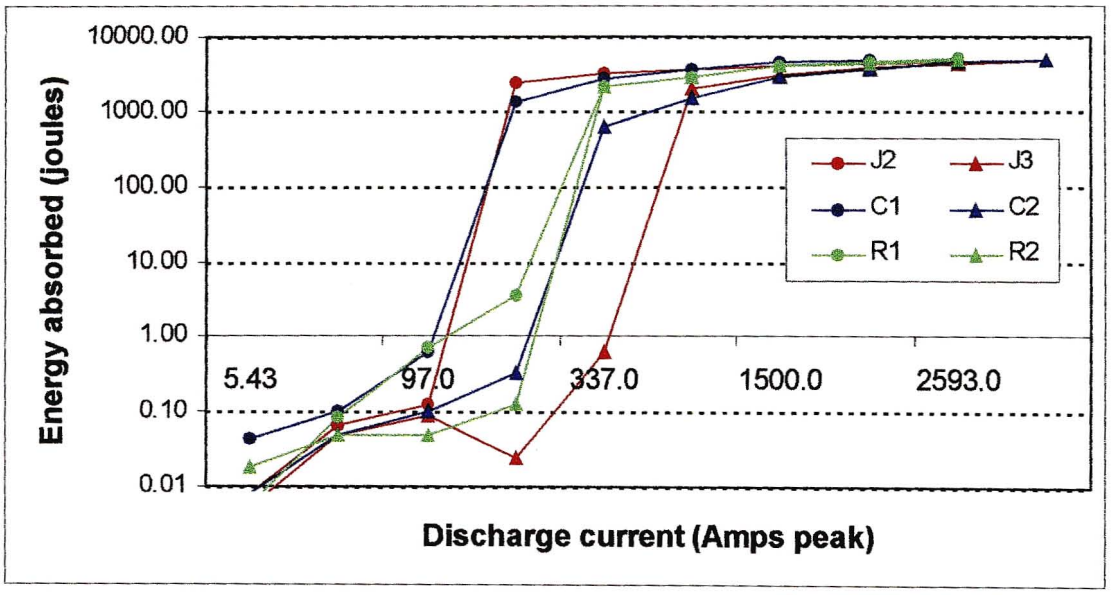

Figure 8.28 Energy absorbed for each MOV block (average discharge current values)

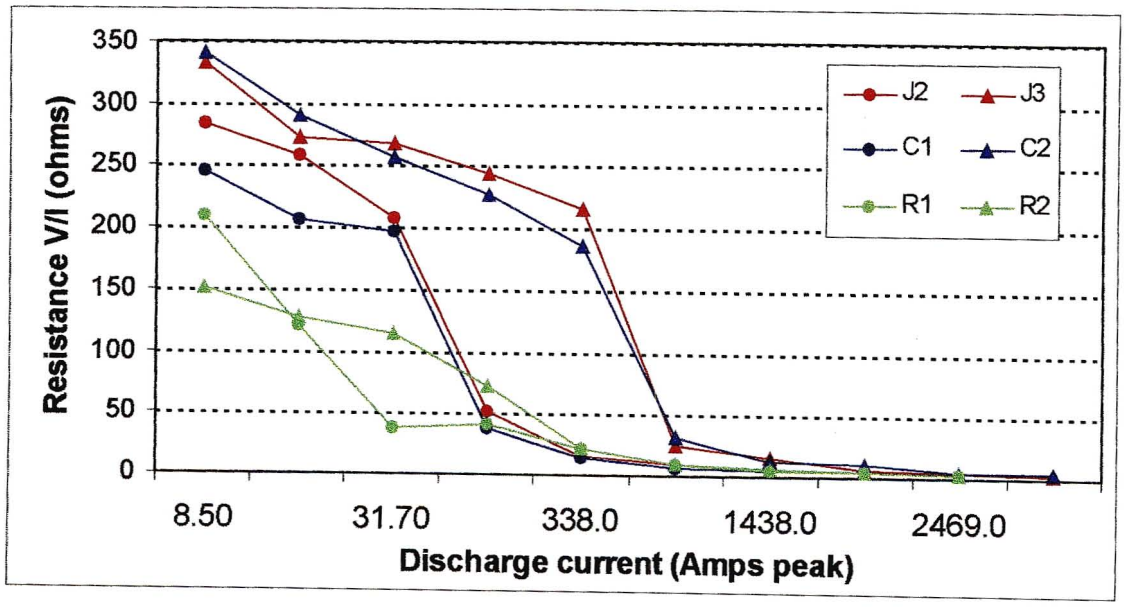

Figure 8.29 Impedance values of the MOV blocks

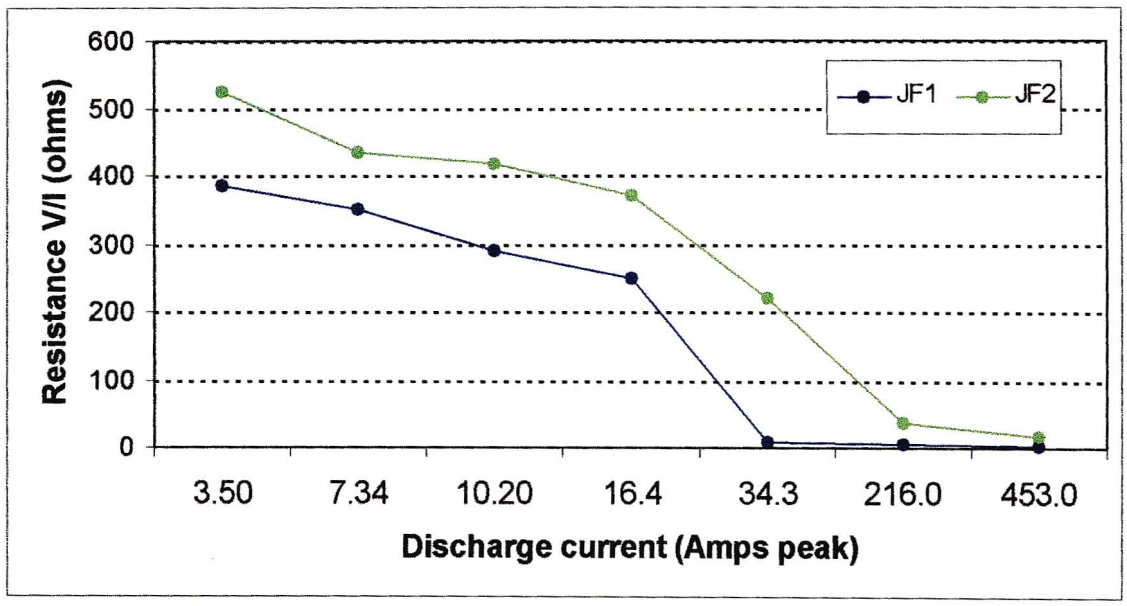

Figure 8.30 Impedance values of the failed MOV blocks

The resistance of MOV blocks (33-52mm diameter with thickness 23mm) at 10kA was recorded at between 0.7 to 1.3Ω (Asokan et al, 2000). It was found that for different MOV block diameters, the resistance decreased at 10kA for increasing block diameter.

ZnO arrester elements are known to exhibit high non-linearity at current magnitudes above a few hundred milliamps. This is due to the fact that the impedance of the block reduces drastically at the onset of the non-linear conduction (Asokan et al, 2000). This can be seen clearly in Figure 8.29.

8.5.4 Failure of MOV Block

During the initial impulse experiments the block J3 was damaged. The failure looked like a classical surface flashover due to surface voltage breakdown. This might have been due to a manufacturing defect. On the top of the block rings can be seen penetrating the surface. It was estimated that the discharge current was about 3.5kA (9 kV peak impulse voltage). This was after two prior impulses of 2 to 3kA.

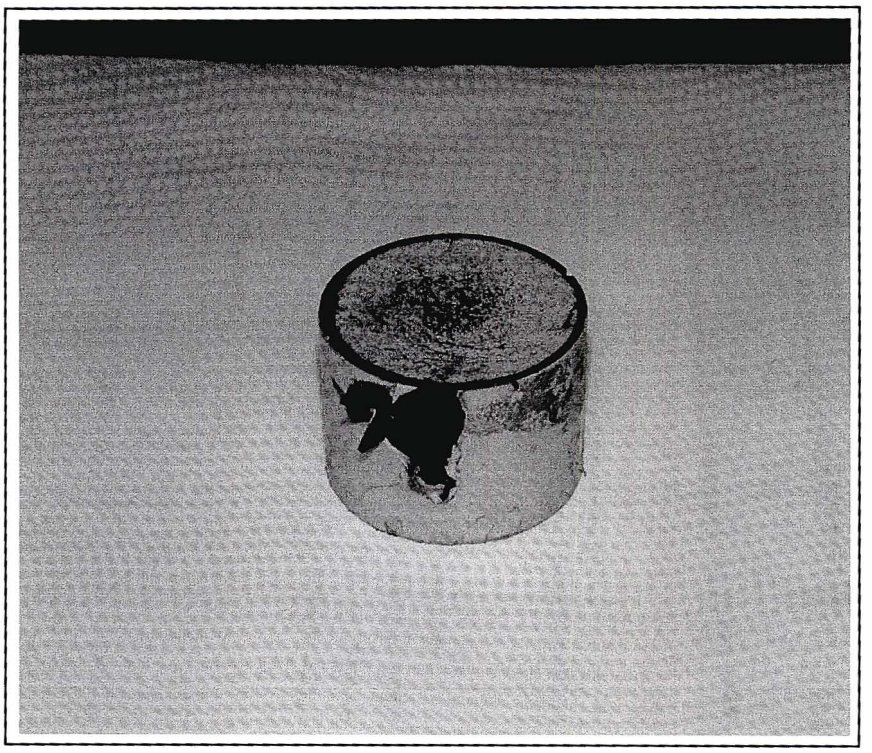

Figure 8.31 Damaged MOV block J3 (damage along the side)

Figure 8.32 Damage visible along the top surface of the block

8.5.5 Current Sharing of Blocks in Parallel

The variation or current sharing between two parallel MOV blocks was quantified by the introduction of current sharing factor of the two block discharge currents. The equation (7.28) was used. A factor K equal to 0 means that there is equal current sharing and a factor K equal to 2 means that one of the MOV blocks discharges the full current and the other block discharges no current. This can be seen in Figure 8.33 below.

Table 8.4 Example of K factor calculations for block C1 and R1 in parallel

Impulse voltage (kV)	C1 discharge current (A peak)	R1 discharge current (A peak)	I max	I min	I ave	K factor
7.00	37.5	543.8	543.8	37.5	290.7	1.742
7.30	113.0	769.0	769.0	113.0	441.0	1.488
7.50	218.0	1031.0	1031.0	218.0	624.5	1.302
7.80	500.0	1531.0	1531.0	500.0	1015.5	1.015
8.00	675.0	1781.0	1781.0	675.0	1228.0	0.901
8.50	1328.0	2688.0	2688.0	1328.0	2008.0	0.677
8.80	1797.0	3203.0	3203.0	1797.0	2500.0	0.562

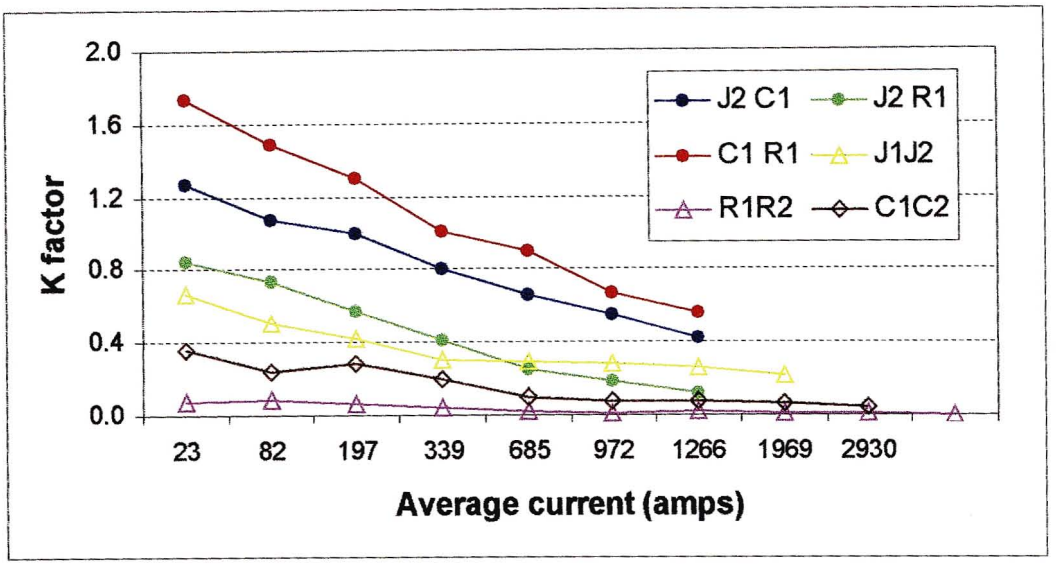

Figure 8.33 K factor for various MOV blocks in parallel

It can be seen that at higher discharge currents the current sharing becomes better. The two MOV blocks in parallel discharge almost the same current. This may be because that at the higher current magnitudes the external measuring circuit plays a bigger role. Figure 8.33 also shows that current sharing is better for blocks from the same manufacturer (solid circle curves) than for different manufacturers (triangle curves).

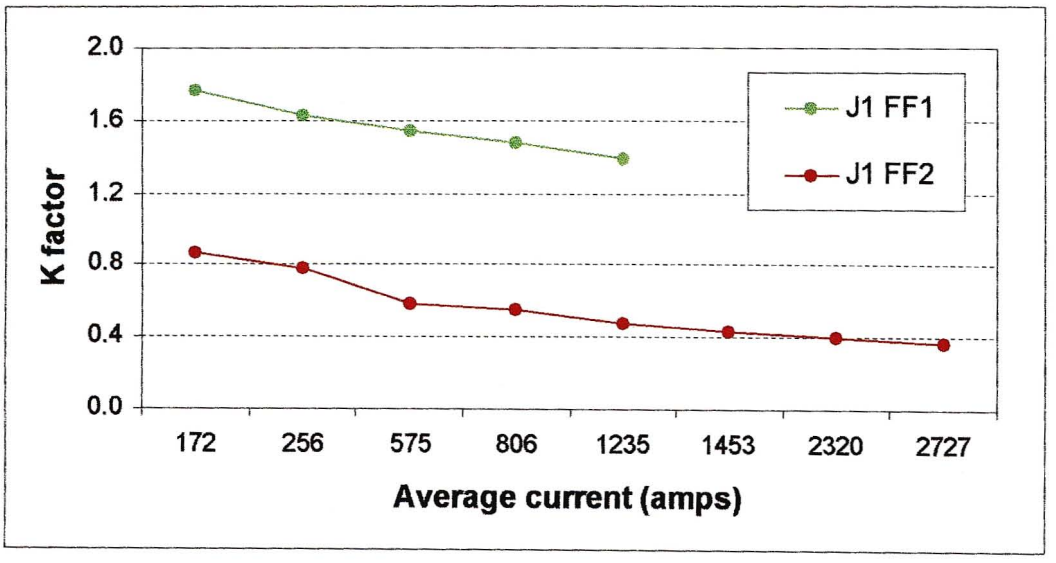

Figure 8.34 K factor for failed blocks in parallel

8.5.6 ATP Model of a MOV Block

A model for an arrester MOV block was proposed in (Schmidt et al, 1989) and discussed in (Hileman et al, 1990). The proposed equivalent circuit was used to describe the impulse behaviour of a MOV block. The model comprises of a capacitor (representing the capacitive component of the discharge current) and a non linear resistance (representing the resistive component of the discharge current). The two circuit components were connected in parallel. In series with this arrangement is an inductor and resistance in series. The series RL combination represents the ZnO grain and the parallel RC combination represents the grain boundary of a MOV block.

R(i) is the steady state resistance and R(θ) is the temperature dependent resistance. R(θ) the high ohmic resistance, represents the behaviour of the block in the low current region (< 1A) and can be ignored for high magnitude impulses (Schmidt et al, 1989). The non-linear resistance consists of the non-linear effect of the grain boundary R(i) and the linear resistance r of the ZnO grain. Both of these effects result in the typical V-I characteristic of a MOV block.

The resistance can be obtained from the residual voltages for 8/20μs current impulses with various peak values of discharge voltages, provided that inductance effects are excluded. Normally the V-I characteristic is measured with a DC voltage at low currents and with impulse currents at higher currents.

For the ATP simulations, the V-I characteristic data curves of arrester manufacturer J were used. The V-I characteristic in the discharge current range 1kA to 10 kA was used and scaled accordingly for a single MOV block.

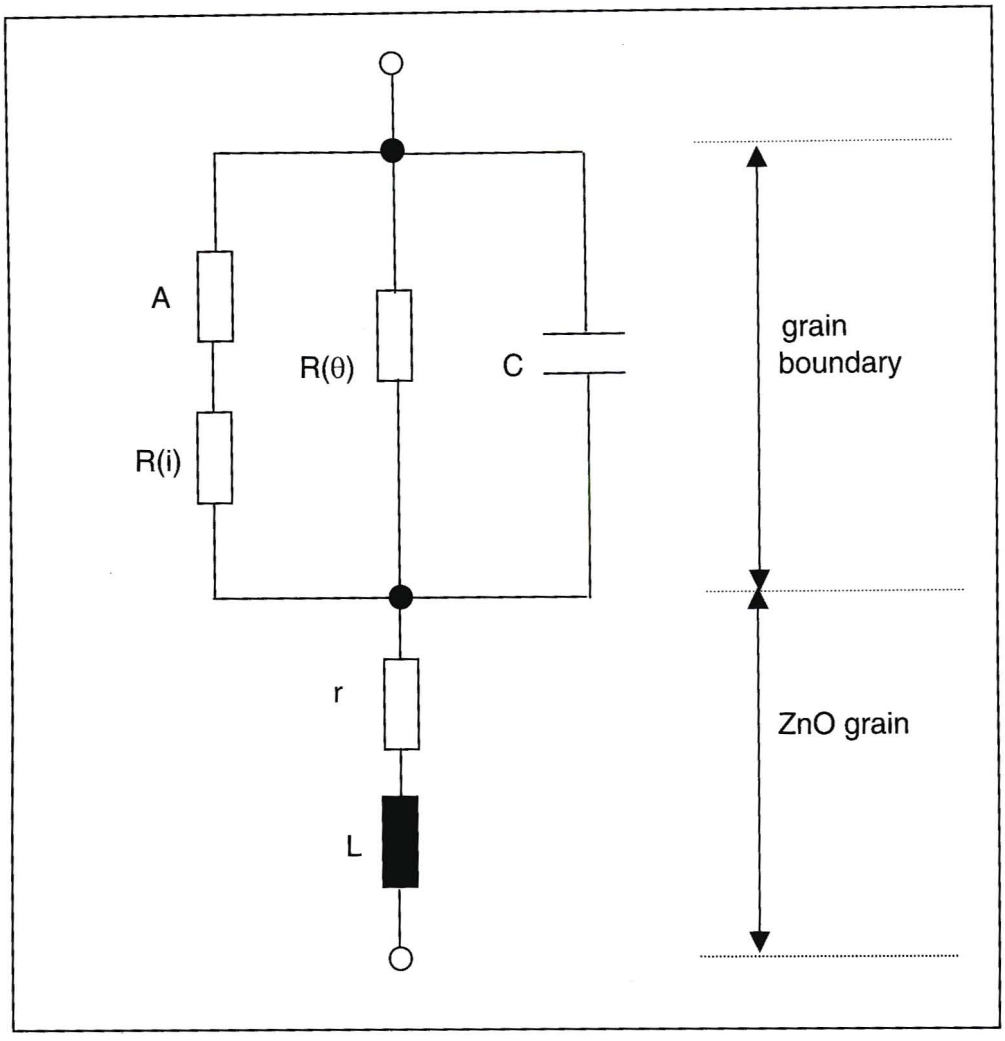

Figure 8.35 Proposed model to simulate the impulse behaviour of a MOV block taken from (Schmidt et al, 1989)

The capacitance C of the block depends on the steepness of the applied transient. In (Schmidt et al, 1989) the capacitance of the block (76mm diameter and 30mm height) was measured to between 0.8nF and 1.5nF. In principle the capacitance is voltage and temperature dependent and varies according to the diameter of the block. The response time variation or clamping behaviour was shown to be influenced by the capacitance (grain boundary) of the block (Asokan et al, 2000).

A represents the turn on element and reflects the dynamic charge distribution at the grain boundary. Its dynamic behaviour depends on the voltage waveshape and the time constant for reaching the equilibrium of electrons and holes at the grain boundary (Schmidt et al, 1989). For the equivalent circuit of the MOV block it is proposed to use a resistance in series with the non-linear resistor to represent the "turn on" time of the MOV block.

This is the time it takes for the block to change from an capacitive behaviour to an ohmic behaviour. This turn on time results in a voltage spike (or overshoot) in measurements of the residual voltage. This overshoot has been reported to range from 50 to 100% (Schmidt et al, 1989).

From the published curves in (Schmidt et al, 1989) the resistance is given as a function of current and the current steepness, Currents of more than 1200A result in a resistance of approximately zero ohms. The other alternative is to use the proposed differential equation describing the conductance in (Hileman et al, 1990). For the ATP simulations a conservative resistance value of 2Ω was used to model the turn on time.

The inductance L represents the inductance of the metal oxide disc and is determined by the geometry of the current flow path. Depending on the calculation procedure used, this can be represented by either an inductance value or a surge impedance with travel time. If one assumes as a rule of thumb an inductance of 1μH/m and the MOV block has a length of 30cm, then the inductance of the MOV block is 0.3μH (Hileman et al, 1990).

The resistance r in series with L, represents the resistance of ZnO grains with an average material resistivity of 0.01Ω.m. Using a length of 30cm this provides a resistance of 0.33Ω for the block (Hileman et al, 1990).

A discussion is presented on the behaviour of MOV blocks under steep front impulses and which block parameters effect the impulse behaviour of the block (Asokan et al, 2000). It was found that the residual voltage decreases as the diameter of the block increases. The rate of rise of current increases as the diameter increases. The ZnO block may respond faster at higher order of current magnitude compared to the same at lower current magnitudes.

8.5.7 Validation of MOV Model

In Figure 8.36 below the ATP model used to simulate the impulse behaviour is shown. The impulse voltage was represented by an ATP defined Heidler voltage source. Figure 8.37 and Figure 8.38 show the type of impulse voltage that was simulated.

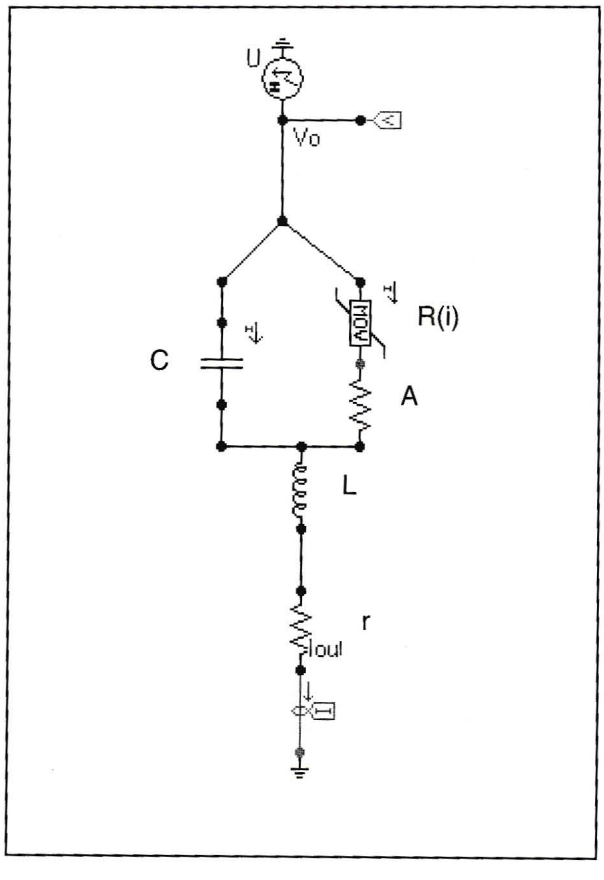

Figure 8.36 ATP model of MOV block for transient studies

The various results can be seen below in the various figures. The figures are in order of increasing applied impulse voltage and discharge currents.

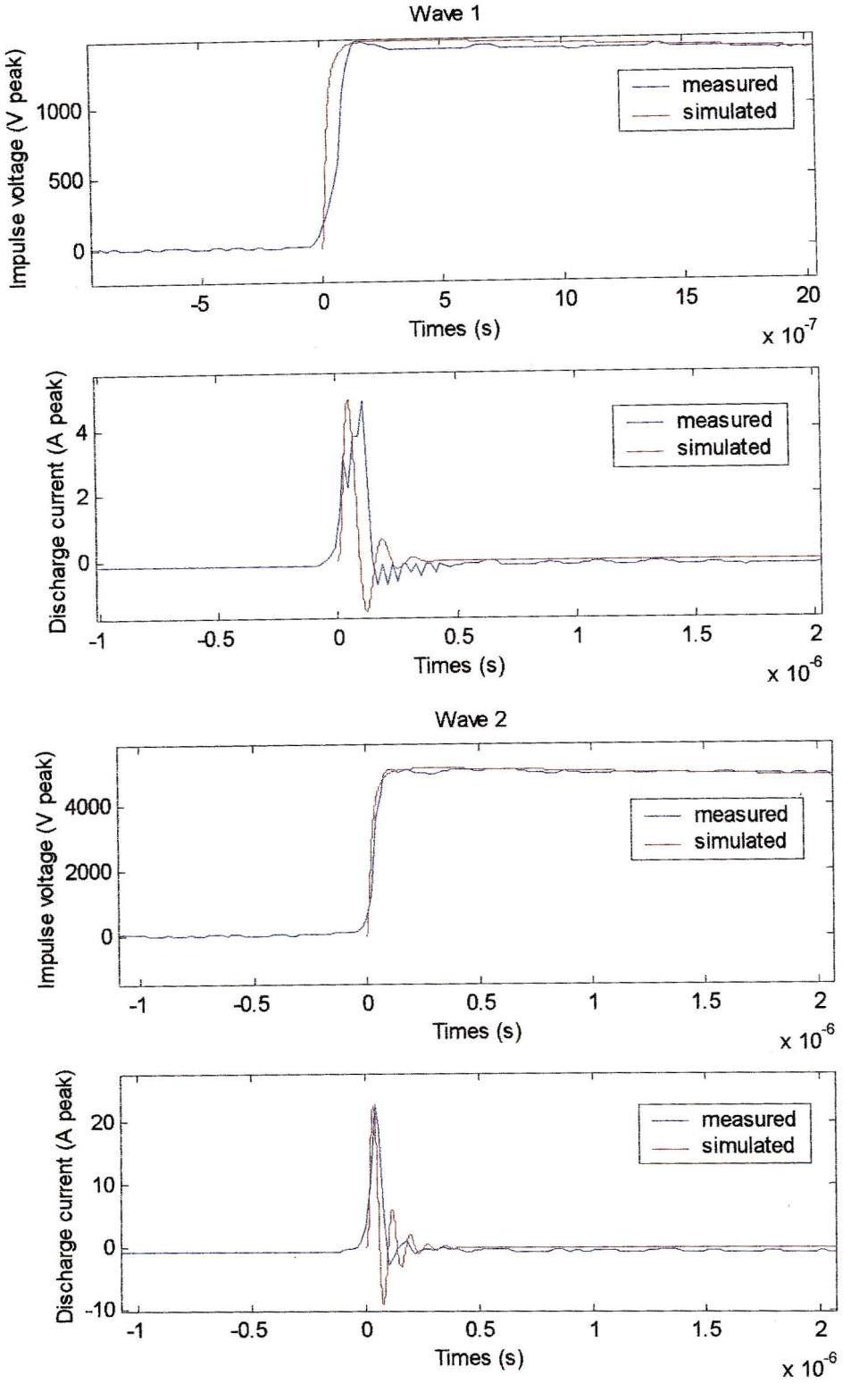

Figure 8.37 Simulated and measured capacitive discharge currents (Wave 1 and Wave 2)

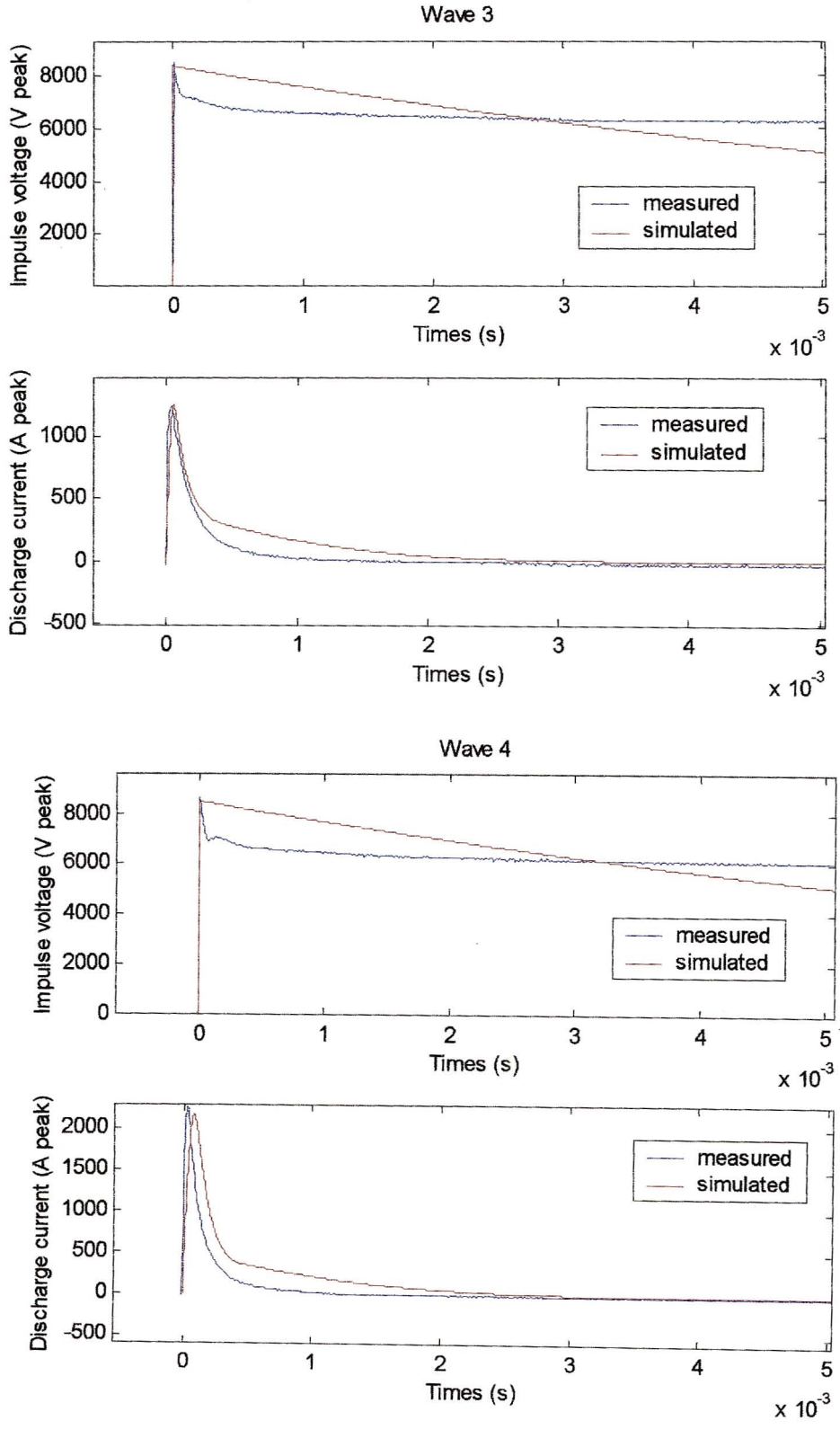

Figure 8.38 Simulated and measured resistive discharge currents (Wave 3 and Wave 4)

Table 8.5 below shows the good agreement between the simulated and measured discharge current waveforms can be seen. One of the problems was trying to simulate the measured voltage impulse in ATP. The available voltage sources in ATP can not accurately replicate the measured impulse voltage waveform of the capacitor bank.

Table 8.5 Error Analysis of simulated and measured waveform

	Peak current magnitudes			Rise time to peak		
	Measured (A)	Simulated (A)	% error	Measured (us)	Simulated (us)	% error
Wave 1	5	4.9	2.0%	0.1	0.07	30.0%
Wave 2	23.1	22.9	0.9%	0.05	0.04	20.0%
Wave 3	1256	1259	-0.2%	47	40	14.9%
Wave 4	2225	2164	2.7%	44	52	-18.2%

8.6 Conclusions

The main finding from the impulse laboratory work was that current sharing between parallel MOV blocks became better at higher currents. It was found that the current sharing of parallel MOV blocks during power frequency experiments was very poor. The power frequency experiments conducted on the MOV blocks were in the AC and start of the transition regions of the V-I curve. The MOV block behaved as a capacitor with the capacitive current component dominant in these regions.

The equivalent circuit of a MOV block for transient studies was proposed and then simulated in ATP. The simulated results were compared to the measured waveforms obtained from the impulse laboratory work. A good agreement between the simulated and measured waveforms was obtained.

CHAPTER 9
DISCUSSION

The transformer data analysis results indicated that the surge arresters in the Distribution Eastern Region were failing during periods of lightning storm activity. Another Eskom transformer investigation in the North West Region (Free State area) had a sample of failed transformers opened up for internal inspection. These inspected transformers showed signs of lightning damage to either the primary side winding or primary lead. The analysis of collected data from one of the national transformer refurbishment companies, indicated that the majority of the failed transformers brought in for repairs had their primary winding damaged.

The proposed failure hypothesis was that the transformers required additional lightning protection of the primary side to protect the transformer against lightning. It seemed that the current specifications of the Eskom distribution class surge arresters were inadequate to offer sufficient lightning protection of the pole mounted transformers. The results from the analysis of the Glencoe TSC fault logbook indicated that for majority of failed transformers with signs of visible damage, all three associated arresters had also failed. The arrester failure mode was either that the arrester had visible physical damage or the disconnector had operated. The collected data could not provide information about whether the transformers and arresters failed at the same time. The analysed data did support the above hypothesis that lightning was responsible for the majority of transformer failures.

The experimental project consisted of three networks in the Glencoe area. The main emphasis of the lightning protection on Glencoe N/B 13 was the use of two distribution class arresters in parallel for each transformer and an understrung conductor arrangement. The network Glencoe N/B 15 had single arresters installed on the transformers and a 600mm wood path in series with an earthed down conductor installed on each intermediate woodpole structure. This was to ensure a BIL of 300kV for the network.

From the literature survey conducted it was found that the double surge arrester configuration had only been used by the electrical utilities in Colombia by CODENSA (the national Colombian utility), and in Japan by the Hokuriku Electric Power Corporation. CODENSA found that the double arrester configuration did not work, but the relevant reference did not provide supporting engineering reasons. The intention of the application of parallel surge arresters in Japan, was to use two 2.5kA rated arresters in parallel instead of a single 5kA rated arrester. This would reduce the financial costs and decrease the risk of failure of the individual arresters protecting the transformers.

The literature survey results showed that the most commonly applied practical methods of improved lightning protection of transformers were :

- Re-location of the MV surge arresters to the transformer tank and the reduction in length of all connecting leads.
- The use of LV surge arresters on the transformer to provide protection against LV side lightning overvoltages.

The current Eskom Distribution MV standard calls for the practice of the arresters to be mounted on the transformer tank and a reduction in connecting lead lengths. It was the experience of Eskom Distribution that LV surge arresters were not required to protect the transformer. There was so far no field experience to support the use of LV arresters as used in Australia and the USA. The disadvantages of using LV arresters would be the additional cost and the increasing complexity of the transformer installation. The LV arresters could also add to the problem of possible nuisance phase to earth faults on the network due to damaged arresters or disconnectors that did not blow away.

An energy based probability of failure characteristic of an arrester based on its energy absorption limit was introduced. For 11kV arresters as used in the experimental project, it was found that the energy absorption rating of 25.5kJ corresponded to almost a zero probability of failure. A 50% probability of failure for the 11kV arresters corresponded to an energy absorption level of 64kJ.

This was 2.5 times greater than the rated energy level of the surge arrester. The current probabilistic capability could be simply stated as 100kA with a zero probability of failure. This current probabilistic capability was based on the required arrester high current test results.

For the period November 1999 to March 2002 not a single transformer or surge arrester had failed due to lightning on the Glencoe N/B 13 network. There were recorded transformer and surge arrester failures on Glencoe N/B 15 and the control network Dundee N/B 18. This was a very positive result and indicated that the practical methods implemented on Glencoe N/B 13 did prevent transformer and arrester failures.

It was found that the practical methods implemented on Glencoe N/B 13 did not have a negative impact on the performance levels of the network. The performance of all three networks had similar cumulative frequency of voltage loss events per 100km per year distribution curves. The analysis of the LPATS collected data showed that the lightning activity in the area surrounding the three networks before project implementation was similar to that activity after the project implementation. The conclusion could be made that the reduction in transformer failures was due to the practical methods implemented and not due to less lightning activity in the area surrounding the networks.

The main finding from the impulse laboratory work was that current sharing between parallel MOV blocks became better at higher currents. This finding was supported by other research work findings, particularly in the field of nuclear fusion research with parallel arresters. It was found that the current sharing of parallel MOV blocks during power frequency experiments was very poor. The power frequency experiments conducted on the MOV blocks were in the ac and start of the transition regions of the V-I curve. The MOV block behaved as a capacitor with the capacitive current component dominant in these regions.

The findings of the ATP parametric simulations showed that the Glencoe N/B 13 network with the parallel arresters and understrung conductor arrangement considerably reduced the energy absorbed by the individual arresters. The effect of the double arrester configuration was to reduce the energy absorbed by the individual arresters even with arresters with different V-I characteristics.

The understrung earth conductor arrangement was the major contributor towards the reduction of the energy absorbed by the arresters. The type of conductor used had negligible effect on the energy absorbed by the arresters.

The pole footing electrode resistance and transformer earth electrode resistance, were found to be important factors effecting the energy absorbed by the arresters. The pole footing resistance had to be as low as possible. Practically this would be difficult as the transient impedance of a 1.5m Copper rod would always be larger than the transient impedance of a crows foot electrode used to earth the transformer. This would be assuming both electrodes were in similar soil resistivities.

The tail half time of the lightning current also had a significant effect on the energy absorbed by the arresters. This was not a parameter that can be controlled by the line designer. The detailed ATP simulations for Glencoe N/B 13 showed that the lightning rise time did effect the energy absorbed by the arresters. This could be due to the fact that the conductor connections were also modelled leading to inductive volt drops that the ATP program would take into account in its energy calculations.

Dundee N/B 18 had the least effect of reducing the energy absorbed by the single arresters. This was due to the network been fully insulated with no discharge path along the network for lightning overvoltages.

For existing reticulation networks with high arrester and transformer failure rates, the double arrester configuration would the most time and cost effective solution. The understrung conductor arrangement did reduce the energy absorbed by the arresters but to due high labour costs and time requirements this would not recommended for existing networks. It is suggested that Eskom investigate this practical method for new lines to be built in high lightning areas. An alternative solution would be to build the 300kV spark gap one structure back but with no understrung conductor as shown in the ATP simulations.

Even with arresters from different manufacturers, the use of the double arrester configuration would decrease the energy absorbed and hence reduce the risk of failure of the arresters protecting the transformer. It was proposed to perform arrester matching by ensuring that the both arresters were from the same manufacturer.

CHAPTER 10
CONCLUSIONS

The following are the conclusions from the findings and results of the dissertation :

- The experimental project at Glencoe was a success with no recorded surge arrester or transformer failures due to lightning on Glencoe N/B 13 for the period November 1999 to March 2002. This proved the success of the practical methods implemented on the network in preventing the failure of transformers and arresters.

- The analysed lightning data from the Eskom LPATS system showed that the success of Glencoe N/B 13 was due to the practical methods implemented and not a reduction in lightning activity in the area surrounding the network.

- The performance level of Glencoe N/B 13 was not negatively affected by the practical methods implemented. The performance of all three networks had similar cumulative frequency of voltage loss events per 100km per year distribution curves.

- A performance benchmark curve for a reticulation woodpole network in a high lightning area was proposed from the collected data in this dissertation.

- The results of the ATP simulations showed that the 300kV BIL applied on Glencoe N/B 15 did help reduce the energy absorbed by the arresters. This method has been proposed for reticulation networks in high lightning density areas. The success of this method could not be validated in the experimental project as there were recorded transformer and arrester failures on Glencoe N/B 15. The reasons for their failures were unknown. There was wood pole splintering found during the audits that provided evidence of voltage flashovers at the 600mm wood path.

- The results of the ATP simulations showed that the fully insulated network Dundee N/B 18 had the least effect on reducing the energy absorbed by the arresters. This practical method was not recommended for networks in high lightning areas.

- The results of the ATP simulations showed that the double arrester configuration and the understrung conductor arrangement on Glencoe N/B 13 had the most effect of reducing the energy absorbed by the individual arresters. This was proven by the successful results of the experimental project.

- The understrung conductor arrangement effectively acted as a spark gap for large overvoltages on the network and was found to be the most influential factor in reducing the energy absorbed by the individual arresters. Evidence of voltage flashover was found on Glencoe N/B 13 network during the network audits. There were signs found of woodpole splintering of the 600mm wood path.

- The type of conductor used for the understrung conductor had negligible effect on the energy absorbed of the arresters.

- The understrung conductor arrangement did reduce the energy absorbed by the arresters but to due the high labour costs and time requirements this was not recommended for existing reticulation networks. An alternative solution would be to build the 300kV spark gap one structure back but with no understrung conductor. This was supported by the results of the ATP simulations.

- It was important to make the pole footing resistance as small as possible. This could be achieved by using a crows foot earth electrode instead of the standard 1.5m Copper rod.

- The ATP simulation results of complete arrester units in parallel and the impulse laboratory experiments on parallel MOV blocks showed that the current sharing became better at higher lightning currents. The current sharing was better in the lightning region (region 3) of the V-I curve of the arresters.

- For existing reticulation networks with high arrester and transformer failure rates, the double arrester configuration would the most the cost effective and practical solution.

- The installation of arresters in parallel did reduce the energy absorbed by the individual arresters even with two arresters with different V-I characteristics. This meant that Eskom field staff could use different make arresters in parallel. This would be especially for the times when replacing failed arresters or a faulty transformer under breakdown conditions when electrical supply had to be restored to the customer as soon as possible.

- Matching of the parallel surge arresters could be crudely performed by ensuring that the arresters were from the same manufacturer.

CHAPTER 11
FUTURE WORK

The following are possible topics for future work based on the results and conclusions of this dissertation :

- Wave-shaping of the capacitor bank output current to provide more realistic lightning type waveforms. The rise time of the waveform can be slowed down to more lightning comparable rise times.

- Use of all available capacitor banks to provide larger magnitude impulse currents so that the current sharing of parallel MOV blocks can be quantified in the lightning region (region 3) of their V-I characteristics.

- The testing of complete surge arrester units in parallel in the high voltage laboratory. The current sharing and energy absorption limits of individual arresters needs to be quantified. The effects of different make arresters under different impulse rise times and tail fall times needs to be quantified.

- The researches at ICLRT will be conducting similar experiments with the double arrester configuration for the line surge arresters in 2002. These experiments are of interest due to the low level long duration lightning currents found at the start of triggered lightning experiments. The energy absorption capability of the double arrester configuration will be quantified.

- The single phase conductor ATP simulations can be expanded to three phase conductor simulations. The voltage flashover mechanism and modelling of pre-discharge currents between conductors will be required to be taken into account. The current sharing between the three single arresters can also be investigated.

- The benefits of using one single station class arrester as compared to two distribution class arresters in parallel can be quantified in the ATP simulations. The financial costs should also be considered.

- The transfer of lightning overvoltages from the MV line to the LV supply of the customer can be investigated. This will require an accurate high frequency transformer model that can be verified in laboratory experiments in the high voltage laboratory.

- Statistical Monte Carlo simulations of the lightning parameters to quantify the probabilistic energy absorption limits of the distribution class surge arresters.

- Investigate further the probabilistic current capability of surge arresters.

APPENDICES

Appendix A

South African Lightning Flash Density Map

Taken from (Gaunt et al, 1989)

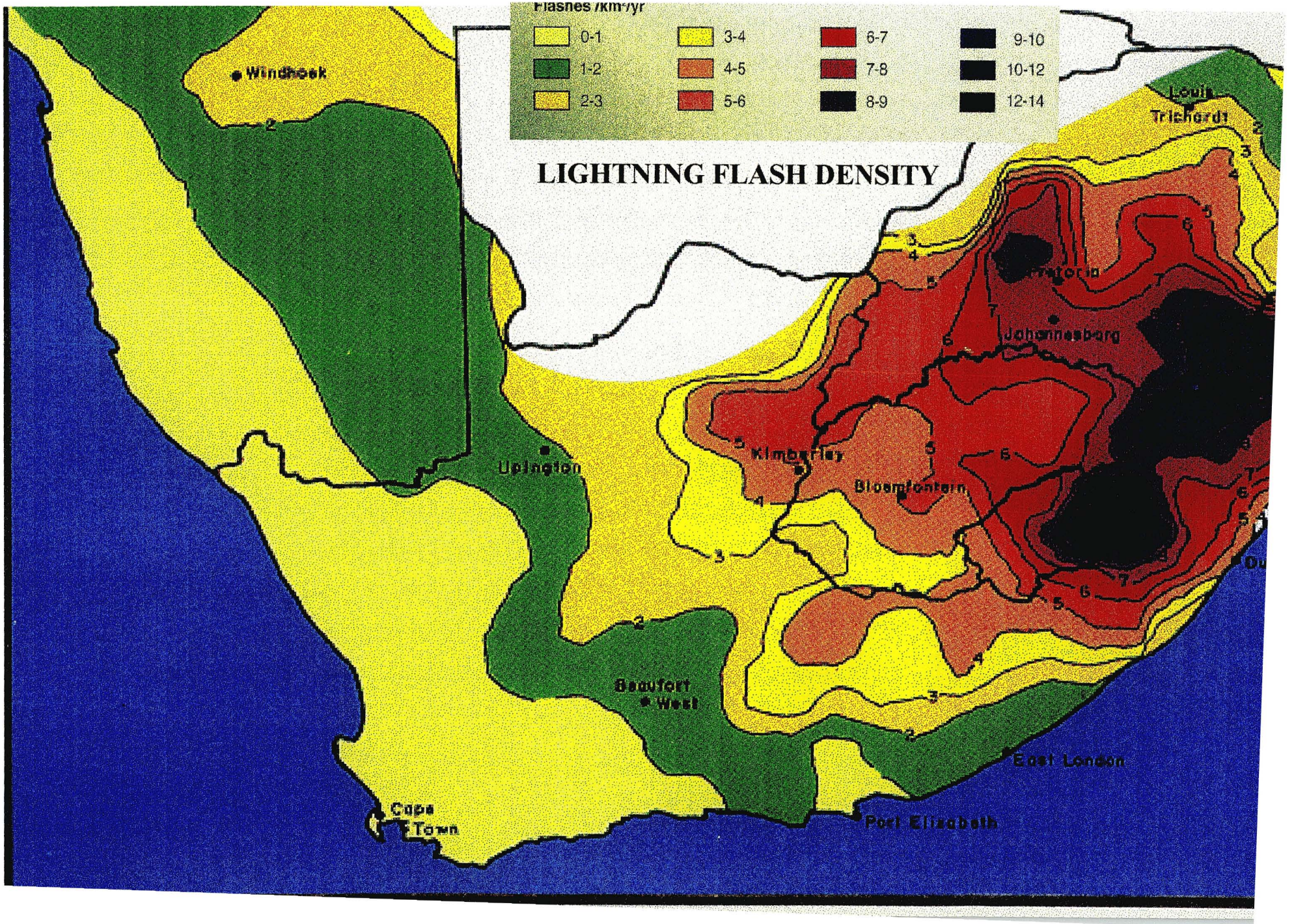
Flashes /km²/yr
0-1
1-2
2-3
3-4
4-5
5-6
6-7
7-8
8-9
9-10
10-12
12-14
LIGHTNING FLASH DENSITY
Windhoek
Louis Trichardt
Johannesburg
Kimberley
Bloemfontein
Upington
Beaufort West
East London
Cape Town
Port Elizabeth

Appendix B

Transformer Audit Questionnaire Sheet

ESKOM	**POLE MOUNTED TRANSFORMER STRUCTURE QUESTIONNAIRE SHEET**	**DTBC rev 2** **Page 1 of 1**

INFORMATION **(Please fill in the details or tick the relevant box where applicable)**

TSC :	**Glencoe**	**N/W Breaker :**		**Make :**	
Date :		**Pole No. :**		**KVA Rating :**	
Time :		**Serial No. :**		**Refurbished Job No. :**	
Substation :	**Glencoe**	**Voltage :**	**11kV**		

Terrain :	**Open ground**	**Tall trees higher than 7m**	**Other lines nearby**	**other(specify)**	

SURGE ARRESTERS AND DROP OUT FUSES

MV surge arrester installed :	**Yes**		**No**	
Surge arrester tails blown :	**1**	**2**	**3**	**0**

MV Drop out fuses present :	**Yes**		**No**	
Number of Drop out fuses blown :	**1**	**2**	**3**	**0**

Position of MV surge arresters :	**Transformer tank**	**On top of crossarm**	**other(specify)**	

EARTHING **(Please tick the correct box)**

Separate MV and LV earth :	
LV earth at pole :	

Common MV and LV earth :	
LV earth one span away :	

Result of Earth Resistance Test:	**Ohms**

Is the hardware on each phase bonded :	**Yes**	**No**

Information supplied by :		**Company :**	
Signature :		**Date :**	

Appendix C

Project Activity Summary

Date	Activity
February 1999 to September 1999	• Project initiation • Background work • Project engineering and design details
October 1999	**Phase 1 of Project** • Glencoe N/B 13 implementation complete • Glencoe N/B 15 implementation complete
November 1999	• First network audits conducted by Duke Engineering • Reference condition of networks established • Vectographs installed on each networks
September 2000	• Second network audits conducted by Duke Engineering
November 2000	First TSI research report • Statistical analysis of NAPI data • Comparison of results of 1st and 2nd network audits • Vectograph data : Nov 1999 to Apr 2000
April 2001	**Phase 2 of Project** • Replace old gapped type surge arresters with MOV type arresters • Re-locate arresters from crossarms to transformer tank
May 2001	Third network audit conducted by Karabo Engineering
July 2001	Second TSI Research report • Comparison of results of 1st, 2nd and 3rd network audits • Vectograph data : Nov 1999 to Mar 2001 • LPATS data analysis • Preliminary ATP simulations
November 2001	• Visit ICLRT, Florida, USA • Spend time at Camp Blanding

Appendix D

V-I Characteristics of J blocks

Table D2-1 Sample J1

Voltage applied (kV rms)	Current leakage (mA rms)
0.48	0.18
1.02	0.34
1.52	0.48
2.12	0.71
2.52	0.85
3.03	1.07
3.50	1.39
3.86	2.06
3.90	2.36
4.03	3.27
4.12	4.71
4.18	5.39
4.21	7.42
4.24	10.15
4.30	14.33
4.36	18.67
4.44	24.82

Table D2-2 Sample J2

Voltage applied (kV rms)	Current leakage (mA rms)
0.51	0.21
0.98	0.39
1.51	0.56
1.93	0.71
2.50	0.93
2.99	1.17
3.48	1.52
3.80	2.12
3.94	3.05
4.03	4.21
4.14	4.89
4.19	6.21
4.20	8.10
4.26	11.3
4.30	16.31
4.35	21.35
4.42	26.21

Appendix E

V-I Characteristics on multiple J blocks in series

Table E1-1 Samples of J1 and J2 in series

Voltage applied (kV rms)	Current leakage (mA rms)
0.51	0.12
1.00	0.18
1.53	0.27
1.98	0.36
2.55	0.43
3.10	0.55
3.57	0.60
4.08	0.71
4.50	0.80
5.10	0.89
5.61	1.01
6.12	1.17
6.63	1.42
7.16	1.70
6.76	2.31
7.83	4.78
8.14	5.15
8.32	8.45
8.52	21.90
8.71	28.60

Table E1-2 Samples of J1, J2 and J3 in series

Voltage applied (kV rms)	Current leakage (mA rms)
2.30	0.09
3.83	0.17
5.35	0.23
6.89	0.28
7.65	0.32
8.42	0.35
9.18	0.39

Appendix F

Software code for harmonic analysis of current and voltage waveforms

Part of this software code was used from the work performed by (Van der Linde, 1999). The code was then modified by the author and additional routines added in. This code normalises the harmonic components to the fundamental 50Hz component. The code produces a normalised vector which is the magnitude of the real and imaginary parts of the DFT. The two normalised vectors, the real and imaginary parts, enable the separation of the capacitive and resistive components of the leakage current. The THD for the resistive component was also calculated.

```
%**********RescurHarm*************************************************************
%***This code is for the harmonic analysis of the resistive component of the
%***Leakage current.
%*****************************************************************************************

cd ('D:\MATLAB Files\Curves')

%load the data file to be analysed
load W9i.dat

%Specify which vectors are the recorded time and voltage magnitudes
time=W9i(:,1);
volt=W9i(:,2);

%obtain current values : using 100 ohm shunt as a factor
current=volt./100;

%specify how many decimal points
format short e;

%Obtain sampling frequency from two arbitary assigned points
Ts=time(5)-time(4);
Fs=1./Ts;

%Specify dft resolution to be used
n=2000;

%Window the data to required length x(1) to x(2001)
curr_wind=current(1:n+1);
```

```
%Perform the n point fft on the data with window
Y=fft(curr_wind,n);

%Magnitude of resulting fft : Fourier co-efficient Cn
y=abs(Y);

%Magnitudes of imaginary and real components
cosmag=abs(real(Y));
sinmag=abs(imag(Y));

%Normilization of vectors
norm=y/max(y);
normcos=cosmag/max(cosmag);
normsin=sinmag/max(sinmag);

%Convert to frequency : up to nyquist frequency Fn
%Fn=0.5*Fs
freq=Fs*(0:(n-1)/2)/n;

%Convert to column vector for operations
freq=freq(:);

%Constant for highest harmonic order to be looked at
rang=15;

%Determine the frequency
k=[0:rang];
pos=k*50;
posn(k+1)=pos/Fs*n+1;

%Calculate the current component harmonics
%Amp = total current
%real comp = capacitive current
%imag comp = resistive current

Amp(k+1)=norm(posn(k+1));
normcos2(k+1)=normcos(posn(k+1));
normsin2(k+1)=normsin(posn(k+1));
resis=(normsin2(k+1))*100;

%Look at the even harmonics
%cap=(normcos2(k+1))*100;

%Output harmonic results percentages for resistive current

format bank;
disp(' ')
disp('Harmonic analysis of resistive current:')
results=[k',resis']

%results=[k',cap']
```

```
%Calculate the THD
THDsum=0;
%Disregard the 50Hz fundamental

for k=2:rang
     resis=(normsin2(k+1))*100;
   THDsum=(resis.^2)+THDsum;
end

 THD=sqrt(THDsum);

 disp('The % THD relative to 50Hz is equal to :')
 results=[THD']


%*****************************************************************************************
%Reconstruct and check the original waveform for samples n=n/2
%Plot the current waveform,reconstructed current waveform resistive and
%the capacitive currents on the same axis
*****************************************************************************************
freq=Fs*(0:(n-1)/2)/n;
sercos=zeros(n/2,1);
sersin=zeros(n/2,1);

for a=2:n/2
   sercos=sercos+real(Y(a))*cos(freq(a)*2*pi.*time(1:n/2));
   sersin=sersin-imag(Y(a))*sin(freq(a)*2*pi.*time(1:n/2));
end

%first element of fft is dc component
%Construct the original waveform

sertot=0.5*Y(1)+sercos+sersin;

plot(current,'r');
hold on;
plot(sertot/1000,'y');
grid;
xlabel('Index');
ylabel('Leakage Current (Amps)');

plot(sersin/1000,'b');
plot(sercos/1000,'g');
```

```
%**********ResisHarm*************************************************************
%***This code is for the harmonic analysis of the applied voltage to the
%***resistor load.
%*************************************************************************************

cd ('D:\MATLAB Files\Clipping')

%load the data file to be analysed
load C1c3v.dat

%Specify which vectors are the recorded time and voltage magnitudes
time=C1c3v(:,1);
volt=C1c3v(:,2);

%specify how many decimal points
format short e;

%Obtain sampling frequency from two arbitrary assigned points
Ts=time(5)-time(4);
Fs=1./Ts;

%Specify dft resolution to be used
n=2000;

%Window the data to required length x(1) to x(2001)
volt_wind=volt(1:n+1);

%Perform the n point fft on the data with window
Y=fft(volt_wind,n);

%Magnitude of resulting fft : Fourier co-efficient Cn
y=abs(Y);

%Magnitudes of imaginary and real components
cosmag=abs(real(Y));
sinmag=abs(imag(Y));

%Normilization of vectors
norm=y/max(y);
normcos=cosmag/max(cosmag);
normsin=sinmag/max(sinmag);

%Convert to frequency : up to nyquist frequency Fn
%Fn=0.5*Fs
freq=Fs*(0:(n-1)/2)/n;

%Convert to column vector for operations
freq=freq(:);

%Constant for highest harmonic order to be looked at
rang=10;
```

```
%Determine the frequency
k=[0:rang];
pos=k*50;
posn(k+1)=pos/Fs*n+1;

%Calculate the current component harmonics
%Amp = total current
%real comp = capacitive current
%imag comp = resistive current

Amp(k+1)=norm(posn(k+1));
normcos2(k+1)=normcos(posn(k+1));
normsin2(k+1)=normsin(posn(k+1));

resis=(normsin2(k+1))*100;

%Look at the even harmonics
%cap=(normcos2(k+1))*100;

%Output harmonic results percentages for resistive current

format bank;
disp(' ')
disp('Harmonic analysis of resistive current:')
results=[k',resis']

%results=[k',cap']

%Calculate the THD
THDsum=0;
%Disregard the 50Hz fundamental
for k=2:rang
      resis=(normsin2(k+1))*100;
   THDsum=(resis.^2)+THDsum;
end

 THD=sqrt(THDsum);

 disp('The % THD relative to 50Hz is equal to :')
 results=[THD']
```

Appendix G

Harmonic analysis of waveforms

Table G1 Harmonic analysis of voltage waveform with resistor as load

H (Order Number)	Frequency (Hz)	% Component (1.04kV rms)	% Component (2.76kV rms)	% Component (4.18kV rms)
2	100	0.02	0.02	0.11
3	150	0.64	0.45	0.30
4	200	0.05	0.06	0.09
5	250	0.21	1.17	0.95
6	300	0.23	0.06	0.04
7	350	0.36	0.13	0.11
8	400	0.05	0.02	0.02
9	450	0.14	0.08	0.16
10	550	0.09	0.06	0.02

Table G2-1 Harmonic analysis of voltage with block J1 at 1.87mA rms

Harmonic Order H	% Harmonic of 50Hz
2	0.14
3	0.81
4	0.02
5	1.32
6	0.01
7	0.11
8	0.01
9	0.33
10	0.07

Table G2-2 Harmonic analysis of voltage with block J1 at 2.34mA rms

Harmonic Order H	% Harmonic of 50Hz
2	0.09
3	0.86
4	0.04
5	0.29
6	0.01
7	0.28
8	0.05
9	0.14
10	0.03

Table G3-1 Harmonic analysis of voltage with block C1 at 1.76mA rms

Harmonic Order H	% Harmonic of 50Hz
2	0.18
3	0
4	0.07
5	0.23
6	0.03
7	0.26
8	0.01
9	0.74
10	0.01

Table G3-2 Harmonic analysis of voltage with block C1 at 2.36mA rms

Harmonic Order H	% Harmonic of 50Hz
2	0.36
3	0.87
4	0
5	3.66
6	0
7	2.04
8	0.09
9	0.33
10	0.05

Table G4 Harmonic analysis of resistive component of block J1

	Wave 2	Wave 4	Wave 6	Wave 9
Harmonic order	**1.61kV rms**	**3.00kV rms**	**3.62kV rms**	**4.00kV rms**
2	0.28	0.23	0.34	0.74
3	39.88	8.62	20.67	33.31
4	0.68	0.17	0.16	0.32
5	15.98	1.79	7.36	38.97
6	0.30	0.13	0.13	0.16
7	5.12	0.97	6.81	13.17
8	1.18	0.00	0.17	0.07
9	22.08	0.16	5.12	4.52
10	0.92	0.13	0.19	0.15
11	8.92	0.58	1.19	0.86
12	1.89	0.03	0.33	0.04
13	6.75	0.38	0.56	0.63
14	0.95	0.13	0.08	0.01
15	3.29	0.04	1.08	1.60

Appendix H

Temperature dependence tests on blocks

Table H1 Temperature tests on Sample J2

Applied Voltage (kV rms)	Temp (Deg C)	Leakage Current (mA rms)
1.28	30	0.53
1.28	50	0.92
1.28	70	1.10
1.28	90	1.39
1.28	110	1.42
1.79	30	0.74
1.79	50	1.28
1.79	70	1.40
1.79	90	1.88
1.79	110	1.97
2.55	30	1.05
2.55	50	1.95
2.55	70	2.10
2.55	90	2.68
2.55	110	2.96
3.06	30	1.38
3.06	50	2.48
3.06	70	2.64
3.06	90	3.51
3.06	110	3.90
3.83	30	2.51
3.83	50	6.16
3.83	70	6.41
3.83	90	8.46
3.83	110	10.50

Table H2 Temperature tests on Sample C2

Applied Voltage (kV rms)	Temp (Deg C)	Leakage Current (mA rms)
1.28	30	0.17
1.28	50	0.19
1.28	70	0.20
1.28	90	0.22
1.28	110	0.23
1.79	30	0.22
1.79	50	0.25
1.79	70	0.26
1.79	90	0.27
1.79	110	0.29
2.55	30	0.33
2.55	50	0.35
2.55	70	0.37
2.55	90	0.38
2.55	110	0.40
3.06	30	0.38
3.06	50	0.43
3.06	70	0.44
3.06	90	0.52
3.06	110	0.55
3.83	30	0.61
3.83	50	0.67
3.83	70	0.79
3.83	90	0.88
3.83	110	0.97

BIBLIOGRAPHY

AIEE (1950) : *"A method of estimating the lightning performance of Transmission lines"*, AIEE Committee Report, AIEE Transactions, Vol. 69, 1950, pp1187-1196.

Akbar M. and Ahmad M. (1998) : *"Failure study of metal-oxide surge arresters"*, Electric Power Systems Research, Elsevier Science, March 1998.

Alexandri I. and Fournarakis E. (1998) *: "Lightning Protection of PPCs distribution networks"*, MEDPOWER 98, IEE, Cyprus, November 1998.

Anderson J. G. (1982) : *"Lightning performance of transmission lines"*, Chapter 12, Transmission Line Reference book 345kV and above, EPRI, 1982.

Anderson R. B. and Eriksson A. J. (1980) : *"Lightning parameters for engineering application"*, Electra No.69, CIGRE, 1980, pp65-101.

Asokan T. and Kishore B. N. (2000) : *"Clamping characteristics of ZnO arrester element under steep front impulses"*, CIGRE Session 2000, Paris, 2000, paper 33-107.

Bartkowiak M., Comber M. G. and Mahan G. D. (1999) : *"Failure modes and energy absorption of ZnO varistors"*, IEEE Transactions on Power Delivery, Vol. 14. No. 1, January 1999, pp152-162.

Bavin D. (1998) : *"Transformer failure analysis 11/07/1996 to 21/01/1998"*, Report CEN00033, Central Engineering Report, Eskom, 1998.

Borghetti A., Nucci C. A. and Paolone M. (1997) : *"Statistical evaluation of lightning performance of Distribution lines"*, Department of Electrical Engineering, University of Bologna, Italy, 1997.

Brady T. W. (1976) : *"Report on lightning arrester failure experiment"*, Report No. 123/2/81, Electrical Research Division, Eskom, September 1976.

Britten A. C. (1992) : *"Insulation Co-ordination of Lines"*, Chapter 8, Eskom and CSIR Course Handouts, 1992.

Bronikowski R. J and du Pont J. P. (1982) : *"Development and testing of MOV arrester elements"*, IEEE Transactions on Power Apparatus and Systems, Vol. PAS-101, No.6, June 1982, pp.1638-1642.

Brown G. W. and Thunander S. (1976) : *"Frequency of distribution arrester discharge currents due to direct strokes"*, IEEE Transactions on Power Apparatus and Systems, Vol. PAS-95, No.5, September 1976, pp1571-1578.

Burger N. (1998) : *"Report on the failure of distribution transformers in the Southern Region"*, Eskom Report, Southern Region, October 1998.

Carneiro S. and Marti J. R. (1991) : *"Evaluation of corona and line models in electromagnetic transients simulations"*, IEEE Transactions on Power Delivery, Vol. 6, No.1, January 1991.

Carter J. F., Darveniza M., Logothetis N. and Parnell T. M. (1976) *: "Investigations of selected high voltage tests on the windings of 11kV distribution transformers"*, Transformer voltage tests, Electrical Engineering Transactions, Australia, 1976, pp89-97.

Chatterton B. G. (1999a) : *"Revised Distribution transformer cost analysis and network performance index impact"*, Eskom Project Report, 2 July 1999.

Chatterton B. G. (1999b) : *"Distribution pole mounted transformer failure analysis project"*, Eskom Project Report, 24 April 1999.

Chatterton B. G., Geldenhuys H. J., Ferguson I., Stephen R. G. and Hoch D. A. (1999c) : *"Distribution pole mounted transformer failure project 1999 short report*, CIGRE/CIRED Working Group 33-01, Eskom Distribution Technology and University of Natal, South Africa, October 1999.

Chatterton B. G. and Kohlmeyer R. E. (2000a) : *"Evaluation of practical methods to reduce transformer failures in Distribution Eastern Region : Progress Report"*, RES/RR/0012139, Technology Research Report, Eskom, November 2000.

Chatterton B. G., Geldenhuys H. J., Ferguson I., Stephen R. G. and Hoch D. A. (2000b) : *"Distribution pole mounted transformer failure analysis and the Eskom experimental program"*, Eskom Distribution Technology and University of Natal, SAUPEC Conference, University of Natal, January 2000.

Chatterton B. G. (2001a) *: "Evaluation of practical methods to reduce transformer failures in Distribution Eastern Region : Progress Report 2 "*, Technology Research Report, RES/RR/01/13736, Eskom, July 2001.

Chatterton B. G., Geldenhuys H. J., Ferguson I., Stephen R. G. and Hoch D. A. (2001b): *"Experimental research on the lightning protection of Reticulation transformers in the Eskom Distribution Eastern Region"*, CIGRE 4th Southern Africa Regional Conference, Cape Town, October 2001.

Chimklai S. and Marti J. R. (1995) : *"Simplified three phase transformer model for electromagnetic transient studies"*, IEEE Transactions on Power Delivery, Vol. 10, No. 3, July 1995.

Chisholm W. A. and Janischevskyj W. (1989) : *"Lightning surge response of ground electrodes"*, IEEE Transactions on Power Delivery, Vol. 4. No.2, April, 1989, pp1329-1337.

CIGRE (1990) *: "Guidelines for representation of network elements when calculating transients"*, Technical Bulletin, WG 02, SC 33, 1990.

CIGRE (1991) : *"Guide to Procedures for estimating the Lightning Performance of Transmission lines"*, WG 01, CIGRE Technical Bulletin 63 October 1991.

CIRED (1997) : *"Protection of MV and LV networks against lightning"*, CIRED/CIGRE WG 05, CIRED Conference, pp 2.28.1 – 2.29.1, June 1997.

Darveniza M., Mercer D. R. and Parnell T. M. (1968) : *"The lightning protection of distribution transformers"*, Transformers and Lightning, Institute of Engineers, Australia, September 1968, pp193-204.

Darveniza M., Sargent M. A., Limbourn G. J., Choy L. A. and Caldwell R. O. (1979a) : *"Modelling for lightning performance calculations"*, IEEE Transactions on Power Apparatus and Systems, Vol. PAS-98, No. 6, Nov/Dec 1979.

Darveniza M., Holcombe B. C. and Stillman R. H. (1979b) : *"An improved method for calculating the impulse strength of wood porcelain insulation"*, IEEE Transactions on Power Apparatus and Systems, Vol. PAS-98, No.6, Nov/Dec 1979.

Darveniza M. (1980) *:"Electrical Properties of wood and line design"*, University of Queensland Press, 1980.

Darveniza M. and Uman M. A. (1982) : *"Lightning protection of distribution systems : Final Report"*, U.S. Department of Energy, DOE/ET/29066-1, September 1982.

Darveniza D. and Uman M. A. (1984) : *"Research into lightning protection of distribution systems – Results from Florida field work 1978 and 1979"*, IEEE Transactions on Power Apparatus and Systems, Vol. PAS-103, No.4, April 1984.

Darveniza M. and Mercer D. R. (1989) : *"Lightning protection of pole mounted transformers"*, IEEE Transactions on Power Delivery, Vol. 4, No. 2, April 1989.

Darveniza M., Mercer D. R. and Tumma L. R. (1991) : *"Stresses on surge arrester blocks caused by multiphase lightning currents"*, ISH 7th, August, 1991.

Darveniza M. and Mercer D. R. (1993) : *"Laboratory studies of the effects of multiphase lightning currents on Distribution surge arresters"*, IEEE Transactions on Power Delivery, Vol.8, No.3, July 1993.

Darveniza M., Roby D. and Tumma L. R. (1994) : *"Laboratory and analytical studies of the effects of multiphase lightning current on metal oxide arresters"*, IEEE Transactions on Power Delivery, Vol. 9, No.2, April 1994.

Darveniza M., Saha T. K. and Wright S. (1999) : *"Studies of in-service and laboratory failures of metal-oxide distribution surge arresters"*, International Symposium on Lightning Protection, Brazil, May 1999, pp39-46.

De la Rosa F., Nucci C. A. and Rakov V. A. (1998) : *"Lightning and its impact on power systems"*, SC 33 International Conference, CIGRE, Croatia, 1998.

De Lorenzi A., Gaio E. and Piovan R. (1987) : *"Performances of ZnO varistors in parallel operation"*, IEEE Pulsed Power Conference, Arlington, 1987, pp623-626.

DME (1994) : *"Analysis of overhead Distribution line outages"*, Report No. EL9001, Department of Mineral and Energy affairs, Pretoria, August 1994.

Dugan R. C. and Smith S. D. (1988) : *"Low-voltage-side current-surge phenomena in single-phase distribution transformer systems"*, IEEE Transactions on Power Delivery, Vol. 3, No. 2, April 1988.

Duke (2000a) : *"Glencoe NB13 Earth Resistance Survey"*, Contract 5RH000001, Duke Engineering, 7 October 2000.

Duke (2000b) : *"Glencoe NB15 Earth Resistance Survey"*, Contract 5RH000001, Duke Engineering, 7 October 2000.

Duke (2000c) : *"Dundee NB18 Earth Resistance Survey"*, Contract 5RH000001, Duke Engineering, 7 October 2000.

ECR (1973) : *"Lightning protection of distribution networks"*, Electricity Council Research, England, June 1973.

Eda K., Iga A. and Matsuoka M. (1980) : *"Degradation mechanism of non-ohmic Zinc oxide ceramics"*, Journal of Applied Physics, Vol.51, No.5, May 1980, pp.2678-2684.

Electrotek (1999) : *"TOP 2000 Users Guide version 4.14"*, Electrotek Concepts, November 1999.

EPRI (1990) : *"Characteristics of lightning surges on distribution lines : First phase report"*, EPRI Research Interim Report, EL-6782, May 1990.

EPRI (1991) : *"Characteristics of lightning surges on distribution lines :Second phase final report"*, EPRI Research Interim Report, TR-100218, December 1991.

EPRI (1997) : *"Testing of lightning arresters and improved lightning protection : Preliminary results"*, EPRI Research Interim Report, TR-109670, December 1997.

Ericksson A. J. and Meal D. V. (1982) : *"Lightning performance and overvoltage surge studies on a rural distribution line"*, IEE Proceedings., Vol. 129 Pt. C, No.2, March 1982.

Ericksson A. J. (1986a) : *"The incidence of lightning strikes to power lines"*, IEEE/PES Winter meeting, New York, February 1986.

Ericksson A. J., Geldenhuys H. J., Kroninger H. and Hefer S. M. (1986b) : *"A study of lightning stresses on metal oxide surge arresters"*, Paper 33-08, CIGRE Session, Paris, August 1986

Ericksson A. J. (1987) : *"An improved electromagnetic model for transmission line shielding analysis"*, IEEE Transactions on Power Delivery, Vol. PWRD-2, No. 3, July 1987.

Fernandez M. I., Rambo K. J., Rakov W. A. and Uman M. A. (1999) : *"Performance of MOV arresters during very close, direct lightning strikes to a power distribution system"*, IEEE Transactions on Power Delivery, Vol. 14, No.2, April 1999.

Fernadez F. and Diaz R. (2001) : *"Metal-oxide arrester model for fast transient simulations"*, IPST '01, Brazil, June 2001.

Funabashi T. (1997) : *"Flashover Modeling of Arcing Horns using the MODELS simulation language"*, IPST '97, Seattle, June 1997, pp295-300.

Gallagher T. J. (1989) : *"Lightning protection of transformers on a 10kV distribution system with isolated neutral"*, ISH 6, New Orleans, USA, 1989.

Gaunt C. T., Britten A. C. and Geldenhuys H. J. (1989) : *"Insulation co-ordination of unshielded distribution lines from 1 kV to 36 kV"*, The High Voltage Co-ordinating Committee Task Force on the Lightning Protection of Distribution Lines, SAIEE, August 1989.

Geldenhuys H. J. (1984) : *"A simulation to predict the effect of line height on the frequency of lightning-induced voltages on distribution lines"*, CSIR, NEERI Report No. I ELEK 328.

Geldenhuys H. J., Stringfellow M. F. and Meal D. V. (1986) : *"Measured lightning discharge duty of distribution surge arresters"*, CIGRE Session, Paris, August 1986.

Geldenhuys H. J. and Oettle E. E. (1987) *: "A discussion of recent work on the prediction of the impulse impedance of earth electrodes"*, source unknown only paper copy of paper, 1987.

Geldenhuys H. J. (1992a) : *"The role of earthing"*, Chapter 5, Lightning Workshop Handout Notes, Eskom and CSIR Course, 1992.

Geldenhuys H. J., Lagesse R. B., Britten A. C., Sadurski K. J. and Van der Merwe W. C. (1992b) *: "Practical insulation co-ordination of woodpole distribution lines in lightning areas"*, Africon '92, IEEE , Swaziland, 1992, pp 503-508.

Goedde G. L., Dugan R. C. and Rowe L. D. (1991) : *"Full scale lightning surge tests of distribution transformers and secondary systems"*, IEEE Transactions on Power Delivery, 1991.

Grainger J. J. and Stevenson W. D. (1994) : *"Power System Analysis"*, 1st edition, McGraw Hill International, 1994.

Greenwood A. , (1991) : *"Electrical Transients in Power Systems"*, 2nd ed, Wiley Interscience, John Wiley and son, 1991.

Haddad A., Fuentas-Rosado J., German D. M. and Waters R. T. (1990) : *"Characterisation of ZnO surge arrester of ZnO surge arrester elements with direct and power frequency voltages"*, IEE Proceedings, Vol. 137, Pt A, No. 5, September 1990, pp269-279.

Hahn B. D. (1997) : *"Essential MATLAB for Scientists and Engineers"*, Prentice Hall, 2nd edition, 1997.

Hart W. C. and Malone E. W. (1979) : *"Lightning and lightning protection"*, Don White Consultants Incorporated, USA, 1979.

Hayashi M., Haba M., Hirano S., Okamoto M. and Watanabe M. (1982) *:"Degradation mechanism of Zinc Oxide varistors under dc bias"*, Journal of Applied Physics, Vol.53, No.8, August 1982, pp.5754-5762.

Hayt W. H. (1994) : *"Engineering Electromagnetics"*, 3rd edition, McGraw Hill International.

Hileman A. R., Roguin J. and Weck K. H. (1990) : *"Metal oxide surge arresters in AC systems – Part 5 : Protection performance of metal oxide surge arresters"*, Electra No. 133, December 1990, pp133-143.

Hileman A. R. (1999) : *"Insulation Coordination for power systems"*, Marcel Deker Inc., 1999.

Holdalen H. K. (1997) : *"Lightning induced voltages in low voltage systems with emphasis on lossy ground effects"*, IPST '97, Seattle, June 1997, pp336-341.

HP (1990) : *"HP 5400 digitizing Oscilloscopes getting started guide"*, Hewlett Packard, August 1990.

Huse J. (1981) : *"Lightning overvoltages and overvoltage protection of distribution transformers"*, CIRED, IEE Publication 197, pp110-113, June 1981.

IEC (1996) *: "Insulation co-ordination Part 1 : Definitions, principles and rules"*, IEC 71-1, IEC international Standard, 1996.

IEEE (1985) : *"A simplified method for estimating the lightning performance of transmission lines"*, IEEE Working Group on lightning performance of transmission lines, IEEE Transactions, PAS-104, April 1985, pp919-932.

IEEE (1991) : *"IEEE Guide for the application of metal-oxide surge arresters for alternating-current systems"*, Standard C62.22 1991.

IEEE (1992) : *"Modeling of metal oxide surge arresters"*, IEEE WG 3.4.11, Application of surge protective devices subcommittee, IEEE Transactions on Power Delivery, Vol.7, No.1, January 1992, pp302-309.

Ikmo K., Funabashi T., Sasaki H. , Hagiwara T. and Kobayashi M. (1996) : *"Study of ZnO arrester model for steep front wave"*, IEEE Transactions on Power Delivery, Vol.11, No.2, April 1996, pp834-841.

Karabo (2001a) : *"Glencoe NB 13 Earth Resistance and Equipment Failure Survey"*, Karabo Engineering, 24 May 2001.

Karabo (2001b) : *"Glencoe NB 15 Earth Resistance and Equipment Failure Survey"*, Karabo Engineering, 24 May 2001.

Karabo (2001c) : *"Dundee NB 18 Earth Resistance and Equipment Failure Survey"*, Karabo Engineering, 24 May 2001.

Kelly R. (1996) : *"Lightning surge propagation from medium voltage to low voltage distribution networks"*, MSc(Eng.) thesis, Department of Electrical Engineering, University of Witwatersrand, South Africa, December 1996.

Kraus J. D. (1992) : *"Electromagnetics"*, 4th ed, McGraw Hill International, 1992.

Leuven (1992) : *"Alternative Transients Program Rule Book"*, Leuven EMTP Center, June 1992.

Liew A. and Darveniza M. (1974) *: "Dynamic model of impulse characteristics of concentrated earths"*, IEE Proceedings, Vol. 121, No.2, February 1974, pp123-135.

Lundquist J., Stenstrom L. Schei A. and Hansen B. (1990) : *"New method for measurement of the resistive leakage currents of metal-oxide surge arresters in service"*, IEEE Transactions on Power Delivery, Vol.5, No.4, November 1990, pp.1811-1829.

Mansoor A. and Grady W. M. (1995) : *"EMTP simulation of lightning and arrester operation"*, Internal Report, Department of Electrical and Computer Engineering, University of Texas, USA, 1995.

Marcuvitz N. (1951) : *"Waveguide Handbook"*, McGraw Hill, New York, 1951.

Marti J. R. (1982) : *"Accurate modelling of frequency dependent transmission lines in electromagnetic transient simulations"*, IEEE Transactions on Power Apparatus and Systems, Vol. PAS-101, No.1, January 1982.

Martinez M. L. B and Zanetta L. C. (1997) *:"A testing method to evaluate the energy withstanding capacity of metal oxide resistors for surge arresters"*, CIGRE SC 33 Colloquium, Toronto, Canada, September 1997.

Mata C. T. (2000) : *"Interaction of lightning with power distribution lines"*, PhD Thesis, Department of Electrical and Computer Engineering, University of Florida, USA, December 2000.

MATLAB (1997) : *"MATLAB function help : FFT"*, Help Desk, MATLAB student version 5.3.

McDermott T. E., Short T. A. and Anderson J. G. (1994) : *"Lightning protection of Distribution lines"*, IEEE Transactions on Power Delivery, Vol. 9, No.1, January 1994, pp138-152.

McMillen C. J., Schoendube C. W. and Caverly D. W. (1982) : *"Susceptibility of distribution transformers to low-voltage side lightning surge failure"*, IEEE Transactions on Power Apparatus and Systems, Vol.PAS-101, No.9, September 1982.

Menter F. E. and Grcev L. (1994) : *"EMTP-Based model for grounding system analysis"*, IEEE Transactions on Power Delivery, Vol. 9, No. 4, October 1994.

Milton J. G. (1989) : *"Energy ratings for metal oxide varistors under repetitively pulsed operation"*, Los Alamos National Laboratory, IEEE, 1989, pp85-88.

Mitchie S. D. (1995) : *"A study of life-cycle costs of distribution transformers and low voltage feeders in urban electricity distribution systems"*, MSc(Eng.) thesis, Department of Electrical Engineering, University of Cape Town, South Africa, July 1995.

Mizuno M., Hayashi M. and Mitani K. (1981) : *"Thermal stability and life of the gapless surge arrester"*, IEEE Transactions on Power Apparatus and Systems, Vol. PAS-100, No.5, May 1981, pp.2664-2671.

Morched A., Marti L. and Ottenvangers J. (1993) : *"A high frequency model for the EMTP"*, IEEE Transactions on Power Delivery, Vol. 8, No. 3, July 1993.

Nixon K. J., Jandrell I. R. and Van Coller J. M. (1998) : *"Evaluation of modelling techniques used to study the transient performance of an earth electrode"*, SAUPEC '98, 1998.

Nixon K. J. (1999) : *"Modelling the lightning transient response of an earth electrode system"*, MSc(Eng) Thesis, Faculty of Engineering, University of Witwatersrand, March 1999.

NRS 016 (1995) *: "Code of practice for the earthing of low-voltage distribution systems"*, NRS Rationalised User Specification, 2nd edition, 1995.

NRS 039 (1995) : *"Guide for the application of gapless metal-oxide surge arresters in distribution systems"*, NRS Rationalised user specification, 1995.

NRS 048 (1996) : *"Electricity Supply Quality of Supply"*, NRS 048, Part 2, South Africa, 1996.

Nucci C. A. and the Task force 33.01 of SC 33 (1995) *: "Lightning induced overvoltages on overhead power lines Part 1 : Return stroke current models with specified channel-base current for the evaluation of the return stroke electromagnetics"*, Electra No. 161, August 1995.

Nucci C. A., Guerrieri S., Correia de Barros M. T. and Rachidi F. (1995) : *"Influence of corona on lightning-induced voltages on overhead power lines"*, Proc. Int. Conf. on Power System transients, Lisbon, 3-7 September 1995.

Oettle E. E. (1987) *: "A new general estimation curve for predicting the impulse impedance of concentrated earth electrodes"*, IEEE Paper No. 87,SM 567-1, IEEE-PES 1987, California, July 1987.

Olsson E. and Dunlop G. L. (1989) : *"The effect of Bi_2O_3 content on the microstructure and electrical properties of ZnO varistor materials"*, Journal of Applied Physics, Vol. 66, No. 9, November 1989, pp4317-4324.

Oppenheim A. V. and Schafer R. W. (1989) : *"Discrete-time signal processing"*, 1st edition, Prentice Hall International, 1989.

Orfanidis S. J. (1996) : *"Introduction to signal processing"*, 1st edition, Prentice Hall International, 1996.

Parnell T. M., Darveniza M. and Fraser S. G. (1968) : *"Impulse testing of transformers with special reference to testing technique"*, Impulse testing of transformers, Electrical Engineering Transactions, Australia, 1968, pp159-167.

Parrish D. E. (1991) : *"Lightning-caused distribution transformer outages on a Florida Distribution system"*, IEEE Transactions on Power Delivery, Vol. 6, No.2, April 1991.

Paul D. and Venugopalan S. I. (1993) : *"Power distribution system equipment overvoltage protection"*, IEEE Transactions on Power Delivery, 1993, pp 1560-1569.

Pinceti P. and Giannettoni M. (1999) *: "A simplified model for zinc oxide surge arresters"*, IEEE Transactions on Power Delivery, Vol.14, No.2, April 1999, pp393-397.

Prikler L. and Holdalen H. K. (1998) : *"ATPDraw for Windows 3.1x/95/NT version 1.0 Users Manual"*, November 1998.

Plummer C. W. (1995) : *"Reduction in distribution transformer failure rates and nuisance outages using improved lightning protection concepts"*, IEEE Transactions on Power Delivery, Vol.10, No.2, April 1995.

Richter B. (1999) : *"Dimensioning, testing and application of metal oxide surge arresters in medium voltage networks"*, ABB Application Guide, revised edition 3, July 1999.

Richter B. (2001) : *"Private communication"*, ABB High Voltage Technologies Ltd, Switzerland, January 2001 to May 2002.

Ringler K. G., Kirby P. and Erven C. C. (1997) : *"The energy absorption capability and time-to-failure of varistors used in station-class metal-oxide arresters"*, IEEE Transactions on Power Delivery, Vol.12, No.1, January 1997.

Robert A. and Marquet J. (1992) : *"Assessing voltage quality with relation to harmonics, flicker and unbalance"*, CIGRE Session 1992, September 1992, paper 36-203.

Rusk, S. (1977) : *"Protection of Distribution lines"*, Chapter No. 23 of Lightning, Vol. 2, Edited by RH Golde, Academic press, London, 1977.

SABS (1979) : *"Standard specification for Distribution transformers"*, SABS 780-1979, South African Bureau of Standards.

SAIEE (1989) : *"The lightning protection of distribution lines"*, Conference Proceedings, August 1989.

Sakshaug E. C. (1979) : "*Influence of rate-of–rise on distribution arrester protective characteristics"*, IEEE Transactions on Power Apparatus and Systems, Vol. PAS-98, No.2, March/April 1979.

Schei A. and Huse J. (1978) : *"Currents through surge arresters due to lightning with main reference to distribution systems"*, CIGRE SC 33, Electra, No.58, 1978, pp41-91.

Schei A. and Weck K. H. (1990) : *"Metal oxide surge arresters in AC systems – Part 1: General properties of the metal oxide surge arrester"*, Electra No. 128, January 1990, pp101-105.

Schei A. (2000) : *"Diagnostic techniques for surge arresters with main reference to on-line measurement of resistive leakage current of metal oxide arresters*", Behalf of CIGRE SC 33, CIGRE Session 2000, P1-05.

Schmidt W., Meppelink J., Richter B., Feser K., Kehl L. and Qiu Q. (1989) : *"Behaviour of MO-surge arrester blocks due to fast transients"*, IEEE Transactions on Power Delivery, Vol.4, No.1, January 1989, pp.292-300.

SCSASAAL9 (1999) : *"Distribution Earthing Standard Part 2 : Section 1 MV and LV Reticulation Earthing"*, Eskom Standard, 1999.

SCSASABE7 (2001) : *"General information and requirements for overhead lines up to 33kV with conductors up to Hare/Oak"*, Eskom Distribution MV Standard, Section 0, September 2001.

SCSSCAAN5 (2000) : *"Specification for distribution class, metal-oxide surge arresters without spark-gaps"*, Eskom Distribution specification, December 2000.

Shirakawa S., Endo F. and Kitajima H. (1988) : *"Maintenance of surge arrester by portable arrester leakage current detector"*, IEEE Transactions on Power Delivery, Vol.3, No.3, July 1988, pp.998-1003.

Smit H. and Pieterse P. R. (1993) : *"Failure of rural transformers in the Stella Area"*, Eskom Report S167/93, Bloemfontein Distributor, 1993.

Spellman C. A. and Haddad A. (1997) *: "A technique for on-line monitoring of ZnO surge arresters"*, 10th ISH Conference, Montreal, Canada, August 1997.

Stenstrom L. (1990) : *"Metal oxide surge arresters in AC systems – Part 6: Selection of metal oxide surge arrester characteristics from the standards*", Electra No. 133, December 1990, pp147-165.

Stenstrom L. and Lundquist J. (1999) : *"Energy stress on a transmission line arresters considering the total lightning charge distribution"*, IEEE Transactions on Power Delivery, Vol. 14, No. 1, January 1999.

Sugimoto H., Akira A., Yokoyama S. and Nakada K. (1999) *: "Effectiveness of installing two pairs of distribution surge arresters in parallel"*, High Voltage Engineering Symposium, IEE, 1999.

Teorres H., Gonzalez D., Rondon D., Quintana C., Salgado M., Avila D., Trujillo O., Herrera F., Amortegui F. and Giraldo O. (1999) : *"Application of a methodology in order to reduce distribution transformer failures due to high lightning activity"*, International Symposium on Lightning Protection, Brazil, May 1999, pp48-53.

Tominaga S., Shibuya Y., Fujiwara Y., Imataki M. and Nitta T. (1980) : *"Stability and long term degradation of metal oxide surge arresters"*, IEEE Transactions on Power Apparatus and Systems, Vol. PAS-99, No.4, July/August 1980.

Umana A. M. and Rianao O. P. (1999) : *"Solutions to the power distribution transformers failures in Colombia"*, International Symposium on Lightning Protection, Brazil, May 1999, pp54-58.

Van Coller J. M. (1993) : *"An Introduction to EMTP"*, Department of Electrical Engineering, University of Witwatersrand, Revision 3.0, 1993.

Van der Linde F. J. (1999) : *"Parameters for a power frequency model of some deteriorated surge arresters"*, MSc(Eng.) thesis, Department of Electrical Engineering, University of Natal, South Africa, January 1999.

Van Niekerk K. (1987) : *"The performance and characteristics of an 11kV wood-porcelain insulated Transmission line"*, MSc(Eng.) Thesis, Department of Electrical Engineering, University of Natal, South Africa, 1987.

Van Schalkwyk W. J. (2001) : *"The placing of line surge arresters and fuses on 11 and 22kV lines to protect equipment against lightning*", M.Eng thesis, University of Stellenbosch, South Africa, March 2001.

Van Wyk S. (1997) : *"Transformer field performance in Sub-Sahara Africa"*, Applitech 97 Conference, July 1997.

Van Wyk S. (1999) : *"Transformer failures in Sub-Sahara Africa : A 1998 Review*", Energize Magazine, , May/June 1999, pp36-39.

Wadhwa C. L. (1995) : *"High Voltage Engineering"*, New age International Limited, 1st reprint, September 1995.

Walter M. W. (1960) : *"The performance of rural distribution type transformers in lightning areas"*, SAIEE Journal, Natal, November 1960.

Woivre V., Arthaud J. P., Ahmed A. and Burais N. (1993) *: "Transient overvoltage study and model for shell-type power transformers",* IEEE Transactions on Power Delivery, Vol.8, No.1, 1993, pp212-220.

Wood H. B. (1988) : *"Mathematics for communication engineering"*, 1st edition, Ellis Horwood Limited, 1988.